A11103 088714

NAT'L INST OF STANDARDS & TECH R.I.C.
A11103088714
International Semina/Ultrasonic tissue c
QC100 .U57 NO.453, 1976 C.2 NBS-PUB-C 19

NBS SPECIAL PUBLICATION 453

U.S. DEPARTMENT OF COMMERCE / National Bureau of Standards

Ultrasonic Tissue Characterization

QC
100
.U57
NO.453
1976
c.2

NATIONAL BUREAU OF STANDARDS

The National Bureau of Standards [1] was established by an act of Congress March 3, 1901. The Bureau's overall goal is to strengthen and advance the Nation's science and technology and facilitate their effective application for public benefit. To this end, the Bureau conducts research and provides: (1) a basis for the Nation's physical measurement system, (2) scientific and technological services for industry and government, (3) a technical basis for equity in trade, and (4) technical services to promote public safety. The Bureau consists of the Institute for Basic Standards, the Institute for Materials Research, the Institute for Applied Technology, the Institute for Computer Sciences and Technology, and the Office for Information Programs.

THE INSTITUTE FOR BASIC STANDARDS provides the central basis within the United States of a complete and consistent system of physical measurement; coordinates that system with measurement systems of other nations; and furnishes essential services leading to accurate and uniform physical measurements throughout the Nation's scientific community, industry, and commerce. The Institute consists of the Office of Measurement Services, the Office of Radiation Measurement and the following Center and divisions:

Applied Mathematics — Electricity — Mechanics — Heat — Optical Physics — Center for Radiation Research: Nuclear Sciences; Applied Radiation — Laboratory Astrophysics [2] — Cryogenics [2] — Electromagnetics [2] — Time and Frequency [2].

THE INSTITUTE FOR MATERIALS RESEARCH conducts materials research leading to improved methods of measurement, standards, and data on the properties of well-characterized materials needed by industry, commerce, educational institutions, and Government; provides advisory and research services to other Government agencies; and develops, produces, and distributes standard reference materials. The Institute consists of the Office of Standard Reference Materials, the Office of Air and Water Measurement, and the following divisions:

Analytical Chemistry — Polymers — Metallurgy — Inorganic Materials — Reactor Radiation — Physical Chemistry.

THE INSTITUTE FOR APPLIED TECHNOLOGY provides technical services to promote the use of available technology and to facilitate technological innovation in industry and Government; cooperates with public and private organizations leading to the development of technological standards (including mandatory safety standards), codes and methods of test; and provides technical advice and services to Government agencies upon request. The Institute consists of the following divisions and Centers:

Standards Application and Analysis — Electronic Technology — Center for Consumer Product Technology: Product Systems Analysis; Product Engineering — Center for Building Technology: Structures, Materials, and Life Safety; Building Environment; Technical Evaluation and Application — Center for Fire Research: Fire Science; Fire Safety Engineering.

THE INSTITUTE FOR COMPUTER SCIENCES AND TECHNOLOGY conducts research and provides technical services designed to aid Government agencies in improving cost effectiveness in the conduct of their programs through the selection, acquisition, and effective utilization of automatic data processing equipment; and serves as the principal focus within the executive branch for the development of Federal standards for automatic data processing equipment, techniques, and computer languages. The Institute consists of the following divisions:

Computer Services — Systems and Software — Computer Systems Engineering — Information Technology.

THE OFFICE FOR INFORMATION PROGRAMS promotes optimum dissemination and accessibility of scientific information generated within NBS and other agencies of the Federal Government; promotes the development of the National Standard Reference Data System and a system of information analysis centers dealing with the broader aspects of the National Measurement System; provides appropriate services to ensure that the NBS staff has optimum accessibility to the scientific information of the world. The Office consists of the following organizational units:

Office of Standard Reference Data — Office of Information Activities — Office of Technical Publications — Library — Office of International Relations — Office of International Standards.

---

[1] Headquarters and Laboratories at Gaithersburg, Maryland, unless otherwise noted; mailing address Washington, D.C. 20234.

[2] Located at Boulder, Colorado 80302.

reau of Standards
6 1976
acc.
00
7
153
6

Ultrasonic Tissue Characterization

t special publication, 104

Proceedings of a Seminar held at the
National Bureau of Standards,
Gaithersburg, Md., May 28 - 30, 1975

Edited by

Melvin Linzer

Institute for Materials Research
National Bureau of Standards
Washington, D.C. 20234

Cosponsored by

National Science Foundation (Research Applied to National Needs, RANN)

National Institutes of Health (Diagnostic Radiology Department, Clinical Center)

National Bureau of Standards (Institute for Materials Research)

U.S. DEPARTMENT OF COMMERCE, Elliot L. Richardson, Secretary
Edward O. Vetter, *Under Secretary*
Dr. Betsy Ancker-Johnson, *Assistant Secretary for Science and Technology*

U.S. NATIONAL BUREAU OF STANDARDS, Ernest Ambler, Acting Director

Issued October 1976

Library of Congress Cataloging in Publication Data
Seminar on Ultrasonic Tissue Characterization, 1st, National Bureau of Standards, 1975.
Ultrasonic tissue characterization.
(NBS special publication ; 453)
Includes indexes.
Supt. of Docs. no.: C 13.10:453
1. Diagnosis, Ultrasonic—Congresses. 2. Ultrasonic waves—Measurement—Congresses. 3. Tissues—Analysis—Congresses. I. Linzer, Melvin. II United States. National Science Foundation. III United States. National Institutes of Health. Clinical Center. IV. United States. National Bureau of Standards. V. Title. VI. Series: United States. National Bureau of Standards. Special publication ; 453.
QC100.U57 no. 453 [RC78.7.U4] 602'.Is [616.07'583]
76-608298

National Bureau of Standards Special Publication 453

Nat. Bur. Stand. (U.S.), Spec. Publ. 453, 274 pages (Oct. 1976)

CODEN: XNBSAV

U.S. GOVERNMENT PRINTING OFFICE
WASHINGTON: 1976

For sale by the Superintendent of Documents, U.S. Government Printing Office, Washington, D.C. 20402
(Order by SD Catalog No. C13.10: 453). Stock No. 003-003-01700-1 Price $3.55 cents.
(Add 25 percent additional for other than U.S. mailing)

FOREWORD

The primary function of the National Bureau of Standards is to provide measurement methods, standards, and data to assure the reliability and effective use of measurements. Among the many areas requiring improved measurement reliability, none is more important than that which supports the Nation's health care system. The application of the physical and engineering sciences to improve the quality of medical diagnosis and treatment is already having enormous impact. Much, however, remains to be done. To fully exploit the advances in these sciences, it will be necessary to foster and maintain an active dialogue among the many diverse groups working to promote improved health care. The materials scientist can also contribute to this goal. In the field of nondestructive evaluation, for example, many of the ultrasonic methods for assessing structural reliability are remarkably similar to those used for medical diagnosis.

The prospect for a synergistic development of techniques for non-invasive medical diagnosis and nondestructive evaluation of materials is an exciting one. The National Bureau of Standards has programs in both areas and thus can play a role in bringing together the biomedical and materials communities in a common effort to improve these two measurement systems.

This Conference makes a truly outstanding contribution to the advancement of these techniques and to their more effective utilization. The National Bureau of Standards is proud to be a cosponsor along with the National Institutes of Health and the National Science Foundation in this important undertaking.

John D. Hoffman
Director
Institute for Materials Research
National Bureau of Standards

PREFACE

This book is the formal report on the proceedings of the first international Seminar on Ultrasonic Tissue Characterization. The meeting was held at the National Bureau of Standards on May 28-30, 1975, and was cosponsored by the National Science Foundation, the National Institutes of Health, and the National Bureau of Standards.

Participants in the Seminar included the foremost researchers in ultrasonic tissue characterization both from within the United States and from abroad. The meeting served as a forum for the examination of the state-of-the-art and prospects for research in the newly-emerging field of ultrasonic parameter measurement.

This volume contains extended versions of 21 of the 22 talks presented at the Seminar. The first chapter of the book covers the introductory session and is followed by chapters on tissue properties, A-scan pattern recognition techniques, attenuation and velocity techniques, absorption techniques, scattering techniques, impedance-profile techniques, and acoustic microscopy.

These proceedings bring together for the first time a comprehensive compilation of definitive articles on ultrasonic tissue parameters and methods for measurement of these properties. It is our belief that publication of this landmark volume will provide directed stimulus to this new and exciting area of medical diagnosis.

An undertaking of this magnitude would not have been possible without the assistance of many individuals. The editor is greatly indebted to his conference co-chairperson, Gil Devey, who originally conceived of the Seminar and provided major financial support through NSF/RANN. His farsighted management of the RANN Instrumentation Program has had considerable impact on establishing a nationally-integrated research effort in medical ultrasound. For this achievement, Gil recently received the first AAMI Foundation Award for distinguished contribution to the advancement of medical instrumentation. In the week following the Seminar, Gil moved to the Office for International Programs at NSF. His presence in the medical ultrasound area will certainly be missed.

Acknowledgement is also given to the contributions of John Doppman (NIH Clinical Center), as well as to Peter Wells (Bristol General Hospital) and Judy Prewitt (NIH) who served as chairpersons of the "Summary and Critique Panel" and "Tissue Signature Panel", respectively. Particular appreciation is due Ron Johnson (NBS/Institute for Materials Research), whose very capable handling of the logistics of the Seminar helped to ensure the physical comfort of the participants and the smooth progress of the meeting. In this effort, he was enthusiastically aided by Gloria Serig and others in the Institute office as well as Sara Torrence and the other members of the NBS conference staff. Finally, special acknowlegement is expressed to Ellen Ring and the staff of the Institute Text-Editing Facility for their skillful typing of the manuscript, to Rosemary Maddock for valuable editorial suggestions, and to Betty Hurdle for coordinating the final stages of publication of these proceedings.

Melvin Linzer
Conference Chairperson
and Moderator

ABSTRACT

An international Seminar on Ultrasonic Tissue Characterization was held at the National Bureau of Standards on May 28-30, 1975. The meeting was co-sponsored by the National Bureau of Standards, the National Science Foundation and the National Institutes of Health. This volume contains extended versions of 21 of the 22 talks presented at the Seminar. Topics covered include techniques for measurement of ultrasonic tissue parameters, the dependence of tissue properties on physical and biological variables (*e.g.*, ultrasonic frequency, temperature) and pattern recognition techniques.

Key Words: A-scan; absorption; acoustic; attenuation; B-scan; frequency; image reconstruction; impedance; medical diagnosis; microscopy; pattern recognition; scattering; tissue characterization; tissue parameters, tissue signature; tumor; ultrasonic spectroscopy; ultrasound; velocity.

CONTENTS

Page

INTRODUCTION 1

CHAPTER 1 - OVERVIEW

1.1 The NSF (RANN) Integrated Program on Medical Ultrasonics - G. B. Devey 7

1.2 Challenges and Opportunities in Ultrasound (Keynote Address) - J. M. Reid 11

CHAPTER 2 - TISSUE PARAMETERS

2.1 Ultrasonic Attenuation, Absorption, and Velocity in Tissues and Organs - F. Dunn 21

2.2 The Scattering of Ultrasound by Tissues - J. M. Reid 29

CHAPTER 3 - A-SCAN PATTERN RECOGNITION TECHNIQUES

3.1 Use of Pattern Recognition for Signal Processing in Ultrasonic Histopathology - K. Preston, Jr., ... 51

3.2 Quantitative A-Scan Analysis of Normal and Cirrhotic Liver - P. N. T. Wells, R. A. Mountford, M. Halliwell, and P. Atkinson 61

3.3 Digital A-Scan Analysis in the Diagnosis of Chronic Splenic Enlargement - K. J. W. Taylor and J. Milan 71

CHAPTER 4 - ATTENUATION AND VELOCITY TECHNIQUES

4.1 Attenuation and Velocity Measurements in Tissue Using Time Delay Spectrometry - D. H. Le Croissette and R. C. Heyser 81

4.2 Methods of Tissue Identification by Ultrasonic Spectra - A. Sokollu, E. W. Purnell, E. Holasek, W. Jennings, and A. Kaya 97

4.3 Algebraic Reconstruction of Spatial Distributions of Refractive Index and Attenuation in Tissues from Time-of-Flight and Amplitude Profiles - J. F. Greenleaf and S. A. Johnson 109

4.4 Measurement of Ultrasonic Tissue Characteristics by Direct and Phase-Contrast Imaging - R. S. Mezrich, D. H. R. Vilkomerson, and K. F. Etzold 121

4.5 Reflection Techniques for Measurement of Attenuation and Velocity - G. Kossoff 135

CHAPTER 5 - ABSORPTION TECHNIQUES

5.1 Ultrasonically-Induced Transient Thermal Gradients: Their Potential Role in Acoustic Parameter Characterization of Tissue - F. J. Fry 143

5.2 TAST: A Non-Invasive Tissue Analytic System - T. D. Sachs, P. T. Anderson, R. S. Grimes, S. J. Wright, Jr., and R. M. P. Donaghy 153

Page

CHAPTER 6 - SCATTERING TECHNIQUES

6.1 Tissue Characterization by Ultrasonic Frequency-Dependent Attenuation and Scattering - P. P. Lele, A. B. Mansfield, A. I. Murphy, J. Namery, and N. Senapati 167

6.2 Frequency and Angular Dependence of Ultrasonic Scattering from Tissue - C. R. Hill 197

6.3 The Scattering of Ultrasound by Red Blood Cells - K. K. Shung, R. A. Sigelmann, and J. M. Reid 207

6.4 Swept-Frequency Ultrasonic Determination of Tissue Macrostructure - R. C. Waag, R. M. Lerner and R. Gramiak 213

CHAPTER 7 - IMPEDANCE PROFILE TECHNIQUES

7.1 Acoustic Impedance Profiling: An Analytical and Physical Model Study - A. C. Kak and F. J. Fry 231

7.2 Current Problems in Ultrasonic Impediography - J. P. Jones 253

CHAPTER 8 - ACOUSTIC MICROSCOPY

8.1 Tissue Characterization by Means of Acoustic Microscopy - L. W. Kessler 261

REGISTRATION LIST 271

AUTHOR INDEX 283

SUBJECT INDEX 287

INTRODUCTION

Recent developments in ultrasonic imaging and grey-scale technology have made it possible to visualize at high resolution the internal texture of tissue and relate the texture to tissue pathology. In spite of these impressive successes, however, current clinical instruments provide data on only two tissue properties, backscattered echo strength and medium attenuation, neither of which is separated experimentally. Because there are many different modes of interaction of ultrasonic energy with tissue, a vast amount of additional information is potentially available from an ultrasonic signal. This includes such basic acoustic parameters as absorption, velocity, attenuation, scattering, impedance, and their dependence on frequency and other physical variables. In principle, suitable *in vivo* techniques could be devised which will extract and separate many of the medically-significant features of the ultrasound interactions. The development of such quantitative techniques for measurement of ultrasonic tissue parameters is only now receiving the attention of the research community and is perhaps the last major frontier in medical ultrasound.

In order to provide focus and direction to this emerging field, an international Seminar on Ultrasonic Tissue Characterization was held at the National Bureau of Standards on May 29-31, 1975. The conference was cosponsored by the National Science Foundation (NSF), National Bureau of Standards (NBS), and National Institutes of Health (NIH). The principal objective of the Seminar was to assess the current status of and prospects for research into the non-invasive characterization of normal and pathological tissue using ultrasound. The Seminar was the first devoted to a comprehensive examination of tissue parameter measurement techniques. Additional topics included the dependence of tissue properties on physical and biological variables (*e.g.*, ultrasonic frequency, temperature), pattern recognition, and the development of a tissue signature library. Because of the extensive coverage of imaging and Doppler techniques provided in the periodic International Symposia on Acoustical Imaging and Holography, these areas were specifically excluded from consideration at the Seminar.

The Seminar was especially noteworthy for the participation of the world's leading researchers in ultrasonic tissue characterization. The attendees, who numbered more than 220, came from the United States, Canada, Europe, Japan, South America and Australia. The group was truly interdisciplinary, comprising life, physical, and materials scientists, physicians, engineers, and physical science and health care administrators. For many of these individuals, the Seminar afforded a first opportunity to communicate with fellow researchers in divergent fields on problems of mutual interest in tissue characterization.

All of the speakers were carefully selected so as to provide a coherent program. Following the introductory remarks and keynote address, the technical program opened with a session on tissue parameters. This was followed by sessions devoted to techniques for measuring individual tissue properties. A major criterion for inclusion of a particular technique was that it be suitable for eventual application to *in vivo* clinical diagnosis.

Two panel discussions followed the technical sessions. The first panel attempted to assess the relative potential of the various methods presented during the Seminar and to delineate the most promising directions for future research. The second panel considered the steps necessary to establish a tissue signature library, including the formulation of standardized test methodology and standardized reporting procedures for diagnostic results. Lively and extensive floor participation occurred throughout both the technical sessions and panel discussions.

The *introductory session* opened with a welcome address by J. D. Hoffman, Director of the Institute for Materials Research (NBS). Dr. Hoffman noted the similarities between standardization and measurement needs in ultrasound for medical non-invasive diagnosis and for nondestructive evaluation of materials. NBS has programs in both areas and perhaps could serve as a bridge between the biomedical and materials communities in ultrasound technology. G. B. Devey, NSF/RANN (Research Applied to National Needs), reviewed the key role which NSF has played in organizing a nationally-integrated program in medical ultrasound. Current RANN programs emphasize tissue characterization techniques and high resolution imaging, with over $1.4 million to be made available in 1976 to support research in these areas. The keynote speaker, J. M. Reid (Institute of Applied Physiology and Medicine, Seattle) spoke of the great promise of ultrasonic parameter measurements for medical diagnosis but deplored the lack of substantive implementation of this approach in current clinical practice. He also discussed some of the problems associated with research on *in vitro* specimens.

The session of *tissue parameters* (p. 21) was partly tutorial. It opened with a discussion by F. Dunn (University of Illinois, Urbana) on the mechanisms of and available data on attenuation, absorption, and velocity parameters, followed by a talk by J. M. Reid on the basic physics of scattering. Dr. Dunn pointed out that the attenuation values observed in tissue fall naturally into categories determined by the relative concentrations of water and structural protein within the tissue.

The major portion of the scientific program was devoted to tissue characterization methods and opened with a session on *A-scan pattern recognition techniques* (p. 51). The session dealt with both human- and computer-based aspects of pattern recognition. The talk by K. C. Ossoinig[1] (University of Iowa, Iowa City) demonstrated how a trained operator, using carefully calibrated equipment, can successfully identify eye pathology from subtle differences in complex A-patterns. This approach is essentially the one-dimensional equivalent of the application of the sophisticated human eye-brain complex in picture pattern recognition, as employed in traditional x-ray and ultrasonic radiology. K. Preston (Carnegie-Mellon University, Pittsburgh) discussed a recently-initiated program concerned with the development of computer-based techniques for *in vivo* liver diagnosis in which biopsies from the insonified regions are being used to establish correlations. He reported some preliminary results on the down-conversion of ultrasonic A-scan signals to the audio frequency range so as to utilize the ear-brain complex for pattern recognition. This approach is borrowed from a target classification scheme employed in sonar. At the end of his talk, the audience was treated to a conference "first" - the opportunity to hear an audio recording of a transformed A-scan from a normal liver.

Two papers by P. N. T. Wells and coworkers (Bristol General Hospital and Bristol Royal Infirmary, Bristol, U.K.) and K. J. W. Taylor and J. Milan (Yale University, New Haven, and Royal Marsden Hospital, Surrey, U.K.) dealt with digital A-scan analysis of echo amplitudes to differentiate liver and splenic pathology, respectively. Because of statistical variations of absolute echo amplitudes among different individuals, this approach would be most useful in monitoring response to therapy.

The session on *attenuation and velocity techniques* (p. 81) covered a variety of methods providing either integrated or localized values of these parameters. The first two talks, by D. H. Le Croissette and R. C. Heyser (Jet Propulsion Lab, Pasadena) and A. Sokollu and coworkers (Case Western Reserve University, Cleveland), discussed transmission measurements in the frequency and time domains and transformations between these domains. Dr. Sokollu also reported on some recent clinical results using chromatic encoding of frequency response. J. F. Greenleaf and S. A. Johnson (Mayo Clinic, Rochester) described a transmission measurement of tissue velocity distributions using computerized axial tomography. Attenuation profiling, however, is much more difficult to achieve with this approach. R. S. Mezrich and coworkers (R.C.A. Labs, Princeton) combined transmission attenuation and velocity measurements with a real-time imaging system exhibiting wide frequency and angular response. The velocity measurement was accomplished by means of a phase-contrast technique which minimizes effects of intervening tissue. G. Kossoff (National Acoustics Lab, Sydney, Australia) suggested several reflection techniques for obtaining velocity and attenuation parameters and their frequency dependence. One of the velocity methods employs two transducers on the same side of the tissue separated by a known distance and is similar in concept to the image reconstruction approach.

The session on *absorption techniques* (p. 143) dealt with two indirect methods for *in vivo* measurement of this parameter. Both methods depend on the detection of the velocity change induced by the temperature increase associated with absorption of ultrasonic energy. In the first talk, F. J. Fry (Fortune-Fry Labs, Indianapolis) described early work and some recent experimental results on the creation of a velocity gradient by ultrasonically heating an absorption gradient within the tissue. Since impedance is proportional to velocity, the resulting change in impedance across the absorption interface could be probed by pulse-echo techniques. T. D. Sachs and coworkers (University of Vermont, Burlington) discussed an extension of this technique to homogenous tissue using a differential velocity measurement and reported experimental results on detecting ventricles and other structures within an excised brain.

---

[1]The manuscript of this talk was unavailable at time of publication.

The session on *scattering techniques* (p. 167) covered theoretical and experimental aspects of both frequency and angular dependence of scattering and included some preliminary clinical results. Talks were presented by P. P. Lele (MIT, Cambridge), C. R. Hill (Institute for Cancer Research, Sutton, U. K.), K. K. Shung and coworkers (University of Washington, Seattle), and R. C. Waag and coworkers (University of Rochester, Rochester). Excellent agreement between theory and experiment was reported by Dr. Shung for scattering from blood and by Dr. Hill for scattering from muscle tissue.

The session on *impedance profile techniques* (p. 231) opened with a talk by A. C. Kak (Purdue University, West Lafayette) and F. J. Fry who described deconvolution techniques for deriving the impulse response of tissue. The idealized model considered was a dispersionless medium consisting of plane-parallel interfaces insonified at normal incidence. In the absence of multiple reflections, integration of the impulse response yields the impedance profile of the medium. Current problems and future directions of impediography were outlined by J. P. Jones (Bolt Beranek and Newman, Cambridge) who pioneered the development of the technique.

The final technical session was on *acoustic microscopy* (p. 261) and featured a description by L. Kessler (Sonoscan, Bensenville, Illinois) of a commercial device capable of measuring impedance, velocity, and attenuation of tissue samples up to 500 MHz. Although not an *in vivo* technique, acoustic microscopy was included on the program because it can provide acoustic parameter information on a more microscopic scale and at higher frequencies. Such studies can serve to clarify the acoustic interactions observed at clinical diagnostic frequencies.

The talks, audience comments, and panel discussions at the Seminar succeeded in presenting a comprehensive picture of the state-of-the art in ultrasonic tissue characterization. It was evident, however, that although the field is now undergoing rapid change, it is still in a preliminary stage of development. Much of the methodology is unable to provide sufficiently quantitative information on the ultrasonic properties of tissue in an experimental or clinical environment. For example, the underlying theory for the interpretation of scattering data is as yet unable to cope with the complexities of tissue structure, while for other parameters, such as absorption, the techniques are not sufficiently developed for *in vivo* application. One can only hope that the improved scientific communication engendered by the Seminar will provide the impetus to overcome many of these hurdles. Increasing support now being given by federal funding agencies such as NSF and NIH, as well as new thrusts underway on quantitative ultrasonic nondestructive evaluation of materials are also certain to stimulate considerable research activity in ultrasonic parameter measurement.

The conference undoubtedly marked a milestone in the development of medical ultrasound as a major non-invasive diagnostic technique. The consensus among the distinguished participants was that the meeting was one of the most significant in the history of ultrasound. As an indication of their enthusiasm, the attendees voted unanimously to return to NBS in about December, 1976 for another Tissue Characterization Seminar. It is anticipated that future Seminars will be convened at eighteen-month intervals and will serve as the principal forums for reporting new advances in ultrasonic parameter measurement. These Seminars would be complemented by the International Symposia on Acoustical Imaging and Holography, also held at 18-month intervals, which are recognized as the major conferences devoted to imaging and Doppler technology. In the periods between these topical meetings, the researchers in ultrasonic parameter and imaging techniques would have the opportunity to communicate results at clinically-oriented conferences, such as the annual AIUM meetings, or physics- and engineering- oriented meetings such as the annual IEEE Ultrasonic Symposia.

The Proceedings of the Seminar, published in this volume, should play a landmark role in the future development of the field. Speakers were invited to submit extended papers to the Proceedings based on their oral presentations at the Seminar. With the cooperation of the authors, these contributions were carefully reviewed and edited to provide a cohesive picture of the current status and potential of ultrasonic tissue parameter measurement.

It is anticipated that by the next Tissue Characterization Seminar, substantial progress will have been made in placing the various techniques on firm theoretical bases and in the refinement of the methodology and instrumentation to permit *in vivo* diagnosis. Success in the clinical measurement of ultrasonic tissue parameters is likely to be accompanied by the development of simultaneous tomographic displays of the parameters in a format suitable

for interpretation by a physician. Such displays could take the form of a color TV presentation in place of the familiar grey-scale display; the different colors would represent basic acoustic parameters, or such physical variables as frequency or temperature response. Regardless of the degree of sophistication achieved in the immediate future, however, there is no question that research into quantitative tissue characterization will ultimately result in dramatic improvements in the capability of medical ultrasound. When combined with real time, high-resolution imaging and implemented routinely in a clinical environment, these techniques could revolutionize medical diagnosis.

Melvin Linzer
Conference Chairman and
Moderator

CHAPTER 1

OVERVIEW

National Bureau of Standards Special Publication 453. Proceedings of Seminar on Ultrasonic Tissue Characterization held at NBS, Gaithersburg, MD, May 28-30, 1975. (Issued Oct. 1976)

CHAPTER 1. OVERVIEW

Paper 1.1: THE NSF (RANN) INTEGRATED PROGRAM ON MEDICAL ULTRASONICS

G. B. Devey[1]

Instrumentation Technology Program
Research Applied to National Needs (RANN)
National Science Foundation
Washington, D. C. 20550

Recommendations made by the National Science Foundation (NSF) Survey Team on Ultrasonic Imaging for the conduct of a Medical Instrumentation Experiment to provide incentives to commercial firms and for the preparation of an R & D agenda for future developments in medical ultrasonics have been implemented. Projects emphasizing substantial improvements in resolution of medical ultrasonic images and investigations into ultrasonic tissue characterization are listed at high priority. The NSF (RANN) Instrumentation Technology program supports research in these areas. In addition to having good potential for making substantial technological advances, the funded projects must also develop the criteria which should be met before results of the research are introduced into clinical medicine. Successful results from a coordinated research and development program in ultrasonic tissue characterization could revolutionize medical diagnosis.

Key Words: Applied research; imaging; instrumentation technology; medical ultrasonics; NSF; RANN; R & D incentives; tissue characterization; tissue signature; ultrasonic diagnosis; ultrasound

1. Introduction

In 1973, the RANN (Research Applied to National Needs) Program of the National Science Foundation (NSF) organized a survey team for the purpose of evaluating the state-of-development of medical ultrasonic diagnostic instruments. The results of the survey are found in the report, "Prospectives for Ultrasonic Imaging in Medical Diagnosis" [1].[2]

One outcome of the NSF survey team recommendations was the establishment of a Medical Instrumentation Experiment (No. 5) by the NSF Office of Experimental Research and Development Incentives (RDI). Twelve industrial firms agreed to participate in the experiment, which was implemented in 1974; the objective is to promote the development of advanced medical ultrasonic diagnostic instruments using existing technology to meet the advanced performance specifications included in the protocol of Experiment No. 5. The incentive to industrial firms is the opportunity for no-cost clinical validation to be made of the instruments to be developed to meet these specifications. The essential validation tests would be conducted by the Veterans Administration (VA) under a $3 million agreement with NSF. An important element of the VA program is the conduct of an extensive training program in medical ultrasonics.

---

[1]Present address: Office of International Programs, National Science Foundation, Washington, DC 20550.

[2]Figures in brackets indicate the literature references at the end of this paper.

The "Prospectives Report" includes a recommendation that an R & D agenda be prepared for future developments in ultrasound. The agenda should include four elements, *viz.*, (1) interaction of ultrasonic energy with biological structures; (2) ultrasonic transducers; (3) displays and scans; and (4) signal processing.

These elements have been examined by four task groups established by the Alliance for Engineering in Medicine and Biology (AEMB) under a grant (ATA 73-03255A03) from NSF. The report, "A 5-Year Research and Development Agendum for Ultrasonic Imaging Diagnostic Instrumentation," is the result of this examination and is available from the NTIS [2].

2. The NSF (RANN) Instrumentation Technology Program

This program area seeks to support applied research projects that hold high promise to make substantial improvements (not incremental improvements) in instrumentation technology. There is a willingness to support "high risk" research. An adequate and unexploited scientific/technological base must exist from which the applied research project can draw. RANN emphasis is on applied research rather than on basic research.

Another feature of RANN-supported applied-research projects is that "exit criteria" must be stated clearly. That is, we want to know in advance how to determine when the project should move from applied research to development to clinical application. An important factor is to determine how and when the results of the research are to be transferred to user groups.

3. Areas of Support

In the current fiscal year (1975), areas of support in medical ultrasound are: (1) high-resolution imaging research, and (2) tissue characterization. Both of these areas are noted as high priority areas by the AEMB Task Groups. The goal for resolution capability, as noted by the AEMB Task Group on "Ultrasonic Transducers: Signal Detection and Preprocessing," is:

Field of view (minimum)	25x25x25 cm^3
Range (minimum)	25 cm
Resolution (minimum)	1x1x1 mm.

The second area of support, tissue characterization, is viewed as developing new, more powerful non-invasive techniques based upon the measurement of ultrasonic parameters of tissue. Successful results from research in the area of ultrasonic tissue characterization would *revolutionize* medical diagnosis, thereby providing great economic and social benefits.

4. Current RANN Projects

The RANN Instrumentation Technology program activity added $715,000 to Federal support of research in medical ultrasonics during fiscal year 1975, as shown in Table 1. The NSF budget request to Congress would increase allocations for the Instrumentation Technology Program area to $1,400,000 in fiscal year 1976.

The area of ultrasonic tissue characterization is viewed as being one where sufficient scientific and technological information exists on which to base a coordinated investigation to develop the concept for introduction into clinical medicine. The scientific and technological base began to be developed some twenty years ago with the pioneering work of Dr. J. M. Reid. Since then, he and a growing number of other investigators have added to the base of knowledge, as demonstrated in the papers read at this Seminar. Important contributions to the advancement of ultrasonic tissue characterization for introduction to clinical medicine have developed in areas unrelated to biology and ultrasound. Developments in low-cost high-capability data processing, pattern recognition, information theory, and large-scale integrated electronic circuits from research and development conducted in the mathematical and physical sciences have provided the technologies needed to demonstrate the concept of tissue characterization. Another important aspect of applied research in ultrasonic tissue characterization is that a reasonable cost and time period for federal support is involved to reach a "go - no go" decision point in determining the value of the concept.

Table 1

Breakdown of RANN-Supported Research in Medical Ultrasound in Fiscal Year 1975

Principal Investigator	Institution	Title	Amount
K. Preston, Jr.	Carnegie-Mellon University	Signal Processing for Ultrasonic Histopathology	$127,000
C. F. Quate	Stanford University	Scanning Acoustic Microscope	108,700
J. H. Busser	Alliance for Engineering in Medicine and Biology	Information Exchange and Problem Assessments in Medical Ultrasound	118,800
M. Linzer	National Bureau of Standards	Seminar on Ultrasonic Tissue Characterization	12,000
D.H.R. Vilkomerson	RCA Laboratories	High Resolution Ultrasonic Annular-Array Imaging	99,000
R. C. Waag	University of Rochester	Tissue Characterization with Ultrasound.	249,000

In NSF (RANN) terminology, a "milestone chart of accomplishments" can be designed, the objectives can be stated with precision, there is an existing data base, and the expected results can be described concisely.

Two policy issues need to be examined during the course of the conduct of applied research projects in tissue characterization. These are: (1) proper "exit criteria" for federal support, and (2) criteria for introduction into clinical medicine. Such issues are becoming more important as we attempt to cope with allocations of limited national resources. The Federal Government should not be expected to support the development of ultrasonic tissue characterization indefinitely, and the concept should not be introduced into the health care system until the consequences of doing so have been thoroughly assessed.

5. Necessary Action

What is needed to accomplish all of this? First, it is important to have a formal mechanism whereby investigators all over the world can exchange information on developments in ultrasonic tissue characterization. Secondly, it is important to establish a formal mechanism for the preparation of plans for the utilization of the results of research in ultrasonic tissue characterization; detailed plans for the operation of a tissue signature library should be drawn. Such plans should be based on the assumption that ultrasonic tissue characterization will be introduced into clinical practice. The cost of doing so is small; little would be lost if the great promise of ultrasonic tissue characterization fails to be realized, but great progress in clinical medicine could happen quickly if the results occur as anticipated.

6. A Challenge

The preparation of criteria for the introduction of a new procedure or technique into clinical medicine is something that researchers and clinicians are unlikely to accept with alacrity. The concept of "acceptance criteria" perhaps is counter to the common view that highly-beneficial developments are adopted quickly and that unsuccessful developments are ignored. But what of mediocre advances? Can the United States (or the World) long afford the luxury of haphazardously subjecting new developments to the vagaries of the clinical medicine marketplace?

To develop criteria for the introduction of new procedures into clinical medicine requires the concerted attention of a multidisciplinary group of scientists, engineers,

physicians, health care administrators, health economists (academic and private insurors representatives), and lawyers. A possible mechanism for examining these issues would be the establishment of an *ad hoc* Committee for Ultrasonic Research Evaluation (CURE).

7. Conclusion

The next few years hold high promise for additional substantial advances to be made in non-invasive medical diagnosis through ultrasonics. Ultrasonic tissue characterization is an area of scientific investigation wherein advances in medicine would "be manifest through the development of practical automated test (diagnostic) instruments and new techniques which will be vastly more efficient and effective than those available today, thereby contributing substantially to our ability to provide quality medical care for all. This well might be one of the most important contributions that engineering can make to the welfare of mankind..." [3].

References

[1] *Prospectives for Ultrasonic Imaging in Medical Diagnosis,* Report of the NSF Survey Team on Ultrasonic Imaging, National Science Foundation, Washington, DC (1973).

[2] *A 5-Year Research and Development Agendum for Ultrasonic Imaging Diagnostic Instrumentation,* (The Alliance for Engineering in Medicine and Biology, Chevy Chase, MD, Publication No. N-1975-1, April 1975), available from the National Technical Information Service, 5285 Port Royal Road, Springfield, Virginia 22151, Publication No. PB-230010/AS.

[3] Devey, G. B., The conference in retrospect, in *Proceedings of the International Conference on Engineering in Automated Multiphase Health Testing,* p. 431 (Engineering Foundation, New York, 1971), Library of Congress Catalog Number 79-175127.

National Bureau of Standards Special Publication 453. Proceedings of Seminar on Ultrasonic Tissue Characterization held at NBS, Gaithersburg, MD, May 28-30, 1975. (Issued Oct. 1976)

Paper 1.2: CHALLENGES AND OPPORTUNITIES IN ULTRASOUND

Keynote Address

John M. Reid

Institute of Applied Physiology and Medicine
and Providence Hospital
Seattle, Washington 98122

The scientific study of the ultrasonic properties of tissue is on the threshold of being able to contribute useful knowledge needed to improve the utility of ultrasonic medical diagnostic instruments. There is ample evidence to support these contentions and to guide our future course.

Key Words: Diagnosis; Doppler effect; optimization; resonance; scattering; tissue characterization; tissue parameters; tumor detection; ultrasound.

Traditional keynote addresses begin by considering why we are here, how we got here, or where we are going. I will follow this format today. This is not a research paper; it nearly always end with the conclusion that "more research needs to be done." The previous speakers have made excellent statements of why we are here. I think it is very exciting to note that this is the first conference devoted entirely to the topic of the passive, that is, information-containing, interactions of ultrasound and tissue. The idea that information could be gathered from tissues through their interactions with sound waves is an old one, but one that certainly was not as accepted as the enthusiastic, sizeable audience here today indicates. In one of the early papers on the effect of tissues on ultrasound, the manuscript suffered a curious change [1].[1] The editor had reversed the title in accordance with long habit and instead of reading "The Effects of Tissues upon the Ultrasound," it was entitled "The Effects of Ultrasound on Tissues!" Of course, we wrote back that this was not what we intended at all, that the ultrasound was doing nothing to the tissues and would they please reverse the caption to have it read the way we had intended. This was done; the title of the paper appeared as we intended, but the running lead on each of the succeeding pages on that article was entitled "The Effects of Ultrasound on Tissues."

1. Present Status

The very existence of this meeting, I believe, signals an end to the empirical era through which most diagnostic equipment and techniques evolved. This was a process of "trying out" what seemed to be good ideas. Equipment parameters were changed in the clinic in attempts, that were not always successful, to contribute useful information about the state of a patient.

Today we are on a threshold. Meetings such as this one present new opportunities which will lead, if followed, to new ways to contribute to the effectiveness of non-invasive diagnosis. This threshold consists of a series of new challenges. Many of the challenges derive from the fact that this is a new field, and that we are involved in establishing a new scientific field of study. We have all seen the symptoms of the birth of this new science. We have had difficulty with the editorial boards of existing publications, our efforts have had difficulty fitting into the organized departmental structure at both universities and hospitals. Our industrial members have seen dismay in the faces of market researchers and sales people as they try to assess the possibilities of diagnostic ultrasound. In many ways, we

[1]Figures in brackets indicate the literature references at the end of this paper.

have been fighting to get new ideas into closed minds, minds that were certain that all that was worthwhile had been discovered, and that nothing new could be added.

To cross this threshold, however, we must face up to the demands placed on a truly scientific field. The medical profession expects a great deal of the underlying sciences. Medicine has dealt largely with fields with scientific foundations for almost the past 100 years and some expectations have developed. These other fields have recently arrived at or passed over their own thresholds. They thus can contribute mightily to the medical practice of the future, and it might be instructive to consider just how and why these fields achieved their present stature.

We now know that x-rays are able to image soft tissue structures. The development of image-reconstruction techniques such as the EMI scanner was due to the ability of some workers in this field to overcome their *a priori* assumptions that x-rays could not image soft tissues. We all knew that this could not be done, and scientific boards governing the allocation of research money refused several times to put money into such an obviously impossible device! It was due to the vision of private industry that this development came about. The ability to image soft structures in completely inaccessible locations such as the head has led to large strides in the diagnosis and care of cerebral disorders. This ability is now available for the whole body. Multi-tube stop-action images appear to be possible for the heart.

The field of nuclear medicine has made a number of specific contributions to diagnosis, but many current workers are not satisfied with these. They are working with carbon compounds which are awkward to use and cannot be stored because of their extremely short half-life. The reason that these heroic efforts are being expended in a very difficult field is not too difficult to appreciate. The use of radioactive carbon compounds will make the entire field of known knowledge in organic chemistry available to the diagnostician. If these efforts of the nuclear medicine field are successful, we can look forward to a tremendous increase in the knowledge of the function of the human body obtained non-invasively with very minimal radioactive dose.

2. The Road Ahead

Our path is littered with questions: Just what is it that we want to do? Why should it be done? And how can we do it? The hardest question is, does evidence exist that knowledge of acoustic properties of tissue will lead to successful characterization? That is, will it increase the ability of ultrasonic diagnostic instruments to perform diagnoses, will it lead to new concepts and new types of equipment? These could be just pious hopes, although we certainly think not. The possibility of self-deception reminds me of W. C. Fields' temperance lecture, which says something like "every drunk thinks the world revolves around himself, and it usually does!". I have some examples which indicate to me that there is considerable promise in the field. This personal conviction arises from that fact that most of these examples are my own, but I hope you will bear with me.

The first example is on the diagnosis of cancer. The first quantitative measurement which characterized a tissue was a measurement from the A-scope trace derived by Wild and Reid in 1952 [2]. The suggestion that cancer diagnosis can be done with ultrasound has not achieved clinical success anywhere except in Japan. Why does present equipment not function well in the diagnosis of cancer? The answer must be that the design of conventional clinical apparatus was based on *a priori* assumptions; mainly, that high resolution and the achievement of geometric localization were the most important design criteria. This led to the use of somewhat lower frequencies to obtain penetration, coupled with wider fractional bandwidths to restore resolution. To further aid in the outlining of structures, fast time-constant, or differentiator circuits were introduced into the video amplifiers. It was subsequently shown that this type of circuit will remove the criteria used by Wild and Reid in their attempt to quantitate the A-scope [3]. The result has been equipment which does some jobs very well. When we are asked why we cannot detect cancer with the equipment, the reply must be that most of the design assumptions are wrong for this application and that a completely different type of machine should be used. We then complete the circular argument by saying "but if we made it that way it wouldn't sell because the pictures would look different."

Why have the Japanese been successful? Their equipment is more like the present clinical machines than like the Wild and Reid equipment, yet papers on the successful diagnosis of breast cancer continue to come from Japan [4]. The techniques used by these workers, however, are considerably different from the techniques used by others. By using a simple parallel or sector scan, they have demonstrated that the shadows (which show the transmission properties of the tumor) contain enough data to make diagnostic decisions. In our usual practice, however, the presence of shadows destroys resolution, and compound scanning is used to fill in the shadows to obtain better looking pictures! Suggestions that compound scanning in some applications can be deleterious to the information are met with skepticism and a firm resolve to increase the use of compound scanning by providing automatic machine-driven compound scans so the operator will have no choice.

There are other, very positive examples of the information that is lurking just around the corner. I refer to the possibility of optimizing the design of present apparatus as well as of suggesting new apparatus based upon knowledge of the mechanism of the ultrasonic tissue interactions with which we are dealing. The first optimization example is the selection of ultrasonic frequency to detect red blood cells. If we know the frequency dependence of the scattering cross-section, as well as of the absorption constants and other factors which govern the strength of the echo, we can look for an optimum frequency.

As reported by K. K. Shung in our paper "The Scattering of Ultrasound By Red Blood Cells," (p. 207, this volume) the frequency dependence of the scattering cross-section per unit volume of red blood cells varies as the 4th power of the frequency. We also know from the accumulated experiences on the absorption of ultrasound (see F. Dunn; "Ultrasonic Attenuation, Absorption, and Velocity in Tissues and Organs," p. 21, this volume) that the product of absorption constant, α, and wavelength, λ, is a constant over the useful frequency range. Since the absorption loss increases with the frequency (decreasing the received signal) and the scattering increases with frequency (increasing the received signal), the product of these two curves will have a maximum. The frequency at this maximum can be found by differentiating the appropriate equations. (See "The Scattering of Ultrasound By Tissues," p. 29, this volume.) For scatterers which "fill" the beam, we use eq. [A-8],

$$\frac{\partial P}{\partial f} = \text{Constant}\ \frac{\partial}{\partial f}\ \eta e^{-4\alpha R} = \text{Constant}\ \frac{\partial}{\partial f}\ f^4 e^{-\frac{4\alpha\lambda R f}{c}} = 0 \qquad (1)$$

at $f = c/\alpha\lambda R$, where c = velocity and R = range to scatterers. For a single scatterer, we use eq. [A-6] similarly,

$$\frac{\partial P}{\partial f} = \text{Constant}\ \frac{\partial}{\partial f}\ f^6 e^{-\frac{4\alpha\lambda R f}{c}} = 0 \qquad (2)$$

at $f = 1.5\ c/\alpha\lambda R$. The resulting optimum frequency is inversely proportional to the depth and is plotted for $\alpha\lambda = 0.03$ in figure 1. The two lines apply to the cases of individual cells in the beam of ultrasound and of a collection of cells completely filling the beam. All other practical cases appear to be intermediate between these two. We see that there is a considerable latitude in the frequency which achieves the maximum signal strength, but also that the operating frequencies of present Doppler flowmeters could be substantially reduced and better depth of penetration obtained.

The other example comes from study of the frequency dependence, using continuous waves, of the reflections from a stretched calf mitral valve. The result is shown in figure 2, which shows the reflection strength in dB below a perfect reflector as a function of frequency corrected for transducer diffraction and frequency response. Note a dip at about 2.9 MHz which indicates that a half-wave resonance effect is taking place in the substance of the mitral valve. This curve explains why the 2 MHz transducers originally used when echocardiography was first introduced in this country always gave stronger signals than the 2.25 to 2.5 MHz transducers currently used in echocardiography. The advantage of the lower frequency ranges between 10 and 20 dB depending on whether we consider the gain at the center frequency or some average over the band.

The absorption constant of the connective tissue comprising the substance of the valve appears to be very low. An absorption per wavelength, $\alpha\lambda$, of about 0.003 was calculated from the dip of figure 2. If other thin, layered connective tissue structures in the body have such low loss, then the possibilities of highly frequency-selective resonances cannot be discounted.

New knowledge of ultrasonic tissue properties would be put to use because there *is* room for improvement in the field as it presently exists. Consider that the same transducer frequencies have been used in medical applications as were previously used in materials-testing applications. These frequencies, at 2, 5 and 10 MHz, are in approximately 2:1 steps. The very coarseness of the steps indicates that not much selective optimization has been done. The design of the apparatus, as stated earlier, has been largely on a "suck it and see" approach. There is considerable room here for improvement. The aircraft industry does not find it necessary to crash many planes these days to prove that a new design can fly. They are able to determine not only that it can fly, but also its profit potential under present fare schedules, while it is still on the drawing board. We are still, in contrast, at the embryonic stage of crashing our designs in the clinic!

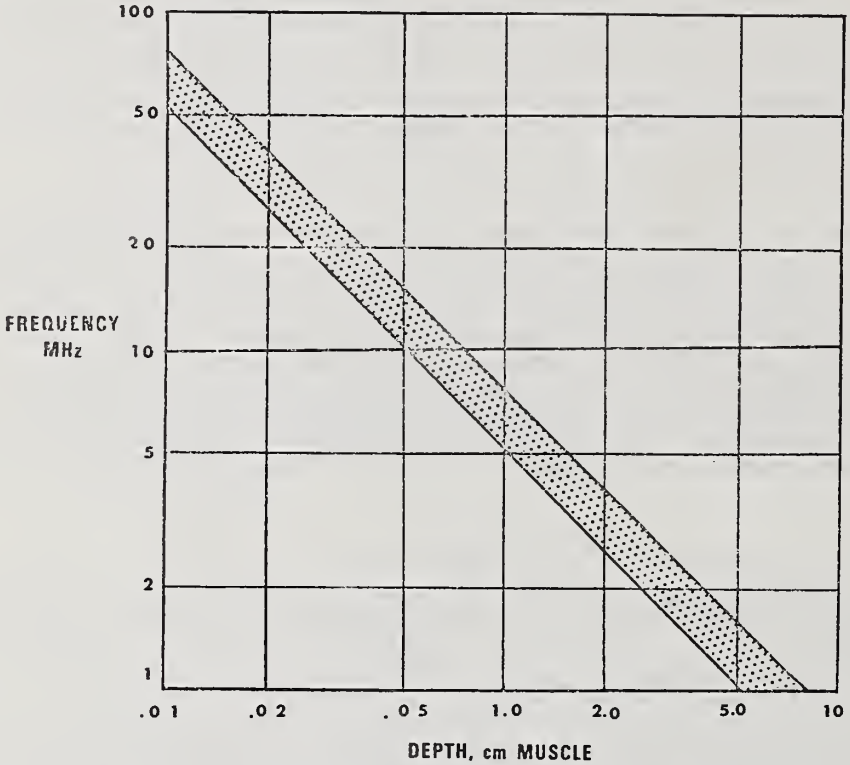

Figure 1. Ultrasound frequency for maximum scattered amplitude for Rayleigh scatterers. Upper limit of optimum frequency area applies to single scatterers and the lower limit to randomly-distributed scatterers which fill the sound beam. The curve predicts the optimum operating frequency for ultrasound Doppler flowmeters.

Further optimization is possible if we understand the effect of tissue parameters in setting fundamental limits to the operation of our equipment. Calculations show that frequency dependence of absorption can result in pulse-stretching by a factor of about 2, that refraction due to subcutaneous fat can deviate the beam by nearly the beam width and hence badly blur the pictures at maximum range of present equipment, and that the possible dispersion of the velocity of sound in absorbing tissues can lead to a considerable spectrum distortion and further pulse stretching at maximum ranges [5].

Another reason for thinking there is considerable hope is the realization that has been forced upon me that engineers and medical doctors are not trained as scientists. Although scientists exist in both fields, they undergo a rather long and rigorous training program. Those without this training have found it even more difficult than those with training to impress medical scientists that the work they propose is valuable and can be done by them. When we speak to our peers in an unfamiliar tongue, we must speak with great clarity to get our points across. Let us increase our communication skills.

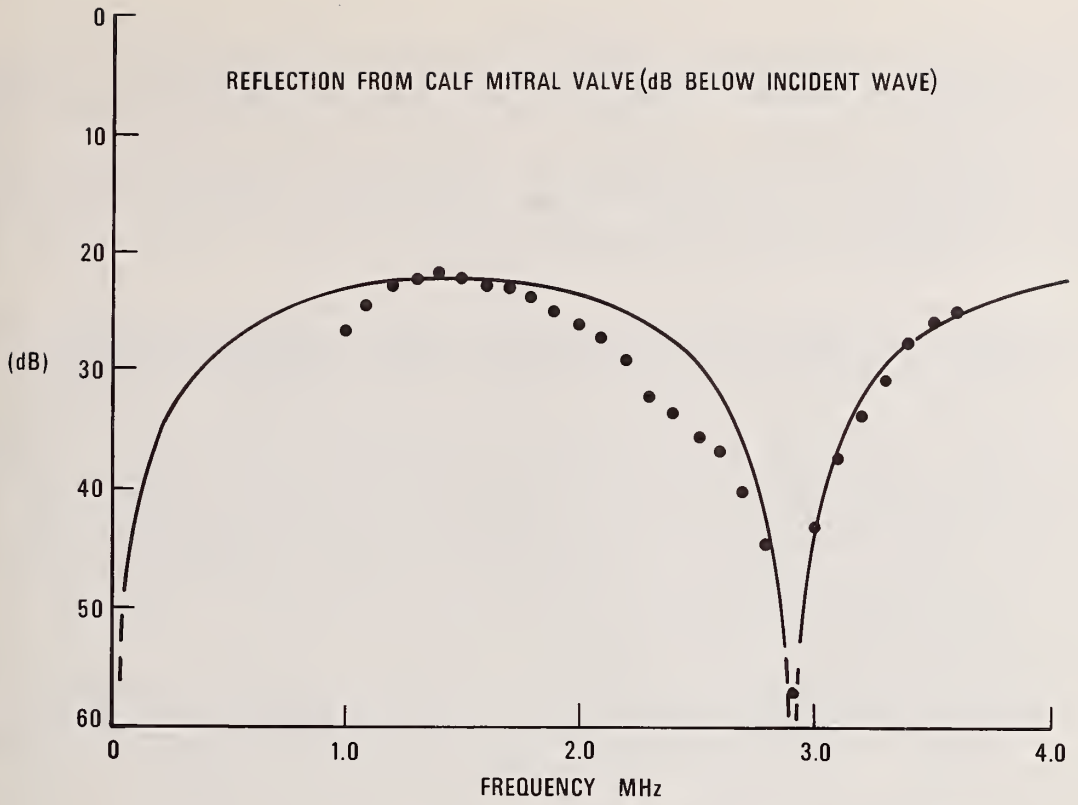

Figure 2. Frequency dependence of continuous wave reflections from calf mitral valves relative to the reflections from a perfect reflector at the same range. Dots are experimental points taken using gated bursts of more than ten cycles. Solid line was calculated for the reflection coefficient of a 1/2 wave, one-dimensional transmission line section. Losses in the model section correspond to $\alpha\lambda = 0.003$.

3. What To Do?

The principal task before us, I believe, is to get on with it. Our job is to plow the corners of our field which are most amenable to our resources and our techniques in the positive expectation that both expected and unexpected benefits will flow from our efforts.

A caution I must add is to please examine the basis for the experiments which you do, so that your work will have the highest possible scientific value and hence the greatest future utility to the field. To obtain system design information which has a scientific basis, and is most useful, requires that the data be gathered in a manner which is independent of the gathering equipment. This is more easily said than done, particularly in the case of scattering measurements where changes in wave shape upon reflection introduce unexpected dependence upon aperture, range and frequency (see "The Scattering of Ultrasound by Tissues," p. 29, this volume).

Scientifically, only measurements which are independent of the measuring system characterize the *tissue*. Observations, such as the often-made observation of echo strength on angle, which are not so reduced, characterize the equipment as well as the tissue. Such observations have limited utility in the exchange of information which is the life-blood of science. Even worse, such observations are practically useless in equipment design.

Only if we have tissue parameters which are independent of the measuring equipment can we choose equipment parameters when designing optimum diagnostic systems. This comes about because the design process consists of steps taken in reverse order to that followed when reducing measurement data to an equipment-independent form. Reduction starts with the raw

measurements obtained in terms of pulse heights or wave energy. Tissue parameters are derived by correcting for the effects of transducer aperture, range, pulse lengths, frequency and so on. The result is a value for scattering cross-section or reflectivity which is independent of the measuring equipment. Consider now the task confronting a designer of a new device. Depending on its intended application, the reflections from a particular tissue may be considered either to contain the information or to be interference and noise which must be suppressed. With both the "noise" and the "signal" parameters available for characterizing the tissues in the propagation path, the designer can choose values for frequency, aperture, range and so on, which will maximize the desired signal.

The very knowledge of the interaction equations will be a great aid in equipment design and use. Consider the transmission or continuous-wave "camera" type imaging systems. The effects of velocity differentials in forming diffraction images have been considered very little. Large organs, such as the kidney, have a near field determined by the size of the organ similar to the near field of a transducer. Diffraction effects will thus be responsible for some detail of the image at distances from the organ which are considerably greater than the size of the human body. This may explain why semi-permeable structures can appear to be either sonolucent or opaque depending on their position in the sound field. Also, the illuminating field for each organ in the abdomen consists of the diffraction fields of all the organs which shadow it. This may be the reason that *in vivo* imaging with these devices has not yielded pictures at all comparable with promising images obtained from the early *in vitro* work. Understanding of the physics of the image-forming process thus could lead to far greater utility for these intriguing devices.

We should give some thought to the parameters which we will choose for tissue characterization and with the definitions that we will use for "tissue signature." The classical parameters of absorption, velocity, scattering cross-section and reflectivity will be covered in the next two papers. The literature abounds, however, with different meanings appended to the term "signature." In the radar field, the target signature is regarded to be the model for the fluctuations of scattering strength. Typical terms are Rayleigh, log normal, *etc.*, depending upon the statistical fluctuations. (There may well be a lesson here for us in that statistical models of tissue parameter fluctuations are almost entirely lacking. A Rayleigh distribution is to be expected from the observed frequency dependence of the scattering from red cells, but we really know nothing about fluctuations from other tissues except that practically all ultrasonic reflections do fluctuate.) We can consider various heirarchies of signatures as used in ultrasonic diagnosis [6]. These range from a B-scan picture obtained on a particular apparatus, to the response of a tissue to a short pulse, to the response to a true impulse which can, theoretically, be derived from the response to a short pulse. The impulse response of the tissue is related through the Fourier transform to the frequency-domain characterization of a tissue, but only if the data are corrected (in both cases) to be independent of equipment parameters which are functions of frequency.

4. Scientific Standards

To perform adequately-detailed scientific studies, inlcuding the studies of mechanisms, will probably require the use of *in vitro* specimens or animals other than man. We must be ever alert to the biological problems posed in the use of such preparations. We are concerned with mechanical properties and must be certain that these are preserved in our specimens. Biomechanics investigators seeking to establish the mechanical properties of blood vessel walls discovered a few years ago, for example, that the state of contraction of the smooth muscles was different in many of the arterial specimens that they were pulling and twisting. The large but accepted biological variability was greatly reduced with pretreatment of the muscles to insure a repeatable contraction state. Apparatus for performing the measurements must be designed with knowledge that tissue is a living thing with requirements of temperature, salinity and nourishment. The equipment must also allow our data to be gathered in a convenient and repeatable fashion. The field will undoubtedly develop concepts, such as useful approximations, and equipment as we learn.

These problems are simply a part of working in a new discipline. As we continue to open this new field, we must always remember to keep our minds as open as we wish the minds of others had been when we began. A closed mind is, perhaps, our worst enemy and it is nowhere as damaging as when the closed mind is our own.

References

[1] Wild, J. J. and Reid, J. M., The effects of biological tissues on 15 mc pulsed ultrasound, *J. Acoust. Soc. Am.*, 25, 270 (1953).

[2] Wild, J. J. and Reid, J. M., Further pilot echographic studies on the histologic structures of tumors of the living intact human breast, *Am. J. Path.*, 28, 839 (1952).

[3] Reid, J. M., An evaluation of intensity-modulated recording for ultrasonic diagnosis, *J. Acoust. Soc. Am.*, 44, 1319 (1968).

[4] Kobayashi, T., Takatani, O., Hattori, N., Kimura, K., Watanabe, H., and Abe, O., Clinical investigation for the differential diagnosis of breast tumor by means of the degraded sensitivity method of ultrasonotomogram (II), *Medical Ultrasonics*, 10, 81 (1972).

[5] Task Group 4: *Ultrasonic Diagnostic Signal Processing*, in *A 5-Year Research and Development Agendum for Ultrasonic Imaging Diagnostic Instrumentation*, (The Alliance for Engineering in Medicine and Biology, Chevy Chase, MD, Publication No. N-1975-1, April 1975), available from the National Technical Information Service, 5285 Port Royal Road, Springfield, Virginia 22151, Publication No. PB-230010/AS.

[6] Task Group 1: *Interaction of Ultrasonic Energy with Biological Structures*, in *A 5-Year Research and Development Agendum for Ultrasonic Imaging Diagnostic Instrumentation*, (The Alliance for Engineering in Medicine and Biology, Chevy Chase, MD, Publication No. N-1975-1, April 1975), available from the National Technical Information Service, 5285 Port Royal Road, Springfield, Virginia 22151, Publication No. PB-230010/AS.

CHAPTER 2

TISSUE PARAMETERS

National Bureau of Standards Special Publication 453. Proceedings of Seminar on Ultrasonic Tissue Characterization held at NBS, Gaithersburg, MD, May 28-30, 1975. (Issued Oct. 1976)

CHAPTER 2. TISSUE PARAMETERS

Paper 2.1: ULTRASONIC ATTENUATION, ABSORPTION, AND VELOCITY IN TISSUES AND ORGANS

F. Dunn

Bioacoustics Research Laboratory
University of Illinois
Urbana, Illinois 61801

Propagation relations for compressional waves in isotropic, elastic media are described briefly and discussed with reference to ultrasonic propagation in biological structures. A selected review of experimentally obtained results from tissues and organs is presented. It is shown that characterization of tissues and organs by their acoustic parameters should be possible.

Key Words: Absorption; attenuation; mammalian tissues; tissue parameters; ultrasound; velocity.

1. Introduction

The "ultrasonic propagation properties of tissues and organs" include the behavior of those measurable acoustic parameters, as functions of state and acoustic variables, which characterize the fate of acoustic signals propagating within the biological environment. The speed with which the signal propagates in the biological medium, the attenuation and/or absorption of wave energy by the medium, and features of the medium responsible for reflection and scattering phenomena, generally embodied in the impedance concept, constitute the properties of interest. The present discussion treats briefly these properties with the view toward identifying characteristics of tissues and organs essential in clinical ultrasonic diagnostic procedures.

2. Propagation Relations

The pertinent relations describing acoustic phenomena in ideal fluid media are presented first. A brief discussion then follows on the alterations that must be made in order to describe events occurring in media which extract energy from the propagating wave process.

The wave equation describing propagation of mechanical disturbances in dissipationless, isotropic, elastic media is

$$\frac{\partial^2 \xi}{\partial t^2} = \frac{K + \frac{4}{3}G}{\rho_o} \nabla\nabla\cdot\xi - G \nabla \times \nabla \times \xi \qquad (1)$$

where ξ is the instantaneous displacement of an element of the medium from its equilibrium position, t is time, K is the adiabatic bulk modulus, G is the modulus of shear rigidity, and ρ_o is the mean density of the medium. The specialization for lossless fluid media is obtained by setting G equal to zero since these are characterized by an inability to

support an elastic shear strain. The one-dimensional elastic wave equation, as it applies to an ideal, linear, homogeneous, perfectly elastic (dissipationless) liquid medium, is

$$\frac{\partial^2 \xi}{\partial t^2} = \frac{1}{\rho_o \beta_s} \frac{\partial^2 \xi}{\partial x^2} \tag{2}$$

where β_s, the adiabatic compressibility, is the reciprocal of the adiabatic elastic bulk modulus. The relations are approximations of the more general hydrodynamic equations valid under the conditions that the particle velocity amplitude, $(\partial \xi/\partial t)_{max}$, is small compared with the speed of sound in the medium and that the adiabatic compressibility is not significantly dependent upon pressure over the range of pressure variations occurring in the sound field. Under such conditions, the free-field sound propagation velocity for compressional waves is

$$v = \frac{1}{\sqrt{\rho_o \beta_s}} \quad . \tag{3}$$

The solution to eq. (2) is

$$\xi(x,t) = Ae^{j(\omega t - kx)} + Be^{j(\omega t + kx)} \tag{4}$$

which includes waves propagating along both directions of x. k is the wave number ω/v, and A and B are the amplitudes of the two wave components. The acoustic pressure in the field can be defined as

$$p = P - P_o \tag{5}$$

where P is the instantaneous pressure at a point of concern in the field and P_o is the constant equilibrium pressure in the medium. The acoustic pressure and the particle displacement are related by

$$p = -\rho_o v^2 \frac{\partial \xi}{\partial x} \quad . \tag{6}$$

The quantity $\rho_o v$, the product of the medium density and the sound velocity, is the characteristic impedance of the medium, *i.e.*,

$$Z_o = \rho_o v = \sqrt{\frac{\rho_o}{\beta_s}} \quad . \tag{7}$$

For plane traveling waves, this quantity is numerically equal to the specific acoustic impedance which is defined as the ratio of the sound pressure p to the particle velocity $\dot{\xi}$ at any point in the field. For other field configurations, *e.g.*, standing waves, the specific acoustic impedance differs numerically from $\rho_o v$ and is, in general, a function of position. Further, the characteristic acoustic impedance is dependent upon the type of wave propagating since the velocity of, for example, shear waves is different from that of compressional waves.

The intensity I of the acoustic wave is defined as the time average of the rate of transport of energy through unit area normal to the direction of propagation. It is related to the sound pressure amplitude P_a and the particle velocity amplitude $\dot{\Xi}_a$ for plane traveling waves

$$I = \frac{P_a^2}{2Z_o} = \frac{P_a \dot{\Xi}_a}{2} = \frac{Z_o \dot{\Xi}_a^2}{2} \quad . \tag{8}$$

The energy density E_o of the wave motion at a specific position in the field is the sum of the kinetic energy per unit volume of the moving element and the potential energy per unit volume of compression (or expansion) of the element. For plane traveling waves, this becomes equal to the ratio of the intensity to the wave velocity, *i.e.*,

$$E_o = \frac{\rho_o \dot{\xi}_a}{2} = \frac{P_a^2}{2\rho_o v^2} = \frac{I}{v} . \tag{9}$$

When an ultrasonic wave propagates in a real fluid, wave energy is irreversibly absorbed by the medium, by any of a variety of physical mechanisms. The occurrence of this phenomenon modifies the phenomenological description of lossless plane-wave propagation by the introduction of an absorption factor, *i.e.*, eq. (4) becomes, for unidirectional propagation in the positive x-direction

$$\xi(x,t) = Ae^{-\alpha x} e^{j(\omega t - kx)} \tag{10}$$

where α is the amplitude absorption coefficient per unit path length. When other loss mechanisms occur, such as scattering (see "The Scattering of Ultrasound by Tissues," p.29, this volume), α can be redefined as the total attenuation coefficient. The Stokes-Kirchhoff classical absorption coefficient is

$$\alpha = \frac{\omega^2}{2\rho_o v^3} \left(\frac{4}{3} \eta_S + \eta_B + \frac{\gamma - 1}{C_p} K \right) \tag{11}$$

where ω is the angular frequency, η_S is the shear viscosity coefficient, η_B is the bulk viscosity coefficient, γ is the ratio of specific heats, C_p is the heat capacity at constant pressure, and K is the thermal conductivity. This relation expresses the view that energy transported by the wave process is converted to heat by virtue of the medium possessing finite viscosity and thermal conductivity. The losses due to viscosity result from the fact that, though a fluid cannot support a static shear, it can support a dynamic one in the form of a viscous drag. The thermal conductivity process occurs because during passage of an ultrasonic wave, temperatures will be greater in the regions of higher acoustic pressure than in the neighboring regions of lower pressure, and heat will flow in response to such gradients. The thermal conductivity term is, for biological media, very much less than the viscosity terms and can be ignored. Equation (11) indicates that the absorption coefficient should vary with the square of the frequency and that the temperature dependence should follow that of the viscosity. However, liquids in general and biological media in particular, do not often exhibit these dependencies in so simple a fashion and it is necessary to consider that other relaxation processes are involved. Such processes reflect the presence of mechanisms of energy transfer which require time [1].[1] In the following equation, the term A represents the classical absorption terms and the second term describes a single relaxation process with f_r being the relaxation frequency:

$$\frac{\alpha}{f^2} = A + \frac{B}{1+(f/f_r)^2} . \tag{12}$$

With regard to the second term, it is seen that at very low frequencies, such that the period of the wave is long compared to the time required for energy transfer, it is constant and has the value B, while at very high frequencies, such that the period of the wave is short compared to the time required for energy transfer, energy is not extracted from the wave process and this term vanishes leaving only the classical term. Again, it does not often happen that a single relaxation process is present and in order to describe observed absorption spectra, it is necessary to consider a number of such processes occurring and to sum on all of them [1], giving

[1]Figures in brackets indicate the literature references at the end of this paper.

$$\frac{\alpha}{f^2} = A + \sum_i \frac{B_i}{1+(f/f_i)^2} \quad . \tag{13}$$

3. Velocity of Ultrasound in Tissues

Goldman and Heuter [2] compiled a detailed list of ultrasonic velocity and attenuation data in animal tissues. Therein, it is seen that the velocity in soft tissues, excluding lung, is very nearly that of dilute salt solutions and varies only slightly among the various tissues, with the exception being that fatty tissue has a velocity about 10% less than that of non-fatty tissues. The reflection properties, which are of considerable importance in clinical diagnostic procedures, can be discussed in terms of elementary considerations for unbounded, lossless, homogeneous and isotropic media for which the magnitude of the reflection coefficient R is, in terms of the characteristic impedances (Z_1, Z_2) of the two contiguous media (see eq. (7)),

$$R = \frac{Z_1 - Z_2}{Z_1 + Z_2} = \frac{(\rho_1/\beta_{s1})^{\frac{1}{2}} - (\rho_2/\beta_{s2})^{\frac{1}{2}}}{(\rho_1/\beta_{s1})^{\frac{1}{2}} + (\rho_2/\beta_{s2})^{\frac{1}{2}}} \quad . \tag{14}$$

As the inertial property exhibits minimal variation among tissues, *viz.*, variations less than about 1% in density, $\rho_1 \approx \rho_2$ and eq. (14) can be written

$$R \approx \frac{\beta_{s2}^{\frac{1}{2}} - \beta_{s1}^{\frac{1}{2}}}{\beta_{s2}^{\frac{1}{2}} + \beta_{s1}^{\frac{1}{2}}} \quad . \tag{15}$$

It is apparent that the reflection characteristics of these media are dependent, for the most part, upon the elastic properties of their components [3]. The speed of sound in lung tissue increases nearly linearly with frequency, in the low megahertz frequency region, but has a value considerably less than other soft tissues [4] and depends upon inflation [5].

Theismann and Pfander [6] measured the speed of sound in specimens of human skull and found it to be approximately twice that of the soft tissues. As the density of bone is considerably greater than that of soft tissues, its impedance thus becomes nearly four times greater (see eq. (7)). More recent studies provide a shear velocity, for freshly frozen dog tibia, or approximately one-half that for longitudinal velocity [7,8].

4. Attenuation and Absorption of Ultrasound in Tissues and Organs

The following is a selected review of the experimentally-observed ultrasonic attenuation and absorption characteristics of biological tissues. Figure 1 shows the dependence of the ultrasonic attenuation coefficient on frequency for a number of tissues [2]. Here, the attenuation per cycle is plotted against the logarithm of frequency, for which classical theory would predict a linear dependence with positive slope if the attenuation were due solely to absorption. The broad shaded regions of figure 1 are partially accounted for by the inclusion of all available data (at time of preparation), *i.e.*, the figure includes measurements by numerous investigators employing different experimental techniques under a variety of physical and biological conditions. Nevertheless, it is possible to discern several relatively simple relationships, *e.g.*, the attenuation per cycle is generally constant over the frequency range considered. In a more recent investigation [9], mammalian kidney tissue was shown to continue this linear dependence of the attenuation on frequency to approximately 100 MHz, after which a quadratic (or greater) dependence prevails. Further, this quantity increases slightly from 1 to 10 MHz for fat, and striated muscle and liver appear to exhibit minima in the neighborhood of 2 MHz.

The important dependence of the absorption coefficient upon temperature has been established as a function of frequency only recently [10,11]. Figure 2 includes observations on mammalian central nervous tissue of neonatal mice (essential poikilotherms) and adult cats (homoeotherms). These data suggest a family of curves whose maxima decrease in magnitude and occur at ever higher temperatures as the frequency increases.

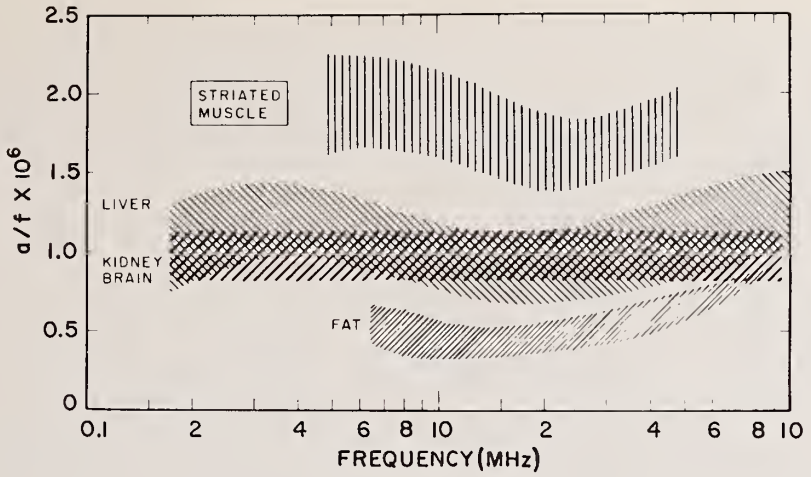

Figure 1. Acoustic attenuation per wavelength (in dB/cm MHz) for several mamalian tissues versus frequency [2].

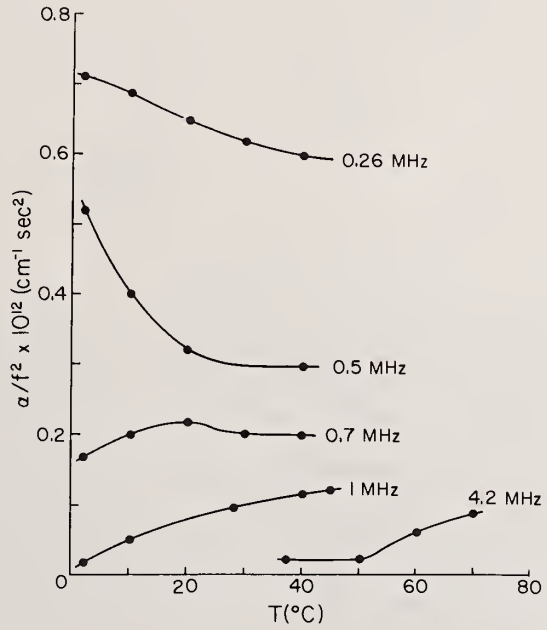

Figure 2. Frequency and temperature dependence of ultrasonic absorption in mammalian central nervous tissue [11].

Several tissues are known to exhibit unique properties. An early study of specially-prepared skull bone in the frequency range 0.6 to 3.5 MHz (25 to 35°C) exhibited a quadratic dependence of the attenuation coefficient upon frequency, with a transition to lower power dependence at high frequencies [12]. The average value for the acoustic amplitude attenuation coefficient per unit path length in skull bone, in the neighborhood of 1 MHz, was found to be of the order of 1 Np cm^{-1} (1 Np = 8.68 dB), approximately an order of magnitude greater than that of soft tissue at the same temperature. Recent observations have called these values into question. Adler and Cook [7] have obtained attenuation measurements of 1.5 Np cm^{-1} and 2.2 Np cm^{-1}, in freshly-frozen dog tibia at, respectively, 3 and 5 MHz. Kishimoto [13] observed a positive temperature coefficient for the ultrasonic attenuation

in horse bone, and values of the shear velocity, approximately one-half that of the longitudinal velocity, have been obtained [7,8]. Tissues such as cartilage, tendon, skin, etc., having high concentrations of collagen, exhibit attenuation values approximating the root-mean-square of those of organs and bone [14]. The acoustic amplitude attenuation coefficient in freshly-excised dog lung at a fraction of residual inflation has recently been shown to increase exponentially with frequency from 4.3 Np cm^{-1} at 1 MHz to 11.6 Np cm^{-1} at 5 MHz [4]. This frequency dependence has also been found for formalin-fixed preparations which have provided some information on the dependence of attenuation on inflation [5].

The acoustic propagation properties of the refractive media of excised calf eyes have have been studied [15], and table 1 is a summary of the data. It is noted that the attenuation for the humors is approximately 50% greater than that of dilute salt solution, suggesting that these media may possess a viscous-type frequency dependence, *viz.*, increasing quadratically with frequency. As the lens contains a relatively high concentration of protein, it is tempting, in the absence of further information, to consider that its frequency dependence resembles that of other soft tissues for which the absorption properties are dominated by the protein content, *viz.*, that it varies approximately linearly with frequency. Investigators concerned with diagnosing disorders of the eye by ultrasonic means feel that Begui's *in vitro* attenuation values are greater than those of the human lens *in vivo* and speciation and measurement and handling techniques, no doubt, provide explanations for the differences.

Table 1. Acoustic Properties of Refractive Media of the Eye [15]

Media	T (°C)	f (MHz)	v (cm/s x 10^5)	α(Np cm^{-1})
Aqueous	27.5	30	1.497	0.35
Vitreous			1.516	0.35
Lens	28.0	3	1.616	0.70

5. Concluding Remarks

The above discussion was intended only as a selected review of the pertinent literature dealing with ultrasonic propagation in tissues and organs. The comprehensive treatment by Dunn *et al.*, [16] and the definitive Workshop Proceedings of the Seattle Conference [17] should be consulted for details. Therein, it will be seen that recent studies have dealt with investigation of protein solutions for clues to the ultrasonic absorption behavior of tissues and organs. It is apparent that a great deal must be accomplished before a complete understanding of ultrasonic velocity and absorption by biological media is obtained. From the previous work, it is possible to determine types of dependencies of the attenuation and/or absorption as a function of some of the important field and state variables and it is possible to classify tissues into rather general categories as regards these dependencies. However, the present state of experimental data does not allow for the desired understanding of the mechanisms for any tissue structure or component relative to even a single physical variable.

Table 2, following Dussik [14], is an attempt to characterize tissues according to their ultrasonic attenuation. It is seen that tissues can be grouped in apparent teleologic fashion with a relatively narrow range of attenuation values within each group. The attenuation approximately doubles from group to group in direction of increasing attenuation. Further, proceeding from group to group in the same direction, tissues of ever-decreasing water content and ever-increasing structural protein content become involved. Thus, it is seen that ultrasonic attenuation can be invoked to characterize tissues according to functional criteria. Possibly, detailed measurements will allow assignment of resolvably unique values to each tissue structure including usefully differentiable values for pathological states. Should this be the case, then ultrasonic attenuation and impedance values, as functions of state and acoustic parameters, media, etc., should specify uniquely tissues for diagnostic purposes.

Table 2. Ultrasonic Attenuation Characterization of Tissues

Attenuation Classification	Attenuation at 1 MHz (Np cm^{-1})	Tissue	Tissue Classification
Very low	0.003	serum	Transport of metabolic materials
	0.01	blood	
Low	0.07	adipose	Storage of fat and water
Medium	0.1	brain	Protoplasmic activity, physiological function
	0.12	liver	
	0.24	muscle	
	0.12	kidney	
High	0.4	integument	Structural, supporting, stress conveying, high in structural proteins (collagen)
	0.5	tendon	
	0.6	cartilage	
Very high	1 or more	mineralized	Framework protection (high in collagen)
	> 4	pulmonary	Gaseous exchange

References

[1] Herzfeld, K. F. and Litovitz, T. A., *Absorption and Dispersion of Ultrasonic Waves* (Academic Press, NY, 1959).

[2] Goldman, D. E. and Hueter, T. F., Tabular data of the velocity and absorption of high-frequency sound in mammalian tissues, *J. Acoust. Soc. Am.* 28, 35 (1956).

[3] Fields, S. and Dunn, F., Correlation of echographic visualizability of tissue with biological composition and physiological state, *J. Acoust. Soc. Am.* 54, 809 (1973).

[4] Dunn, F., Attenuation and speed of ultrasound in lung, *J. Acoust. Soc. Am.* 56, 1638 (1974).

[5] Bauld, T. J. and Schwan, H. P., Attenuation and reflection of ultrasound in canine lung tissue, *J. Acoust. Soc. Am.* 56, 1630 (1974).

[6] Theismann, H. and Pfander F., Uber die durchlassigkeit des knochens fur ultraschall, *Strahlentherapie,* 80, 607 (1949).

[7] Adler, L. and Cook, K. W., Ultrasonic parameters of freshly frozen dog tibia, *J. Acoust. Soc. Am.* 58, 1107 (1975).

[8] Lang, S. B., Ultrasonic method for measuring elastic coefficiency of bone and results on fresh and dried bovine bones, *IEEE Trans. Biomed. Engr.* BME-17, 101 (1970).

[9] Kessler, L. W., VHF ultrasonic attenuation in mammalian tissue, *J. Acoust. Soc. Am.* 53, 1759 (1973).

[10] Dunn, F. and Brady, J. K., Pogloshchenie ul'trazvyeka v biologicheskikh sredakh, *Biofizika* 18, 1063 (1973).

[11] Dunn, F. and Brady, J. K., Temperature and frequency dependence of ultrasonic absorption in tissue, in *Proceedings of 8th International Congress on Acoustics,* p. 366c (1974).

[12] Hueter, T. F., Messung der ultraschall absorption im menschlichen schadelknocken und ihre abhangegkeit von der frequenz, *Naturwissenschaften,* 39, 21 (1952).

[13] Kishimoto, T., Ultrasonic absorption in bones, *Acoustica,* 8, 179 (1958).

[14] Dussik, K. T., Kyriazidov, M., Fritch, D. J., and Sear, R. S., Measurement of articular tissues with ultrasound, *Amer. J. Phys. Med.* 37, 160 (1958).

[15] Begui, Z. E., Acoustic properties of the refractive media of the eye, *J. Acoust. Soc. Am.* 26, 365 (1954).

[16] Dunn, F., Edmonds, P. O., and Fry, W. J., Absorption and dispersion of ultrasound in biological media, in *Biological Engineering,* H. P. Schwan, ed., Chapter 3, p. 205 (McGraw-Hill, NY, 1969).

[17] *Interaction of Ultrasound and Biological Tissues,* Workshop Proceedings, J. M. Reid and M. R. Sikov, eds. (Bureau of Radiological Health, 73-8008, 1973).

National Bureau of Standards Special Publication 453. Proceedings of Seminar on Ultrasonic Tissue Characterization held at NBS, Gaithersburg, MD, May 28-30, 1975. (Issued Oct. 1976)

Paper 2.2: THE SCATTERING OF ULTRASOUND BY TISSUES

John M. Reid

Institute of Applied Physiology and Medicine
Seattle, Washington 98122

Most ultrasonic diagnostic equipment are based on the observation of the waves scattered by tissues. Although these instruments generally perform useful clinicaldiagnosis, they do not provide quantitative measurements of the detailed characteristics of the scattered waves. Such measurements should significantly improve the diagnostic capability of medical ultrasound. The properties responsible for scattering have been shown to be differences in compressibility and density between adjacent tissue structures. The rationale of scattering measurements is considered through a review of direct measurements and substitution techniques which correct for wave shape changes. The necessity of correcting for apparatus parameters and the effects of overlying tissue attenuation is considered. Equations are derived which relate the scattered power to the scattering parameters of tissues and the measuring equipment constants for a number of useful cases.

Key Words: Blood; cross-section; diagnosis; scattering; standardization; tissue characterization; ultrasound.

1. Introduction

The scattering of ultrasound by tissues was established experimentally long before the mechanism of scattering could be ascertained with certainty and before any practical utility of the scattered waves could be found in clinical medicine. Today, the subject of scattering by tissues is extremely important from a practical sense. Pulse-echo and Doppler apparatus which employ these scattered waves to investigate the structure and function of tissues have found secure places in clinical medicine. Tissue identification and diagnosis are being routinely performed by observation of scattered ultrasonic waves in most hospitals. The excellent probability that even more useful systems can be devised has been dealt with in the Keynote Address (p. 11, this volume). For example, the introduction of grey scale apparatus has refocused attention on the small amplitude echoes which are observed from the interior of many organs within the body. Knowledge of the exact structures and tissue properties responsible for these echoes would be immediately useful since clinicians using existing technology could exploit this knowledge.

This paper will attempt a clear distinction between *observation* and *measurement* of scattering. As useful as observation has been, there are many differences of opinion between laboratories and clinics about what can be diagnosed. This results since observations are not quantitative and cannot be compared readily. Measurements are quantitative and can be compared. More importantly, measurements of *tissue properties*, by definition, should be independent of the apparatus used. This is not easily achieved in the case of scattering measurements. Both observations and measurements are made with a particular piece of equipment and the results are colored by the particular acoustical and electronic characteristics of the apparatus.

Scattering measurements are inherently more difficult to make than are transmission measurements such as velocity and attenuation; these measurements result, at any given frequency, in two numbers. In the scattering process, however, a new wave is generated and must be

specified. A number is also required to express the scattering strength. The scattered wave thus requires a function and an amplitude for characterization, both of which are frequency-dependent.

Fortunately, approximations for ideal types of scatterers exist which are very useful in characterizing interfaces and cellular scattering. Agreement between theory and careful experiment is excellent. Work on the red cell (See Shung, Sigelmann, and Reid, p. 207, this volume) has achieved excellent correspondence between scattering measurements and fundamental physical properties of the cell. Further extension of these methods to tissue is being pursued.

The basic thesis of measurement, as expanded below, is that one must separate the properties of the tissues from the properties of the equipment. By reducing the data obtained with a particular apparatus to a form which is independent of the parameters chosen for that apparatus, one may express the scattering parameters in a form which applies to the tissue alone. This step insures comparable results between laboratories if the other biological precautions have been taken properly.

The data reduction may be accomplished in two ways; by the use of substitution methods of measurement (see below), or by the use of exact equations expressing the echo strength as a function of the apparatus parameters as well as of the tissue properties. An unexpected benefit of the mathematical approach is that the equations will also be useful to the equipment designer. By using them "backwards" from the data reduction approach, new equipment parameters can be chosen so as to allow the equipment to achieve the visualization or differentiation of particular types of structure. The substitution method can be used today with any type of equipment which is linear in echo amplitude. The analytic approach has been solved only for far-field conditions (see Appendix).

One example of the necessity of separating the influence of equipment parameters from tissue parameters will be developed later. Briefly, it will be shown that the observations of the influence of angle of incidence on echo amplitude, as has been made in a number of laboratories, primarily gives information about the beam pattern of the transducer that was used. The statement that the echo falls off so many dB in so many degrees, thus, is a characterization of the *transducer* and says nothing at all about the properties of approximately-plane tissue interfaces. If we had design equations relating transducer response to interface tilt, we could approach the design of transducers capable of imaging interfaces at angles of incidence considerably away from normal incidence. An intensity-responsive receiver processing with large apertures is an excellent possibility. There are many large aperture transducer systems in use which employ lenses or phased arrays. When an interface examined with such a system is tilted, the reflected energy is usually still reaching some portion of the transducer over a larger angular range than is possible with a smaller aperture transducer. As long as such angular-dependent reflection properties are considered to be related to the tissue interface, attention is diverted away from the transducer design question where the problem might be solved.

2. Scattering Mechanisms

Since the original observations [1,2][1] that echoes could be received from biological tissues, a lively debate has centered around the mechanisms causing such reflections. It was known that the densities of many soft tissues varied little from that of water. Early investigations of tissue velocity showed by implication that the elastic properties would not vary greatly from water [3]. Since the velocity of sound in soft tissues is approximately the same as in water, we usually use the equations which apply to compressional waves in a liquid. The velocity, c, is given by

$$c = \sqrt{\kappa/\rho} \tag{1}$$

[1]Figures in brackets indicate the literature references at the end of this paper.

where κ is the adiabatic bulk elastic modulus and ρ is the density of the medium. Since the specific acoustic impedance, Z, is given by

$$Z = \rho c \tag{2}$$

we can write

$$Z = \sqrt{\kappa\rho} \tag{3}$$

for unbounded plane waves normally incident on the interface between media of differing properties. The fraction of the incident intensity which is reflected is given by k^2, where, at normal incidence,

$$k = \frac{\sqrt{\kappa_2\rho_2} - \sqrt{\kappa_1\rho_1}}{\sqrt{\kappa_1\rho_1} + \sqrt{\kappa_2\rho_2}} . \tag{4}$$

The subscripts refer to the media on the two sides of the interface. These equations describe the relationships between the basic medium parameters of elastic modulus or density and the observed quantities of reflection constant and velocity. Interface echoes can be produced by tissue elements whose elastic modulus *or* density differs from the adjacent tissues. Equations are also known which apply to structures much smaller than the acoustic wavelength, to the red cell, and possibly to other tissue structures. The importance of these equations for small-scatterers is that they can be extended to structures of arbitrary shape. The scattering from complicated structures is the vector sum of the scattering from its component elements, if these elements are small. The elemental scattering is calculated from [4]

$$\sigma_d = \frac{1}{9}\left(\frac{2\pi}{\lambda}\right)^4 a^6 \left[\frac{K_e - K}{K} + \frac{3\rho_e - 3\rho}{2\rho_e + \rho}\cos\theta\right]^2 \tag{5}$$

where,

σ_d = differential scattering cross-section
λ = wavelength
a = scatterer radius, $<< \lambda$
K = adiabatic compressibility of embedding medium = $1/\kappa$
K_e = adiabatic compressibility of scatterer
ρ = density of medium
ρ_e = density of scatterer
θ = angle between scattered ray and direction of incident plane wave (θ=0° for backscatter).

The scattered power per unit solid angle is given by the product of incident intensity and σ_d. Integration over the face of the receiving transducer then yields the acoustic power in the echo. Measurement of σ_d is discussed in the next section. Equation (5) applies strictly to media without viscosity. If viscosity is present, the second term in parentheses is replaced by a more complicated function of viscosity, scatterer size, and density with the same cos θ dependence [5].

The scattering from some structures is explained by the preceding equations for cases where material properties are known and where scattering has been investigated quantitatively. In other cases, useful inferences can be drawn from extensive clinical experience. Both approaches are combined to provide a good understanding of scattering. Ultrasound scattering is produced by very small differences in density and in elastic modulus (or compressibility). This energy may be used to detect variations caused by disease processes.

The reflection coefficient of biological interfaces may be calculated from basic data using eq. (4) [6]. The amplitudes of the reflected wave range between 30-40 dB less than that of the incident wave for all soft tissue interfaces. It is extremely fortunate that the value is small, since the abstraction of energy from the propagating wave by these interfaces is negligible and thus, interrogations are possible at appreciable depths of tissue. The calculated values have been measured *in vitro* for mitral valves (see Keynote Address, fig. 2, p. 11, this volume). Transcutaneous determinations *in vivo* have shown that a value of impedance differing from blood by 1-5% would, when corrected for absorption, account for the observed echo strength [7].

Such small impedance variations could be produced by differences in either density or bulk elastic modulus for tissue organizational elements of a size on the order of 1 mm. Generally, values of compressibility and density are not obtained for tissue elements this small by conventional methods. Thus, one must use ultrasonic means of measurement. The use of ultrasonic velocity to measure particle compressibility is well known. Effective values of density and elastic modulus must be considered, since if these properties undergo relaxational changes, they become functions of frequency. Changes in elastic modulus which affect sound waves are not the static values, but rather the high-frequency values. At frequencies of several Hz, these values are functions of the general level of stress and, for some biological tissues, the stress history of the material [8].

Early in the development of diagnostic ultrasound, some experiments were done which shed light on the mechanism of echo production from within skeletal muscle and tumors [9]. The strength of muscle echoes was highly dependent upon orientation and was strongest when the sound beam was normally incident upon the muscle bundles. This anisotropy implicated the muscle bundles in the echo-production process. It was not clear, however, whether the extra-cellular fluid between the bundles was the origin of the echoes or whether the elastic and connective tissues which organized the contractile elements into bundles were responsible. This same investigation showed that internal echoes could be observed within tumors and that these could be used in diagnosis. During the intervening years, a number of clinical observations, primarily by those using grey scale apparatus, have helped delineate the fact that different echo patterns arise from the interior of many organs.

Many of the clinical observations and investigations into the origin of scattering within tissues by E. Kelly Fry and G. Kossoff were considered in a review by Fields and Dunn [10]. Based on the correlation between connective tissue growth and disease processes, they showed that impedance discontinuties between connective tissue with high collagen content and other soft tissue play a primary role in producing echoes from within tissues. Although their argument refers to the large differences in the static Young's modulus of elasticity within these tissues rather than to the small differences in the high-frequency bulk modulus which governs the impedance, their general conclusion is still valid. Investigations of the approximate value of the velocity in high-collagen-content tissues such as blood vessel walls and mitral valve structures have found variations only up to 10% from the average velocity of other soft tissue. However, these differences are near the upper range of velocity differences observed within soft tissue. Furthermore, in analogy to the case of red blood cells (see Shung's paper, p. 207, this volume), differences in the compressibility and density of these structures and other soft tissue could be of the same order of magnitude.

3. Tissue Scattering

Many organs within the body can be visualized by means of the echoes which arise from their surfaces. These organs, such as kidney, liver, stomach, bowel, etc., have connective tissue membranes enclosing their structure. The echoes are strong and highly angle-dependent, indicating that specular or mirrorlike reflections from the surface are responsible. The role of half-wave resonance within these membranes, which has been demonstrated for the mitral valve (see Keynote Address, p. 11, this volume) is not known for these other connective tissue structures. These echoes are widely used by clinical pulse-echo machines to determine the shape and position of normal body structures. Blood vessel walls may also be in this category, although reflections from internal layers probably contribute.

The scattering patterns of the interior of muscle have some interesting properties. The apparent size of the scattering centers and their distribution leads to different

textures in the grey-scale echo pattern [11]. This texture difference is useful in allowing the differentiation of muscles which lie close to each other. The primary clinical utility of this information is the differentiation of the placenta from the uterine wall. This ability to locate the placenta has made the pulse-echo device almost a standard fixture in obstetrical departments. The scattering from heart muscle interior has been shown to be quite independent of angle at 5 MHz [12]. These myocardial echoes may not even appear on standard echocardiographic machines which usually display the strong surface reflections. At high gain, however, the muscles can be observed by means of these internal echoes. The influence of infarct on internal myocardium echoes is being investigated.

Many efforts have been made to characterize tumors by their scattering, as observed with B-mode scanners. If such characterization could show not only the presence but the nature, *e.g.*, malignancy or non-malignancy, of a tumor, the method would be extremely valuable. These efforts are distinguished by a considerable lack of agreement between investigators, and illustrate the difficulties involved when interpreting simple echo strength and position data as representing tissue properties. The height of the echo on the A-mode display (or the brightness of a B-mode display) is the result of the interaction of all factors present. These include not only the scattering parameters, but the attenuation of the tissue being investigated and of all overlying tissues, as well as the frequency, beamwidth, pulse length, and signal processing of the examining equipment.

It is not our purpose to review the state of cancer detection. Various investigators have generally used equipment whose characteristics differ considerably. The result is that a number of equipment parameters make intercomparison difficult. These are: the frequency of operation, transducer aperture, pulse length, receiver/detector law, video processing, and characteristics of the display. Frequency is an extremely important variable since the attenuation for all tissues is known to be frequency-dependent. The echo height could be influenced differently in different frequency ranges because of this effect. The effects of aperture and pulse length are to average the signals received over different volumes of tissue. The ultrasound carrier frequency is converted to a frequency suitable for the display in a detector which is highly nonlinear in most clinical equipment. Low-level thresholds, high-level limiting, and a frequency-dependent response are the rule rather than the exception. Video processing can involve differentiation or integration of the raw video signal plus signal compression. The display apparatus ranges from bistable memory tubes to grey-scale apparatus and color displays. These may be nonlinear and can include other effects such as integration due to finite spot size and proportional or super-proportional response.

It is clear that more work needs to be done in the tumor field, one of the most promising for clinical payoff of tissue-characterization studies. Quantitative measurements of echo height as well as scattering will be discussed below. These techniques appear to be suitable for application to the tumor characterization problems. Many examples of scattering observations can be found in any issue of the *Journal of Clinical Ultrasound* and *Ultrasound in Medicine and Biology*. Similar articles are appearing with increasing frequency in various medical specialty journals.

The differentiation of tumors by scattering measurement has been more successful [9]. In an extensive review of his work on ultrasound in ophthalmology [13], Ossoinig shows how it is possible to differentiate malignant melanoma of the choroid and to categorize other lesions into five groups. He uses both blood and the smooth scleral surface for substitution standards.

The primary tissue which is well characterized with regard to scattering is blood. (See Shung, "The Scattering of Ultrasound by Red Blood Cells," p. 207, this volume). The scattering has been measured from blood as a function of frequency and angle, and from these quantities exact tissue parameters have been derived. Comparison of scattering cross-section of the red cell with the results of calculation from relatively simple models shows excellent agreement. We are able to separate the contributions due to the changes of compressibility from those due to changes in density. Fluctuations in blood scattering were studied by Atkinson and Berry [14]. They found that a two-particle correlation function satisfactorily defines the fluctuations, so that multiple scattering may be neglected.

Whole blood is less well characterized than is the cell. The angular dependence has only been observable in dilute concentrations. This work obviously needs extension to higher hematocrits and must consider the influence of flow rate. Fluctuation as a function of flow rate has prevented quantitative work from being done at high hematocrits, although this effect may be an artifact due to the measuring apparatus. One item which is under scrutiny at present is the observation that the scattering from suspensions of red cell ghosts, that is the membranes alone, is nearly the same as the scattering from whole blood. This finding does not invalidate the theoretical model since the values of compressibility which were used were derived basically from sound velocity measurements in which the cell was treated as a unit. The implication seems to be that the compressibility may well be a property of the membrane rather than of the interior of the cells.

The most inconsistent data has been obtained for lung tissue. Lung containing the normal amounts of air present due to respiration strongly scatters sound and distorts the sound beam in space as well as the pulse shape in time [15]. Scattering measurements reported to date, however, have used relatively short pulses which have not allowed the steady state to be reached. This situation precludes the exact application of theories of propagation or scattering. Measurements on cut lung samples are consistent [16,17]. There is little hope of using the lung as a propagation path to reach the heart with present techniques, since indications are that the lung diffuses sound passing through it. Considerable interest is attached to the detection of fluid in the lung and the possibility of detecting clinically-significant emboli in the lung. These applications, which have shown some preliminary clinical feasibility, appear to warrant expenditure of more effort on lung scattering.

Measurements of the angular dependence of scattering hold great promise since these are basically relative determinations that could be applied clinically. The work of Lele, Waag, and of Hill in this area are reported in this volume.

4. Scattering Measurements - General

Measurements of scattering from biological tissues present challenging problems. Techniques exist to solve some of these, and can clearly be developed to handle most cases. This section considers in some detail the nature of scattering measurements and how they are made. This discussion attempts to relate various types of scattering measurements to each other and to the basic physics upon which these measurements depend.

Scattering is difficult to specify, primarily because the scattered wave is a new wave which depends on frequency and angle, as well as on the fundamental elastic properties that give rise to the scattered wave. This contrasts with the case of velocity and absorption measurement where waves of essentially the same shape are compared for arrival time and amplitude.

Additional problems associated with measuring scattering from biological tissues arise from three factors. First, the tissue of interest may not be in the far field of the apertures used to generate and receive the scattered waves, so the known equations and approximations do not apply. In other fields, *e.g.*, military radar, investigation of planets, etc., the targets are all at a considerable distance relative to the dimensions of the aperture. Large aperture medical systems average angular variations in the wave over the aperture. Diagnostically-significant angular variations may well be destroyed by the averaging process.

The second problem is the extremely wide bandwidth of the pulses which are generally used. Fractional bandwidths of approximately 50% are in common use, and are often necessary to obtain time separation of the echoes from closely-spaced structures. To analyze such structure echoes requires short time-duration pulses and the information is obtained over a very wide bandwidth. Unless spectrum analysis is used to separate the effects of the scattering on the discrete frequencies of the pulse, the wide bandwidth may also act to smear or obscure highly frequency-dependent terms in the scattered wave. (Spectrum analysis is only one step in the measurement process outlined here.)

The third problem comes from the presence of significant absorption in the medium being investigated. Most microwave radar and optical propagation are characterized by a

loss due to inverse-square spreading only. We, however, must deal with a strong frequency-dependent absorption in the material we are investigating. This absorption interacts with the reflections so that, although we can observe the amplitude of a scattered wave, we have some difficulty in separating the effects of absorption and scattering strength that contribute to the observed amplitude. This latter problem has been solved for cases where the absorption is known (see Appendix). Analytic methods are available which allow the complete separation of absorption and scattering-strength effects under some experimental conditions. The formalism exists to extend these techniques eventually to *in vivo* measurements, as is shown in table 1, below.

Table 1. Levels of Scattering Measurement

Level	Correction Required	Standards or Methods
1. Observed wave	None	External
2. Source function	Overlying tissue absorption	Reflection: known reflectivity, or Absorption: known or negligible
3. Effective values	Wave-shape, equipment parameter interaction	Reflection: known reflectivity
k^2		plane
σ		sphere
η		distribution
		(Calculations needed unless paired standard is used)
4. Actual values σ η	Sample tissue absorption	Same as # 3, plus known absorption
5. Per cell or structure σ	Concentration effect	Same as above, plus variation of sample concentration or volume

To measure scattering requires two sequential steps to overcome these problems. The first is to define the functional dependence of the scattered wave, *i.e.*, to determine the shape of this wave. The second step is to measure the amplitude of the scattered wave. The functional dependence can be defined by making measurements of the effect of range and transducer aperture on the received echoes. A small transducer can be used to probe the angular dependence of the wave. The functional dependence for far-field conditions for spherical waves and plane waves is known (see Appendix).

To measure the scattering properties of the tissue requires reducing the actual scattering data for comparison to a suitable absolute measure of scattering. The standard of acoustic reflectivity is the perfect reflector, *i.e.*, an interface which returns all of the energy which is incident upon it without changing the shape of the wave. This is realized in a practical form by a plane interface of known reflectivity [18]. Thus, a scattering measurement is a relative quantity. This is really not different from the measurement of absorption where the wave leaving the region is specified relative to the wave entering the region.

Such a standard of acoustic reflectivity requires modification for use in cases where the shape of the scattered wave is changed. A plane-reflecting surface reflects a wave of unchanged shape whose strength is specified relative to that of a wave reflected from a perfect interface. In the case of a very small scatterer, a non-planar wave is radiated. The strength of the scattering source is then conveniently specified in terms of a "piece" of a perfect reflector. This area is referred to as a scattering cross-section.

Cross-sections are expressed in several forms and sometimes the literature does not carefully identify which form is being used. The total scattering cross-section, σ, is usually given without subscript and refers to the total scattered power. This cannot be related to the power received by the receiving transducer unless the angular dependence is known. If the scattering is a function of angle, the differential scattering cross-section, $\sigma_d(\theta)$ is used. This scattering cross-section gives the power scattered per unit solid angle in the direction θ. This scattered wave must be integrated over the surface of the transducer and is treated further in the Appendix. The backscattering cross-section is the scattering cross-section observed by the usual pulse-echo technique where the transmitter and receiver are at the same location. In the case of an isotropic scatterer, in the far-field, the backscattering cross-section is equal to the total scattering cross-section, σ, or $4\pi\sigma_d$ (180°).

The scattering cross-section equations for discrete scatterers are extremely useful since such scatterers are elementary wave sources. Theoretically, more complicated scatterers can be regarded as a distribution of elementary discrete scatterers and the scattering found by a summation over the individual scatterers. Summation generally requires the use of computers if the object is at all large, but randomly-distributed scatterers can be handled analytically in closed form. In the case of volume distributions, the scattering is described by a scattering cross-section per unit volume of tissue. These scattering cross-sections per unit volume are usually designated by η and there are obviously as many forms of η as there are of σ, as described above.

The second step of the measuring procedure, the determination of the scattered amplitude once the shape of a scattered wave is known, can be done in three basic ways. The first two involve analytical reduction of the data so that suitable equations relating the observed wave amplitudes and the equipment parameters are needed. Reducing the data to terms involving the standards of reflectivity mentioned above can make the measurements independent of the parameters of the measuring apparatus. Because, at the present time, we have only equations which are suitable for analysis in the far-field region (see Appendix), these two methods have limited utility. The transition zone between the near- and far-field regions of the transducers is often used. This zone is the region of narrowest field and maximum intensity. It is not very different from the far field and future workers may be able to derive suitable corrections and approximations to allow analytical design to be done in this region. Through the use of the substitution method, to be discussed below, it is possible to use any region of the transducer field to make scattering measurements.

The most straightforward means of measuring the scattering is to measure the field incident upon the scattering tissue volume and separately to measure the scattered field at the location of the receiving transducer. These two quantities can then be inserted into a suitable scattering equation to derive either the interface reflectivity or the scattering cross-section. The equations can be written only for the strict far-field case at present. This restriction and the reduced accuracy which results from the separate measurements severely limit the utility of the separate measurement technique; it is not recommended because simpler and better methods exist.

The most useful measurement technique is based on a substitution method. In its basic form, it has been used to measure the scattering cross-section of the red cell and is applicable to many types of scattering problems. The measurement is performed by measuring the amplitude of the wave scattered from a particular region of tissue. The tissue is then replaced by a standardized scattering target and a second determination made of the signal from the known scattering target. If the far-field restriction has been met in the measurement, then equations giving the scattering strength in terms of the equipment parameters and the tissue scattering parameter apply (see Appendix). These equations can be solved for the scattering parameter in terms of the equipment parameters and the *ratio* of the wave amplitudes received in the two cases just mentioned. The result is that the tissue scattering parameter is obtained independent of the apparatus parameters and without the necessity of making absolute measurements of acoustic power. Another advantage of this method over the separate measurement of the acoustic waves is that the substitution method can eliminate all corrections due to the frequency response of the transducers and electronic equipment. Pulse methods can be used for the time-selection of adjacent structures, and the spectrum of gated echoes can be obtained. Corrections are needed, however, if the wavelength or other frequency-dependent terms do not divide out of the equations. To obtain the true spectrum, the observed spectrum must be weighted to account for this effect.

An exceedingly simple measurement situation results if the standardizing target and the biological tissue scatter waves are of the same shape. By the same shape, we refer to the characterization of the wave as spherical, cylindrical, or plane. In this case, when the scattered power from the tissue is compared to the scattered power from the target (typical equations that govern the scattering are given the Appendix), it is found that all of the terms involving the transducer, frequency, and other apparatus parameters divide out. This is rather obvious when measuring the reflectivity of an interface using a planar standardizing reflector. The ratio of the two scattered waves can be expressed in decibels below a perfect reflector and no geometrical corrections are necessary.

In summary, the substitution method of scattering involves replacing the actual scatterer by a standardized scattering target and making a comparison of the two amplitudes. If the observation is done under conditions in which the dependence of the received echo upon the geometrical factors, such as transducer aperture and range and operating frequency, are all known, then any target, *e.g.*, a standardizing target giving any conveniently shaped wave, can be used as a standardizing means for the actual scatterers. This has been done in the quantitative measurement of scattering by red blood cells in which the plane wave target was used to standardize the scattering from distribution of red blood cells. Suitable equations (eq. (12), multiplied by the ratio of pulse length to pulse period, and eq. (A-11), in the Appendix) were solved for the scattering cross-section per unit volume in terms of the ratio of the received power. Had a distribution been chosen for standardizing, two equations of the form of eq. (A-11) would have resulted. All the apparatus terms would divide out in the final results. Therefore, if similar equations exist for other ultrasonic field regions, the equipment terms will similarly divide out. It is necessary that tissue and target be at the same range, not only for the range to divide out, but also for wave shape identity in both cases.

Various standardizing targets are available which have a known scattered wave shape, *e.g.*, plane standardizing targets of glass or stainless steel. Spherical wave scattering can be standardized by using a perfectly-reflecting sphere. If such a sphere is much larger than the wavelength, the scattering cross-section equals the geometrical cross-section, and is independent of frequency. Many biological materials appear to be distributions of scatterers, and substitution methods can be used, provided that suitable distributions can be found.

Original observations by Wild and Reid [9] were quantitative in that the scattering from pathological tissues in the human breast was compared to the scattering from the normal tissue at the same range in the opposite side. This is a substitution scattering measurement in which the scattering can be expressed in decibels relative to normal tissue. If the scattering from the normal tissues had been known, this would also have been a true quantitative measurement. A considerable field exists in the characterization of both *in vivo* and *in vitro* secondary standards by the more exact methods outlined here.

Some of the earliest work on measuring scattering used packed red blood cells as a standardizing means [13]. This was not a true absolute measurement since absolute reflectivity of the packed red cells has not been measured. This extension is certainly possible and will undoubtedly be done in the future, although artificial distributions of scatterers will probably be more convenient.

5. Scattering Measurements - Corrections

A number of steps are necessary for reducing raw observations of scattered power to scattering parameters which characterize the tissue. It is necessary to correct the observed scattering for the effects of attenuation due to both the overlying tissue (in the case of *in vivo* measurements) and to the tissue of interest, and as has been noted, for changes in shape of wave caused by the use of various types of standardizing objects. The steps are summarized in table 1. This table shows the five levels of scattering measurements which have been reached so far.

The first level consists of the external measurement of the power of the ultrasonic waves scattered by the tissue. The measurements may be made relative to suitable standards, *e.g.*, an externally-mounted perfect reflector. Thus, the scattered power is determined relative to the incident power in decibels below that scattered by the perfect reflector.

Any of the other types of reflector discussed above may be used. Measurements have also been made of the scattering by using the signal loss in a column of paraffin oil to obtain a factor which expresses the ratio of the scattered wave to the incident wave. It is usually more useful to reach the second level in Table 1, the determination of what is termed the source-scattering function.

The source-scattering function, level 2, is the scattering from a region of tissue corrected for the absorption caused by the overlying tissue. If the absorption of the overlying tissue is so small that it can be neglected, this source function is the same as the scattered power measured in the first level. It is a reasonable assumption to neglect this loss in the case of the eyeball and perhaps also for low-loss organs such as the liver and spleen (see papers by Wells and by Taylor, pages 61, 71, this volume). If the absorption of the overlying tissue can be determined from a separate measurement or by a calculation from known values, this correction can be made. To perform the correction for an *in vivo* situation will eventually require the use of internal standards. These standards must have a known reflectivity, but no well-characterized internal standardizing structures are available at the present time. It is quite possible, however, that *in vitro* work may determine that tissue structures, such as smooth lining membranes, bones or even red blood cells, might be used for internal standardization. It is necessary, of course, for these internal standards to be so positioned that the tissue between the standard and the transducer has the same absorption as the tissue between the tissue being measured and the transducer.

It is of great practical importance to correct measurements to the second level. Not only may the loss of overlying tissue be high, but the frequency and angular dependence may be controlled by this tissue. An example is the strong influence of the frequency dependence of absorption which can mask even the fourth-power dependence of frequency of the scatter from blood (or any small scatterers). It has been shown (see Keynote Address, p. 11, this volume) that the received power increases with frequency, peaks, and then decreases!

The third level of the table is the first level at which a scattering parameter can be determined independent of the measuring apparatus. In this step, effective measures of scattering strength, that is, k^2, σ, or η, can be determined. The third step differs from the second only by the use of a scattering standard which has the same scattered wave shape as the tissue being investigated or subjecting the fields being measured to calculated corrections. In this latter case, equations which govern the influence of equipment parameters on the observed echo strength are needed. These effective values of scattering parameters are corrected for the equipment parameters and, thus, characterize the tissue. The values can be used for equipment design or for the derivation of diagnostic criteria. They will be most useful in equipment design if the equations which relate the observed echo height with the tissue and equipment parameters are found for both the transition- and near-field cases. In this case, the designer can manipulate his equations to maximize particular echo information with respect to whatever constitutes the noise in his particular system.

It is of great interest, however, to reduce the data to the fourth level, which allows comparison with theory. Only if this step is taken, can the scattering mechanisms be determined with certainty and the full predictive power of this knowledge be applied to the design of new equipment and the development of diagnostic methods. This fourth level is the derivation of the actual scattering magnitudes by separating out the effects of absorption in the tissue being investigated. The analytical expressions required to obtain actual values of σ or η are known only for the case of randomly-distributed scatterers which scatter spherical waves (see Appendix). The various formulas for scattering cross-sections found in textbooks can be compared with measured values only if this stage of data reduction is reached.

One further step is possible in the case of distributions of scatterers, the extraction of the σ value per scatterer. Although determination of the volumetric scattering cross-section is useful, in the case of red blood cells it was necessary to go to this final fifth level, the derivation of the scattering cross-section per cell to compare with theory. This step is necessary to determine the scattering mechanism for the small structural elements responsible for volumetric scattering. To reach this level, the law of combination of waves must be determined. In the case of blood, the law was determined by varying the

concentration of red cells and extrapolating the σ value per cell to zero concentration. This technique cannot be done for more highly-organized tissue, although the sample volume could be varied and similarly extrapolated to zero.

One subject not covered here is the fluctuation in range or time of scattering from small fixed-position structures. It is well known in radar that the range fluctuations are Rayleigh-distributed, a characteristic of truly random scatterers. Since it is doubtful that organized biological tissue is truly random, knowledge of actual statistics may very well be useful in tissue characterization.

6. Measuring Equipment

It is important to use suitable equipment and techniques in connection with the measurements. Electronic units of sufficiently wide bandwidth, linearity and so on are available. In general, clinical apparatus is not useful for making measurements unless the waves can be recorded and suitably processed prior to detection. Most clinical apparatus contains thresholding, fast time-constant circuits, and, in some cases, detectors of special characteristics which do considerable processing of the echo information. If this processing is included when measuring tissue parameters, then some of the *a priori* assumptions made by the designer of the equipment are automatically adopted and the measurements no longer characterize the tissue alone.

Special transducers designed to help separate the echoes to be measured from interfering echoes are of great help in both *in vivo* and *in vitro* work. Those interested in making measurements should give some thought to acquiring sets of transducers whose focusing and frequency-response characteristics are designed to ease the data gathering step. Transducers and mountings should allow the range and aperture parameters to be varied to find the shape of the scattered wave.

Control of the geometry of the sample while making reflection measurements is particularly important. The area of the sample being measured, *i.e.*, the region where the sound beam investigates the sample, must be determinable and stay constant as frequency, range, aperture, and angle are varied. For illustration, the apparatus used in our laboratory is shown in figure 1. It is a dovetail channel in which alignment jigs and sample holders are inserted. A ball-ended rod is used for the initial alignment of the investigating sound beam. The transducer is moved back and forth to vary the range. Adjustments to make the sound beam parallel to the axis of the apparatus are made at the transducer. When tissue is to be mounted onto the holder, the pointed rod is mounted from the left (figure 1) to

Figure 1. Apparatus for holding tissue specimens which allows accurate determination of region being examined. Ball-ended rod for transducer alignment is shown mounted. A holder for heart valves is on the table. Pointed rod is a transfer marker used only for initial alignment. This apparatus is suspended in a temperature-controlled saline bath for measurements.

indicate the exact center of the ball-ended rod. The tissue is tied, pinned, or otherwise fastened to a holder. A valve holder, suitably baffled with sound absorbing rubber, is shown on the table in front of the apparatus. When the tissue is mounted in place of the ball-ended rod, the area of the tissue to be investigated is selected by reference to the pointed rod. The pointed rod can then be removed and the measurement made. If an internal region is to be measured, the pointed rod can be offset toward the transducer. Both the vertical and horizontal axes of rotation of the apparatus are carefully adjusted with the aid of a dial indicator to intersect at the exact tip of the pointed rod. Other holders are used for standardizing targets.

To maintain the biological integrity of *in vitro* samples requires the maintenance of normal values of fluid content, temperature, and elasticity of the sample. This last item is new to such a list and is necessary to insure that the variational values of elastic modulus are similar to those found in life. Since the variational value of elastic constants of biological materials is a function of the stress level, the degree of tonus in muscle, for example, may turn out to be important. The influence of age must also be considered, since death of the tissue liberates decay enzymes to attack the normal structures.

Fluid balance is necessary for two reasons. First, fluid-filled spaces such as arteries, veins, lymph channels and interstitial spaces should be maintained. This may require techniques to keep these from collapsing. Secondly, to avoid osmotic gradients and retain normal water balance, the sample should be maintained in normal saline, *i.e.*, water of 9 grams per liter NaCl content.

Body temperature (37°C) must also be maintained unless the process studied is independent of temperature.

7. Conclusion

The quantitative study of scattering characteristics appears to be a fruitful field for further investigation. Recent studies in this field are discussed in this volume (see Chapter 6, "Scattering Techniques," p. 167, this volume), as well as in References 19 and 20. Information derived from scattering measurements could very well be clinically useful in a relatively short period of time. Further implementation of clinical and *in vivo* experiments for determining scattering is required. Relatively few tissues have been measured in a comprehensive manner, which is probably normal for a developing field. As new information-exchange mechanisms, such as this Conference and the proposed Tissue Characterization Library, are developed, we may expect the state of knowledge to increase rapidly. Work remains to be done at the theoretical, laboratory, and clinical levels. Fortunately, the means to obtain good data and understanding of mechanisms are at hand.

Appendix

Tissue Interaction Equations

The emphasis throughout this development is on methods to obtain measurable quantities which characterize scattering tissues. Most of the literature dealing with scattering problems in random media use a theoretical approach which is based on many-particle correlation or probability functions. These functions are completely unknown for biological tissues. They may become known (heuristically, at least) by comparing the theoretical results with the results of measurement. Thus, the determinations of measurable quantities should have a high priority.

To be of greatest utility, tissue scattering parameters must be measured in a quantitative sense and be independent of the apparatus used to perform the scattering measurements. This independence frequently requires knowledge of the equations which describe the interaction between tissue parameters and equipment parameters.

It is important to know these interaction equations for two purposes. First is the reduction of the output of the data to provide the tissue parameters. The second purpose is the design of equipment to maximize the probability of detecting echoes from any particular type of tissue. Knowledge of scattering parameters as well as of interactions may very well suggest new possibilities for system design.

The simplest interaction equations are derived by considering continuous-wave operation in the far-field of a transducer for the cases of plane and spherical waves. Three classes of targets can be handled by these equations; the reflecting interface, the spherical scatterer, and distributions of spherical scatterers [21]. Angle-dependent scattering from large scatterers can be handled later through the formalism of the differential scattering cross-section. We begin with the case of the simplest echo-ranging equation which yields the received echo power in terms of the transmitted power and the various parameters describing the transducers, propagating medium, and the target or reflecting tissue structure.

The intensity on the axis of the main beam of radiation at a distance, d, from the transducer can be written:

$$I_d = \left(\frac{P_t}{4\pi d^2}\right)\left(\frac{4\pi A}{\lambda^2}\right) \tag{A-1}$$

where P_t is the transmitted acoustic power and λ the wavelength. The first factor is the intensity of d if all the power were radiated isotropically. The second factor is the gain of a directional radiator over an isotropic radiator. This factor holds for acoustic radiators larger than two wavelengths in diameter. The factor A is the effective area of the transducer, which equals the geometric area if it vibrates as a piston.

The effect of the medium in which the waves propagate on their way to the target will be taken as that of attenuation alone, that is, scattering by these tissues will be included only insofar as they weaken the wave. The received intensity is thus reduced by a factor:

$$e^{-4\alpha R} \tag{A-2}$$

where α is the plane wave amplitude attenuation coefficient and R is the range to the reflecting tissue structure being considered. The received intensity from a particular target structure will depend upon the shape and composition of the structure, but the three limiting cases discussed above can be treated. First, we consider a target which is small compared to the beamwidth and sufficiently small compared to the wavelength so that the wave can be considered to be scattered isotropically and to propagate as a spherical wave. The reradiated power is found by multiplying the "scattering cross-section," an area, by the incident intensity. The received intensity is thus obtained from

$$\frac{P_t A}{R^2 \lambda^2} \quad \frac{\sigma}{4\pi R^2} \quad e^{-4\alpha R} \quad , \tag{A-3}$$

where the first factor is eq. (A-1) with d = R. In the second, or target factor, σ = the total scattering cross-section.

The second limiting case is exemplified by the scattering or reflection from relatively large smooth tissue interfaces. This is also the case which applies to the perfect reflector block which is often used for calibration. The model for such large area targets is a plane mirror. For normal orientation to the beam, the fraction of the incident intensity which is reflected is given by the reflection coefficient. Since we are considering far-field radiation and nearly plane wavefronts, the fractional reflectivity of the interface between two media of different acoustic impedance is k^2, where k is the usual amplitude-reflection coefficient. With mirror reflection, the incident field is folded back toward the receiving transducer by the interface and the geometrical factors governing received intensity are the same as if the receiving transducer were in front of the transmitted transducer at a distance d = 2R. Making this substitution in eq. (A-1) and including the absorption factor, we obtain the received intensity:

$$\frac{P_t A}{4R^2 \lambda^2} \, k^2 \quad e^{-4\alpha R} \quad . \tag{A-4}$$

The third type of target is a distribution of isotropic scatterers. For first-order scattering, we find the echo intensity by summing eq. (A-3) over the scatterers. The total scattering cross-section is given by the product of a volume occupied by the outgoing pulse and the scattering cross-section per unit volume, η. In the far-field, the width of the pulse volume is $KR\lambda/a$, where K is a factor defining the effective beamwidth and is usually taken as 1.2 for round transducers. Since the pulse length in distance is $c\tau/2$, where c is the velocity of propagation and τ is the pulse length, the pulse volume is

$$\pi \left(\frac{KR\lambda}{a} \right)^2 \quad \frac{c\tau}{2} \quad .$$

Substituting the above in eq. (A-1) and including the absorption factor, we find the returned intensity to be

$$\frac{P_t \pi K^2}{4R^2} \quad \frac{c\tau}{2} \quad \eta e^{-4\alpha R} \quad . \tag{A-5}$$

Equations (A-3), (A-4), and (A-5) above yield only the received intensity. We can put them in a final form in terms of the electrical transmitted and received power. The actual power received is the product of the reflected intensity at the position of the receiving transducer and the same effective area, A, previously discussed in connection with eq. (A-1). This received acoustic power is an available power. It is the power that would be absorbed by a matched transducer. If we define a receiving available power efficiency, T, we can find the electrical power available, P_r, by multiplying the received acoustic power by T. This is the electrical power which would be delivered to a matched load and is given by the square of the open circuit voltage divided by four times the real part of the transducer impedance. It is a measurable quantity which can be obtained by purely electrical measurements on the terminals of a transducer. The transmitted acoustic power, P_t in eq. (A-1), is found by multiplying the electrical power output of the transmitter, P_o, by the transmitting power efficiency. This transmitting power efficiency has the same value as the available power efficiency of the receiver.

Making the above substitutions, which introduce P_o and P_r, and multiplying the previous equations by an additional factor as T^2A, we obtain the final equations:

for an isotropic radiator,

$$\frac{P_r}{P_o} = \frac{T^2 A^2}{R^4} \frac{e^{-4\alpha R}}{4\pi\lambda^2} \sigma \qquad \text{(A-6)}$$

for a plane interface,

$$\frac{P_r}{P_o} = \frac{T^2 A^2}{R^2} \frac{e^{-4\alpha R}}{4\lambda^2} k^2 \qquad \text{(A-7)}$$

for a distribution of isotropic scatterers,

$$\frac{P_r}{P_o} = \frac{T^2 A}{R^2} \frac{K^2 \pi e^{-4\alpha R}}{4} \frac{c\tau}{2} \eta \, . \qquad \text{(A-8)}$$

Modifications to these equations are required for transducer frequency response, sample volume effects, pulse operation, attenuation in the sample volume, and angular variation. Examples are given below, with no intention of being exhaustive.

In actual measurements, the open circuit voltage is not observed. The actual voltage is related to open circuit voltage by a function involving the complex transducer impedance as well as the complex value of impedance connected across the transducer terminals due to both the transmitting device and the receiver input circuits. To make corrections for this electrical loading over the full frequency range of short pulses not only requires computer methods, but also can lead to considerable inaccuracies. The ratio between the open circuit voltages found with reflection standards and with the actual tissues, however, is the same as the ratio between the loaded voltages in these same two conditions. The substitution method of scattering measurement, thus, eliminates the entire problem of correcting for frequency response of the transducer. If the substitution method is not used, T and A must be known. A separate experiment and eq. (A-2) can be used to find T and the effective area, A. This is equivalent to a self-reciprocity calibration, but is more complete [22].

If masks or apertures in the measurement system define the beamwidth, then the actual beam area, S, should be retained in eq. (A-8) to yield

$$\frac{P_r}{P_o} = \frac{T^2 A^2 S e^{-4\alpha R}}{4\pi R^4 \lambda^2} \frac{c\tau}{2} \eta \, . \qquad \text{(A-9)}$$

The main difference in this case is that the frequency dependence is changed because we have eliminated the effects of the variation in beamwidth with frequency in the far field.

The extension of these equations to pulse-echo systems is relatively simple. Equations (A-6) through (A-9) apply to the peak values of power during the pulse. To apply to average values, the equations must be multiplied by the ratio of the observation time to the total interpulse period time. The observation time in the case of an oscillographic display is simply the pulse length, τ. For quantitative measurements, it is more convenient to use recording instruments such as rms voltmeters followed by recording devices for averaging out the fluctuations. When this is done, the observation time is the width of the time slot through which the instruments observe the scattered echoes. This is usually a gate in the receiver which is "on" for some time interval Δt.

This correction to eqs. (A-8) or (A-9) is only an approximate one if the medium containing the scatterers is lossy. With loss, the field at each scatterer will progressively diminish as the pulse traverses the volume of scatterers. The exact equation for this

case was derived analytically by Sigelman [23] and the result will be summarized here. We can interpret eq. (A-9) as applying to a situation in which the loss factor α over the range R accounts for all the loss to the wave up to the first surface of the distribution of scatterers. We will change the notation at this point to let α_m describe the absorption constant in the media outside the distribution of scatterers and retain α as the absorption coefficient which is effective within the distribution. This absorption inside the distribution must include losses due to all sources, particularly scattering losses. Two new terms must be introduced. We let t_1 stand for the time during which the interrogating wave travels between the first surface of the scattering volume and the opening of the observation gate. Also, t_2 is the time between the wave entering the scattering volume and the closing of the observation gate. The actual observation time, Δt, is given by:

$$\Delta t = t_2 - t_1 \ . \tag{A-10}$$

The average value of our ratio P_r/P_o is now

$$\frac{P_r}{P_o} = \frac{T^2 A^2 S \eta e^{-4\alpha_m R}}{32\pi T_p R^4 \lambda^2 \alpha^2 c} \quad (e^{-2\alpha c t_1} - e^{-2\alpha c t_2})(e^{\alpha c \tau} - e^{-\alpha c \tau}) \ . \tag{A-11}$$

In the case of small absorption within the scattering medium, eq. (A-11) can be shown to reduce to eq. (A-9) as modified by the ratio of observation time, Δt, to the interpulse period time, T_p. Equation (A-11) differs from equations in reference 23, which used the differential volumetric scattering cross-section. (See eq. (23) in reference 23.)

Further modifications of the previous equations are needed if the scatterer is not isotropic. We shall now derive another form of eq. (A-6) which applies to a small scatterer whose scattering function varies with angle. This is a very practical case since, as has been determined by Shung (p. 207, this volume), the red cell is of this type. Now we return to the discussion preceding eq. (A-3) to consider the power incident upon our non-isotropic scatterer which is

$$\frac{P_t A}{d^2 \lambda^2} \ e^{-2\alpha R} \ , \tag{A-12}$$

where the terms have all been defined previously. Non-isotropic scattering objects can be described by a scattering cross-section which is a function of angle. This differential scattering cross-section is usually termed $\sigma_d(\Theta)$. This scattering cross-section is an area which, when multiplied by the incident intensity, yields the power scattered *per unit solid angle* in the direction Θ. The power scattered per unit solid angle toward the receiving transducer can then be written as

$$\frac{P_t A}{R^2 \lambda^2} \ \sigma_d(\Theta) e^{-2\alpha R} \tag{A-13}$$

in units of watts per steradian. The power which is received by any receiving transducer at any angle Θ can be obtained by integrating eq. (A-13) over the face of the receiving transducer. Assume for simplicity that the receiving transducer is at a sufficient distance from the non-isotropic scatterer so that the scattered field varies slowly with Θ over the face of the receiving transducer. If this transducer is at a range D from the scatterer and has an area A_r, the solid angle which it subtends at the scatterer is given by

$$\frac{A_r}{D^2} \tag{A-14}$$

steradians. The total received power thus can be written;

$$\frac{P_t A\, A_r}{R^2 D^2 \lambda^2}\ \sigma_d(\Theta) e^{-2\alpha(R+D)} \quad . \tag{A-15}$$

In the particular case of backscattering, $\Theta = 180°$, and, assuming we use the same transducer for both transmission and reception, we obtain the ratio between the received and transmitted electrical powers as

$$\frac{P_r}{P_o} = \frac{T^2 A^2}{R^4 \lambda^2}\ \sigma_d(180°) e^{-4\alpha R} \quad . \tag{A-16}$$

Equation (A-16) can be compared directly with eq. (A-6), which is written for the same case, and we see that

$$\sigma = 4\pi\ \sigma_d(180°) \quad . \tag{A-17}$$

By analogy, we can also write

$$\eta = 4\pi\eta d\ (180°). \tag{A-18}$$

The more general treatment of angular-dependent scattering can be written following the above discussion, but will not be expanded here. Briefly, the field incident upon the distribution of simple scatterers with a known angular scattering function must be treated point by point. For each point in the scattering volume, the scattered wave must be integrated over the receiving transducer aperture. The appropriate distance and area functions are introduced into the calculation and this summation repeated over all points of scattering volume. For some measurement purposes, it is obviously much simpler to arrange the apparatus so that the approximations leading to eq. (A-16) are valid. This same formulation can be extended to take account of absorption by using eq. (A-11) with eq. (A-18).

Two cases of angular variation should be carefully distinguished. We know that many biological structures have a scattering function which varies with angle. If these are rotated in front of a pulse-echo system, the received scattered wave will change in amplitude. The angle-dependent scattering which has been found with red cells, however, is due to the dipole term introduced by the density difference (see eq. (5)). This angular variation is defined with respect to the direction of the incident wave and is thus "frozen" into a wave coordinate system rather than the target coordinate system. Rotation of a red cell in front of a pulse-echo system would thus result in no change of received wave with angle, although translation of a separate receiving transducer around the red cell would record the angular variation which was actually observed [24].

Equations expressing the influence of apparatus parameters on angular dependence of interface reflections have apparently not been worked out but would be extremely valuable. As figure 2 shows, when an interface is inclined to the sound beam of a pulse echo apparatus, a reflection is sent back toward the transducer displaced by twice the angle of rotation of the interface. Thus, all plane interfaces at a particular range will appear to have the same angular-distribution function. The angular-distribution function, in the case of large ranges, is identical with the beam spread function of the transducer as integrated over an area whose solid angle equals that subtended by the transducer at twice the range of the actual interface. This change with range has been observed by Wells [25].

A number of clinical measurements of the angular dependence of the scattering from biological interfaces have been made and interpreted as if the interfaces possessed this angular dependence of scattering. As figure 2 should make clear, the angular dependence on scattering is a property of the transducer and its beam shape. The angular scattering function of an interface for plane waves should be strictly an impulse function. The observed response is the convolution of the impulse response and the actual beam pattern. A deconvolution operation is needed to derive the angular distribution functions which

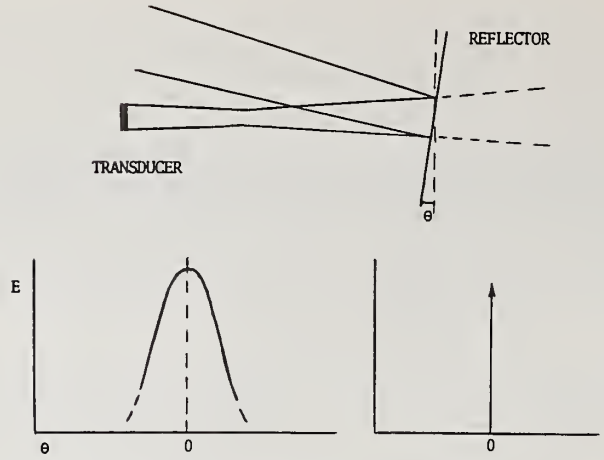

Figure 2. Typical apparatus arrangement for measuring angular dependence of interface reflectivity. As the interface tilts through the angle Θ, the reflected beam sweeps past the send-receive transducer (top). The transducer output, E, varies as a function of angle and transducer directivity function. The true interface directivity function is an impulse (bottom right). Measurements such as these define transducer, not interface, properties.

characterize biological interfaces. Since increasing the angular range over which interface reflections can be received without sacrificing lateral resolution is a high priority design goal for most pulse-echo apparatus, a better understanding of the interactions of the transducer beam pattern parameters and the tissue angular dependence scattering parameters would be very useful.

References

[1] Wild, J. J., Use of ultrasonic pulses for measurement of biological tissues and detection of tissue density changes, *Surgery*, 27, 183 (1950).

[2] Ludwig, G. E. and Struthers, F. W., Considerations underlying the use of ultrasound to detect gallstones and foreign bodies in tissues, Naval Medical Research Institute Project, MM 004 001 Report #4, June 1949; Ludwig, G. E. in *Report of 81st Meeting of the Society of Clinical Surgery,* (Boston, MA, November 4-5, 1949).

[3] Ludwig, G. E., The velocity of sound through tissues and the acoustic impedance of tissues, *J. Acoust. Soc. Am.* 22, 862 (1950).

[4] Morse, P. M. and Ingard, K. U., *Theoretical Acoustics* (McGraw-Hill Book Co., NY, 1968).

[5] Ahuja, A. S., Effect of particle viscosity on propagation of sound in suspensions and emulsions, *J. Acoust. Soc. Am.* 51, 182 (1972).

[6] Wells, P. N. T., *Physical Principles of Ultrasonic Diagnosis,* p. 13 (Academic Press, London, 1969).

[7] Reid, J. M., *Ultrasonic Diagnostic Methods in Cardiology,* Ph.D. Thesis, University of Pennsylvania, p. 91, Order No. 66-4638 (University Microfilms, Ann Arbor, MI, 1965).

[8] Fung, Y. C. B., Stress-strain-history relations of soft tissues in simple elongation, in *Biomechanics: Its Foundations and Objectives,* Y. C. B. Fung, *et al.,* eds. (Prentice-Hall, Inc., NJ, 1972).

[9] Wild, J. J. and Reid, J. M., The effect of biological tissue on 15 Mc pulsed ultrasound, *J. Acoust. Soc. Am.* 25, 270 (1953).

[10] Fields, S. and Dunn, F., Correlation of echographic visualizability of tissue with biological composition and physiological state, *J. Acoust. Soc. Am.* 54, 809 (1973).

[11] Reid, J. M., Diagnostic applications of ultrasound, *Proc. IRE*, 47, 1963 (1959).

[12] Sigelmann, R. A. and Reid, J. M., Scattering of ultrasound by biological tissues, in *Interaction of Ultrasound and Biological Tissues*, Workshop proceedings, J. M. Reid and M. R. Sikov, eds., p. 245 (Bureau of Radiological Health, 73-8008, 1973).

[13] Ossoinig, K. C., Quantitative echography--the basis of tissue differentiation, *J. Clin. Ultrasound*, 2, 33 (1974).

[14] Atkinson, P. and Berry, M. V., Random noise in ultrasonic echoes diffracted by blood, *J. Phys. A: Math., Nucl. Gen.* 7, 1293 (1974).

[15] Reid, J. M., *Ultrasonic Diagnostic Methods in Cardiology*, Ph.D. Thesis, University of Pennsylvania, Appendix I, Order No. 66-4638 (University Microfilms, Ann Arbor, MI, 1965).

[16] Bauld, T. J. and Schwan, H. P., Attenuation and reflection of ultrasound in canine lung tissue, *J. Acoust. Soc. Am.* 56, 1630 (1974).

[17] Dunn, F., Attenuation and speed of ultrasound in lung, *J. Acoust. Soc. Am.* 56, 1638 (1974).

[18] *Standard Specification of Echoscope Sensitivity and Noise Level, Including Recommended Practice for Such Measurements* (American Institute for Ultrasound in Medicine, 1973).

[19] Chivers, R. C. and Hill, C. R., A spectral approach to ultrasonic scattering from human tissue: methods, objectives and backscattering measurements, *Phys. Med. Biol.* 20, 799 (1975).

[20] Nicholas, D. and Hill, C. R., Acoustic Bragg diffraction from human tissues, *Nature*, 257, 305 (1975).

[21] This derivation of the echo-ranging equation is based on the development used in radar. The rationale is discussed at greater length in: Skolnik, M. I., *Introduction to Radar Systems*, Chapters 1 and 2 (McGraw-Hill, NY, 1962); and *Radar System Engineering*, L. N. Ridenour, ed., Chapter 2 (McGraw-Hill, NY, 1947). References to radar practice refer to these sources.

[22] Reid, J. M., Self-reciprocity calibration of echo ranging transducers, *J. Acoust. Soc. Am.* 55, 862 (1974).

[23] Sigelmann, R. A. and Reid, J. M., Analysis of ultrasound backscattering from an ensemble of scatterers excited by sinewave bursts, *J. Acoust. Soc. Am.* 53, 1351 (1973).

[24] Shung, K. K., Sigelmann, R. A., and Reid, J. M., Angular dependence of scattering of ultrasound from blood, *IEEE Trans. Biomed. Engnr.* (in press).

[25] Wells, P. N. T., *Physical Principles of Ultrasonic Diagnosis*, p. 90 (Academic Press, London, 1969).

CHAPTER 3

A-SCAN PATTERN RECOGNITION TECHNIQUES

National Bureau of Standards Special Publication 453. Proceedings of Seminar on Ultrasonic Tissue Characterization held at NBS, Gaithersburg, MD, May 28-30, 1975. (Issued Oct. 1976)

CHAPTER 3. A-SCAN PATTERN RECOGNITION TECHNIQUES

Paper 3.1: USE OF PATTERN RECOGNITION FOR SIGNAL PROCESSING IN ULTRASONIC HISTOPATHOLOGY

K. Preston, Jr.

Department of Electrical Engineering
Carnegie-Mellon University
Pittsburgh, Pennsylvania 15213

New developments in high-speed electronics have made possible real-time digitization of the ultrasonic A-scan as a block of binary words. This makes computer processing of such blocks feasible using techniques previously developed in time-series analysis for communications, speech processing, word recognition, etc. The research reported here is concentrating on: (1) advanced digitization techniques having variable block length and skip-block capability; (2) application of speech spectrogram representation and analysis to A-scan processing; and (3) use of human audition (of the recorded A-scan, properly frequency-translated) to assist in defining the features most useful for A-scan pattern recognition.

Key Words: Analog-digital converter; A-scan; digitization; pattern recognition; speech spectrogram; ultrasound.

1. Introduction

The purpose of the research reported here is to determine the feasibility of conducting useful tissue analysis by computer processing of ultrasonic pulse echoes. At the present time, only the gross macrostructure of organs is observable through either the ordinary or "grey-level" ultrasonic B-scan. However, it has been reported by many researchers and quantitated by some that detailed features of individual A-scans may be useful in analyzing the structure of the tissue to be examined [1-5].[1]

Under a grant from the National Science Foundation (NSF), the Department of Electrical Engineering of Carnegie-Mellon University has been funded to conduct a study of the utility of detailed computer analysis of A-scans in determining tissue characteristics *in vivo*. This will be accomplished by 12-bit digitization at 10 megasamples per second using a total storage of 4096 words, and a 1 kHz interrogation rate. The record length will be variable from 128 to 4096 words (*i.e.*, a depth of 2 to 60 centimeters). Record spacing will be variable from 1 interpulse interval to 1024 interpulse intervals making possible recordings over periods of time as long as 32 seconds (and as short as 12.8 microseconds). Blocks, *i.e.*, the number of records digitized per patient, will be variable from 1 to 32 within the existing memory capacity. Synchronization with the cardiac cycle will also be included. By means of this instrumentation, both liver and kidney in normal and abnormal patients are to be studied over a population of approximately 100 patients. For most of the abnormal patients, a biopsy core will be obtained coaxial with the A-scan.

2. Pattern Recognition

A flowchart of the program to be conducted is shown in figure 1. This flowchart is diagrammed in terms of the basic pattern recognition formalism which shows a series of four mappings from signal space to data space to measurement space to classification space.

---

[1]Figures in brackets indicate the literature references at the end of this paper.

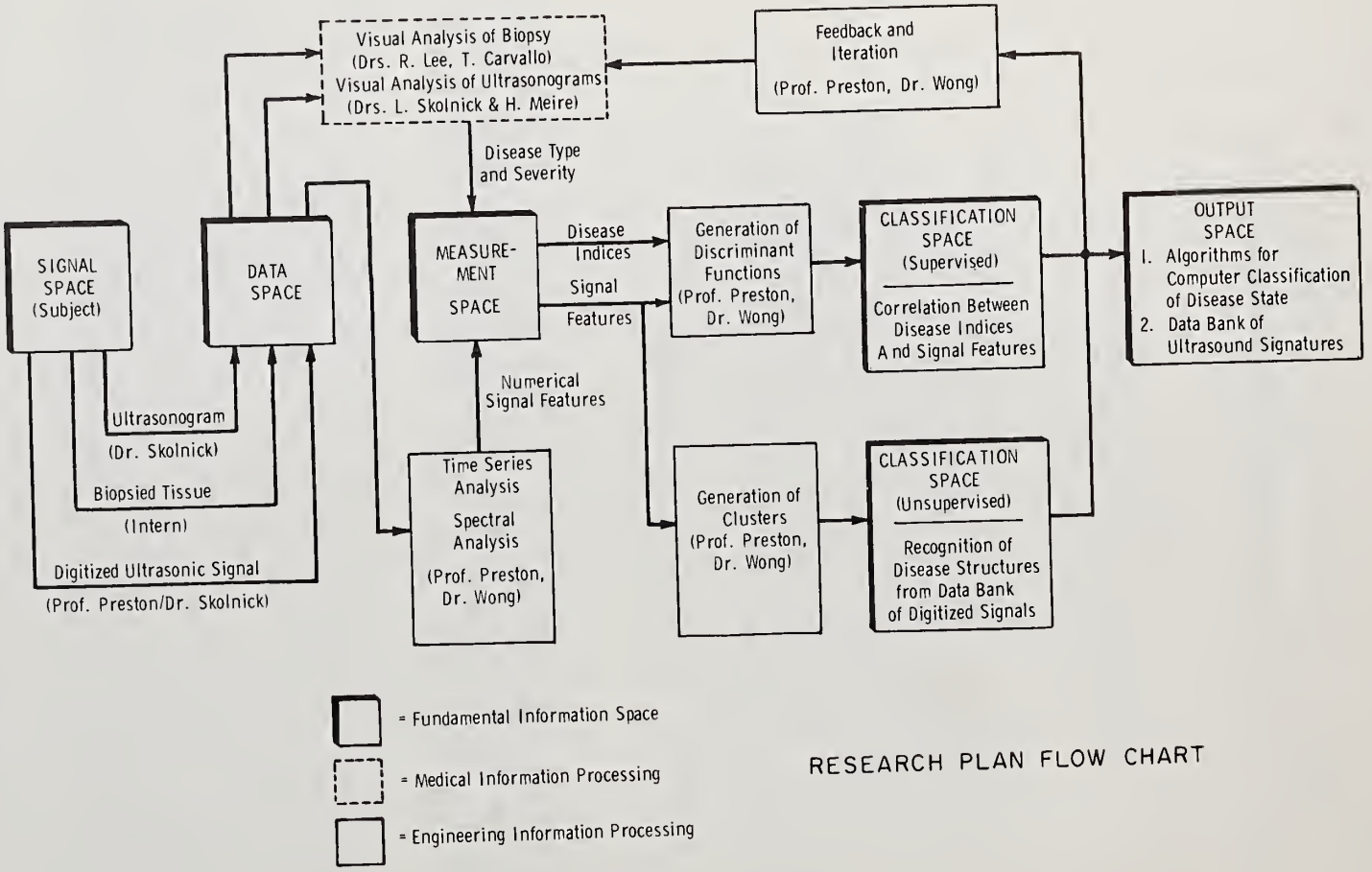

Figure 1. Flow chart of the joint Carnegie-Mellon University - University of Pittsburgh liver and kidney research program for comparing computer analysis of digitized ultrasonic pulse echoes with the visual diagnosis of these organs from simultaneous coaxial biopsies.

In the case of the study undertaken for NSF, the individual patient (or, more exactly, the organ to be examined in the individual patient) is the signal space, the ultrasonic transmit-receive system is used to gather data (the digitized A-scans), measurements are generated from digitized data by time-series analysis, and classification is determined either in a deterministic learning mode or by means of comparison with the simultaneously-extracted biopsy core as analyzed by traditional pathology. Hence, the term "ultrasonic histopathology."

3. Histopathology

Figure 2 shows a field of view of abnormal liver tissue. The purpose of this illustration is to indicate the structural levels at which the pathologist examines an abnormal tissue sample. This particular sample represents a case of toxic hepatitis.

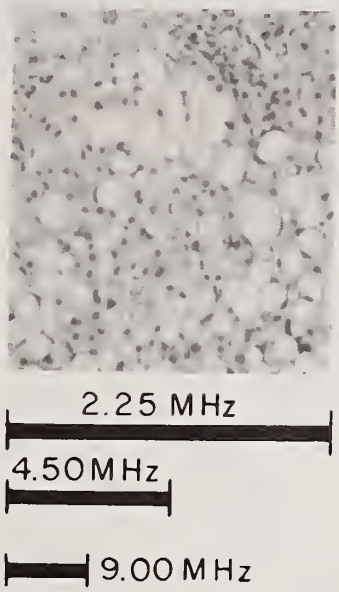

Figure 2. Photomicrograph of a portion (0.5 mm x 0.5 mm) of a section of liver tissue of a patient exhibiting toxic hepatitis. Hepatic cell nuclei, leukocytes, fatty cells, balloon cells and sinusoids are evident. The ultrasonic resolution at various frequencies in liver tissue is given on the bar chart for purposes of scale.

It is useful to compare optical with ultrasonic resolution, *i.e.*, the resolution achievable under the optical microscope with that achievable by the A-scan. In ultrasonic pulse-echo systems, the maximum achievable resolution is the reciprocal of twice the 3 dB bandwidth of the pulse. The 3 bars in figure 2 are made to correspond to half wavelengths at 2, 4, and 8 MHz. It is clear from the dimensions of the ultrasonic wavelength that considerable averaging will be carried out over the structural details observable in the photomicrograph. For example, leukocyte nuclei, even at 8 MHz, are an order of magnitude smaller than the acoustic resolution. Even the hepatic cell is smaller than the acoustic resolution as are the fatty cells shown. This means that acoustic scattering will be from a more of less random collection of scattering sites whose dimensions are considerably below the acoustic resolution. However, leukocyte clusters within the tissue from inflamatory leukocyte infiltration, such structures as biliary ducts, clusters of fatty cells, etc., will in many cases be of the order of, or greater, than the acoustic resolution. Thus, the full spectrum of structural detail must be considered in studying its effect on the received and digitized A-scan. The computer can be used in this analysis, as is shown in figure 3.

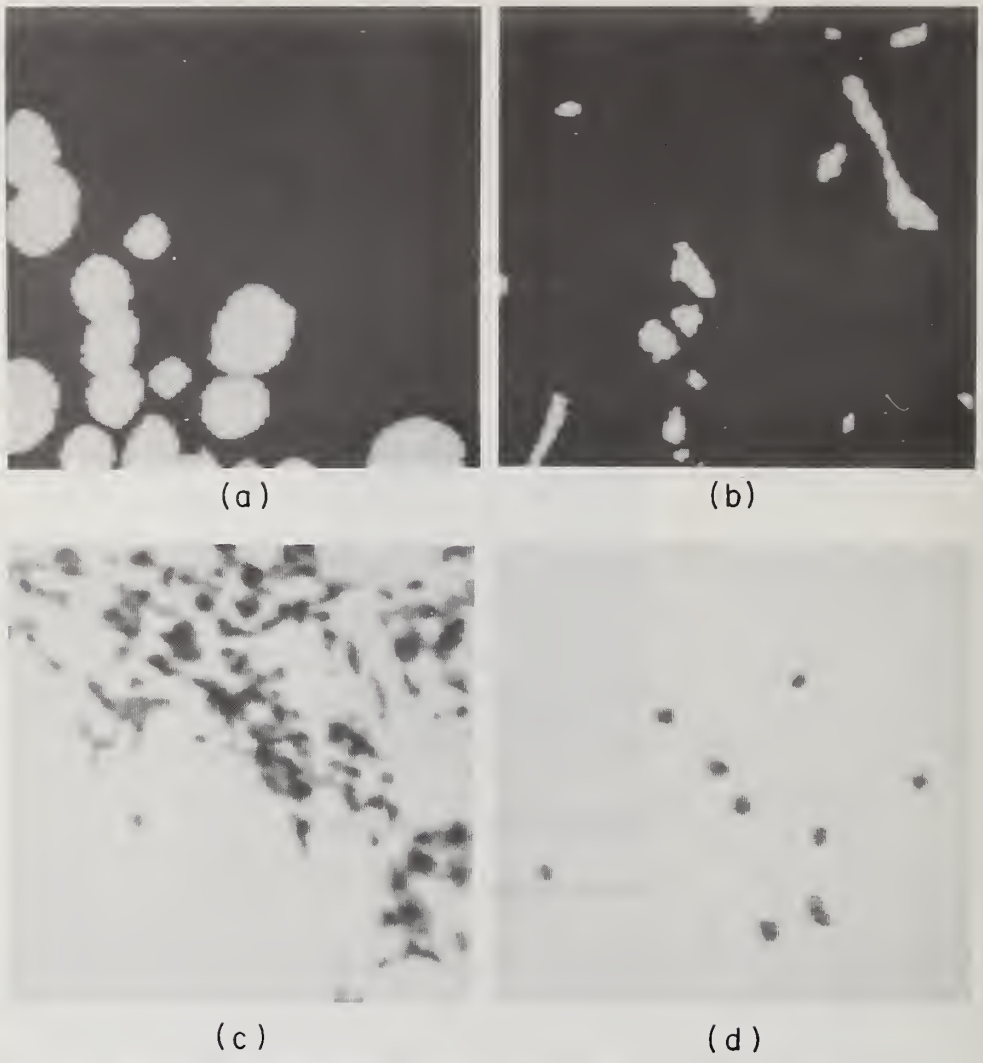

Figure 3. Computer analysis performed of the upper right hand portion of figure 2 at Carnegie-Mellon University using a program coded in PICPAC. The program has separated (a) fatty cells, (b) sinusoids and balloon cells, (c) leukocytes, and (d) hepatic cell nuclei.

4. A-Scan Statistics

Another purpose of this research is to determine the uniqueness of the statistical properties of both normal and abnormal liver and kidney over a statistically-significant population of patients. At this present writing, since the program is only 6 weeks past its starting date, statistically-significant results are not available. Only technique and approach can be reported here. Typical statistical measurements which may be made on the probability density function of the A-scan voltage waveform include not only its mean and standard deviation but also such measures as skew and kurtosis. These measures have been found useful in the analysis of other biological structures [6]. Other statistical measures which are useful in this type of analysis include the n-gram statistics which provide first-order correlation of nearest neighbors in the A-scan time-series. This statistic is also known as the transitional probability density function. It is a two-dimensional function and is best shown in matrix form, as is indicated in figure 4, which shows the transitional probability density function for the first 8 letters of the alphabet in English text. The utility of this statistic in treating digitized A-scans is under investigation.

Second Letter of Di-Gram	First Letter of Di-Gram: A	B	C	D	E	F
A	0.02	0.08	0.44	0.45	1.31	0.21
B	0.32	--	--	0.18	0.11	0.02
C	0.39	--	0.12	0.04	0.64	0.09
D	0.15	--	--	0.10	1.07	0.01
E	--	0.58	0.55	0.39	0.39	0.25
F	0.10	--	0.01	0.12	0.23	0.14

Figure 4. The transitional probability histogram (Di-Gram) of Englist text.

Other quasi-statistical measures on the A-scan include the Wiener spectrum. Its properties are being investigated by many workers [7-10]. The Wiener spectrum is simply a projection of the time-series on the Fourier polynomials and represents a graph of the magnitude of the resultant Fourier coefficients. Whether the Fourier polynomials form a valuable basis for the analysis of A-scans is unknown and an investigation of other bases is planned. For example, we intend to study the eigenvectors of the A-scan time-series itself using the Karhunen-Loeve expansion. If this expansion yields a basis similar to the Fourier polynomials, then the validity of these polynomials will be proven.

5. Auditory Analysis

Each digitized echo is akin to a word or, perhaps, to a phoneme. Thus, a single echo or a series of echoes may be represented in "speech-spectrogram" form as shown in figure 5.

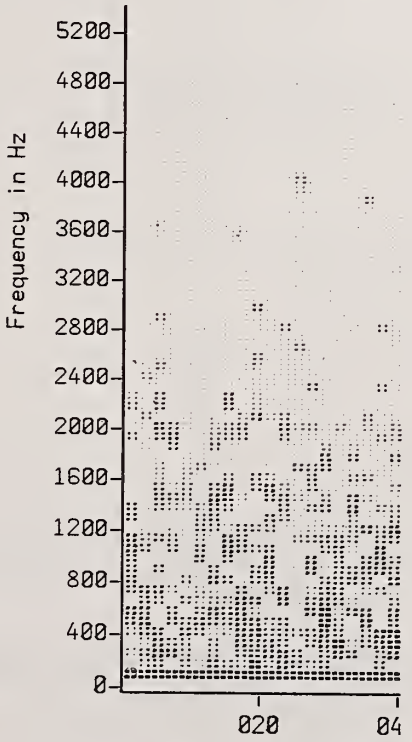

Figure 5. An ultrasonic A-scan time-series (obtained from Dr. R. A. Mountford, British Royal Infirmary, Great Britain) presented in speech spectrogram format for the purpose of applying speech analysis to medical ultrasonic pulse echoes.

Echoes in this form may be analyzed using "voiceprint" recognition techniques as pioneered by Kersta [11]. A single echo or a series of echoes may be converted to audible sound and analyzed by the most sophisticated of all acoustic pattern recognition systems, the human ear-brain complex. It is well known that the human cannot only recognize the well-enunciated speech of his fellows but also distinguish a wide variety of noises: the bark of a dog, the meow of a cat, the trill of a bird, the chirp of a cricket, etc. This may also be done (to some extent) by computer processing of the audible signal, as exemplified by the HEARSAY project at Carnegie-Mellon University [12]. But the ear-brain complex is more sophisticated than the computer and can also distinguish much more subtle features such as the bark of one (well-known) dog from a pack of the same species. Thus, it is logical to use the human ear-brain system in studies of A-scan time-series recognition. To do this, requires a careful selection of the transduction method employed to convert the string of binary words, which are the digital representation of the echo, into the audible signal or "enunciation" presented to the listener. Also, it would be particularly useful if the researchers were familiar with sonar, a field in which there are many skilled workers familiar with the problem of classifying undersea objects by listening to the pulse-echo signal.

Let us consider the characteristics of human speech and determine how the ultrasonic time-series may be treated as a speech signal. The power spectrum of human speech is shown in figure 6. As can be seen, the speech spectrum covers a range of 6 octaves (approximately 128 to 4096 Hertz) with the majority of the spectral energy concentrated in the two-octave region from 128 to 512 Hertz. In order to produce speech-like sounds in the familiar spectrum, it is necessary to shift the A-scan time-series both in frequency and time.

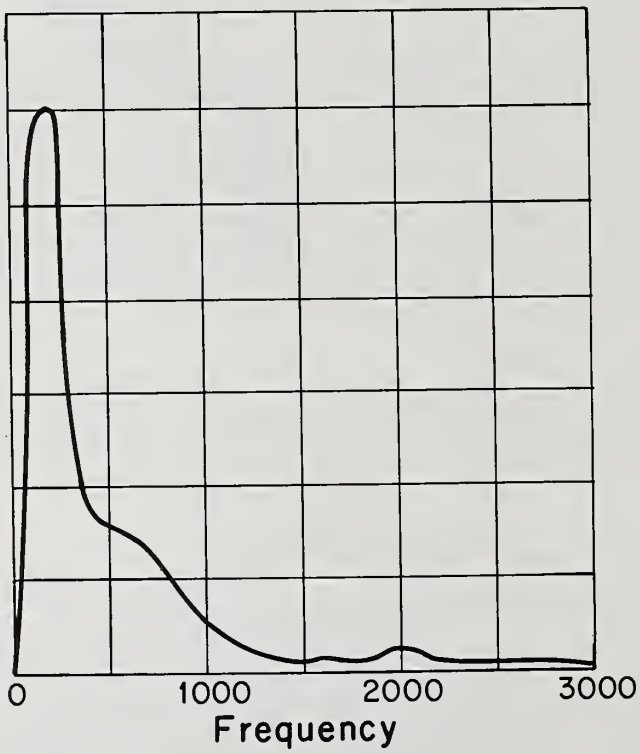

Figure 6. The power spectrum (Wiener spectrum) of male human speech.

Let us assume that there are N samples of the time-series. A Fourier analysis of this time-series will result in N spectral components of which the first is the value of the mean and, since the values of the time-series are real, only (N-1)/2 are significant in determining the amplitude and phase of the spectral components. Neglecting the mean value, we can then state that the time-series represents a signal occupying a number of octaves given by the equation:

$$n_{oct} = \log_2[(N-1)/2] \doteq \log_2(N/2) \tag{1}$$

For typical commercial time-series digitizers, the number N ranges from 128 to 1024 and therefore n_{oct} is between 7 and 10. The distribution of energy in the spectrum is unknown, but we can assume that it is not concentrated in the first 2 octaves. It is therefore likely that both frequency redistribution and time multiplication are necessary in translating the recorded time-series into the speech spectrum. If we assume that the Fourier analysis of the spectrum has produced the coefficients a_n and ϕ_n, then linear frequency translation leads to

$$s(t_k) = \sum_{n=1}^{n=N/2} a_n \cos\left[2\pi(f_c + \frac{n}{T})t_k - \phi_n\right] \tag{2}$$

where $s(t_k)$ is the frequency-translated signal sampled at time t_k, f_c is the "carrier" frequency, using the terminology of a single-sideband communications [13], and T is the enunciation time. If we let $f_c = c/T$, the number of octaves occupied by the signal expressed in the above equation is $\log_2(q+c)/c$ where $q = (N-1)/2$. Therefore, the number of octaves by which the original signal is reduced is given approximately by $\log_2 c$.

One of the first choices to be made, of course, is the value of the enunciation time of the "word" represented by the A-scan time-series. The other choice is of the quantity c which provides an approximation to the lowest frequency in the audible playback. This frequency is given by $(c+1)/T$. Table 1 provides enunciation times (in milliseconds) for many practical cases. The table gives the reader some idea as to the range of choices of enunciation times as a function of the lowest frequency, (f_c+1/T), of the audible signal as a function of the number of octaves present in the audible signal and the number of words in the original time-series.

Table 1. Enunciation Times for Linear Frequency Translation

		q = 64		q = 128		q = 512	
f_c(Hz)	n_{oct}	c	T(ms)	c	T(ms)	c	T(ms)
64	1	64	1000	128	2000	512	8000
	2	21	333	43	667	171	2667
	3	9	143	18	286	73	1143
128	1	64	500	128	1000	512	4000
	2	21	167	43	333	171	1333
	3	9	71	18	143	73	571
256	1	64	250	128	500	512	2000
	2	21	83	43	167	171	667
	3	9	36	18	71	73	286

LInear Frequency Translation (LIFT), as can be seen from table 1, exhibits a rapid decrease in the enunciation time as the number of octaves utilized are increased from unity. LIFT does not take into account the fact that the resolution of the human ear is logarithmic, not linear, and provides a nonuniform number of samples per octave. In the higher octaves, this produces more samples than the human ear can resolve. If we utilize the tonal scale common in Western music, then only 12 frequencies should be utilized per octave, independent of the octave selected. The resultant enunciation would be given by the equation:

$$s_{k+j-1} = \sum_{n=1}^{n=12n_{oct}} a_{nj}\cos\left[(1+\alpha)^{n-1} f_o t_{k+j-1} - \phi_{nj}\right] \qquad (3)$$

where f_o is comparable to the "carrier" frequency of eq. (1). The quantity α is 0.06, *i.e.*, one minus the 12th root of 2. This yields LOgarithmic Frequency Translation (LOFT) wherein the frequencies utilized are not harmonics. In determining the enunciation time, therefore, we can only approximate the situation treated in eq. (1) by defining a "pseudo-enunciation time" given simply by

$$T' = (0.06 f_o)^{-1} . \qquad (4)$$

Table 2 provides pseudo enunciation times in a format comparable to table 1.

Table 2. Pseudo-Enunciation Times for Logarithmic Frequency Translation

		q = 64	q = 128	q = 512
f_{min}(Hz)	n_{oct}	T(ms)	T(ms)	T(ms)
64	1	1000	2000	8000
	2	500	1000	4000
	3	333	667	2667
128	1	500	1000	4000
	2	250	500	2000
	3	168	333	1333
256	1	250	500	2000
	2	125	250	1000
	3	83	168	667

6. Illustrative Example

As part of the oral presentation of this paper, several audible playbacks were rendered which were generated from LIFT renditions of audible signals produced from recordings taken of ultrasonic pulse echoes from human liver *in vivo*.

References

[1] King, J. C. and Wang, A. K. C., Computer analysis of transcranial somotographic B-scans, *J. Comp. Biomed. Res.* 5, 190 (1972).

[2] Mountford, R. A. and Wells, P. N. T., Ultrasonic linear scanning: the quantitative analysis of the normal A-scan, *Phys. Med. Biol.* 17, 14 (1972).

[3] Mountford, R. A., *et al*, Ultrasonic linear scanning: automatic A-scan analysis, *Phys. Med. Biol.* 17, 559 (1973).

[4] Waag, R. C. and Gramiak, R., New concepts for acquiring, processing, and imaging cardiac data, in *Ultrasonics in Medicine*, M. de Vlieger, *et al.*, eds., p. 239 (Excerpta Medica, Amsterdam, 1974).

[5] Goldstein, A., University of Kansas (personal communication).

[6] Hall, E. L., Crawford, W. O., Preston, K., and Roberts, F. E., Computer classification of coal workers' pneumoconiosis, in *Proceedings of the 1st International Conference on Pattern Recognition*, p. 77 (Washington, D.C., 1973).

[7] Gericke, O. R., Defect determination by ultrasonic spectroscopy, *J. Metals*, 932 (1966).

[8] Lele, P. P. and Namery, Jr., Detection of myocardial infarction by ultrasound, in *Proceedings of 25th Annual Conference on Engineering in Medicine and Biology*, p. 135 (1972).

[9] Chivers, R. C., Hill, C. R., and Nicholas, D., Frequency dependence of ultrasound backscattering cross-section: an indicator of tissue structure characteristics, in *Ultrasound in Medicine*, M. de Vlieger, *et al.*, eds., p. 300 (Excerpta Medica, Amsterdam, 1974).

[10] Jones, J. P., Impediography: a new ultrasonic technique for diagnostic medicine, in *Proceedings of AIUM Fall Conference* (1974).

[11] Kersta, L. N., Voiceprints, Inc., N. J.

[12] Lesser, R. R., *et al*, Organization of the HEARSAY II speech understanding system, in *Proc. IEEE Symp. on Speech Recognition*, (Pittsburgh, PA, 1974).

[13] Taub, H. and Schilling, D. L., *Principles of Communications Systems*, Ch. 3 (McGraw-Hill, Inc., 1971).

National Bureau of Standards Special Publication 453. Proceedings of Seminar on Ultrasonic Tissue Characterization held at NBS, Gaithersburg, MD, May 28-30, 1975. (Issued Oct. 1976)

Paper 3.2: QUANTITATIVE A-SCAN ANALYSIS OF NORMAL AND CIRRHOTIC LIVER

P. N. T. Wells, R. A. Mountford,[1] M. Halliwell, and P. Atkinson

Department of Medical Physics
Bristol General Hospital
Bristol, BS1 6SY, United Kingdom

The development of quantitative methods of analyzing ultrasonic liver scans is reviewed. These methods are based on measurements of intrahepatic echo amplitudes or echo spacings. Simple techniques indicate that the echo amplitude tends to be increased in cirrhosis. Using a frequency of approximately 1-5 MHz, this was confirmed by computer analysis of the measurements of 100 consecutive cycles of the ultrasonic echo wavetrains in each of 30 separate scans from each of 30 individuals with normal livers, and 13 with cirrhosis. These data were acquired manually. In cirrhotics, the mean echo amplitude was 6 dB greater than in normals. Similar results were obtained with an automated system of data acquisition. The results are compatible with a model in which the observed structure is a random noise effect; the dimensions of the pulse determines the scale of the fluctuation which is observed. The echoes from cirrhotic liver, higher in amplitude but otherwise very similar to those from the normal, could be due to similar targets with greater characteristic impedance mismatches.

Key Words: A-scan; attenuation; computer analysis; impedance; liver cirrhosis; ultrasonics.

1. Introduction

Although the early literature refers to the visualization of liver abnormalities in two-dimensional B-scans [1-3],[2] the interpretation of these scans was left to the judgement of the observer. Likewise, the assessment of early A-scans was subjective [4]. The first quantitative approach to the possibility of distinguishing between normal and abnormal liver seems to be that of Schentke and Renger [5], who reported that both the mean echo amplitude and the echo frequency are increased in various abnormalities including cirrhosis. Following this, Wells, *et al.* [6] took up a suggestion made by Wild and Reid [7] in connection with the diagnosis of breast disease, and for a series of normal patients, and a series of patients with various liver abnormalities, they calculated an index

$$\sum_i h_i/T \ ,$$

[1]Department of Radiodiagnosis, Bristol Royal Infirmary, Bristol, BS2 8HW, United Kingdom.

[2]Figures in brackets indicate the literature references at the end of this paper.

where h_i is the amplitude of the i^{th} internal echo and T is the duration of the echo train subjected to analysis. For each individual, they used two demodulated A-scans made along different paths through the liver, and they standardized the system operating conditions, including swept gain rate and sensitivity. The positions of the A-scans were marked by intensifying the corresponding lines on two-dimensional compound B-scans made in the same subcostal planes, and echoes of large amplitude--supposed, probably often erroneously, to arise from the concave inferior surface of the liver--were "identified" on the B-scans, and the corresponding echoes were somewhat arbitrarily neglected in the A-scan analyses. The mean index for each abnormal liver was compared with the value for a corresponding normal control, and found to be greater in 25 out of 32 patients with cirrhosis.

A rather similar method of analysis was used by Czarnecki and Kubicki [8], who not surprisingly found that the diagnosis was more reliable, the more advanced the disease.

2. Quantitative Analysis of the A-Scan

Mountford and Wells [9,10] used a refinement of earlier methods of quantitatively analyzing the A-scan to determine variations in the echo amplitudes in normal liver and in cirrhosis, and to estimate the effective attenuation of ultrasound in the liver assuming a random spatial distribution of intrahepatic targets. They also investigated the effects of variations in the characteristics of the anterior abdominal wall, since it had been suggested by Wells *et al.* [6] that, at a frequency of 1.5 MHz, an increase of 10 mm in fat thickness might cause an increase of 0.5 dB in intrahepatic echo amplitude, while the same increase in muscle thickness might cause a decrease of 4.5 dB. The obliquity of the scan angle and the air bubble content of the pores of the skin, could also introduce errors.

A block diagram of the measuring apparatus is shown in figure 1. Provision was made for standardizing the system sensitivity, but this is not shown in the diagram. The pulse repetition rate was 1000 s^{-1}, and the transducer had a diameter of 20 mm, a zero-crossing frequency of 1.67 MHz, and a 20 dB bandwidth of 1.2 MHz. The field was reasonably regular at ranges beyond 50 mm. The waveform displayed on the cathode ray oscilloscope corresponded to echoes selected by the adjustable delay to have originated from the range interval commencing at 50 mm and extending to approximately 100 mm. The parts of the circuitry which processed this signal were linear. The conventional demodulated A-scan was presented on a second cathode ray tube, and with experience it was possible to be certain, by studying this display, that the ultrasonic beam was passing through the liver, and that the range interval 50-100 mm lay entirely within the liver.

For each individual examined, the cathode ray oscilloscope display was photographed 30 times, each with a new position of the probe. These photographs were analyzed by measuring the amplitude of each cycle from the peak to the succeeding trough. The measurements were begun at the graticule line corresponding to a range of 50 mm, and were repeated sequentially for 100 cycles. Generally, these cycles were regularly spaced, and occupied a range interval of about 47.5 mm. Each amplitude was measured to the nearest millimeter; the maximum amplitude which could be contained on the photograph was 56 mm, so that the maximum measurement precision was equivalent to a word length of between 5 and 6 bits. There were 3,000 data points for each individual.

Thus, each scan consisted of 100 data points. These data points may be regarded as samples of echo amplitude y at regular intervals of distance x. Therefore, for each individual, there were 100 x-values, each with 30 data point estimates of y. The analysis was based on the assumption that these echoes originated from targets within the liver, randomly distributed spatially.

Since the echo amplitude might be expected *a priori* to decay exponentially with range, then the regression of the logarithm of the mean values of the 30 data point estimates of y for each value of x (*i.e.*, $\ln \bar{y}$) against x should be linear. Moreover, the slope of the regression line should reflect the attenuation of ultrasound within the liver.

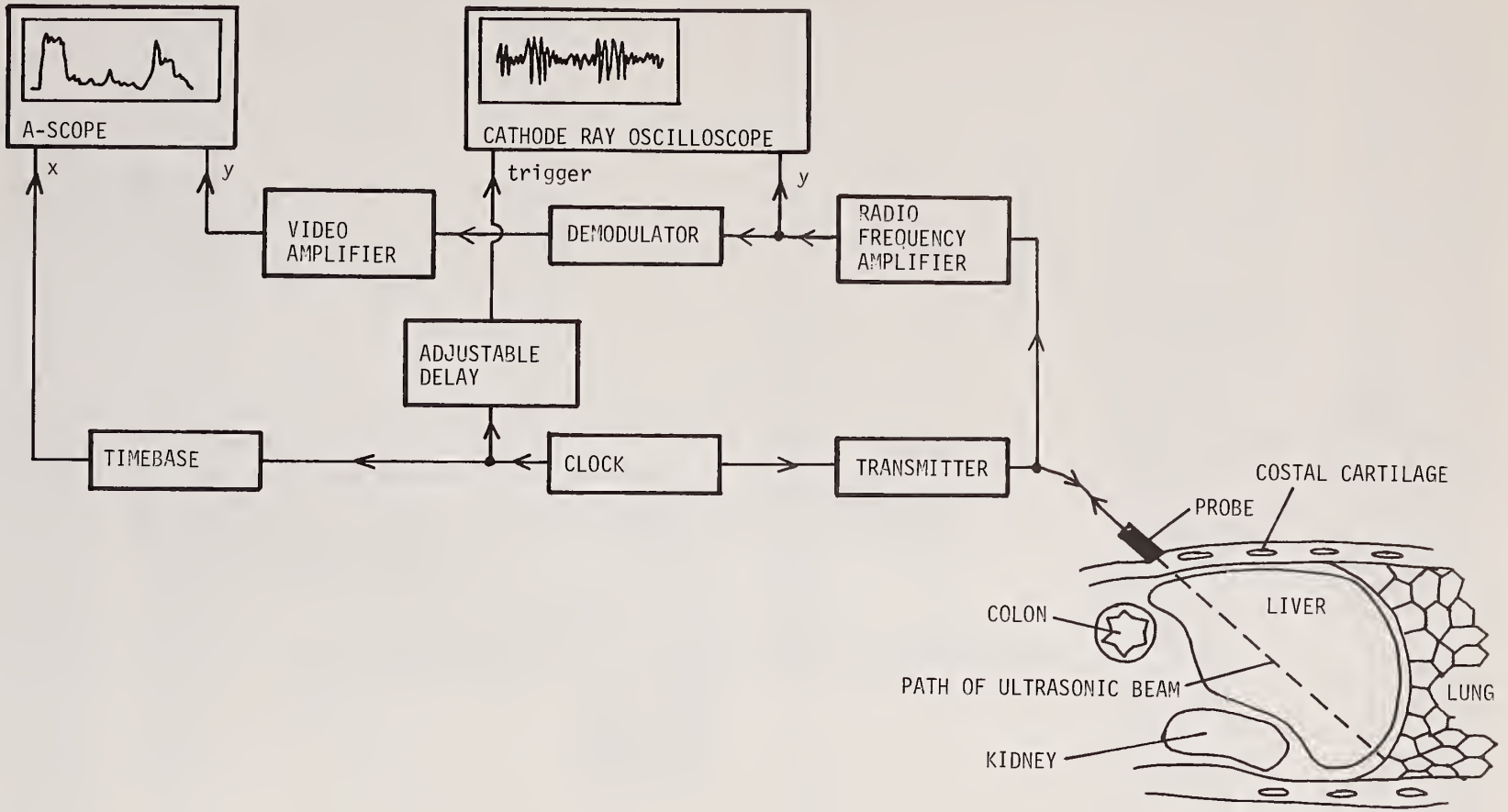

Figure 1. Block diagram showing the ultrasonic apparatus used by Mountford and Wells [9]. The position of the ultrasonic probe is illustrated by a longitudinal section through the right side of the patient, who is viewed from the left.

Thirty individuals with normal livers were studied [9]. Pooling the results for the whole groups revealed a very good linear relationship between ln y and x. Echo amplitude was approximately log-normally distributed about this line. The apparent attenuation rate of the pooled group was 1.76 dB cm^{-1}. Investigation of the echo amplitude values failed to confirm the anxiety of Wells *et al.* [6], referred to previously in this section, concerning the possible importance of variations in the characteristics of the body wall according to somatotype. On the contrary, individuals with high mesomorphy ratings tended to have higher echo amplitudes.

The results obtained with normal livers were compared with corresponding measurements in 13 patients with cirrhosis. The differences between the slopes of the regression lines were not significant (although generally the attenuation was lower in cirrhosis than in normals), but the echo amplitudes in the cirrhotics were always greater than those in the normals, the separation being greatest when the amplitudes corresponding to the ln y intercepts of the regression lines at x = 50 were compared. (In this scheme, x is the cycle number, and the limits of range of the sampled tissue are $0 < x < 100$.) This separation is illustrated in figure 2, and is equivalent to 6 dB.

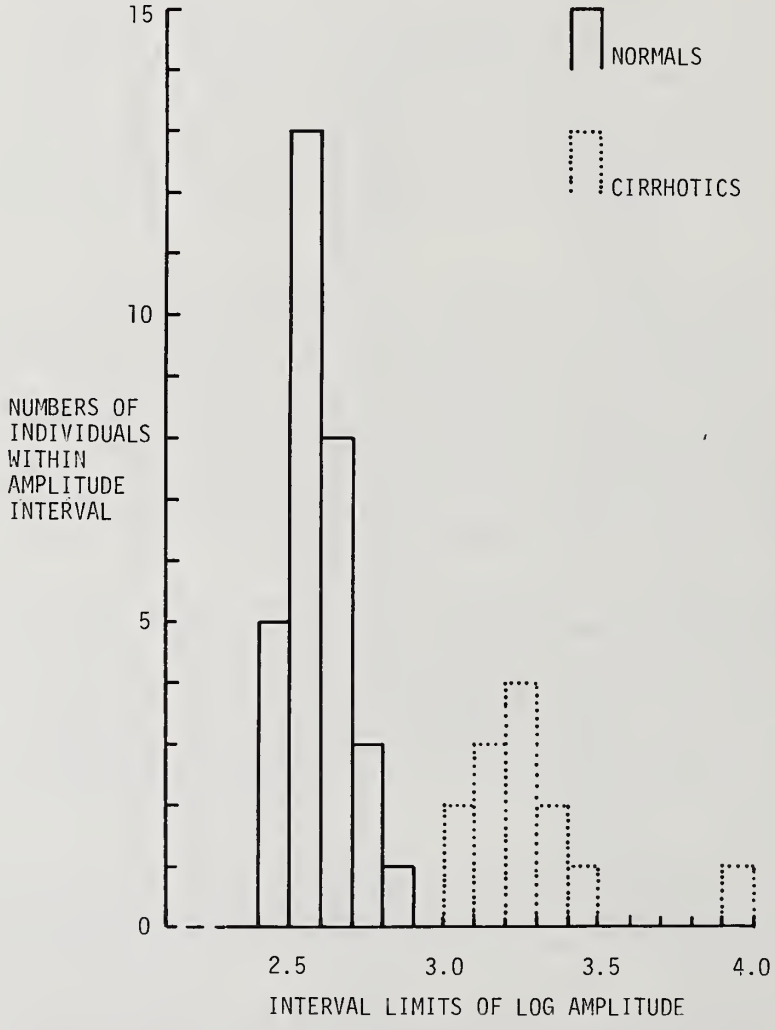

Figure 2. Histogram showing the distribution of midpoint amplitude (ln $\bar{y}$ at x = 50) for all 43 individuals in Mountford and Wells' [9,10] study. The absolute values of amplitude were determined by the conditions of measurement, but the data illustrate that the cirrhotic group does not overlap the normals. (From Mountford and Wells [10].)

For each individual set of data, the effect of the exponential regression was removed by adding the appropriate factor to each value of ln y. Consecutive values of ln y may be regarded as equidistant samples of the echo envelope. A typical result is given in figure 3. Averaging all the data in the normal group and in the cirrhotic group allowed the mean echo envelope shapes (trough-to-trough) to be compared, as shown in figure 4. In relation to the normals, the cirrhotics had significantly faster rise-times, and significantly fewer peaks and troughs.

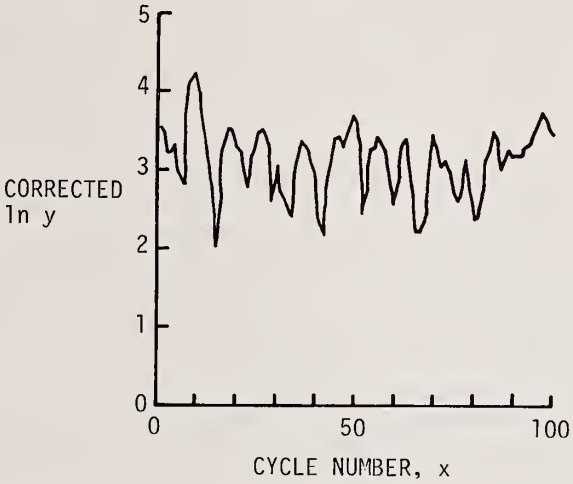

Figure 3. Typical graph (for one scan) of ln y, corrected for regression (mean value for 30 scans of the same individual). Normal liver. The corrections are referred to x = 0. (From Mountford and Wells [10].)

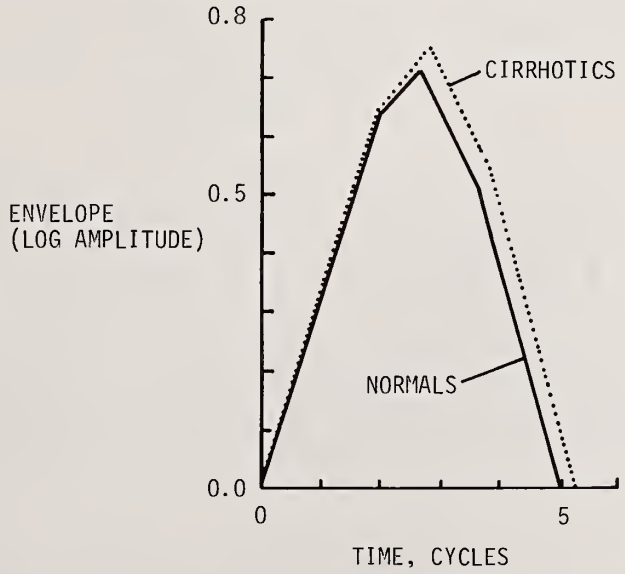

Figure 4. Mean echo envelope shapes for 30 normals and 13 cirrhotics. The envelope (log amplitude) is expressed in units of difference values in ln y. The time is expressed in units of cycles, one cycle corresponding to approximately 0.6 μs. (From Mountford and Wells [10].)

3. Automated Data Acquisition and Analysis

In the method of analysis described in the previous section, large numbers of measurements were made manually from the photographs of the scans, and these were punched onto cards for processing by computer. Four techniques of analyzing liver echograms, which avoid most of the drudgery of manual work, have been described.

Grossman [11] has developed an instrument, using analog circuits, in which the number of echoes occurring along a gated section of the A-scan is counted automatically. This does not seem to have been used clinically, nor would it be expected to be helpful since the echo frequency is not a good index of diffuse abnormality, nor can it be related to localized abnormalities unless it is presented as a pattern on a two-dimensional scan.

Two-dimensional grey-scale liver scans have been used by Rettenmaier [12] to identify appropriate areas of the image for analysis, the brightnesses of the intrahepatic diffuse echo patterns being correlated with clinical conditions. In relation to normals, scans of slightly fatty livers have lower brightness, while the brightness becomes increasingly greater in chronic hepatitis, moderately and severely fatty liver, and cirrhosis. To this extent, the method is similar to that of McCarthy *et al.* [13], who concluded from subjective comparisons of echo patterns that scans of cirrhotic livers were indistinguishable from those of normals made with an increase of 2.5 dB in system sensitivity. (Subsequently, Mountford and Wells [10] estimated this difference to be equivalent to 6 dB; see previous section.) Furthermore, Rettenmaier [12] estimated attenuation from the change in brightness with increasing range (using a parallel line scan pattern). Slightly fatty livers have lower attenuation than normals, and the attenuation becomes increasingly greater in chronic hepatitis, severe and moderately fatty liver, and cirrhosis.

Having similarly localized an area for analysis on a two-dimensional B-scan, Fields *et al.* [14] photographed a series of separate A-scans through this area. From the illustrations of their article, it appears that the demodulated A-scan was used. An image of this was projected onto a screen where the amplitudes and positions of the peaks were digitized with a GRAF/pen interfaced with a PDP-11 computer. They seem to have analyzed only six A-scans from each patient, and so it is hardly surprising that the standard deviations of their results were rather large.

Mountford *et al.* [15] automated the method used previously by Mountford and Wells [9,10]. Figure 5 is a block diagram of the arrangement. Again the system operated linearly at 1.5 MHz without swept gain, but the receiver output was demodulated before being digitized by a 128-word, 6-bit transient recorder. Satisfactory recording of the video waveform required a sampling frequency of 5 MHz, and this corresponds to about 25 μs of storage time, or a range of only about 20 mm in soft tissues. Since the earlier study had demonstrated that the analysis at a range of 75 mm was most efficient, it was arranged that the transient recorder commenced sampling after a delay of 85 μs corresponding to a range of about 65 mm. The data from a single A-scan having been stored in the transient recorder, the words were punched onto 8-column paper tape. Complete word sequences were separated by lengths of blank paper. The sequences were arranged in blocks of 30, each block representing a single set of measurements. Six blocks were collected for each individual studied. An individual could be examined in about 10 min.

The first 120 words in each sequence were used for analysis by an IBM 1130 computer with 16 K store. From each word, the mean recorded baseline level was subtracted to yield the true sample amplitude. Logarithms of these amplitudes were taken and a regression line was fitted by the method of least squares. The slope and midpoint amplitude of this line were calculated. Thus for each block, one value of slope and one of amplitude were calculated.

Ten individuals with normal livers, and three with cirrhosis, were examined using this method. At maximal inspiration, the mean amplitudes of the cirrhotic group were all greater than those of the normals, and there was no overlap between the two groups at the level of one standard deviation. With only one exception, the mean amplitudes of the normals fell as a result of inspiration.

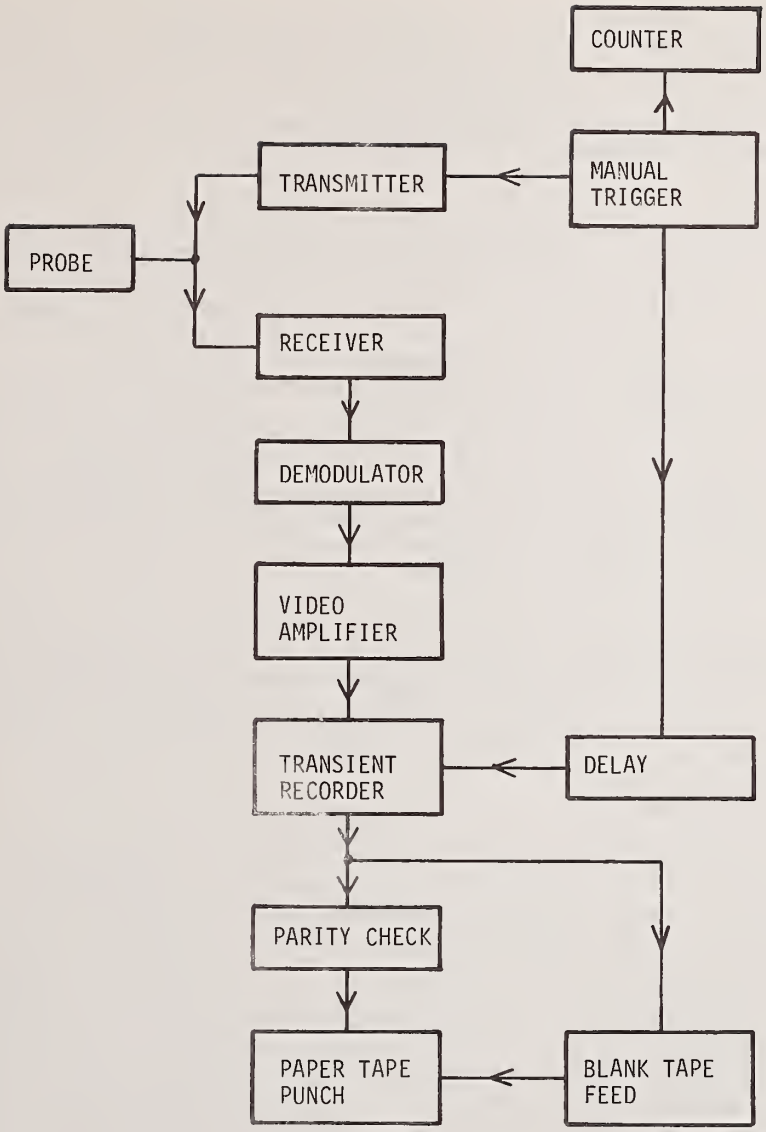

Figure 5. Block diagram of the automatic data analysis system (Mountford *et al.* [15]). The counter records the number of single shots which have been made in collecting the complete set of data. The circuit is arranged as a conventional A-scope while the operator is searching to satisfy the criteria of echogram acceptability.

The estimates of slope using the automated system were subject to rather large values of standard deviation. Doubtless, the chief cause of this was the relatively short length of data available for analysis.

4. Discussion

In an unlimited lossless homogeneous medium, the wave velocity $c = (K/\rho)^{\frac{1}{2}}$, where K is the bulk modulus, and ρ is the density. Furthermore, the characteristic impedance $Z = \rho c$. Combining these two equations yields the result $Z = (K\rho)^{\frac{1}{2}}$.

According to Fields and Dunn [16], the density variation of soft tissues is 1% or less. They concluded that it is variations in elasticity which largely account for

echoes from within soft tissue structures. (Note that the density of fat is 0.92 g ml^{-1}, and that of muscle is 1.07 g ml^{-1}; this is a difference of more than 15%. Moreover, the different constituents of tissue of the cellular level have a larger range of densities. Therefore, it may not be valid to neglect variations in density as contributors to echoes.) Collagenous fibers exhibit an elastic modulus greater by a factor of about 1,000 than that of other soft tissues, and they hypothesized that the amount of collagen may be the dominant factor in determining characteristic impedance. This could account for the observation of Fry *et al.* [17] that pig liver, with well-developed connective tissue between lobules, returns high-amplitude echoes, whereas echoes from cat liver, in which the connective tissue is poorly developed, are of low amplitude. Similarly, there is an increase in echo density in the post-menopausal breast [18], in which there is an increase in fibrous tissue in relation to the pre-menopausal breast. The data for liver cirrhosis are consistent with the finding of Boyett and Sullivan [19] that there may be a three-fold increase in collagen content in the disease. On the other hand, Rettenmaier [12] concluded that the high-amplitude echoes seen in cirrhotic liver should not be considered to result from an increase in connective tissue, because comparable echo amplitudes occur in high-degree fatty liver without essential fibrosis. He suggested that the pattern originates at the interfaces between hepatocytic plates and the fine vascular network. A similar mechanism was proposed by Mountford and Wells [10], who wrote that the echoes produced by cirrhotic liver, higher in amplitude but otherwise very similar to those of the normal, could be due to similar targets with greater characteristic impedance mismatches.

Although there are no sharp distinctions, biological targets may be considered to fall into three categories. The extensive boundaries of major structures and organs represent a large-obstacle situation: the reflection is specular at frequencies at which the surface irregularities are very small in relation to the wavelength. Subcellular, cellular and tissue structures are small in relation to the wavelength, and the scattering is a statistical function of both space and time. Thirdly, other biological targets lie between these two extremes.

The echo wavetrain received from liver tissue irradiated by a short ultrasonic pulse consists of cycles quite regularly spaced in time at a frequency corresponding to that of the ultrasonic pulse. The amplitude decays at a rate which is approximately exponential with range. At first sight, the echo amplitude spacing on the A-scan suggests that liver has a structure on the corresponding scale. While this might be the case, it would remain remarkable that there seems to be such a close relationship between the pattern and the wavelength, in terms of the regular cyclical spacing of successive peaks and troughs. The implication is that the observed structure is a random noise effect, in which the dimensions of the ultrasonic pulse determine the scale of the fluctuation which is observed. Considerable support for this theory exists in relation to the echoes from blood [20]. The situation in blood is certainly much less complicated than that in liver, which contains blood vessels and bile ducts of dimensions varying from the relatively large down to the cellular organization of the parenchyma. In liver, the echo is the sum of a great number of statistically-independent contributions, because there are many reflectors of very different shapes within the relatively large resolution cell. Moreover, in life, blood flow and other physiological movements change the target orientation so that the echo pattern fluctuates with time.

The method of Mountford and Wells [9,10] was not sensitive to echo shape, although, as mentioned in Section 2, it did show that the echo envelope has a significantly longer trough-to-trough duration in cirrhotics than in normals. This suggests that the actual target spacing may be slightly increased in cirrhosis--perhaps due to portal hypertension--and this may provide the basis for any success which might be achieved in liver tissue characterization in terms of measurements of the dependence of scattering on frequency or direction. These possibilities have been discussed by Hill [21], and in this connection it may be helpful to point out that all attempts at tissue characterization up to the present time seem to have been essentially two-dimensional. This paper deals mainly with measurements of amplitude with changing range at a particular frequency, or group of frequencies. Other investigators have studied velocity, absorption and dispersion: see, for example, Kossoff [22] and Wells [23]. Finally, the spectral studies of scattering are concerned with measurements, at a fixed range, of changes in amplitude either with frequency or with angle. Some of these approaches are more

promising than others; all have limitations. Some of the methods are capable of refinement: thus, areas of interest identified on two-dimensional scans could be subjected to numerical analyses. The time has now come to begin to use these various methods in parallel: for example, it might be useful to generate three-dimensional displays, illustrating the variation of the frequency spectrum with range. More generally, computer-based pattern recognition methods, now being developed in geophysics [24], could be used to identify the features which distinguish the echoes produced by different tissues.

We are grateful for grants from the Board of Governors of the United Bristol Hospitals, the Department of Health and Social Security, and the Medical Research Council.

References

[1] Howry, D. H., A brief atlas of diagnostic ultrasonic radiologic results, *Radiol. Clin. N. Am.*, 3, 433 (1965).

[2] Holmes, J. H., Ultrasonic diagnosis of liver disease, in *Diagnostic Ultrasound*, C. C. Grossman *et al.*, ed., p. 249 (Plenum Press, New York, 1966).

[3] Evans, K. T., McCarthy, C. F., Read, A. E. A., and Wells, P. N. T., Ultrasound in the diagnosis of liver disease, *Br. Med. J.*, 2, 1368 (1966).

[4] An, S., Wang, T., An, S., Chu, S., Wu, H., Hsü, C., and Yü, K., The use of pulsed ultrasound in clinical diagnosis, *Chin. Med. J.*, 81, 315 (1962).

[5] Schentke, K. U. and Renger, F., Uber die diagnostische verwertbarkeit des ultraschallhepatogramms, *Z. Ges. Inn. Med.*, 21, 239 (1964).

[6] Wells, P. N. T., McCarthy, C. R., Ross, F. G. M., and Read, A. E. A., Comparison of A-scan and compound B-scan ultrasonography in the diagnosis of liver disease, *Br. J. Radiol.*, 42, 818 (1969).

[7] Wild, J. J. and Reid, J. M., Further pilot echographic studies on the histologic structure of tumors of the living intact human breast, *Am. J. Path.*, 28, 839 (1952).

[8] Czarnecki, T. and Kubicki, S., Observations on the application of ultrasounds in the diagnosis of diffuse liver disease, *Pol. Med. J.*, 9, 79 (1970).

[9] Mountford, R. A. and Wells, P. N. T., Ultrasonic liver scanning: the quantitative analysis of the normal A-scan, *Phys. Med. Biol.*, 17, 14 (1972).

[10] Mountford, R. A. and Wells, P. N. T., Ultrasonic liver scanning: the A-scan in the normal and cirrhosis, *Phys. Med. Biol.* 17, 261 (1972).

[11] Grossman, H., Automatische echogrammauswertung bei der ultraschall-leberdiagnostik, *Nachrichtentechnik*, 21, 64 (1971).

[12] Rettenmaier, G., Quantitative criteria of intrahepatic echo patterns correlated with structural alterations, in *Ultrasonics in Medicine*, M. de Vlieger *et al.*, ed., p. 199 (Excerpta Medica, Amsterdam, 1974).

[13] McCarthy, C. F., Read, A. E. A., Ross, F. G. M., and Wells, P. N. T., Ultrasonic scanning of the liver, *Quart. Med. J.*, 36, 517 (1967).

[14] Fields, S. I., Bowie, J. D., Pai, A. L., and Lichtor, J. L., Tissue differentiation by semi-automated quantitative analysis of A-scan echography, in *Ultrasound in Medicine*, Vol. 1, D. N. White, ed., p. 439 (1975).

[15] Mountford, R. A., Halliwell, M., and Atkinson, P., Ultrasonic liver scanning: automated A-scan analysis, *Phys. Med. Biol.*, 18, 559 (1973).

[16] Fields, S. and Dunn, F., Correlation of echographic vizualizability of tissue with biological composition and physiological state, *J. Acoust. Soc. Am.*, 54, 809 (1973).

[17] Fry, E. K., Okuyama, D., and Fry, F. J., The influence of biological and instrumentation variables on the characteristics of echosonograms, in *Ultrasonographia Medica*, J. Böck, *et al.*, ed., Vol. 1, p. 387 (Wiener Medizinischen Akademie, Vienna, 1971).

[18] Fry, E. K., Kossoff, G., and Lindeman, H. A., The potential of ultrasound vizualization for detecting the presence of abnormal structures within the female breast, *Proceedings of IEEE Ultrasonics Symposium*, p. 25 (IEEE Cat. No. 72CHO 708-8 SU, IEEE, New York, 1972).

[19] Boyett, J. D. and Sullivan, J. F., Zinc and collagen content of cirrhotic liver, *Am. J. Dig. Dis.*, 15, 797 (1970).

[20] Atkinson, P. and Berry, M. V., Random noise in ultrasonic echoes diffracted by blood, *J. Phys. A*, 7, 1293 (1974).

[21] Hill, C. R., Interactions of ultrasound with tissues, in *Ultrasonics in Medicine*, M. de Vlieger *et al.*, ed., p. 14 (Excerpta Medica, Amsterdam, 1974).

[22] Kossoff, G., Progress in pulse-echo techniques, in *Ultrasonics in Medicine*, M. de Vlieger *et al.*, ed., p. 37 (Excerpta Medica, Amsterdam, 1974).

[23] Wells, P. N. T., Absorption and dispersion of ultrasound in biological tissues, *Ultrasound Med. Biol.*, 1, 369 (1975).

[24] Pace, N. G., Sediment identification using acoustic techniques, in *Ultrasonics International 1975 Abstracts*, p. 20 (IPC Science and Technology Press, Guildford, 1975).

National Bureau of Standards Special Publication 453. Proceedings of Seminar on Ultrasonic Tissue Characterization held at NBS, Gaithersburg, MD, May 28-30, 1975. (Issued Oct. 1976)

Paper 3.3: DIGITAL A-SCAN ANALYSIS IN THE DIAGNOSIS OF CHRONIC SPLENIC ENLARGEMENT

K. J. W. Taylor

Yale University School of Medicine
New Haven, Connecticut 06510

and

J. Milan

Department of Physics
Royal Marsden Hospital and Institute of Cancer Research
Sutton, Surrey, United Kingdom

Before the availability of grey-scale ultrasound machines, signal processing only permitted the display of the layer echoes which were specularly reflected at large discontinuities of acoustic impedance. The enhanced signal-to-noise ratio inherent in the grey-scale technique permits, in addition, the display of the internal structure of soft tissue. The amplitude of these low-level echoes is relatively independent of beam orientation and appears to be more dependent on the nature of the interface so that the pattern of the tissue may be specific to each pathology. From clinical observations, high-level echoes are usually associated with benign causes of splenic enlargement, while cellular infiltration, as in many malignancies, results in decreased echo amplitude. Digital A-scan analysis concerns and quantitates this difference.

Key Words: A-scan analysis; digital; grey-scale ultrasound; spleen; splenomegaly.

1. Introduction

An important feature of recent developments in grey-scale ultrasonography is the retention and display of low-amplitude echo information [1][1]. Conventional machines, developed mainly for displaying specular echoes originating at large discontinuities of acoustic impedance such as the fetal skull or placental/fluid interfaces, reject low-level echoes as "noise" or "grass" either in the signal processing or display system. Indeed, the disparity between the range of echoes from tissues and the dynamic range of the display systems makes it easier to suppress the smaller echoes, thereby decreasing the range for display.

Conventional systems largely involve the display of specular echoes and the quantitative analysis of these is unlikely to be informative on the nature of the tissue being interrogated. This is because the amplitude of specular echoes largely depends upon the rather random orientation of the reflecting surface with respect to the beam and this, in turn, is markedly affected by the scanning technique of the operator and the degree of compounding involved.

However, although the precise mechanisms involved are far from clear, the physical principles pertaining to the low-level echoes displayed in grey-scale ultrasonography appear to be different from those pertaining to specular reflections. The grey-scale technique involves the selective amplification of low-level echoes and these appear to be much less

[1]Figures in brackets indicate the literature references at the end of this paper.

dependent on the angle of incidence. Although these may be backscattered echoes, it is also possible they could be specular ones from small, spherical reflectors which would thus be more omnidirectional. Whatever the mechanism, the important conclusion is that the amplitude of these low-level echoes that are retained and displayed in grey-scale techniques are relatively independent of the orientation of the beam and this raises the possibility that the echo amplitude is mainly dependent upon the nature of the interface and hence on the consistency of the tissue. In this situation, an analysis of the amplitude of echoes arising from tissues could produce quantitative data which may have diagnostic value. There is considerable clinical and empirical evidence to encourage this view; from the B-scan display, it is known that in some clinical conditions such as cirrhosis of the liver and other states producing an increased fibrous content of the liver, brighter echoes are produced. Mountford and Wells [2] quantitated the echoes emanating from cirrhotic livers and found them to be significantly higher than those from normal livers. This raises the possibility of identifying certain disease states from the echo amplitude returned and, by serial scanning, to produce an objective measure of progressive pathology. Such data would be of great interest in monitoring industrial exposure to a wide variety of potentially hepato-toxic chemicals.

Before considering the means of digital A-scan analysis, it is interesting and of great importance clinically in connection with interpretation of scans, to consider the possible sites of echo formation and how the echo amplitude may vary with the nature of the interface. The classical formula for the magnitude of the reflected component R of an incident ultrasound beam is:

$$R = \frac{\rho_1 C_1 - \rho_2 C_2}{\rho_1 C_1 + \rho_2 C_2} \qquad (1)$$

where ρ_1, ρ_2 are the densities and C_1, C_2 the velocities of sound in the media at the interface. Fields and Dunn [3] pointed out that this expression made it difficult to account for the magnitude of the reflected component, since, to a first approximation, there is little variation in the velocity of sound in different soft tissues. Thus, a possible site of echo formation becomes more apparent if the expression:

$$C = \sqrt{\frac{B}{\rho}}$$

is substituted in Eq. (1). Thus, assuming little variation in density between the different tissues,

$$R \cong \left(\frac{B_1^{\frac{1}{2}} - B_2^{\frac{1}{2}}}{B_1^{\frac{1}{2}} + B_2^{\frac{1}{2}}} \right) \qquad (2)$$

where B_1 and B_2 are the bulk moduli of the media at the interface. Fields and Dunn [3] examined the figures available for the bulk moduli of various soft tissues and found that these did vary by several orders of magnitude. In particular, tissue elements of a supporting nature, such as collagen and elastin, could constitute a major site of echo formation.

This is consistent with past clinical observations and those reported in this paper. When a tumor replaces the normal fibrous skeleton of an organ, a defect is apparent in the normal anatomy while various causes of increased fibrous tissue within the liver, such as inflammatory states and the rare, successfully treated metastases, produce increased echo amplitudes [4,5].

This concept is also supported quantitatively by the work of Mountford and Wells [2] who reported that the amplitude of echoes from the livers of patients with cirrhosis were significantly higher than those with normal livers. This quantitated past clinical observations on the ultrasonic appearance of cirrhosis [6,7]. However, it seems unlikely that all data on echo amplitude can be ascribed merely to the supporting tissue content and indeed we have noted that fatty infiltration is also associated with high-level echoes but in a recognizably different pattern from those seen in established cirrhosis or chronic inflam-

matory states. It, therefore, appears that the spatial distribution of echoes is of equal importance to the amplitude of echoes in the differential diagnosis of liver disease. Such pattern recognition is easier for the trained diagnostician whose interpretation at present is superior to that obtained by computer technology. Interest is focused on the spleen as an experimental model, since the pattern seems relatively constant in different pathologies while the relative echo amplitude permits differentiation of various pathologies.

The clinical results obtained on ultrasound scanning of enlarged spleens were reported by Taylor and Milan [8]. They found that of 30 large spleens returning very low-level echoes, all were malignant (either leukemias or lymphomas). Conversely, of nine spleens returning very high-level echoes, six were chronic inflammatory states and hence contained abnormal amounts of fibrous tissue, while two of the remaining three were benign causes of splenic enlargement in patients with malignancy elsewhere. Furthermore, one of these was found in a myeloproliferative disorder in which excessive collagen is present in the spleen. Thus, in pathologies in which an increase of fibrous tissue could be expected, there were high-level echoes, while abnormal cellular masses were characterized by echoes of similar or lower amplitude than the normal spleen. A third intermediate group was also described, again largely benign, in which the amplitudes of the echoes returned lay between the two previous groups--the commonest disease in this group was splenic enlargement due to cirrhosis of the liver with consequent portal hypertension. Digital analysis was undertaken on these groups of patients to confirm and quantitate these clinical observations. The method and the preliminary results are reported here.

2. Method

The equipment used in these studies was custom-built [9] on the principles described by Kossoff [1]. The resulting scans have markedly more signal-to-noise ratio than conventional equipment available and to date it is not clear whether the commercially-available grey-scale systems are equally suitable for this examination. The ultrasound equipment was used to produce a B-scan display of the spleen by scanning either longitudinally, transversely or obliquely, depending on the size of the spleen. The computer was then switched on-line and the scan repeated. During this process, the signals from the scanner were digitized and stored in a Digital Equipment Corporation PDP 8/E computer, which had 12 k words of memory and 1.6 M word magnetic disc.

In order to produce standardized data when the computer was on-line, a constant tissue absorption correction was maintained, no attenuation was used, and the echo signal range was compressed by means of a full-range logarithmic amplifier. The output from this was processed by means of a peak detector and 128 samples of each A-scan contributing to the B-scan display were digitized to a precision of 6 bits. The signals from the positional potentiometers were digitized separately to a precision of 12 bits and both sets of data were stored on the magnetic disc in real time.

When the scan was complete, the data stored on the disc were processed to produce a B-scan display on a color television display system. This display has a resolution of 96 x 96 points and uses the temperature scale (red-orange-yellow-white) to represent echo amplitude [10]. An advantage of such a color scheme is that half-tone photographs are meaningful. A facility was provided in the processing program to superimpose on the display a pair of crosswires which were positioned to delineate a particular area of interest. The data stored on the disc were then processed to extract quantitative information on all the echoes within the delineated area. The mean and standard deviation of echo size were calculated and a histogram produced of echo amplitude against frequency of occurrence.

3. Results

Typical results of the B-scans in the three groups of patients are shown in figures 1, 2, and 3. Figure 1 shows moderate enlargement of the spleen while the consistency returns very low-level echoes which, with the present signal-to-noise ratio, cannot be reliably distinguished from the normal consistency. In both situations, the echoes are too low to be recorded although this will obviously vary with the machine settings, and in particular, with the type of equipment used. However, with the same equipment settings, there is an obvious difference between the brightness of the echoes seen in figure 1 from those seen in figures 2 and 3. Figure 2 is a case of non-tropical splenomegaly--a benign

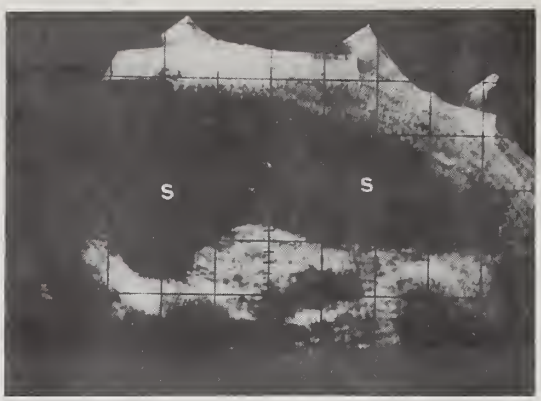

Figure 1. Oblique ultrasonogram of enlarged spleen (S) which appears black indicating that very low level echoes emanate from within it. This was an acute leukemic spleen.

Figure 2. Transverse ultrasonogram of spleen (S) lying to the left of the vertebra (V) and an enlarged splenic artery (a) is seen. Note the medium level echoes which are found in benign conditions and in this patient was due to non-tropical splenomegaly.

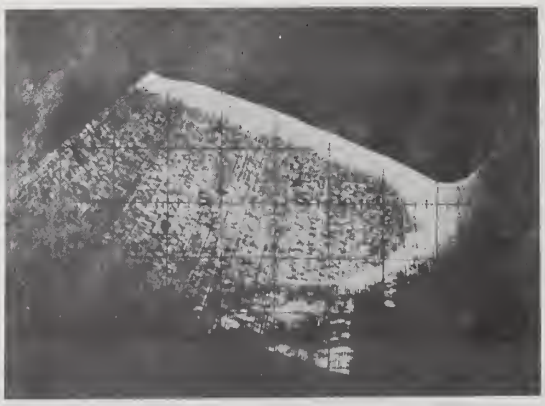

Figure 3. Longitudinal scan of spleen (S) showing very high-level echoes from within it so that the consistency appears white. This patient suffered from a chronic inflammatory state.

condition--while figure 3 shows the scan of the patient with tuberculosis and the very high-level echoes are apparent on the brightness-modulated scan.

The digital analysis permits these results to be substantiated and quantitated without operator bias or modification by equipment settings. The histogram corresponding to figure 1 is shown in figure 4, which confirms that low-level echoes are produced. Figure 5 is the histogram obtained from the type of splenic consistency displayed in figure 2 when intermediate echoes are obtained. The apparent bimodal distribution on the histogram we believe to be due to the lower tail of the Gaussian curve appearing in the first bin because of insufficient signal-to-noise ratio. Figure 6 is striking since the echo amplitudes in this case are of a similar magnitude to those seen in cirrhosis of the liver using this equipment. Thus, the difference between most malignant consistencies are vastly different from those seen in most of the benign causes of splenic enlargement. Although this is apparent on the B-scans, the difference can be confirmed and quantitated by this technique, free of operator bias.

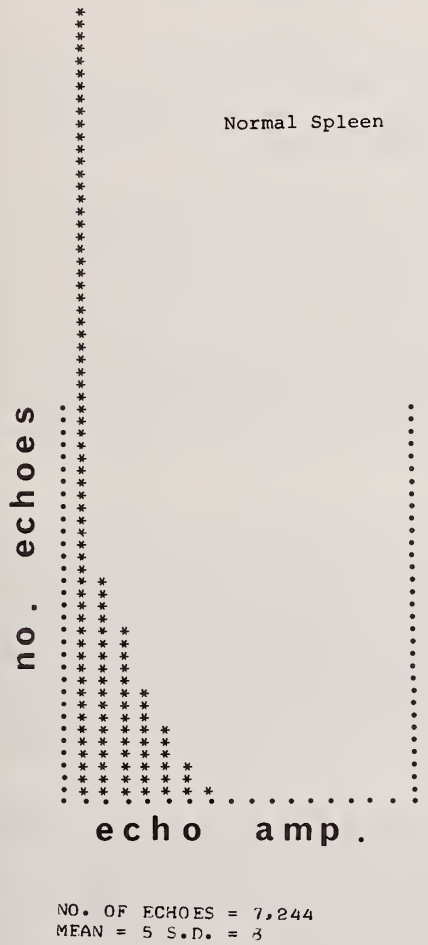

Figure 4. Histogram of echo amplitudes corresponding to the spleen shown in figure 1.

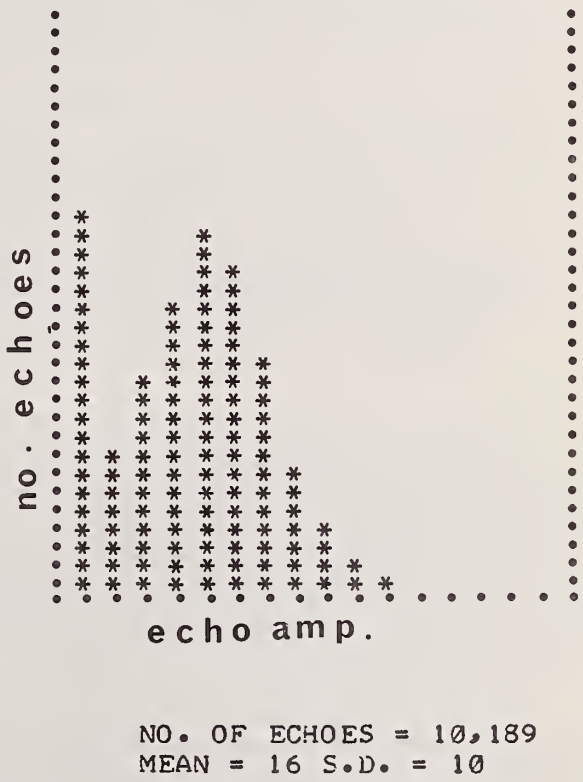

Figure 5. Histogram of echo amplitude corresponding to the spleen seen in figure 2.

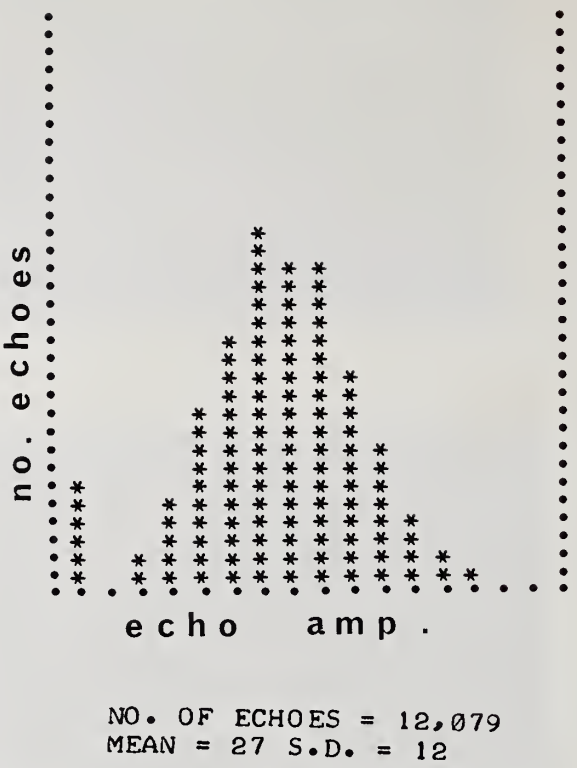

Figure 6. Histogram of echo amplitudes corresponding to the spleen seen in figure 3. Note the progressive shift towards the right in these three figures.

4. Discussion

The main value of a computer system such as we have described here is that it may be used to provide objective information about echo signal strength. The mean amplitude of the echoes from the splenic tissue will depend partly upon the pathological state in a particular patient and partly upon other factors, including the quantity and nature of the tissue between the analyzed area of the spleen and the transducer in contact with the patient's skin. The passage of the beam through the intervening tissue may cause significant variations within groups of normal or abnormal patients and thus, although the mean echo amplitude is a useful aid to the diagnosis of gross abnormalities, it is of less value when the abnormalities are slight.

However, in individual cases, the factors other than splenic pathology which contribute to variations in echo amplitude may be expected to remain relatively constant with respect to time so that small variations in echo intensity may be significant. For example, we have noted that successful and energetic treatment of the leukemias is frequently accompanied by an apparent increase in the low-level echoes which is more marked in the deeper tissues (fig. 7) due to depth-attenuation compensation. This may provide an objective means for monitoring response to treatment. A similar change may be found in the liver when there appears to be an increase in echo amplitude in response to therapy. Such a change may precede the clinical improvement in the patient's involvement by malignancy [5] There are further possibilities in monitoring progressive liver damage occurring through social exposure to alcohol or industrial exposure to hepato-toxic agents such as vinyl chloride. There is also evidence that grey-scale ultrasonography may be valuable in the latter respect [11].

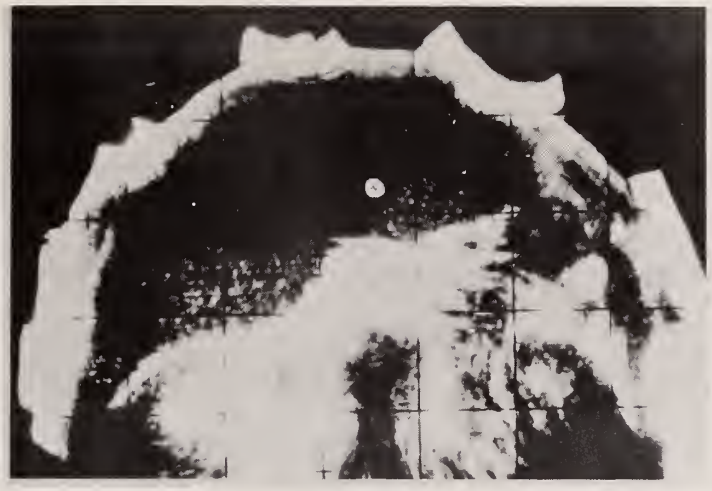

Figure 7. Longitudinal scan of spleen in chronic lymphatic leukemia after extensive treatment. Low-level echoes are apparent compared with figure 1 and these are accentuated by the depth-attenuation correction (TGC). Thus, effective treatment of malignancies may cause some increase in echo amplitude towards medium-level echoes.

The histograms in figures 4 through 6 show wide standard deviations. Despite this, given a sufficiently large sample, small differences in mean amplitude will nonetheless be significant. However, the versatility of the technique would be extended if the standard deviation could be reduced. In this preliminary work, in which we were not able to digitize in real time, much of the variation apparent in the histograms is due to the digitization process rather than variations in echo amplitude. Improvements in the digitization technique, currently under development, will produce true histograms of echo intensity and also allow comparison of different sections of the same A-scan. The latter will be the first step towards recognizing changes in the patterns as well as changes in intensity which occur with progressive pathology in soft tissues.

References

[1] Kossoff, G., Display techniques in ultrasound pulse echo investigations: a review, *J. Clin. Ultrasound*, 2, 61 (1974).

[2] Mountford, R. A. and Wells, P. N. T., Ultrasonic liver scanning: the A-scan in the normal and in cirrhosis, *Phys. Med. Biol.* 17, 261 (1972).

[3] Fields, S. and Dunn, F., Correlation of echographic visualizability of tissue with biological composition and physiological state, *J. Acoust. Soc. Am.*, 54, 809 (1973).

[4] Taylor, K. J. W., Carpenter, D. A., McCready, V. R., Grey-scale echography in the diagnosis of intrahepatic disease, *J. Clin. Ultrasound*, 1, 284 (1973).

[5] Gilby, E. D. and Taylor, K. J. W., Ultrasound monitoring of hepatic metastases during chemotherapy, *Brit. Med. J.*, 1, 371 (1975).

[6] Holmes, J. H., Ultrasonic diagnosis in liver disease, in *Diagnostic Ultrasound*, C. C. Grossman, J. H. Holmes, C. Joyner, and E. W. Purnell, eds., p. 249 (Plenum Press, New York, 1966).

[7] Holm, H. H., Ultrasonic scanning in the diagnosis of space-occupying lesions of the upper abdomen, *Brit. J. Radiol.* 44, 24 (1971).

[8] Taylor, K. J. W. and Milan, J., Differential diagnosis of chronic splenomegaly: clinical observations and digital A-scan analysis, *Brit. J. Radiol.* (in press).

[9] Hill, C. R. and Carpenter, D. A., Ultrasonic echo imaging of tissue: instrumentation, *Brit. J. Radiol.* (in press).

[10] Milan, J. and Taylor, K. J. W., The application of the temperature colour scale to ultrasonic imaging, *J. Clin. Ultrasound*, 3, 171 (1975).

[11] Taylor, K. J. W., Williams, D. M. J., Smith, P. M. and Duck, B., Grey-scale ultrasonography for monitoring industrial exposure to hepato-toxic agents, *Lancet*, 1, 1222 (1975).

CHAPTER 4

ATTENUATION AND VELOCITY TECHNIQUES

National Bureau of Standards Special Publication 453. Proceedings of Seminar on Ultrasonic Tissue Characterization held at NBS, Gaithersburg, MD, May 28-30, 1975. (Issued Oct. 1976)

CHAPTER 4. ATTENUATION AND VELOCITY TECHNIQUES

Paper 4.1: ATTENUATION AND VELOCITY MEASUREMENTS IN TISSUE USING TIME DELAY SPECTROMETRY

D. H. Le Croissette and R. C. Heyser

Jet Propulsion Laboratory
California Institute of Technology
Pasadena, California 91103

A practical ultrasound system is described which is capable of making measurements of attenuation and velocity in tissue as a function of frequency. This method is based upon a technique known as Time Delay Spectrometry which employs a swept frequency signal and has the ability to provide anechoic ultrasonic measurements. A system operating between 2 and 3 MHz has already been shown to be capable of producing images in soft tissue with a resolution of less than 2 mm. Preliminary measurements on excised tissue using this system have indicated a frequency dependence of attenuation in pathological tissue that is substantially different from that of normal tissue. The method generates the time domain response simultaneously with the received frequency sweep. It is shown that the time response in the apparatus is available as a displayed phasor quantity and that the arrival time of the directly-received signal can therefore be measured to within a few nanoseconds.

Key Words: Attenuation; phase; swept frequency; time delay spectrometry; tissue; transmission; velocity.

1. Introduction

The possibilities of using ultrasound measurements for detection and identification of the pathological state of soft tissue have recently received attention [1-5],[1] although the feasibility of the concept has been shown much earlier [6]. There are a number of ultrasonic transmission and reflection characteristics which might give information concerning the pathological or morphological status of tissue. If one or more of these can be identified, the tissue can be said to have a signature. In this paper, the following definition will be made.

SIGNATURE - The set of identifiable properties or attributes that places one thing apart from another.

Tissue characteristics that might produce signature data are listed in Table 1 [3].

Table 1. Tissue Characteristics That Might Produce Signature Data [3]

Reflectivity
Absorptivity
Scattering parameters
Propagation velocity
Specific acoustic impedance
Density.

[1]Figures in brackets indicate the literature references at the end of this paper.

Although medical ultrasound in the pulse-echo reflection mode has been used for diagnosis for more than twenty years, there is not a great deal of knowledge of the characteristics listed above. There are several reasons for this. First, many of the quantities vary widely with age, sex and physical condition of the subject. Secondly, the measurements are difficult to make accurately with most of the existing equipment. Thirdly, absorption and scattering, which together constitute attenuation, are difficult to separate in conventional measurements. Lastly, and perhaps the most important factor to date, there has so far been little need expressed for an accurate measure of these quantities in the design and operation of pulse-echo diagnostic ultrasound imaging devices.

If tissue identification is to become a reality, signature identifiers must be found and enough data gathered for confidence to be established in the method. At the present time, some well-known identifiers are already being used in a subjective manner by ultrasonographers in clinical practice. The recognition of these characteristic signatures is based upon years of clinical experience in interpreting ultrasonograms. Scientific measurements on which interpretations can be based, however, are lacking.

One of the principal uses of ultrasound in providing tissue identification at the present time is in the differentiation of solid and cystic masses. In general, a cystic mass may be recognized by the absence of echoes as the receiver sensitivity is increased. By contrast, solid masses are not sonically homogeneous and show an abundance of echoes. This method is not completely reliable, however, as discussed by Birnholz [7], who shows that solid but cellularly-homogeneous masses may be confused with cysts using this criterion.

Two other methods are used to identify a homogeneous tumor mass. Both rely upon the known higher attenuation of sound in tumor tissue versus the minimal attenuation in a fluid-filled cyst. The two methods are (1) to observe whether there is "shadowing" in the image behind the mass which, if present, indicates that a substantial fraction of the energy is attenuated, and (2) to observe the ratio of the amplitudes of the reflection from the front and back surfaces of the mass as given on an A-scan trace.

In all three of these methods, the presence of the mass, whether cystic or solid has first to be observed in the B-scan image. Thus, a mass which has dimensions less than the resolution of the system (typically 10 mm) is unlikely to be noticed. Furthermore, the presence or absence of a solid tumor or cyst is inferred from a secondary measurement such as loss of energy with distance in the ultrasonic beam. The diagnosis is therefore critically dependent on the skill and experience of the ultrasonographer/physician.

In order to distinguish one tissue from another, it is necessary to be able to identify characteristics in the signature that can be correlated with the type or status of the tissue. In the pulse-echo systems presently available, the signal processing through the system allows very few signal characteristics to be retained in the final image. In a bistable imaging system, only the presence of an echo above the threshold level can be detected. In a system which displays a grey-scale image, there is amplitude information on the echo returns but nothing more. Any changes in shape of the returning pulse, indicating frequency or phase changes in transit or upon reflection, are lost. Furthermore, signal shaping to give some edge enhancement occurs in most units. The emphasis is placed on producing a clear, sharp picture even at the expense of losing information.

The shape of the transmitted pulse in a commercial pulse-echo system is mainly determined by the characteristics of the transducer. Since the primary object in current pulse-echo systems is time discrimination, the transducer is heavily damped to produce a short pulse and no attempt is made to control the frequency spectrum. As the ultrasonic energy travels through soft tissue, it suffers attenuation which increases with frequency. As the path length increases, the total attenuation is increased and the relative reduction in the high-frequency components is greater. In the time domain, the pulse broadens and its amplitude decreases. In a typical pulse-echo system, therefore, the propagating signal decreases in amplitude, the pulse width broadens and the high-frequency components preferentially diminish along the path.

Although the pulse-echo system does not seem to be the optimum method for obtaining tissue characteristic information, it may be used for this purpose. This may be done by comparing the received pulse with the transmitted pulse and so determine the transfer function of the medium, including reflection from a tissue boundary if that occurs. The correlation of this with the morphological or pathological state of the tissue will allow the signature characteristic to be determined.

Since there is a considerable amount of signal processing carried out after the signal is received back at the transducer in a commercial pulse-echo system, a conventional ultrasonic unit cannot be used for this measurement without considerable modification. It is necessary to obtain the raw transducer output before processing has taken place. Comparison and analysis of the signals can then be made bearing in mind that the shape of the pulse is determined, in practice, by the transducer characteristics which are normally selected for high spatial acuity only. A computer analysis of the data will probably be required because of the need for sampling and conversion of the inputs into other formats.

Measurements of some tissue properties (velocity, attenuation, etc.) have also been made at a number of discrete frequencies using continuous-wave techniques. These measurements, although useful, have suffered from the problems of reverberation, unwanted echoes, standing waves, etc. There is no way of distinguishing among any one wave in a continuous wave train of single frequency and so it is difficult to select only the direct signal. To use the continuous-wave technique successfully, an anechoic method is required which has the capability of making measurements over the frequency range of interest in medical ultrasound. A method of this type was devised in 1967 by Heyser [8] to make anechoic acoustical measurements on audio transducers. This system overcomes most of the usual problems encountered with continuous-wave systems. It employs a swept-frequency measuring technique called Time Delay Spectrometry [9]. The method will be only briefly outlined here since its adaptation to medical ultrasound systems has been published elsewhere [10].

2. Time Delay Spectrometry (TDS)

The system presently in use at JPL utilizes an ultrasonic transmission signal repetitively swept in a linear manner from 3 to 2 MHz approximately 25 times per second. At the receiver, the signal has the same format, delayed by the transmission time through the subject. Under conditions of no velocity dispersion, the transmission time is constant throughout the sweep. Since the frequency is a linear function of time through the sweep, there is a constant offset frequency between the transmitted signal and the received signal at each moment that will be proportional to the time delay between them. A frequency-shifted version of the transmitted signal can be heterodyned against the received signal to produce a nearly constant frequency difference that contains the received signal information. This narrow bandwidth signal may in turn be passed through a narrow passband filter to remove those signal components that did not arrive with the time delay that is selected for the measurement. Using oscillators with suitable phase stability, a repetitive frequency spectrum including both amplitude and phase is set by the operator and direct measurements of the characteristics of the medium may be obtained as the sweep progresses.

TDS is a dynamic system-testing process which breaks away from the rigid concepts of a steady-state sinewave excitation on the one hand and wide bandwidth impulse excitation on the other hand. It is a coherent communication process in which both the time domain and frequency domain are utilized, even if interest centers wholly on one domain. The transmitted signal discussed above has a predetermined frequency spectrum with the equivalent of a time tag to each frequency component. In the simplest case considered here, this consists of a linear frequency sweep with time in which the tag is the moment of occurrence of each frequency. Upon emergence from the specimen, the frequency components with a given time delay are reassembled to yield the frequency spectrum. This is the time-delayed spectrum for which the process is named.

This method provides the amplitude and phase of the complex signal over the spectrum. In addition, signal components due to longer path lengths, such as those caused by scattering, are effectively suppressed because their spectrum time tags reject

them. The accepted signal is therefore the anechoic frequency response of the combined transducers and tissue path. If a multipath situation is encountered in which the desired signal is closely followed by an undesired signal which traveled a slightly different path, it is possible to center the acceptance of TDS to the specific arrival time of interest and narrow the time window to the extent necessary to insure that the appropriate path is selected, within the limits of the experimental equipment.

Time Delay Spectrometry has been used for visualization of soft biological tissue. Resolution of at least 2 mm was obtained together with a dynamic range in intensity of about 80 dB. This was electronically compressed down to the 20 dB range available for CRT display and subsequent photographic reproduction [10].

Because of the linear relationship between time and frequency, there is an easy transformation between the two domains. The operator has control over the range of frequencies being utilized and can thus bound the frequency range over which the measurement or analysis is carried out. The significance of this to medical ultrasound measurements is that Time Delay Spectrometry simultaneously yields data on the time-domain vector and frequency-domain vector that represent wave propagation through the body. In so doing, a wide range of measurements at high sensitivity is available for time-of-arrival measurements and their spectrum measure.

3. Attenuation Measurements

The system outlined above has been used to make preliminary measurements of the change in attenuation as a function of frequency over the range of 1.5 to 4.0 MHz. As presently configured, the apparatus can be used for imaging and tissue measurements over the frequencies from 2 to 3 MHz and for measurement only over the remainder of the range.

One of the possible ultrasound properties that may yield tissue information is the frequency dependence of attenuation. In order to check this property by means of Time Delay Spectrometry, the transmitting and receiving crystals are placed a convenient distance apart, such as 20 cm. The transmitter is swept through the frequency range, causing the transmitting crystal to emit an acoustic signal with the same frequency sweep. The first sound due to this signal will arrive at the receiving crystal with a definite delay due to the finite propagation velocity in the material interposed between the transmitting and receiving crystals. The first sound that arrives will always be due to the direct transmission path through the intervening medium. The later arriving sound is generally composed of either reverberant signal components or of longer path length signals such as those due to off-axis crystal sounds that are reflected or refracted through a longer path from transmitter to receiver.

All of these received signals are amplified and passed through a narrow bandwidth tracking filter. This filter is tuned so that only the first sound arrivals, due to the direct path, are passed on for further analysis. Reverberant sounds are minimized, if not eliminated from the measurement, and crystal polar response is effectively sharpened without the need for external focusing lenses.

The output of the tracking filter is processed to produce a cathode ray tube display of the frequency response of the first sound arrivals. Since the whole process is continuously repeated, the observer can move the probes to different portions of a specimen and tune the delay path for optimum display and observe the results almost instantaneously.

The resultant response will naturally include the imperfect response of the ultrasound crystals. This does not compromise the data since the entire system can be used to measure the response of the crystals and associated electronics for subsequent data removal.

In the frequency domain, the net frequency response is the product of the individual frequency responses. If the response of the transmitting crystal is $F_X(\omega)$, the response of the tissue is $F_T(\omega)$ and $F_R(\omega)$ is the receiver response, then the combined response is

$$S(\omega) = F_X(\omega) \cdot F_T(\omega) \cdot F_R(\omega) \ . \qquad (1)$$

If the logarithm of the combined response is taken, this can be expressed as

$$\ln S(\omega) = \ln F_X(\omega) + \ln F_T(\omega) + \ln F_R(\omega)$$

$$= [\ln F_X(\omega) + \ln F_R(\omega)] + \ln F_T(\omega) \ . \qquad (2)$$

If a measurement is made by removing the tissue and replacing its displaced volume with an equal volume of water, then this is a measure of the system response and is identical to the term

$$[\ln F_X(\omega) + \ln F_R(\omega)].$$

This term can then be readily subtracted from the tissue measurement to remove the imperfections due to the crystal frequency response.

The manner in which this is done is shown in figure 1. The figure displays the system response over the frequency range of 1.5 to 4.0 MHz. The crystals have a nominal 2.5 MHz resonance.

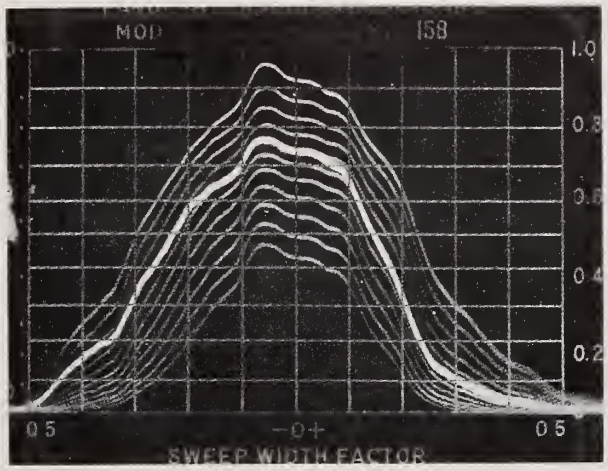

Figure 1. System response over 1.5 to 4.0 MHz. The top curve is the frequency response of the system with a water path between the transducers. Each faint curve below this represents a 2 dB drop in energy of excitation. The bright curve is the response when the specimen is inserted.

A logarithmic amplifier is used for the display of signal amplitude. The top curve is the frequency response of the system with a water path between the transducers. Each faint curve below this represents a 2 dB drop in energy of excitation. The bright curve is the response when the specimen is inserted and the system excitation is the same as that for the top curve.

The data are accumulated for convenience as a multiple exposure on a Polaroid film taken of the sweeping spectrum analyzer. All that is necessary to determine the tissue ultrasound attenuation versus frequency is a decibel subtraction of the bright curve from the top curve. By using a precision attenuator with multiple exposures to determine the system response in dB or fractional dB steps, even the possible errors in the analyzer logarithmic amplifier or in reading the cathode ray screen are minimized.

An example of one data measurement using this technique is shown in figure 2. The frequency dependence of the central portion of a glioblastoma is compared against a

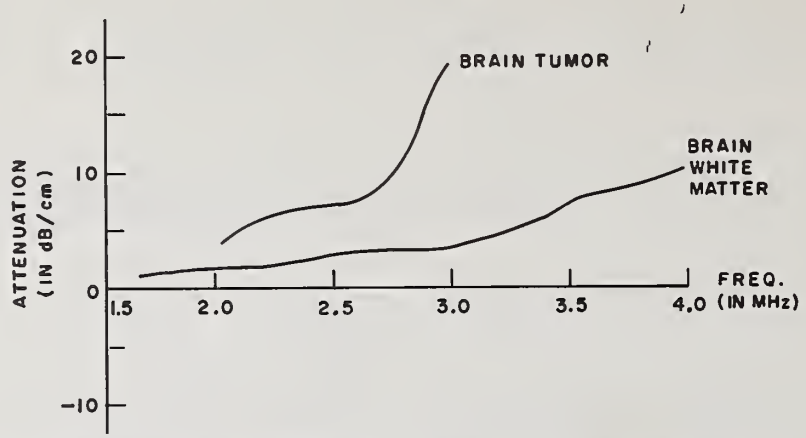

Figure 2. Attenuation as a function of frequency for two regions in a fixed specimen from the posterior thalamus.

measurement made on the white matter adjacent to the tumor. The brain section was formalin-fixed for this measurement. An interesting point of this measurement is that the frequency dependence of attenuation of the tumor shows a decided departure from that of non-tumorous tissue. If this behavior should prove to be general, then we could infer a possible signature in this frequency dependence. This data is also consistent with an overall attenuation that has been reported elsewhere [11].

A few of the data on variation in tissue attenuation with frequency measured with time delay spectrometry methods are shown in figure 3. These data are preliminary since

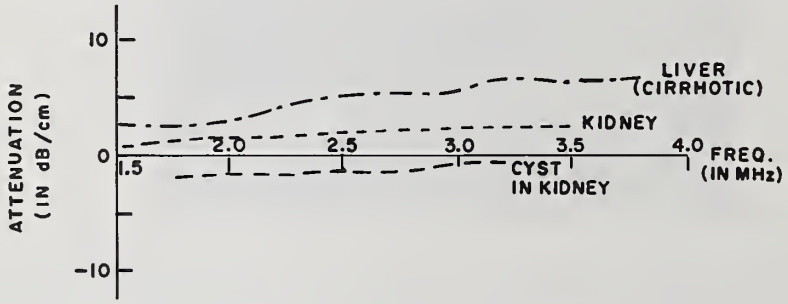

Figure 3. Variation of tissue attenuation with frequency.

measurements have been taken on only one or two specimens of each type of tissue at the present time. The data are taken on unfixed autopsy specimens which had a known pathology.

Of considerable interest are the data for the cyst, which shows not as an attenuation but a gain of 1 or 2 dB cm^{-1}. To understand this phenomena it must be realized that the system is accepting only the energy which arrives with the minimum time delay. It is believed that the cyst which has a near spherical shape and is filled with fluid acts as a focusing lens and permits more energy to be received by the receiving transducer than in the case of normal tissue. In the case of a pulse-echo system "anti-shadowing" has been reported to occur behind a cyst [12]. Since most pulse-echo units operate with swept-gain in the B-scan system, it is difficult to evaluate the magnitude of the effect. The use of a TDS transmission measuring system allows the measurement of this effect in detail. At the present time, our preliminary measurements indicate that we have a method of distinguishing between a solid mass and a cyst. In one instance, a tissue measurement gave such

a strong indication of a cyst signature that the specimen was opened by scalpel at the indicated location and a cyst was found exactly as indicated.

4. Time Measurement

The process of swept-frequency measurement is in effect a frequency-domain technique. By taking the Fourier transform of the frequency spectrum during the frequency sweep, it is possible to generate the time-domain response simultaneously with the frequency-domain response.

There are several advantages to doing this. First, the fact that the time response is computed from the frequency response means that it is possible to measure in a non-causal manner. That is, since the time coordinate is computed rather than corresponding to laboratory time, it is possible to dwell on a measurement representing one moment in time or even to present the results of a reversed time axis. Of course, the computed measurement always results after the swept stimulus giving rise to it. A second advantage lies in the fact that the computation may readily be made for the single-sided frequency spectrum. This yields a time response that is a phasor quantity consisting of an amplitude and a phase. Furthermore, the frequency spectrum chosen for this computation can be a rectangular band with a predetermined low frequency and high frequency cutoff and no spectrum component existing beyond these limits. This is another noncausal measurement but the results, rather than being merely of theoretical interest, are actually of great practical value.

The fact that the time response is a phasor can lead to some new signature characteristics that are not apparent from pulse-echo measurements. The magnitude of the time-response phasor is a direct measurement of the total energy density of the received energy as a function of time. The phase of the time response phasor is a direct measurement of the partitioning of that total energy density into kinetic and potential energy density components. A computation of the received time signal for a specific moment in time, say 90 microseconds after the transmitter pulse is sent, will have a phase angle that is a very sensitive measurement of the path length and acoustic velocity of the tissue through which the ultrasound passed on its way to the receiving pulse. In the case of the equipment described in this paper, one degree of phase retardation of this phasor corresponds to approximately one nanosecond of additional path delay. Thus, the probes may be positioned at a desired point for transmission measurement and the computation made for the peak energy of the first sound passing through the specimen. An oscilloscope display of such a time phasor measurement is shown in figure 4. This display is refreshed 25 times per second and, so long as the probes remain fixed in location, is steady on the screen. If the probes are now moved to an adjacent position on the test specimen, the phasor will change its amplitude and phase corresponding to the attenuation and time retardation of

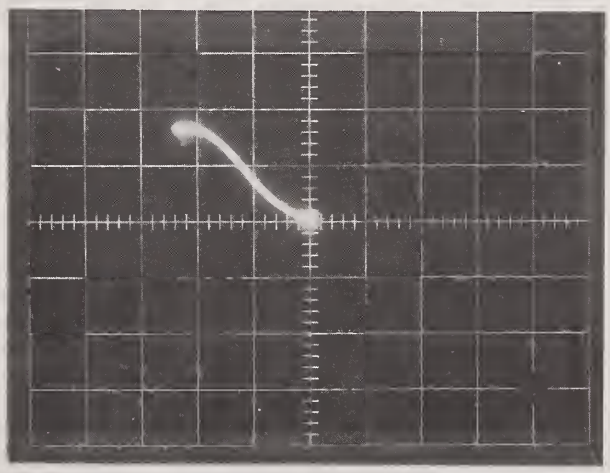

Figure 4. Time phasor recorded on a cathode ray tube.

the new portion transinsonified. If the velocity of the first sound in the new test position is such as to cause an arrival time change of 5 nanoseconds relative to the previous position, the phasor will swing by 5 degrees in a direction indicating whether it is a retardation or advance in arrival time.

Some measure of the sensitivity offered can be appreciated by the fact that a full 360 degrees of phasor angle change is brought about by a change corresponding to 0.5 mm of equivalent water path delay, independent of the total separation between transmitting and receiving probes. If the direct path component passes through a medium which is, for example, 10 cm in extent with an average acoustic velocity of 1500 m/s, then a 1 mm thick inclusion with an average velocity of 1540 m/s will cause an advancement of 18 nanoseconds of arrival time over that of the bulk tissue. The resultant 18 degrees of phase change is readily discerned in a time delay spectrometer, while it is unlikely that a comparable arrival time advancement would be evident with conventional pulse technology. A 3 MHz continuous wave system would show the same phase change but would not be capable of isolating the direct path from other flanking and reverberant sound paths.

With such an enormous sensitivity to arrival time, it might appear at first glance that *in vivo* measurements would be unnecessarily restrictive on subject mobility. This is not the case as has been determined by laboratory measurements. A reasonable amount of motion along the direct path length of ultrasound incurs no net phase change because the net path length of the subject medium always remains constant. Motion perpendicular to the ultrasound path causes a change only if it is sufficient magnitude to cause a different part of the tissue to come under measurement.

In the practical matter of tissue signatures, the time-domain phasor has a greater spatial resolution than the frequency-domain phasor. This is because the Fourier transformation process effectively collapses the measurement to a particular moment in time with a very narrow acceptance of time components prior to and subsequent to the selected moment. For a frequency sweep of 1 MHz and an average acoustic velocity of propagation corresponding to water, the time measurement effectively rejects path lengths which differ by more than 1.5 mm from the selected path. For wider frequency sweeps, the path acceptance is correspondingly reduced. This rejection, incidently, takes place even for ultrasound crystals that have little or no polar angle selectivity in their own right as has been demonstrated previously [10].

Tissue characteristics relating to absorptivity and scattering may be obtained from the time phasor. A homogeneous tissue structure definitely shows a uniform phasor transmission as the direct sound path is scanned through the specimen. Disrupted tissue structure tends to show a very erratic phase angle change with little or no amplitude change.

A homogeneous inclusion has a tendency to create a transmission characteristic known as minimum phase in communication theory. A highly scattering inclusion, creating a large number of closely-spaced multipath arrivals, produces a non-minimum phase transmission characteristic.

By changing the frequency sweep width, the "window" of the computed time response may be altered to include more scattered energy in order to examine the probable extent of a non-minimum phase inclusion. In a similar fashion, the average sweep frequency can be altered to observe the amount of dispersion in a given region.

With a wide frequency sweep, dispersion may be determined from observing the phase behavior of either the complex frequency response or, what amounts to the same thing, the detailed behavior of the Fourier integral from which the time phasor is computed. The oscilloscope picture of figure 4 is actually the trajectory of the complex Fourier transform as it is in process of computation. That is why there is a curve from the center of the screen to the terminal position rather than a straight line. The spot at the center of the screen is mathematically that component of the Fourier transform from negative infinite frequency to positive 2 MHz. It is zero simply because no signal frequency components are allowed below 2 MHz. The arching curve is the component of the Fourier transform from positive 2 MHz to positive 3 MHz, and is the data of interest. The terminal of this curve, which is a point, corresponds to the remainder of the Fourier integral from positive 3 MHz to positive infinity. Again, because no frequency components exist above 3 MHz, this is a null addition to the phasor.

Exactly as in the case of the frequency response, the imperfections of the crystal and electronics can be removed from a time-domain measurement by first measuring the system with a known acoustic medium, then removing those characteristics from a measurement made through the unknown tissue.

5. Summary

A practical system of measurement has been described which is capable of great flexibility in determining tissue ultrasound characteristics. While a substantial amount of experimental data on tissue visualization and measurement using this technique has been accumulated in the past few years by the authors, this paper has primarily been directed at the description of the manner in which tissue signatures may be obtained. Particular emphasis has been placed on the important roles played by both the frequency domain and time domain, and in the advantage of recognizing the complex phasor representation in both domains.

The capability of simultaneous measurement in the time and frequency domain has been found to give a synergism not presently found with conventional analysis.

We acknowledge the medical advice and assistance of Robert L. Wilson, M.D. of the Los Angeles County - University of Southern California Medical Center. This paper presents the results of one phase of research carried out at the Jet Propulsion Laboratory, California Institute of Technology, under Contract No. NAS7-100, sponsored by the National Aeronautics and Space Administration.

References

[1] *Interaction of Ultrasonic Energy with Biological Structures* in *A 5-Year Research and Development Agendum for Ultrasonic Imaging Diagnostic Instrumentation*, (The Alliance for Engineering in Medicine and Biology, Chevy Chase, MD, Publication No. N-1975-1, April 1975), available from the National Technical Information Service, 5285 Port Royal Road, Springfield, Virginia 22151, Publication No. PB-230010/AS.

[2] *Ultrasonic Transducers: Signal Detection and Preprocessing* in *A 5-Year Research and Development Agendum for Ultrasonic Imaging Diagnostic Instrumentation*, (The Alliance for Engineering in Medicine and Biology, Chevy Chase, MD, Publication No. N-1975-1, April 1975), available from the National Technical Information Service, 5285 Port Royal Road, Springfield, Virginia 22151, Publication No. PB-230010/AS.

[3] *Ultrasonic Diagnostic Scanning and Display Systems* in *A 5-Year Research and Development Agendum for Ultrasonic Imaging Diagnostic Instrumentation*, (The Alliance for Engineering in Medicine and Biology, Chevy Chase, MD, Publication No. N-1975-1, April 1975), available from the National Technical Information Service, 5285 Port Royal Road, Springfield, Virginia 22151, Publication No. PB-230010/AS.

[4] *Ultrasonic Diagnostic Signal Processing* in *A 5-Year Research and Development Agendum for Ultrasonic Imaging Diagnostic Instrumentation*, (The Alliance for Engineering in Medicine and Biology, Chevy Chase, MD, Publication No. N-1975-1, April 1975), available from the National Technical Information Service, 5285 Port Royal Road, Springfield, Virginia 22151, Publication No. PB-230010/AS.

[5] *Summary* in *A 5-Year Research and Development Agendum for Ultrasonic Imaging Diagnostic Instrumentation*, (The Alliance for Engineering in Medicine and Biology, Chevy Chase, MD, Publication No. N-1975-1, April 1975), available from the National Technical Information Service, 5285 Port Royal Road, Springfield, Virginia 22151, Publication No. PB-230010/AS.

[6] Wild, J. J. and Reid, J. M., Progress in the techniques of soft tissue examination by 15 Mc pulsed ultrasound, in *Ultrasound in Biology and Medicine*, E. Kelly, ed., p. 30 (Am. Inst. of Biol. Sciences, Washington, 1957).

[7] Birnholz, J. C., Sonic differentiation of cysts and homogeneous solid masses, *Radiology*, 108, 699 (1973).

[8] Heyser, R. C., Acoustical measurements by time delay spectrometry, *J. Audio Eng. Soc.* 15, 370 (1967).

[9] Heyser, R. C., Time delay spectrometer, U. S. Patent 3,466,652 (1969).

[10] Heyser, R. C. and Le Croissette, D. H., A new ultrasonic imaging system using time delay spectrometry, *Ultrasound in Med. and Biol.* 1, 119 (1974).

[11] Fishman, L. S., Heyser, R. C., and Le Croissette, D. H., Ultrasonic transmission measurements on human brain sections, *Radiology*, 112, 211 (1974).

[12] Kossoff, G., Display techniques in ultrasound pulse echo investigations: a review, *J. Clin. Ultrasound*, 2, 61 (1974).

Appendix

Time and Frequency Relationships

Let a signal, $w(t)$, be applied to a network with impulse response, $s(t)$, as shown below:

$$w(t) \longrightarrow \boxed{s(t)} \longrightarrow r(t). \tag{A-1}$$

The output, $r(t)$, is the convolution of $w(t)$ and $s(t)$ and is given by

$$r(t) = \int_{-\infty}^{\infty} w(x-t)\, s(x)\, dx \equiv w(t) * s(t). \tag{A-2}$$

If, in particular, $w(t)$ is a constant-amplitude, linear frequency sweep given by

$$w(t) = e^{i\frac{a}{2}t^2}, \tag{A-3}$$

then the output $r(t)$ is

$$r(t) = \int_{-\infty}^{\infty} e^{i\frac{a}{2}(x-t)^2}\, s(x)\, dx = e^{i\frac{a}{2}t^2} \int_{-\infty}^{\infty} s(x)\, e^{i\frac{a}{2}x^2}\, e^{-iatx}\, dx. \tag{A-4}$$

The frequency response, $S(\omega)$, of the network with impulse response $s(t)$ is

$$S(\omega) = \int_{-\infty}^{\infty} s(t)\, e^{-i\omega t}\, dt. \tag{A-5}$$

Since it is known that the Fourier transform of a product of functions is the convolution of the transforms of the functions, it follows that

$$r(t) = w(t)\, [S(at) * W(at)], \tag{A-6}$$

where $W(\omega)$ is the Fourier transform of $w(t)$.

This is a remarkable result since it demonstrates that a special excitation applied to a network produces an output which is expressible as a time dependence, but has the functional form of the Fourier transform. Functionally, the two domains have been interchanged.

If a fixed delay of τ seconds is experienced by the signal, and if it is desired that the epoch defined at $t = 0$ occur at the network output, then the following figure shows how this can be achieved. The excitation $w(t)$ must now be advanced in time dependence to become $w(t-\tau)$.

$$w(t-\tau) \longrightarrow \boxed{s(t)} \longrightarrow \boxed{e^{i\omega\tau}} \longrightarrow w(t)\, [S(at) * W(at)]. \tag{A-7}$$

If this signal is now multiplied by a frequency-translated version of the complex conjugate of $w(t)$, and this product used as a signal input to a filter network with impulse response $i(t)$, the signals are as shown below:

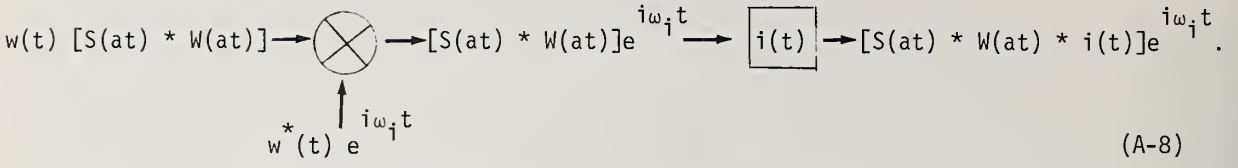

(A-8)

Multiplying by a complex conjugate removed the product dependence of w(t). The offset frequency multiplication performs a translation in what is commonly referred to as a heterodyne of all signal components upward by a fixed frequency, ω_i. The network with response i(t) is a narrow bandwidth filter centered at frequency ω_i and hence is what is commonly called the intermediate-frequency selectivity network. This signal, after selectivity can be translated downward by multiplying by the complex conjugate of the up-conversion signal as shown below:

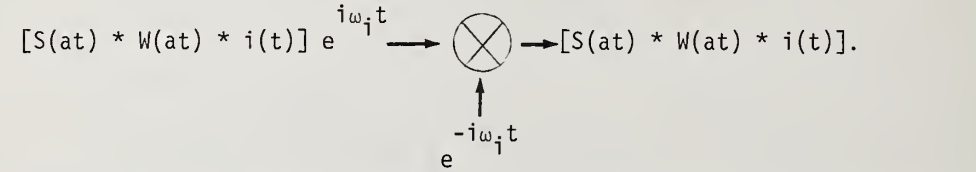

(A-9)

The function w(t) has the further remarkable property that it is its own Fourier transform with complex conjugation. That is,

$$W(at) = \sqrt{\frac{2\pi i}{a}}\, w^*(t) \qquad \text{(A-10)}$$

$$= \sqrt{\frac{2\pi i}{a}}\, e^{-i\frac{a}{2}t^2}.$$

Thus, the output of the process shown in the equation above is the convolution, omitting constant multipliers,

$$S(at) * A(t)$$

where,

$$A(t) = e^{-i\frac{a}{2}t^2} * i(t). \qquad \text{(A-11)}$$

This is the desired result of a Time Delay Spectrometer. A signal w(t) which is of constant energy but with defined time-dependent frequency is fed to a network to be analyzed. The signal in passing through this network will undergo a spectrum change by $S(\omega)$ and suffer a time delay, τ. The signal thus emerging from the network is multiplied by the complex conjugate of the original signal delayed by a time τ. This product is passed through a narrow bandwidth filter. The result is that the output signal is the Fourier transform of the impulse response of that network with the delay τ. The time-domain selectivity producing the apodization of the desired signal, A(t), is performed by the joint action of filter bandwidth and excitation. Signals with an earlier or later arrival time than τ will be suppressed by A(t) while signals arriving at time τ will be shaped (apodized) in a manner producing the best representation of $S(\omega)$ consistent with suppression of improper arrival times.

The signal w(t) represents one sweep through all frequencies. Since interest normally is centered on a restricted band of frequencies, w(t) may be allowed to become repetitive

in this band in a sawtooth fashion of frequency versus time with no loss of generality in the foregoing analysis. When this is done, the output of the network of the above figure may be displayed on one axis of an oscilloscope with the other axis driven by a sawtooth signal synchronized to the sawtooth excitation w(t). This repetitive display now indicates the frequency spectrum of that path representing a fixed and known time delay--hence, the name Time Delay Spectrometry.

In order to yield the time-domain information from this frequency-domain display, it is necessary to perform a Fourier transform. Because the time- and frequency-domain representations are interchanged in a TDS, this is readily accomplished by the method shown below:

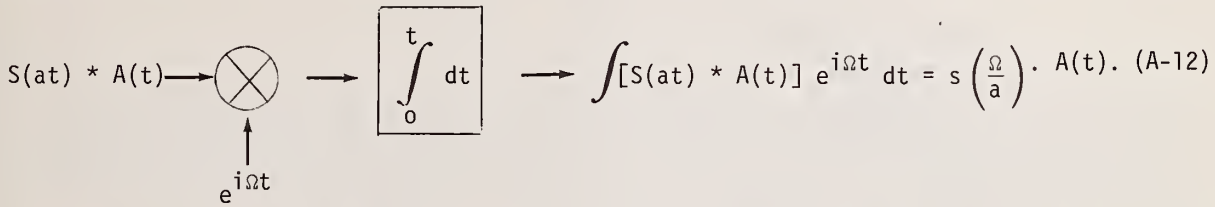

$$\rightarrow \int [S(at) * A(t)]\, e^{i\Omega t}\, dt = s\left(\frac{\Omega}{a}\right) \cdot A(t). \quad \text{(A-12)}$$

The frequency spectrum S(at) is convolved with its time apodization, A(t), then multiplied by a cisoid representing the desired epoch, Ω, and integrated from the beginning of the sweep w(t) to its end. The output of this integration at the end of the sweep is the desired Fourier transform as can be seen from the figure above. A single complex number is produced which corresponds to the moment of arrival selected by the frequency Ω. If this frequency is zero (d.c.), then the moment selected is τ sections after the system excitation by w(t).

The foregoing analysis presumes that the system has been optimized for the proper path delay. If the delay adjustment is not optimum, then the measured response, both for frequency domain and time domain, will be diminished from the optimum response. The selectivity of a TDS is determined by the reduction in response as a function of offset from optimum delay.

The selectivity of the frequency domain measurement yielding $S(\omega)$ is determined by the frequency selectivity of the intermediate-frequency network. Since the frequency of excitation is proportional to time, and since the distance traveled at constant velocity is also proportional to time, it follows that distance may be equated to frequency. With a sweep rate of $\Delta F/\Delta T$ hertz per second, propagation velocity c and offset frequency B hertz, the distance ΔX, traveled by the signal is,

$$\Delta X = \frac{B \cdot C}{(\Delta F/\Delta T)} . \quad \text{(A-13)}$$

If B is the electrical bandwidth of the selectivity network, then ΔX is a space-equivalent bandwidth measuring the amount by which longer pathlength signals are suppressed from an optimum adjustment for direct path. Besides determining the space-equivalent selectivity, the sweep rate and electrical bandwidth perform a smoothing operation on the resultant spectrum $S(\omega)$. This smoothing is the apodization $A(\omega)$ developed above. Because we are using information in both the time domain for selectivity and the frequency domain for measurement, it is not surprising that there is an uncertainty relationship governing the choice of bandwidth and sweep rate. The amount by which the frequency spectrum is smoothed, B, and the amount of space, ΔX, from which signals are smoothed due to velocity c is such that

$$\Delta X \cdot B \sim c. \quad \text{(A-14)}$$

This relationship is not unique to TDS but derives quite generally from the physics of the measurement.

The time-domain measurement is derived from the frequency domain by a direct Fourier transformation. Accordingly, the selectivity in the time domain is governed by Fourier-transform relationships. The spectrum $S(\omega)$ developed by a TDS is quite unique in that it is the true single-sided spectrum and is nil for all frequencies except those bounded by the sweeping signal. Let the sweeping function $W(t)$ start at frequency f_1, sweep uniformly to f_2, then terminate. This is an accurate description of one sweep in a TDS. The Fourier integral may be broken into three integrals as follows:

$$\int_{-\infty}^{\infty} = \int_{-\infty}^{f_1} + \int_{f_1}^{f_2} + \int_{f_2}^{\infty} .$$

By definition, the integrand for the integration from $-\infty$ to f_1 and for f_2 to $+\infty$ is zero. Thus, the only active integral is that from f_1 to f_2. Accordingly, the transformation to the time domain involves a convolution of the true impulse response with the transform of a frequency multiplier which is unity for all frequencies from f_1 to f_2 and nil elsewhere. This term thus becomes the time-domain selectivity and is of the form

$$\frac{\sin X}{X} \equiv \text{sinc}(X). \tag{A-15}$$

The equivocation of time and distance still holds and the offset distance at which the first null of the sinc function occurs is still the uncertainty relation,

$$(\Delta X)(\Delta f) = c. \tag{A-16}$$

The ability of Time Delay Spectrometry to resolve multipath signals is shown in figure A-1. Time-domain resolution is of the form $(\sin X)/X$. The peak to first null is typically 1.5 mm for a water path and 1 MHz in spectrum width.

In the frequency domain, the energy-versus-distance curve has the shape of the spectrum analyzer selectivity versus frequency. This determines the minimum time spacing of the adjacent signals that can be resolved. For a constant signal velocity, the distance resolution is given by

$$X = \frac{Bc}{(dF/dt)} \tag{A-17}$$

where the terms are as defined in figure A-1. A typical set of parameters used in this work is a sweep rate of 20 MHz per second, analyzer bandwidth of 100 Hz, and a water path velocity of 1,500 meters per second. This yields a distance resolution of 7.5 mm.

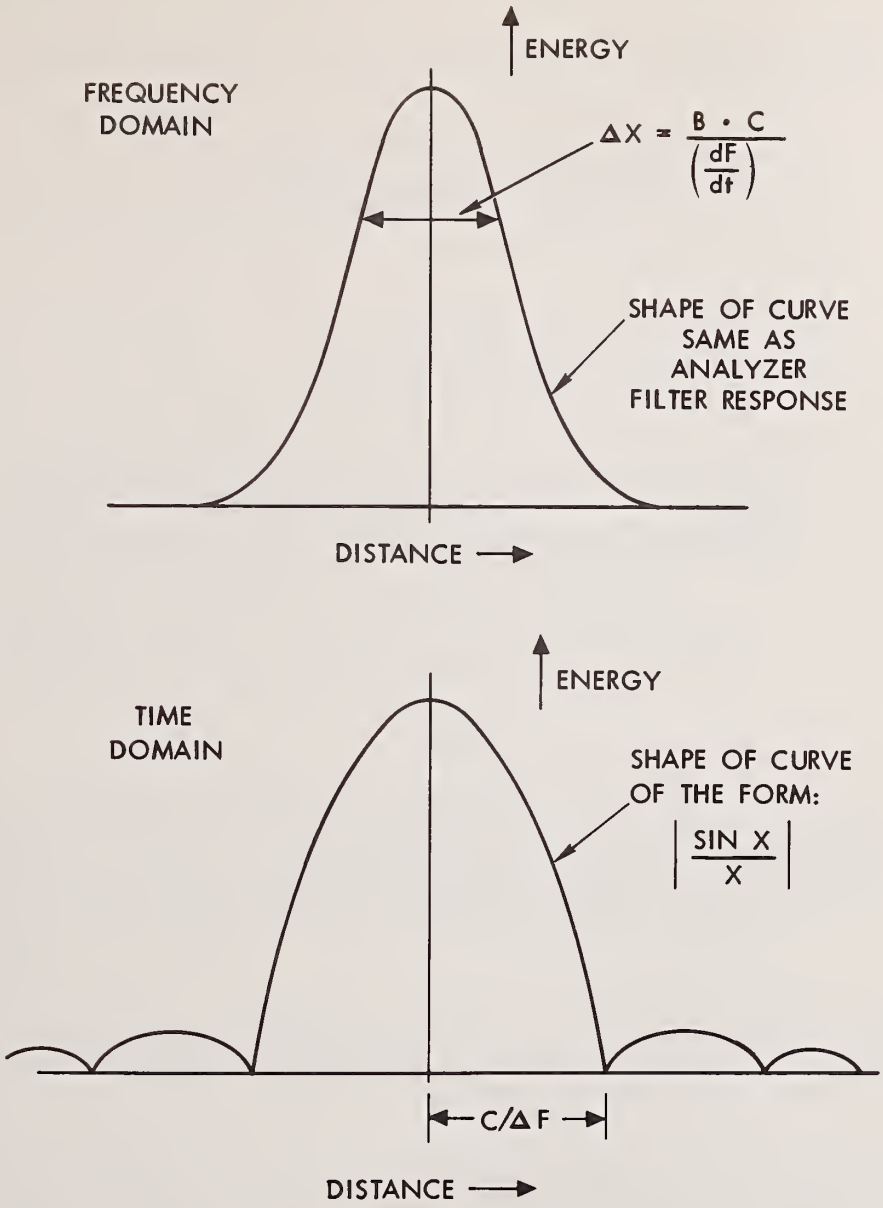

B = SPECTRUM ANALYZER BANDWIDTH, Hz

C = VELOCITY OF SOUND IN METERS · SEC^{-1}

$\frac{dF}{dt}$ = SWEEP RATE IN Hz · SEC^{-1}

ΔF = FREQUENCY SPECTRUM WIDTH IN Hz

Figure A-1. Theoretical system resolution.

National Bureau of Standards Special Publication 453. Proceedings of Seminar on Ultrasonic Tissue Characterization held at NBS, Gaithersburg, MD, May 28-30, 1975. (Issued Oct. 1976)

Paper 4.2: METHODS OF TISSUE IDENTIFICATION BY ULTRASONIC SPECTRA

A. Sokollu, E. W. Purnell, E. Holasek, and W. Jennings

Case Western Reserve University
Cleveland, Ohio 44106

and

A. Kaya

University of Akron
Akron, Ohio 44304

Ultrasonic spectral characterization of tissue is based on the retrieval of latent frequency information not normally detected in intensity-modulated B-scan displays. The results of tissue studies and tissue-model studies are presented and discussed. A method for color coding this frequency information into a B-scan display for clinical use is described.

Key Words: Color-coded B-scan; Fourier transform; spectral analysis; tissue structure; ultrasound.

1. Introduction

Recent technological developments have brought the display capabilities of B-scan ultrasonography close to the theoretical boundaries delimited by the frequency range and intensity level of ultrasonic pulses needed to safely penetrate to the required tissue depth. In spite of our technological achievements, we remain dissatisfied with our accuracy in interpreting the displayed pattern. There are a variety of reasons for this displeasure. Some investigators are displeased with the lack of resolution, and others with the distorted signal display.

Since the phosphors of cathode ray tubes are not capable of presenting echoes in their true intensity (over a range of 80 dB), we resort to various electronic stratagems to compress this range into the 25 dB capability of the phosphors. As a result of this compression, there is signal degradation. Distorted signals affect the outcome of tissue evaluation.

Until recent years, all abdominal scans were displayed on storage scopes without any detailed intensity information. Only after the recent introduction of scan converters and grey-scale storage tubes, have some physicians been able to see tissue in grey-scale. Ophthalmologists, on the other hand, were fortunate enough to have had grey-scale display for many years; the short distances examined made possible faster scan times which permitted the use of long-persistence CRT's with grey-scale capability.

During the last two decades of development in medical ultrasound, major efforts have centered about the improvement of resolving power and patient comfort but no significant breakthrough in the area of basic principles has occurred. We thus learned to recognize pathology in tissue by the abnormal geometry of displayed images, and to conclude from a certain shadow cast what the character of a tissue complex may be. Even with improvements in grey-scale and the use of color-coded amplitude display, there remains considerable uncertainty in interpreting disease states on the basis of ultrasound alone. These and other shortcomings of B-scan methods make it imperative to explore other interactions of sound with tissue as the basis for improving our reliability in diagnosis.

In B-mode scanning, ultrasonic signals are usually sent through the tissue and the received echoes are displayed according to their amplitudes. We totally disregard the frequency components actually reflected from various types of tissue, although we know that all tissues do not reflect all frequencies of sound with equal intensity.

Motivated by these thoughts, we decided to approach the problem of tissue identification from a totally different point of view. We attempted to apply the method of spectral analysis, as used in optics, to ultrasonic diagnosis. The fundamental idea of ultrasonic spectral analysis of tissue is based on the retrieval of the latent frequency information hidden in the shape of echo pulses which is normally not extracted in the processing of intensity-modulated B-scan displays. Feasibility studies were carried out in a series of experiments by measuring the spectral attenuation of various tissue samples in the through-transmission mode [1,2].[1]

The block diagram of the experimental arrangement is shown in figure 1. Two transducers of similar frequency characteristics were placed so as to face each other in axial alignment. Tissues samples were placed between the two transducers. One of the transducers was pulsed to generate wide band sound while the other acted as a receiver. The receiving transducer was connected to a spectrum analyzer (Tektronix, Model 7L12) and the signal gated through a double-balanced mixer to permit only the original pulse to enter the spectrum analyzer, screening out all reverberation echoes that might have been created in the path between the transducers. Several matched transducer pairs were tried to achieve the broadest frequency. The transducers were separated by about 75 mm in a water tank designed for this purpose with all the necessary alignment screws.

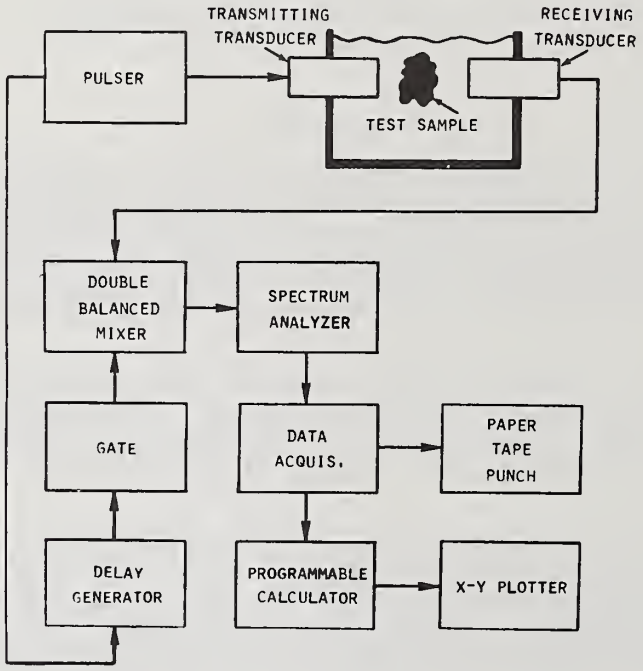

Figure 1. Through-transmission spectrum analysis instrumentation.

To aid in our interpretation of spectral data, we employed a Hewlett Packard 9820 Programmable Calculator with an X-Y plotter in our laboratory. We designed a data acquisition system to accommodate a large volume of data necessary for statistically

[1]Figures in brackets indicate the literature references at the end of this paper.

significant spectral-analysis studies. The data acquisition system consists of a high-speed (6 microsecond) analog-to-digital converter which has a resolution of one part in 4096 (12 binary bits). Peak-detected analog data is converted into digital information at the rate of 2000 samples per second. Our data acquisition system has been designed with the capacity to store a maximum of 960 words (12 bits each). The data acquisition memory transfers stored data either to the programmable calculator or to the paper tape punch. The data record, in standard ASCII code, is then available for use with a variety of computers.

2. Preliminary Results of Through-Transmission Studies

We first established the energy spectrum of the system (figure 1) without any tissue sample. Then we introduced the tissue and determined the spectral distribution. The ratio in dB between the two spectra was the attenuation spectrum of the sample relative to water.

We used natural sponges as tissue models for ease of experimentation [3]. Sponges do not degenerate with time and thus lend themselves to repeatable evaluations. We first discovered that the sponge attenuation spectra were independent of the shape of the incident pulse. Two pulses of radically different spectral content were transmitted through the same sponge (modifications in the frequency content of the pulse were made by changing the energy and damping constants of the excitation pulses). The same attenuation curve was obtained for both.

Secondly, we found the essential shape and nature of the spectral attenuation curve were not significantly altered by repositioning the sponge or by testing different pieces of the same sponge. A thicker piece showed greater overall attenuation but the general shape of the attenuation curve remained unchanged. This observation was of crucial value, since it supports the thesis that tissue types may be identified according to their spectral attenuation characteristics.

The spectral curves of two different sponges are shown in figure 2. Although the curves appear similar in overall shape, the difference curve, figure 3, reveals a significant difference in attenuation.

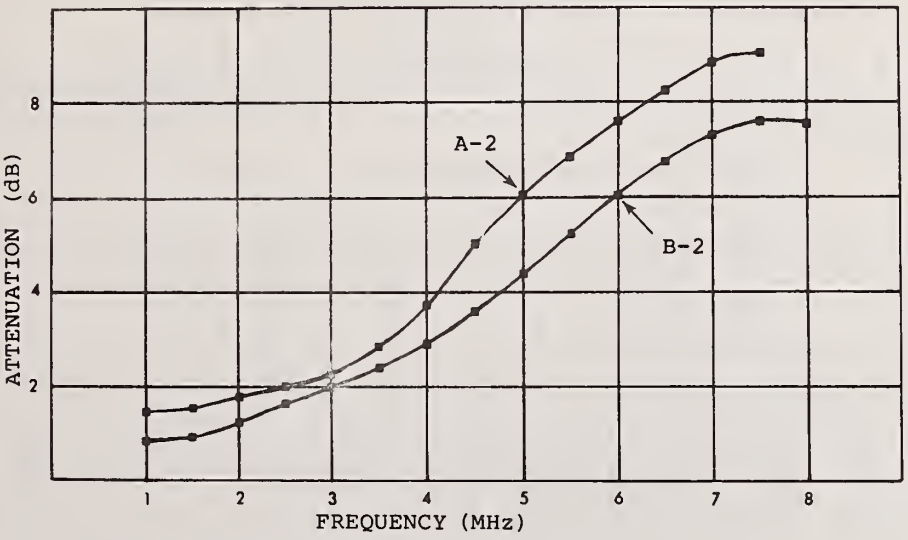

Figure 2. Spectra attenuation curves of two sponges, A-2 and B-2.

Deformation of a sponge by compression was tried next as a means of demonstrating that structural changes in a material induce spectral changes in the material. Figure 4 shows the attenuation spectra of a sponge before and after compression. The difference curve, figure 5, shows the expected changes in the spectrum due to compression.

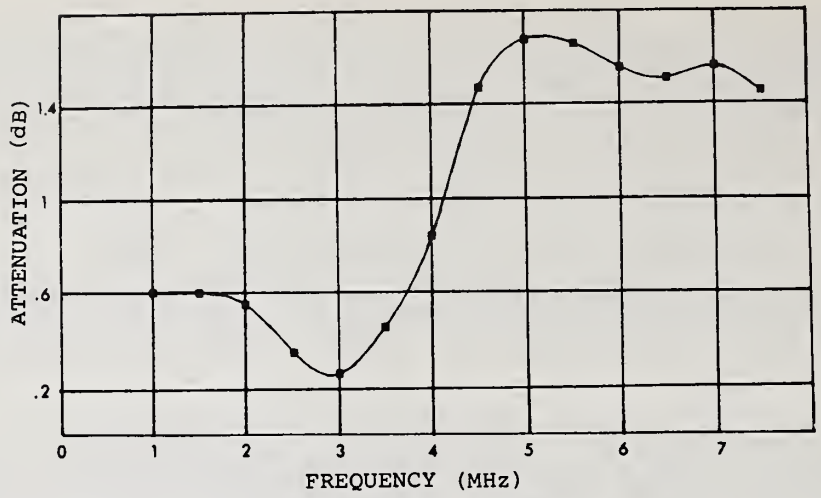

Figure 3. Curve of attenuation difference between sponges A-2 and B-2.

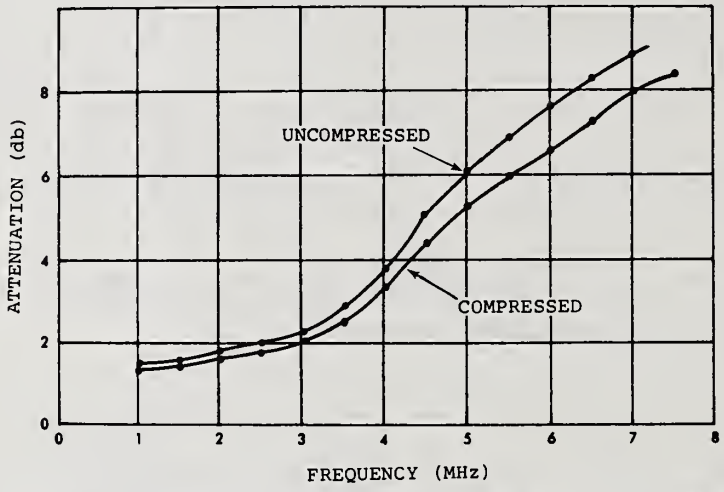

Figure 4. Attenuation versus frequency for uncompressed and compressed sponge.

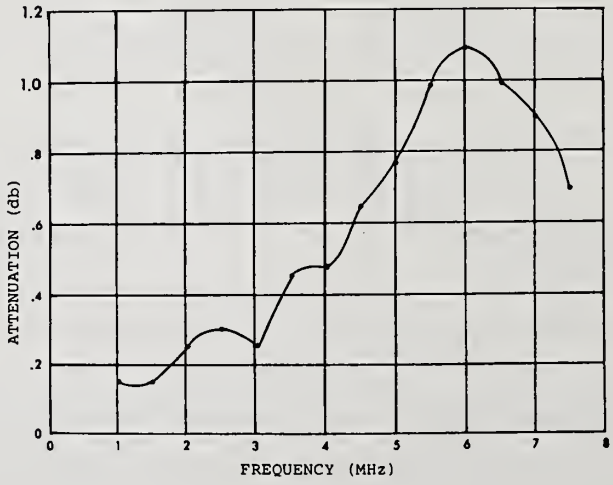

Figure 5. Compression difference curve taken from curves of figure 4.

3. Computer Studies

Our first analysis consisted of taking a polynomial regression of various degrees on our spectral attenuation curves. We were looking for a signature of tissue types in terms of the coefficients of the various powers of frequencies present in the spectral curve.

It was assumed that the linear term corresponds to the non-structural absorption, as classically measured by homogenizing the tissue [4], and that deviations from this dependence represents structural variations in the tissue. This analysis was applied to several sponge types, and each had a very different set of coefficients.

From the literature [5], we found spectral absorption curves for liver homogenate. We compared these values to our own results for spectral attenuation for a particular sponge. This comparison, along with the computed linear approximation to our own data, is shown in figure 6. The computed difference between the slopes of these two straight lines is only 0.2%. The deviation from the linear approximation to the sponge attenuation curve represent the heterogeneities of the sponge due to its coarse texture.

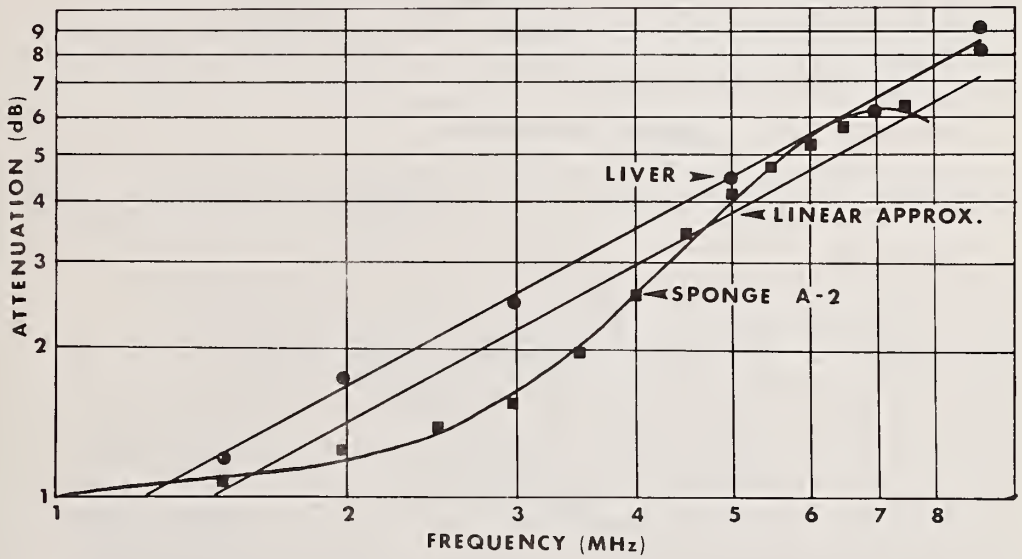

Figure 6. Attenuation versus frequency for homogeneous liver and sponge A-2, and linear approximation to sponge A-2.

4. Determination of Energy Attenuation Spectra of Tissue by Fourier Transform

In parallel to the spectrum analyzer studies, a Fourier-transform computer study has been performed to determine attenuation spectra from time-domain signals. The same sponge samples were used for both studies and the results were compared. Only two sponge samples from several tested are shown. Figure 7 indicates the time-domain pulse shapes observed from a typical test. Figure 7a is the time-domain display of a signal in a through-transmission system with water as the sonic medium. Figure 7b is the pulse shape after passage through the sponge sample A-2. Figure 7c shows the change in the shape and pulse amplitude after passage through a different sponge sample, D-2. Spectral analysis of these time-domain signals were obtained by means of Fourier-transformation, utilizing an IBM-370 computer.

The frequency response of tissue $A(j\omega)$ can be determined from the Fourier transform of the signal through the tissue in water divided by the Fourier transform of the signal through water.

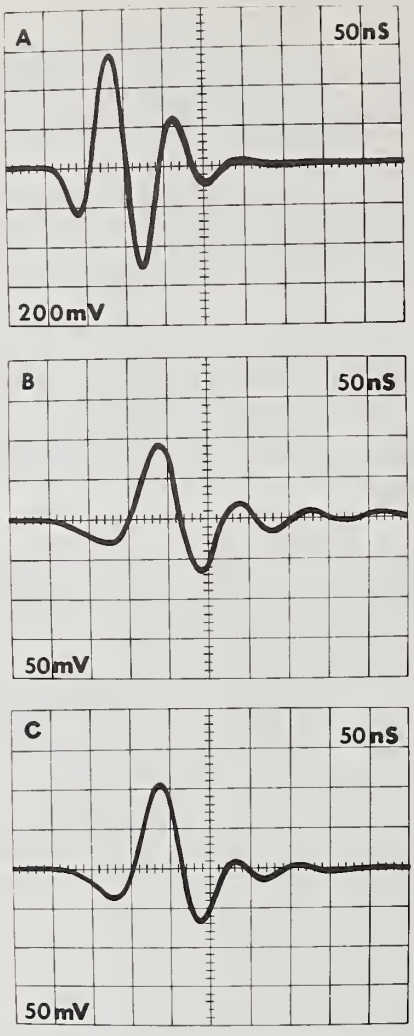

Figure 7. Time-domain pulse shapes received for wide band transmission: (a) through water medium, only; (b) through water and A-2; and (c) through water and D-2.

$$\text{Frequency Response of Tissue} = A(j\omega) = \frac{(\text{signal through tissue})}{(\text{signal through water})} \qquad (1)$$

Of course, $A(j\omega)$ carries both amplitude and phase information. The energy attenuation spectrum of the tissue (energy lost in tissue for each frequency) can be calculated from:

$$\text{Energy Loss of Tissue} = \frac{|A(j\omega)|^2}{Z} \qquad (2)$$

where $Z = 50$ was assumed as the equivalent impedance. The energy attenuation of sponge A-2 is given in figure 8. Similar results were obtained for sponge D-2, as shown in figure 9.

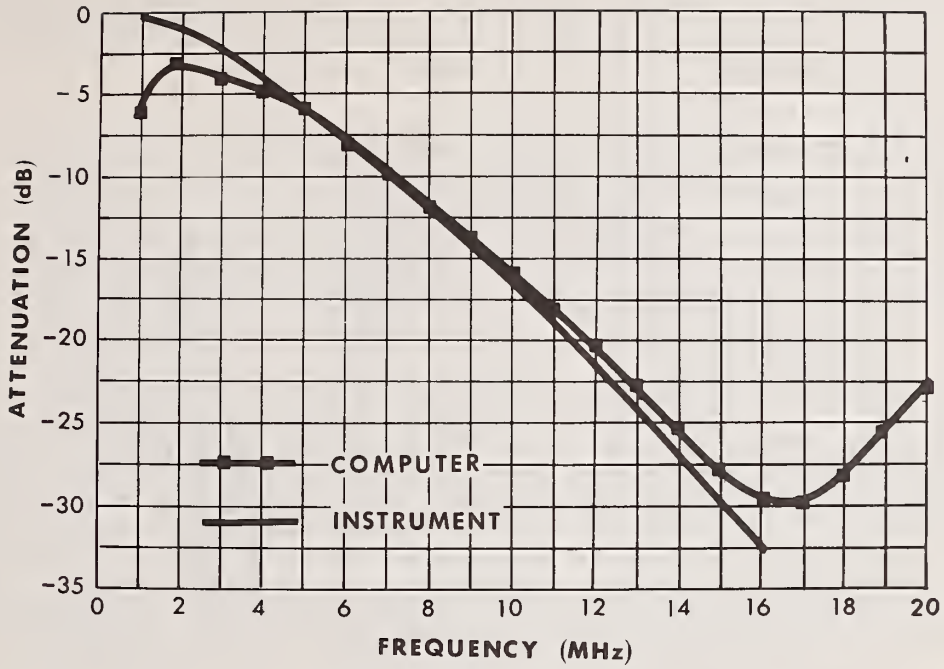

Figure 8. Energy absorption of sponge A-2, obtained by computer, compared with absorption obtained by spectrum analyzer.

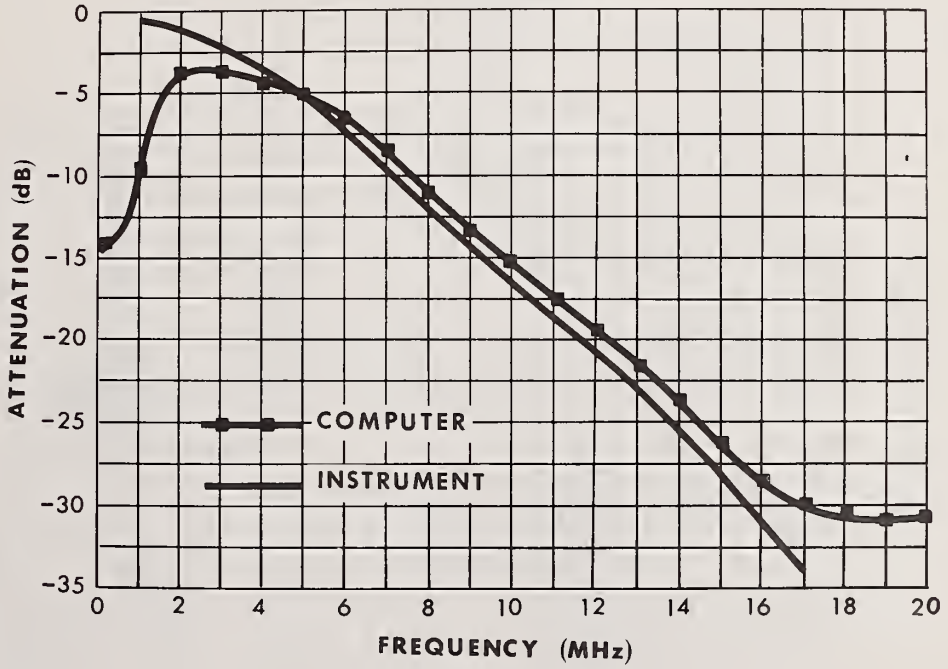

Figure 9. Energy absorption of sponge D-2, obtained by computer, compared with absorption obtained by spectrum analyzer.

The analytical results obtained by means of the spectrum analyzer approach agreed with the Fourier-transform calculations within the frequency range of the spectrum analyzer, 1-16 MHz, as shown in the figures. However, the Fourier-transform results were obtained for sponges A-2 and D-2 over a larger frequency range, 0.1-40 MHz, as shown in figures 10 and 11, respectively.

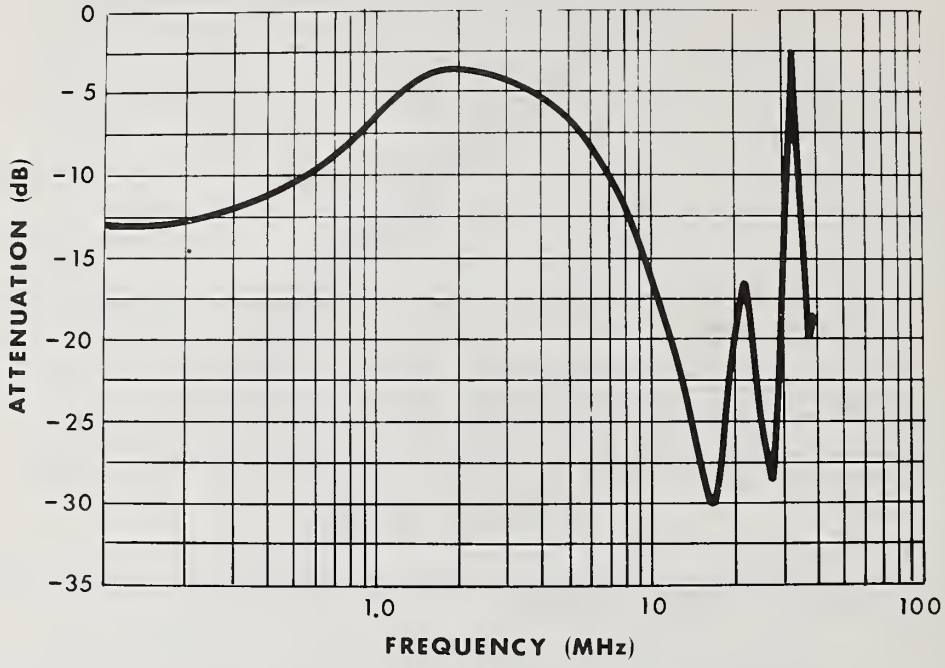

Figure 10. Energy absorption plotted by computer for sponge A-2.

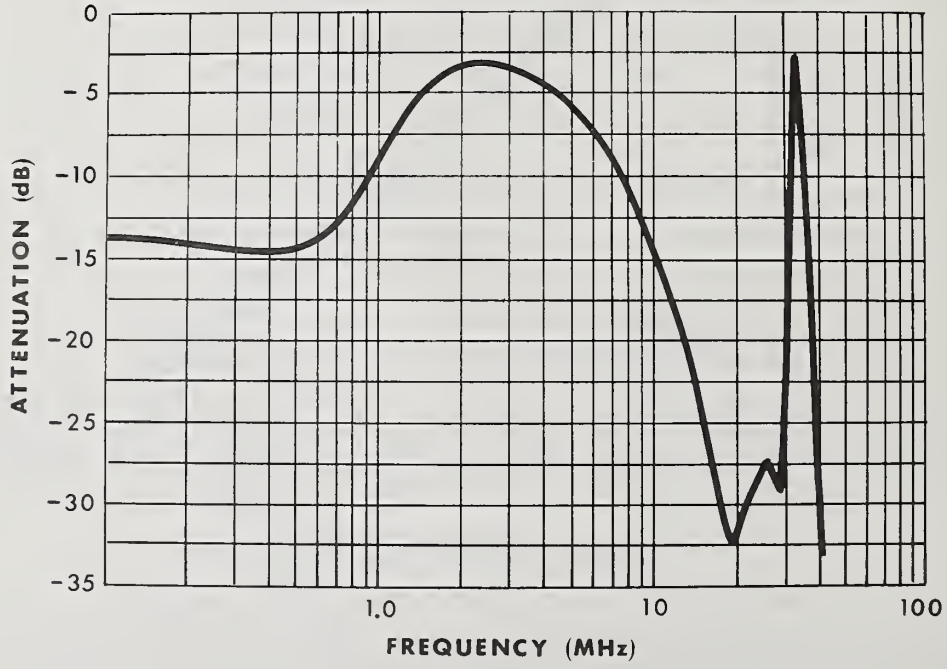

Figure 11. Energy absorption plotted by computer for sponge D-2.

The capability of the Fourier-transform approach in determining phase information in addition to the energy spectrum will be useful in understanding energy transmission in tissue and hence will lead to better recognition of tissue structures.

5. Frequency-Selective Color-Coding of Echoes

Echo analysis presented new problems for spectral identification. The most notable is that of gating specific parts of the echo complex for analysis in order to determine spatial information. The gate shape and duration has been found to influence greatly the echo spectra. We are currently working on a solution to this problem. In the meantime, we have resorted to a more pragmatic approach by separating the echo response into three frequency sub-bands, using analog filtering. Each band was assigned a certain color of light, thus providing the basis for a frequency color-coded B-mode display. We call this Spectra-Color Ultrasonography (S.C.U.), to distinguish it from methods employing amplitude-color coding.

The instrumentation for S.C.U. is composed of a high resolution, digitally-controlled, sector scanner designed for ophthalmic application. A full sector scan of 22.5 degrees is performed in 0.5 seconds. Each sector contains 400 lines of intensity modulated B-scan. The transducer is mounted in a mechanical stage and coupled to a water bath which permits immersion of various experimental target and physical models. For clinical use, it is coupled to a special pair of goggles which are worn by patients for scans of the eye and orbit.

A block diagram of the instrumentation is shown in figure 12. The *transmitter* sends a high-energy pulse which excites the ultrasonic transducer. The *transducer* is wide-

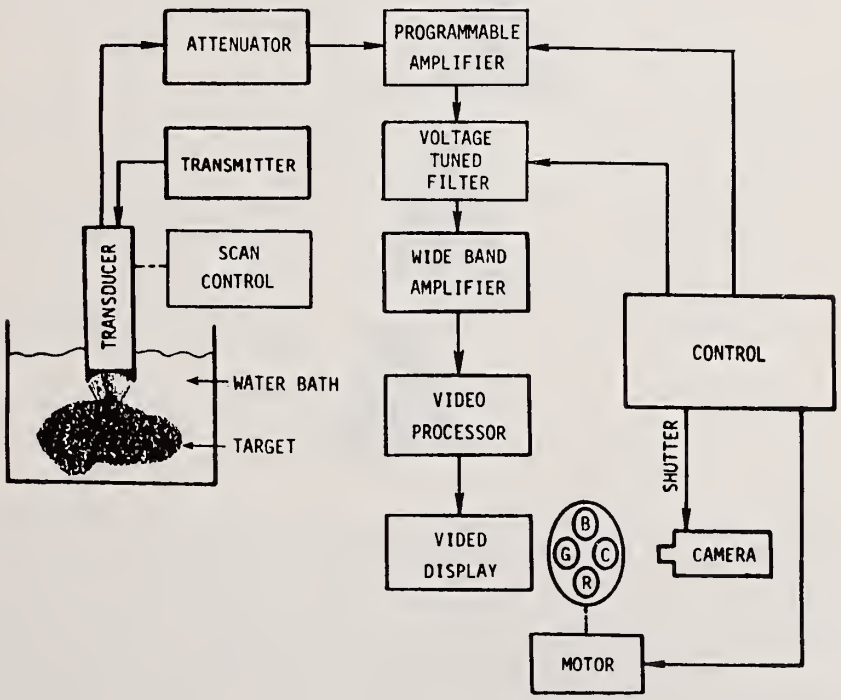

Figure 12. Block diagram of instrumentation for Spectra-Color Ultrasonography.

band, with a center frequency of 9 MHz and a fractional bandwidth of 66%, covering the frequency range from 6 MHz to 12 MHz. The ultrasound is focused by an acoustic lens with a focal length of 77 mm. Axial resolution is 0.3 mm in soft tissue. Lateral resolution varies from 0.4 mm to 1.0 mm, depending on the signal strength. Eighty decibels of amplification is provided by two *amplifiers* of 35 MHz bandwidth. The range of amplification is controlled by an *attenuator*. The intensity-modulated display has a five inch diameter and a spot size of approximately 0.1 mm. The S.C.U. is taken by a *camera* mounted in front of the display. A *voltage-tuned filter* receives three successive DC voltages and, operating on the varactor principle, generates the component frequency bands. Figure 13 shows the three component bands, designated low, middle and high, having center frequencies of 7 MHz, 9 MHz, and 11 MHz, with 2 MHz bandwidth. These frequencies are arbitrarily assigned the three primary colors of light, red, green, and blue, respectively, by introducing light filters between the *video display* and the *camera* (fig. 12). The filters are mounted in a light filter wheel which is rotated by a stepping *motor* to sequentially interpose each of the filters in coordination with each of three successive sector scans. The filters are Kodak Wratten Gelatin, No. 25 (red), No. 57 (green), and No. 47 (blue).

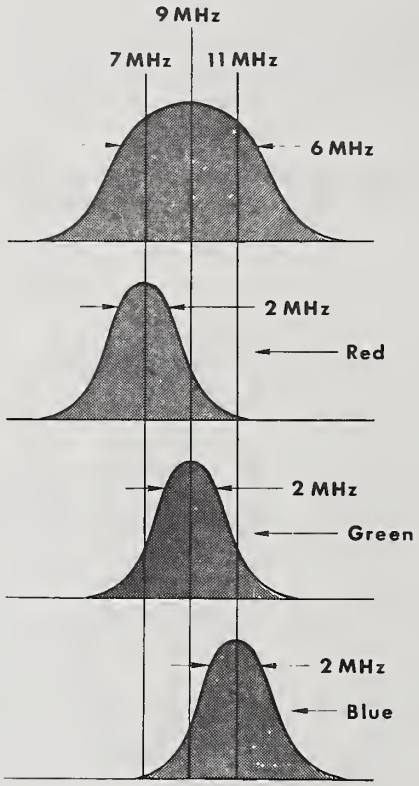

The *color control* device (fig. 12) opens the camera shutter, sequentially applies the DC voltage corresponding to each frequency band, positions the light filter wheel to interpose the respective light filter for three successive sector scans, and controls a *programmable amplifier* for normalizing the signals of the three bands. A single frame of film records the low-frequency response through the red filter, the middle-frequency response through the green filter, and the high-frequency response through the blue filter. Where the primary colors are equally represented, the result is pure white. Where the proportion of the three primary colors is varied, the Spectra-Color Ultrasonogram will record that hue of the light spectrum which is specific to that proportion.

The S.C.U. is recorded on Kodak high-speed Ektachrome, ASA 125 tungsten type, exposed over three sector scan sweeps at a lens opening of f2.8, and processed for a film speed of ASA 300. This emulsion type provided the proper color balance.

Our preliminary investigations indicate that the various color patterns observed with S.C.U. depend on a number of factors. Some of these include the signal strength, the structure of tissue, the resolution of the system, and the shadowing of one tissue by another.

The clinical system was calibrated by adjustments of the gain and attenuator controls so that echoes of the combined three frequency ranges from the major reflecting structures in the normal eye, produced a near-white spectra color ultrasonogram.

A number of patients with diseased eyes were studied by S.C.U. to correlate the spectral reflectivity of these abnormal eyes with a specific pathological diagnosis. Spectra-Color Ultrasonograms of diseased eyes have been characterized by a "breakdown" in the white display, and yield patterns with a variety of hues.

The choroidal melanomas have consistently been represented by spectral color combinations of the mid- and lower-frequency ranges. Separated retinal tissue has consistently been represented by the predominance of the lower frequency range. However, as yet, there is insufficient experience with this method to compare abnormal tissue of different cell types with similar size and location within the eye.

At this stage of the investigation, the many parameters which affect the spectral display are not completely understood. However, the results of this investigation have shown this method workable and easily adaptable to clinical application, and should further our ability to more precisely identify tissue by diagnostic ultrasound.

References

[1] Sokollu, A., Purnell, E. W., Holasek, E., and Jennings, W. D., Tissue identification by ultrasonic spectra, in *Abstracts of the Annual Meeting of Am. Inst. of Ultrasonics in Medicine,* p. 10 (Ann Arbor, Michigan, 1973).

[2] Holasek, E., Jennings, W. D., Sokollu, A., Purnell, E. W., Recognition of tissue patterns by ultrasonic spectroscopy, in *Proceedings of 1973 Ultrasonics Symposium,* p. 73 (IEEE Cat. No. 73 CHO 807-8 SU, 1973).

[3] Sokollu, A. and Holasek, E., Model study of propagation of ultrasonic waves in ocular media, in *Opthalmic Ultrasound*, Gitter, Keely, Sarin, and Meyer, eds., p. 88 (The C. V. Mosby Company, 1964).

[4] Dunn, F., Edmonds, P. D., and Fry, W. J., Absorption and dispersion of ultrasound in biological media, in *Biological Engineering*, Herman P. Schwan, ed., p. 205 (McGraw Hill Book Company, 1969).

[5] Pauly, H. and Schwan, H. P., Mechanism of absorption of ultrasound in liver tissue, *J. Acoust. Soc. Am.* 50, 692 (1971).

National Bureau of Standards Special Publication 453. Proceedings of Seminar on Ultrasonic Tissue Characterization held at NBS, Gaithersburg, MD, May 28-30, 1975. (Issued Oct. 1976)

Paper 4.3: ALGEBRAIC RECONSTRUCTION OF SPATIAL DISTRIBUTIONS OF REFRACTIVE INDEX AND ATTENUATION IN TISSUES FROM TIME-OF-FLIGHT AND AMPLITUDE PROFILES

J. F. Greenleaf and S. A. Johnson

Biophysical Sciences Unit
Mayo Medical School
Rochester, Minnesota 55901

Two-dimensional distributions of refractive index and attenuation were measured in transverse sections through intact isolated organs, using reconstruction techniques. Profiles of time-of-flight (TOF) and/or amplitude of 10 MHz pulses through the specimen were obtained by rectilinearly scanning two opposing transducers along either side of the specimen in the plane of interest. The received pulses were digitized at a rate of one 8-bit sample per 10 ns for 512 samples, and were analyzed with a computer algorithm which calculated the TOF of the pulse to within ± 10 ns and/or its amplitude. Typically, 256 measurements of TOF and/or amplitude were made in each profile scan for each of 37 angles of view separated by 5°. TOF's through tissue, normalized by TOF through water, were used to calculate velocity and, hence, refractive index within the specimen, using an algebraic reconstruction technique (ART). A similar approach was taken to calculate attenuation distributions. Images obtained represented acoustic velocities and/or attenuation in individual cross sections within the tissue specimen with a resolution of 64 by 64 elements (< 2 mm^2). The disadvantage of TOF and attenuation reconstruction is that transmission scanning is required. Advantages over B- and C-scan imaging are: (1) dynamic changes in receiver gain are not required; (2) attenuation occurs on only one traversal through tissue; and (3) the absolute values of important acoustic parameters (velocity and attenuation) are determined which may have significant diagnostic value.

Key Words: Acoustic attenuation; acoustic velocity; breast tumor; computerized tomography; heart; reconstruction; refractive index; synthetic focus; tissues; ultrasound.

1. Introduction

It has been known for some time that three-dimensional functions can be determined from their two-dimensional projections, *i.e.*, line integrals along paths through the three-dimensional function [1].[1] Obtaining a solution for three-dimensional distributions of functions from their two-dimensional projections is popularly called "reconstruction" or computer-assisted tomography (CAT). The recent uses of CAT in medical radiology have had a tremendous impact on the field of neuroradiology [2]. For the first time in the history of roentgenography, the radiologist can obtain quantitative measures of the spatial distribution of roentgen absorption coefficients within the body. Medically-valuable applications of reconstruction methods have been developed in many areas of medical research using forms of energy such as x-radiation [3,4], electrons [5], and more recently, ultrasound [6,7].

[1]Figures in brackets indicate the literature references at the end of this paper.

Historically, ultrasound has been used to obtain images such as B-scans, which correspond to geometric distributions of the gradient of acoustic impedance, and transmission C-scans, which produce images corresponding to acoustic attenuation [8]. Images representing quantitative distributions of basic mechanical tissue properties or values of acoustic parameters such as those recently obtained in this laboratory [7], may be intrinsically more valuable than qualitative images representing only tissue interfaces and geometries. Since fundamental mechanical tissue parameters such as adiabatic compressibility and density can be calculated from measured values of other acoustic parameters [9], quantitative images representing two-dimensional distributions of such fundamental properties may be possible with the reconstruction techniques recently developed in this laboratory.

The purpose of this paper is to describe initial results of applying reconstruction techniques for obtaining quantitative images representing acoustic refractive indices and attenuation coefficients within isolated tissues and phantoms. These images are calculated from profiles of propagation delay time and acoustic intensity obtained by transmission scanning with a single pair of transducers, one on each side of the region of interest.

The theory for mathematically and quantitatively reconstructing two-dimensional spatial distributions of acoustic parameters such as attenuation, speed of sound, and other functions which can be related through line integrals to their shadow images, will be described. In figure 1, an acoustic ray traverses a space divided into n^2 finite elements or picture cells (pixels). We assume that the local value of some acoustic parameter in pixel i is constant

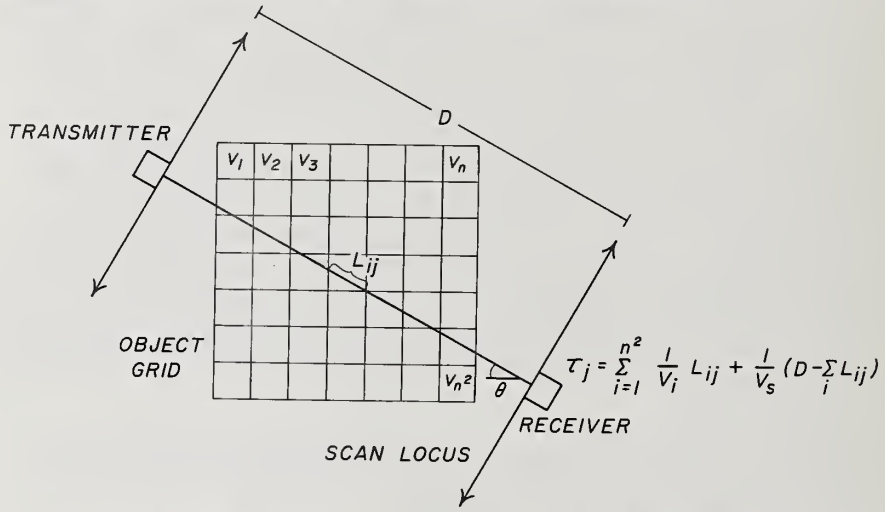

Figure 1. Geometry of ultrasound transmission for algebraic reconstruction. Grid is fixed to coordinates of object. Speed of sound, V_i, is assumed to be constant and isotropic within each pixel. L_{ij} can be varied according to curvature of ray path, which need not be straight. The equation represents propagation delay of pulse through reconstruction region (grid). Number of measurements (*i.e.*, equations) required for solution of set of linear equations is obtained by rectilinearly scanning object at many angles of view.

within the pixel and is denoted by F_i. Let L_{ij} be the length of the path of ray j as it traverses pixel i. Further, let us suppose that the cumulative effect of the interaction of the acoustic energy with the material along ray j can be measured as an integral or sum and has a value G_j. Then the following relationship holds:

$$G_j = \sum_{i=1}^{n^2} L_{ij} F_i \qquad \text{for each ray } j = 1,2,\ldots,M. \tag{1}$$

We note that each ray j has an associated value G_j and that given sufficient independence and a sufficient number of equations M, the set of simultaneous equations representing these measurements can be solved for the values of F_i since the L_{ij} are known from geometric

considerations. Although eq. (1) appears to be merely a set of linear simultaneous equations, the fact that n is 64 or greater precludes direct solutions to the set of equations and requires special treatment of the problem. However, many techniques for solving this set of equations have been devised [10]. In general, the solutions shown in this paper will be for conditions in which n is 64 and the set of equations have been solved using an iterative technique (algebraic reconstruction technique, ART) [3,4].

The specific equations for applying this technique to solutions of attenuation and index of refraction are given below and are derived relative to the geometry shown in figure 1.

Attenuation: assume attenuation can be described by the relationship

$$\frac{I_j}{I_o} = \exp\left(-\sum_{i=1}^{n^2} \alpha_i L_{ij}\right), \tag{2}$$

where I_o is the incident intensity, α_i is the acoustic attenuation in pixel i and L_{ij} is the length of ray j in pixel i. Then the acoustic "density" D can be obtained from the following set of linear equations with some suitable reconstruction algorithm,

$$D_j = \ln\left(\frac{I_o}{I_j}\right) = \sum_{i=1}^{n^2} \alpha_i L_{ij} \quad j = 1,2,\ldots,M. \tag{3}$$

Index of Refraction: assume the propagation time for an acoustic ray j traversing a length L_{ij} of pixel i is τ_i. Then the total time of propagation of the ray through the grid of figure 1 is

$$T_j = \sum_{i=1}^{n^2} \tau_i = \frac{1}{V_F} \sum_{i=1}^{n^2} \eta_i L_{ij}, \tag{4}$$

where η_i is the acoustic index of refraction defined as V_F/V_{ti}, the ratio of acoustic velocity in the surrounding fluid to the velocity in tissue for pixel i.

In practice, the difference between the arrival time of the pulse through a fluid-filled gap ($\tau_F = L/V_F$, figure 1) and that of the pulse through the tissue (eq. (4)) is the actual values measured by the equipment giving

$$\tau_F - \tau_j = \frac{1}{V_F} \sum_{i=1}^{n^2} (1 - \eta_{ti}) L_{ij}, \tag{5}$$

for each ray j = 1,2,...,M, where

$$\eta_{ti} = \frac{V_F}{V_{ti}} .$$

The procedure of obtaining solutions for α_i and η_{ti} from eqs. (3) and (4), respectively, requires one to obtain at least as many measurements (*i.e.*, independent equations) as there are unknowns. The way in which this is done is to make measurements of propagation time or intensity for as many rays through the tissue as possible, given the available geometry. Typically, this is accomplished by rectilinearly scanning the tissue at each of several angles of rotation (about an axis perpendicular to the scan plane) of the tissue relative to the scanning transducers.

2. Data Acquisition

Data for reconstructing acoustic properties within phantoms and excised organs were obtained by transmitting acoustic pulses through the tissue to be studied utilizing transmit and receive transducers arranged in the geometry shown in figure 2. The use of a focused lens

on the transmitter maximizes the energy intensity, while minimizing the area being illuminated by ultrasound, thus minimizing the probability of measuring pulses arriving at the receiver through multiple pathways. The use of a focused lens on the receiving assembly insures that the acoustic energy passes through a relatively small window in space before being detected by the receiver transducer. The normalized error response of this particular geometry as a function of the distance of the transmitter-receiver axis (with fixed gap length) from the center of a cylinder having an index of refraction of 0.94, is also shown in figure 2. Note that the error is smallest for the geometry in which the receiver is next to the cylinder and the transmitter is furthest away from the radius of the cylinder (B_T = 4 cm). These calculations did not include the effects of total reflection at the critical angle.

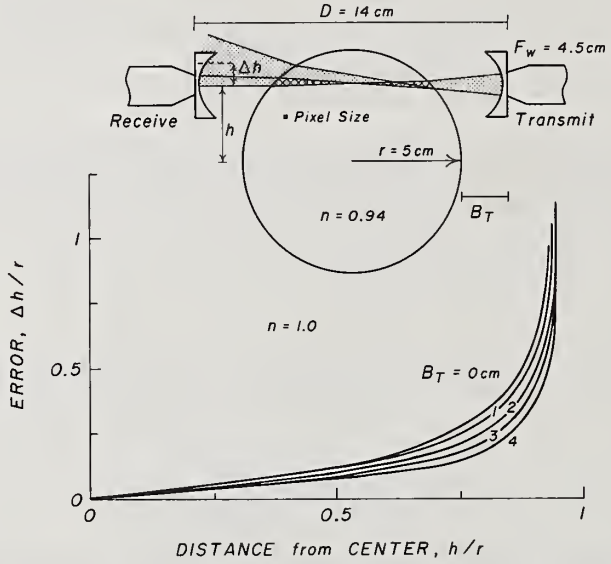

Figure 2. Lens-transducer system used to obtain ultrasound reconstruction data. Cylindrical model is used for analysis of acoustic refraction. Central ray of beam is refracted by amount ΔH depending on distance ΔH/r from center of cylinder and depending on distance from transmitter to cylinder B_T. F_W is the focal length in water. Gap length D was fixed for error analysis.

The transmitter-receiver assembly was scanned on either side of the region being studied using a specially-modified computer-controlled Magna IV scintiscanner [7]. The sample was rotated utilizing a computer-controlled stepper motor (Fig. 3) which was rotated in integer multiples of 1.8°. Signals from the receiver were amplified with a Panametrics PR 50 50 amplifier and subsequently input into a Biomation Model 8100 transient recorder (BTR) and digitized at rates of up to one 8 bit sample per 10 nanoseconds for up to 1,024 consecutive samples. Specific details of the data acquisition system are described elsewhere [7].

Figure 4 illustrates representative examples of digitized signals detected by the receiver and digitized by the BTR and demonstrates the change in propagation time of acoustic pulses through various materials. The arrival times through this particular tissue (canine heart) vary over a range of about 2.5 microseconds, indicating that a digitizing resolution of 10 nanoseconds gives an accuracy of one part in 200 over the signal range. However, since the total propagation time was approximately 100 microseconds, the absolute accuracy of the measurement was about one part in 10^4.

An example of the entire set of data obtained during one scan across the tissue is shown in figure 5. A computer algorithm was utilized which scanned each horizontal line depicted in figure 5 and calculated the point at which the signal changed in amplitude more negative than two standard deviations of the background noise (defined as the noise in the first 12 samples representing the baseline). The algorithm then searched backwards down the first pulse to that point representing the zero crossover (baseline average) using

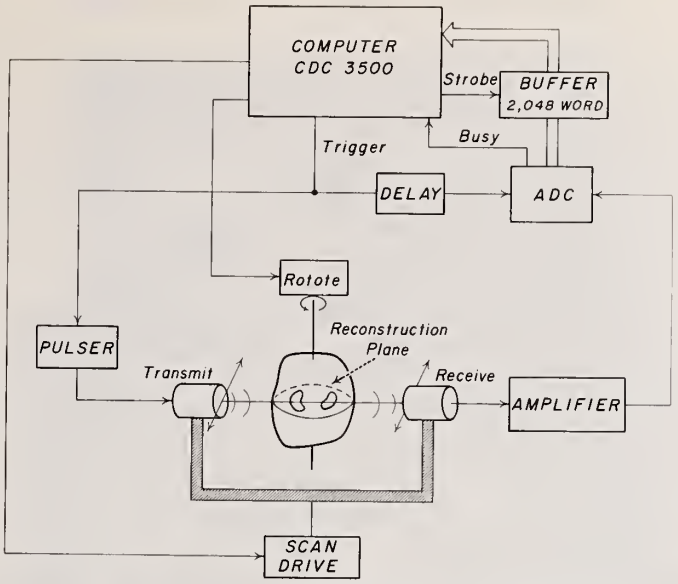

Figure 3. Schematic of computer-controlled data acquisition system which obtains digitized ultrasonic pulses from transmission scans to be used for reconstruction. Pulser and A/D converter are triggered by computer at 256 equally-spaced points along the scan length of about 12 cm. Received signal is digitized at rates of up to 100 samples-per-microsecond. After digitization of pulses received along one rectilinear scan, sample is rotated by stepper motor and the process is repeated through 180°.

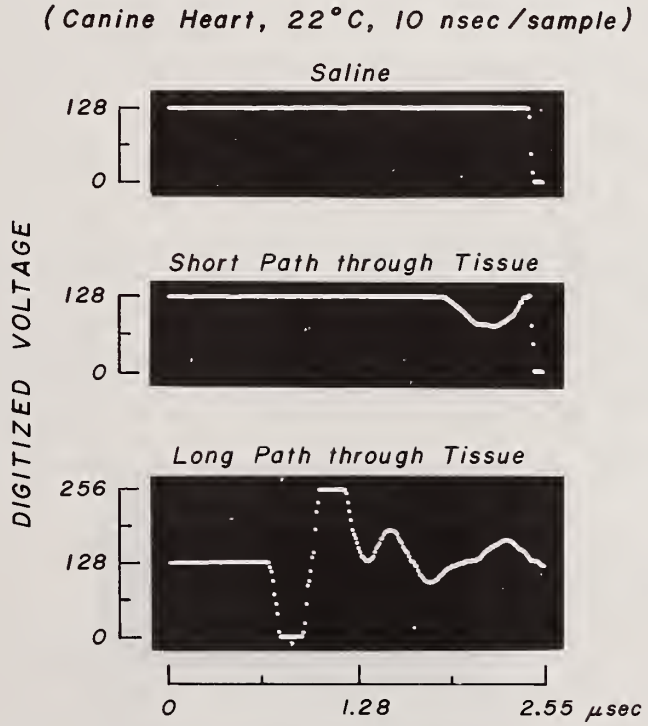

Figure 4. Digitized ultrasound pulses after transmission through saline and two different path lengths of tissue. Received signal is digitized into 256 8-bit samples separated by 10 nanoseconds. Arrival time, determined by computer algorithm, is defined as earliest negative-going portion of signal to emerge from noise. Arrival time through tissues such as cardiac muscle are usually earlier than for saline-filled gap.

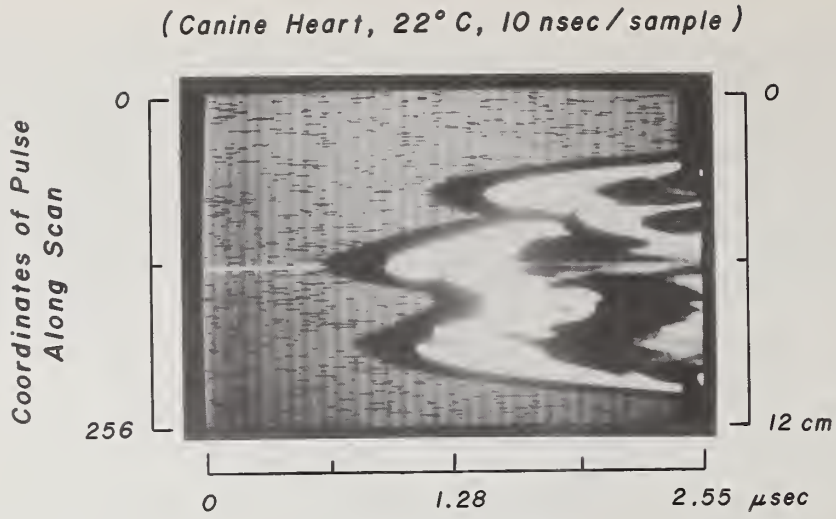

Figure 5. Digitized ultrasonic pulses: arrival time (left-to-right) versus position along scan traversal (top-to-bottom). Intensity of image is proportional to received signal intensity (black < 0.0, white > 0.0 volts). Arrival time through saline (top several lines) is relatively stable and later than arrival times through tissue. Brightened line indicates waveform depicted in A-scan format in bottom panel of figure 4.

the nearest sample time as the arrival time. In certain experiments, the gain of the amplifiers was set so as not to clip the signal, in which case the computer program also calculated the amplitude of the peak of the first negative-going portion of the pulse and utilized the logarithm of this value in calculating profiles representing the acoustic attenuation of the arriving ultrasonic pulse. Computer analysis of the data depicted in figure 5 results in a set of profiles for the propagation delays through the tissue and, depending on the experiment, another set of profiles representing the amplitudes of the arriving ultrasound pulses to be utilized for subsequent reconstruction of two-dimensional distributions of acoustic refractive indices and/or acoustic attenuation coefficients, respectively.

An example of "time-of-flight" profiles obtained by computer analysis of the data shown in figure 5 is represented in figure 6. In general, these profiles are adjusted so that their value for the time-of-flight or intensity through the immersing liquid is zero giving a background in the subsequent reconstruction images which depicts the representative parameter in the immersing fluid as black. In general, 36 to 60 profiles, each containing about 256 time-of-flight or intensity values, were obtained representing time-of-flight or intensity profiles for the multiple views around the object through a range of 180°.

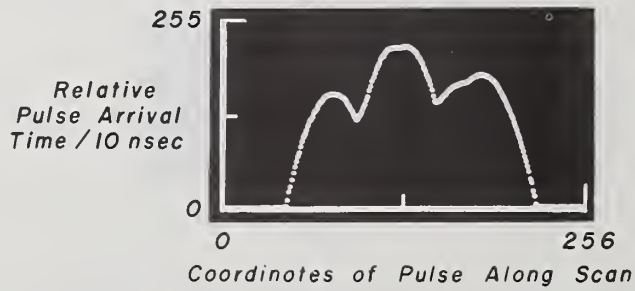

Figure 6. Computer-generated profile of ultrasound propagation delay through saline-immersed, saline-filled canine heart. Computer algorithm calculated arrival times from digitized pulses represented in figure 5. Dynamic range of arrival times is about 2.5 microseconds.

3. Results

The ability to quantitatively determine the value of acoustic indices of refraction was tested using a phantom consisting of rubber finger cots filled with different concentrations of saline. Concentrations of saline ranging from 1 to 8 gm of sodium chloride per 100 ml of distilled water were utilized. Thirty-six angles of view separated by 5.4 degrees were obtained with the scanning system described previously, resulting in measurements of the propagation delay time at 256 points along each profile. The resulting reconstruction is shown in figure 7. Although it is not clear that the various regions of saline have a

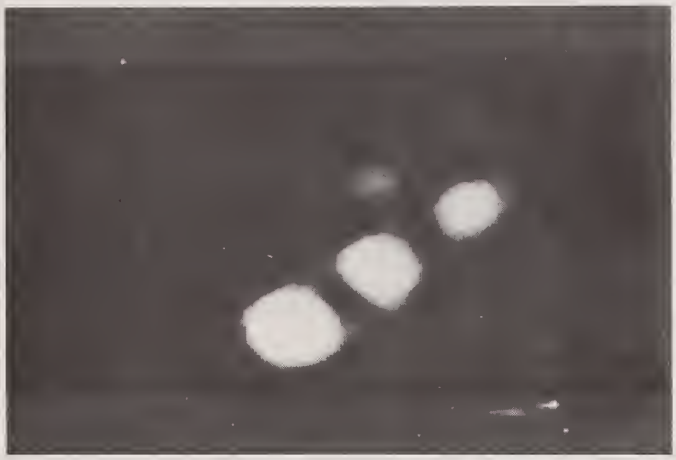

Figure 7. Reconstruction of acoustic index of refraction in saline-filled phantom. Five finger cots were filled with saline concentrations of 1, 2, 4, 6, and 8 gm of sodium chloride per 100 ml distilled water. Phantom was scanned in manner described previously. Speed of sound is proportional to salinity, the highest speed of sound in brightest region of image is 0.64% greater than that of surrounding water.

direct relationship to acoustic velocity, it seems evident that the size of the regions imaged varies with the acoustic velocity. This is apparently the net result of the particular parameters chosen for display and photographic reproduction acting in combination with the refractive properties of the transducer-lens system which was not designed to obtain optimal spatial resolution for this particular test of velocity resolution. The relationship between the averaged reconstructed velocities (five values from the 64 x 64 array of reconstructed velocities were averaged from each finger cot image) and the concentration of sodium chloride is shown in figure 8. The acoustic velocity in water is proportional to sodium chloride concentration in this region of concentrations [11] and, therefore, the plot should be a straight line. It is clear that the errors encountered in this technique are relatively small considering that the change in acoustic velocity was 0.16% between the 2 g/100 ml saline solution and the surrounding water. The high accuracy of the results of this test are not too surprising considering one can measure arrival times of acoustic pulses to within one part in several thousand. Whether this accuracy can be obtained *in vivo* is yet to be proven.

To test the reconstruction technique on tissue models, we first chose to reconstruct the regional distributions of acoustic index of refraction within an isolated canine heart. The isolated heart was immersed in water, filled with water and rectilinearly scanned for each view as it was rotated in five degree increments about its vertical axis through a range of 180°. The left panel on figure 9 represents a reconstruction of the refractive indices through a transverse plane at which the tissue was subsequently sliced after freezing. A photograph of the surface of the sliced heart is shown in the right panel. One can see the ventricular papillary muscles, the endocardial surface of the right ventricle, and the epicardial surface. That the variations in index of refraction within the interior of the myocardial wall are true variations in velocity is suspected but unproven.

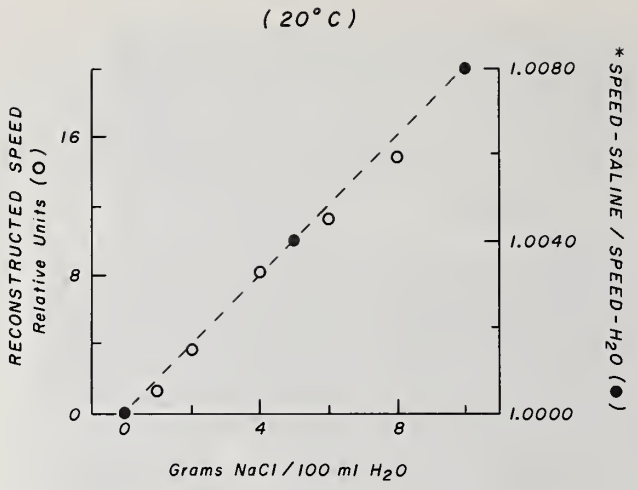

*Millero and Kubinski, J Acoust Soc Am 57(2): 312-319, 1975

Figure 8. Reconstruction of speed of sound within rubber finger cot phantom containing different saline concentrations. Five points in the center of each finger cot image shown in figure 7 were averaged to obtain values shown by circles in this graph. Filled circles indicate acoustic velocities of selected saline concentrations obtained from literature. Accuracy of results is due to ability to measure pulse arrival time to 1 part in 10^4, allowing extremely accurate measurements of refractive index (right ordinate).

Figure 9. Reconstructions of refractive index within canine heart (left) compared to photograph of section through corresponding level (right). Reconstruction of 64 x 64 array of pixels was linearly interpolated up to 128 x 128 pixels. Papillary, epicardial and endocardial surfaces are represented with good fidelity; however, detail shown here of acoustic velocity within the myocardial tissue is not yet substantiated.

Figure 10 illustrates reconstructions of acoustic attenuation (left panel) and acoustic index of refraction (right panel) within a coronal section through a human female breast obtained from subcutaneous mastectomy post mortem. The distribution of reconstructed refractive indices correlated in a qualitative way with the distribution of fat (dark areas) and connective tissue (light areas) in the breast as judged from the gross specimen. The

position of the nipple and associated ducts can be seen as the dark hole in the upper left central region of both images. The ring-like region around each reconstruction probably occurred as a result of critical-angle reflection causing inconsistencies in the reconstruction equations.

Figure 10. Reconstruction of refractive index (right) and acoustic attenuation coefficients (left) within normal excised human breast tissue obtained from post mortem subcutaneous mastectomy in a 21-year-old woman. Scan data were obtained in a manner similar to that described in figure 1. However, both arrival time and amplitude profiles were calculated from the digitized pulses to obtain velocity and attenuation images, respectively. Although these images are uncorrected for refraction errors, the detail seems promising. The ducts associated with the nipple can be seen in the upper left central region of each image. The dissimilarity of these two images indicate that these two acoustic parameters are relatively independent.

Although the quantitative details of these reconstructions cannot yet be correlated with individual breast tissues, it is clear that the two types of reconstruction images represent nearly independent acoustic parameters. It is the independence of acoustic parameters such as refractive index and attenuation which may allow accurate differential characterization of tissue types in healthy and diseased organs, particularly the breast.

4. Discussion

Computer-assisted tomography (CAT) has been applied to the measurement of the two-dimensional spatial distribution of two acoustic parameters, attenuation and refractive index. Arrival times of acoustic pulses propagated by transmission through a tissue specimen at many angles of view have been used to reconstruct the refractive indices within selected excised tissue samples. The intensities of acoustic pulses have been used as an indication of attenuation and have been utilized for reconstruction of the two-dimensional distribution of attenuation coefficients within breast tissues.

The use of the arrival time of the pulse as an indication of propagation delay tends to minimize the undesirable effects of refraction since in a homogeneous material such as tissue, whose index of refraction varies less than a few percent, the earliest arrival time will in general represent the shortest and thus straightest path through the tissue. The use of arrival time is particularly sensitive to detection of small inclusions or regions in which the speed of sound is higher than its surroundings since in this case the straight ray through the inclusion is the first to arrive at the detector. The fidelity of the reconstruction of distributions of index of refraction was qualitatively shown to be good in tissue and the accuracy of calculated refractive indices within a phantom was shown to be accurate to within a few parts in a thousand. Reconstructions of the two-dimensional distributions of attenuation coefficient could only be qualitatively described since the assumption was made that attenuation is an exponential function, independent of the

direction of propagation. This assumption is probably true for situations where the major portion of attenuation is caused by absorption and isotropic scattering, while reflection and anisotropic scatter are minimal.

The effect of refraction on the assumption that the paths of acoustic energy through the tissue are straight lines seemed to be minimal, especially for the relatively coarse reconstruction resolution of 64 x 64 pixels per image. For reconstructions of higher spatial resolution, it will become imperative that the effect of refraction on the ray paths be taken into account. The use of the algebraic reconstruction technique (ART) allows one to use curved ray paths in reconstruction. This may allow one to use ray tracing [12] in order to solve for the actual paths of the rays through the tissue and thus obtain higher-fidelity reconstructions.

Accurate reconstructions of the refractive index may lead to a method of correcting for refraction in compound B-scans and allow for the subsequent calculation of acoustic impedance. It is clear that all acoustic images are distorted to some degree due to refraction; therefore, techniques of obtaining accurate distributions of refractive index could be utilized for the reduction of distortion in almost all types of acoustic images. A technique termed "synthetic-focus imaging," developed in our laboratory [13], has the property of retaining maximum information as to the nature of reflection and scattering over wide angles because it retains intensity and phase information by digitization of the total signal received by an array of transducers. Since "synthetic focusing" is accomplished by computer algorithms, aberrations due to refraction can be corrected for using refractive-index distributions determined by the image reconstruction technique.

Although arrival times and intensities of the acoustic pulses were calculated using computer algorithms, analog techniques could be used after optimal methods of finding these parameters have been determined by computer simulation. Complex algorithms for calculation of arrival times from digitized pulses could also be implemented on special-purpose digital devices such as microprocessors in order to decrease the calculation time.

The use of high-speed, high-fidelity signal processing methods [14] in combination with techniques of computer-assisted tomography may allow quantitative imaging of basic acoustic properties within the intact human. The quantitative determination of two-dimensional spatial distributions of parameters relating to the basic mechanical properties of tissues may provide significant increases in the ability to distinguish and characterize the various tissues of the body in both healthy and diseased states.

The authors wish to thank Dr. Richard A. Robb for assistance in programming the BTR and Mrs. Jean Frank and coworkers for their secretarial and graphic assistance. Mr. William Samayoa and Mr. Francis Duck assisted in algorithm programming and data collection. Dr. Gary Glover of General Electric Corporation assisted in the design of the saline phantom. Dr. Titus Evans has provided valuable administrative and technical assistance.

This research was supported by grants NO1-HT-4-2904, HL04664, and RR-7 and HL00060 from the National Institutes of Health, United States Public Health Service: AF 44620-71-C-0069 from the United States Air Force.

References

[1] Bracewell, R. N., Strip integration in radio astronomy, *Austral. J. Phys.* 9, 198 (1956).

[2] Baker, H. L., Jr., Campbell, J. K., and Houser, O. W., Computer-assisted tomography of the head: an early evaluation, *Mayo Clinic Proceedings*, 49, 17 (1974).

[3] Gordon, R. and Herman, G. T., Three-dimensional reconstruction from projections: a review of algorithms, *International Reviews of Cytology*, 38, 111 (1974).

[4] Johnson, S. A., Robb, R. A. and Greenleaf, J. F., Dynamic three-dimensional reconstructio of beating heart and lungs from multiplanar roentgen-television images, *Mayo Clinic Proceedings*, 49, 958 (1974).

[5] Klug, A. and Crowther, R. A., Three-dimensional image reconstruction from the viewpoint of information theory, *Nature (London)*, 238, 435 (1972).

[6] Greenleaf, J. F., Johnson, S. A., Lee, S. L., Herman, G. T., and Wood, E. H., Algebraic reconstruction of spatial distributions of acoustic absorption within tissue from their two-dimensional acoustic projections, in *Acoustical Holography, Vol. 5*, P. S. Green, ed., p. 591 (Plenum Press, New York, 1974).

[7] Greenleaf, J. F., Johnson, S. A., Samayoa, W. F., and Duck, F. A., Algebraic reconstruction of spatial distributions of acoustic velocities in tissue from their time of flight profiles, in *Acoustical Holography, Vol. 6*, N. Booth, ed., p. 71 (Plenum Press, New York, 1975).

[8] Green, P. S., Schaefer, L. F., Jones, E. D, and Suarez, J. R., A new high performance ultrasonic camera system, in *Acoustical Holography, Vol. 5*, P. S. Green, ed., p. 493 (Plenum Press, New York, 1974).

[9] Kinsler, L. E. and Frey, A. R., *Fundamentals of Acoustics*, (John Wiley and Sons, Inc., New York, 1950).

[10] Gordon, R. and Herman, G. T., Reconstruction of pictures from their projections, *Communications of the ACM*, 14, 759 (1971).

[11] Millero, F. J. and Kubinski, T., Speed sound in sea water as a function of temperature and salinity at 1 atm, *J. Acoust. Soc. Am.* 57, 312 (1975).

[12] Jacobson, M. J., Siagmann, W. L., Weinberg, M. L. and Clark, J. G., Pertubation method for determining acoustic rays in a two-dimensional sound speed medium, *J. Acoust. Soc. Am.* 57, 843 (1975).

[13] Johnson, S. A., Greenleaf, J. F., Duck, F. A., Chu, A., Samayoa, W. F., and Gilbert, B. K., Digital computer simulation study of a real-time collection, post-processing synthetic focusing ultrasound cardiac camera, in *Acoustical Holography, Vol. 6*, N. Booth, ed., p. 193 (Plenum Press, New York, 1975).

[14] Gilbert, B. K., Storma, M. T., James, C. E., Hobrock, L. W., Yang, E. S., Ballard, K. C., and Wood, E. H., A real-time hardware system for digital processing of wideband video images, *IEEE Trans Computers* (manuscript in preparation).

National Bureau of Standards Special Publication 453. Proceedings of Seminar on Ultrasonic Tissue Characterization held at NBS, Gaithersburg, MD, May 28-30, 1975. (Issued Oct. 1976)

Paper 4.4: MEASUREMENT OF ULTRASONIC TISSUE CHARACTERISTICS BY DIRECT AND PHASE-CONTRAST IMAGING

R. S. Mezrich, D. H. R. Vilkomerson, and K. F. Etzold

RCA Laboratories
Princeton, New Jersey 08540

This paper describes methods for measurement of the ultrasonic attenuation and acoustic velocity of biological tissue. Initial results are given for a series of measurements on excised breast tissue that quantitatively demonstrate the correlation between ultrasonic attenuation and pathological state. A method for measuring changes in phase (due to velocity and thickness differences) in a wave as it passes through tissue, based on the phase-contrast technique, is described and demonstrated. The principal advantage of this method over other phase measurement techniques is that it is not as sensitive to the effects of structure overlying the region of interest.

Key Words: Attenuation; breast tissue; broadband; high resolution; imaging; large aperture; pathology; pellicle; phase-contrast; transmission; ultrasound; velocity.

1. Introduction

One of the goals of the research on ultrasonic interactions with biological tissue has been to develop methods of acoustical characterization in order to be able to determine pathological states and as an aid to the design of new instruments for ultrasonic visualization. Since 1952, when Wild and Reid [1][1] reported on differences between the ultrasonic echoes from malignant and benign tumors, there have been a number of studies of the characteristic interaction of sound including, for example, such effects as attenuation [2], scattering [3], and variations in acoustic velocity [4]. These studies have not been complete and, more important, lack the quantitative nature needed for the effective determination of tissue characteristics.

This report describes the application of a new system [5] for the measurement and visualization of ultrasonic waves to the study of attenuation and acoustic wave velocity in tissue. The important characteristics of the system are: a uniform frequency response from 0.5 to 10 MHz; a large angular acceptance (0-40°) which, with acoustic lenses, allows wavelength-limited resolution; a large aperture (to 6 inches); and the ability to measure the tissue characteristic reproducibly and accurately while the acoustic image is displayed. The ultrasonic transmissivity of tissues is measured by detecting the ultrasonic intensity at each point of the acoustic image. Acoustic velocity differences in tissue can be measured by using the principles of phase-contrast microscopy.

Figure 1 illustrates one application of the system to tissue characterization. Part A is an optical image of an excised breast section with a malignant tumor. Part B is an ultrasonic image (at 3 MHz) to the same scale, photographed from the display CRT of the system. Regions of high acoustic transmissivity appear light while regions of low relative transmissivity are darker. The section was held on a plastic frame and the metal screws, seen in both images, were used as markers. As will be discussed

[1]Figures in brackets indicate the literature references at the end of this paper.

below, the electrical signal used to modulate the brightness of the CRT at each point of the image is directly proportional to the acoustic intensity and is measured as the signal is displayed to determine the relative tissue transmissivity. In this particular tissue, the transmissivity through the normal region of the section (1 cm thick) was -4 dB (relative to the transmission through water) while that through the malignant region was -20 dB. It is important to note that these values are not averages over large cross-sections of tissue, but rather accurate measurements of the local tissue transmissivity; the lateral resolution in the image, limited by the F:2 acoustic lenses, was < 2 mm.

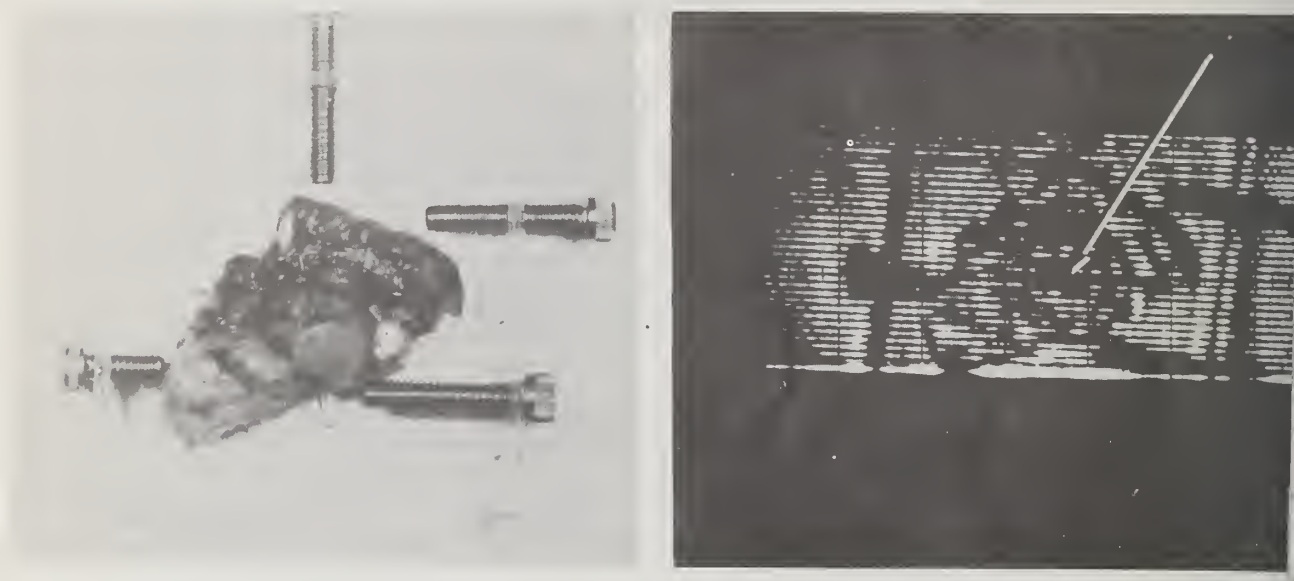

Figure 1. Optical and acoustic image of excised breast tissue with malignancy (dark region in acoustic image). Screws were used as markers.

In the following sections, we shall briefly describe the operation of the ultrasonic imaging system, discuss and illustrate its application to tissue characterization, including recent results on the measurement of differing ultrasonic attenuation in benign and malignant breast tumors, and demonstrate the implementation of the phase-contrast method to display and measure ultrasonic velocity differences.

2. Ultrasonic System

The arrangement used to display and measure ultrasonic waves is schematically illustrated in figure 2. The structure to be displayed (tissue section, phantom, etc.) is placed on the object plane, insonified, and imaged by plastic acoustic lenses onto a thin metallized plastic film (pellicle). The pellicle is so thin ($\sim$ 6 μm) that its motion at every point is almost exactly equal (> 99%) to the displacement amplitude of the ultrasonic wave passing through it. The ultrasonic displacement amplitude is measured by interferometrically detecting the motion of the pellicle. By scanning a laser beam over the pellicle, a signal is produced which is proportional to the displacement amplitude. This signal can be measured and simultaneously processed to modulate the brightness of a CRT.

The following analysis demonstrates the sensitivity and linearity and indicates the means for achieving stability in an interferometric detection system. The arrangement used is the Michelson interferometer, the essential elements of which are shown in figure 3.

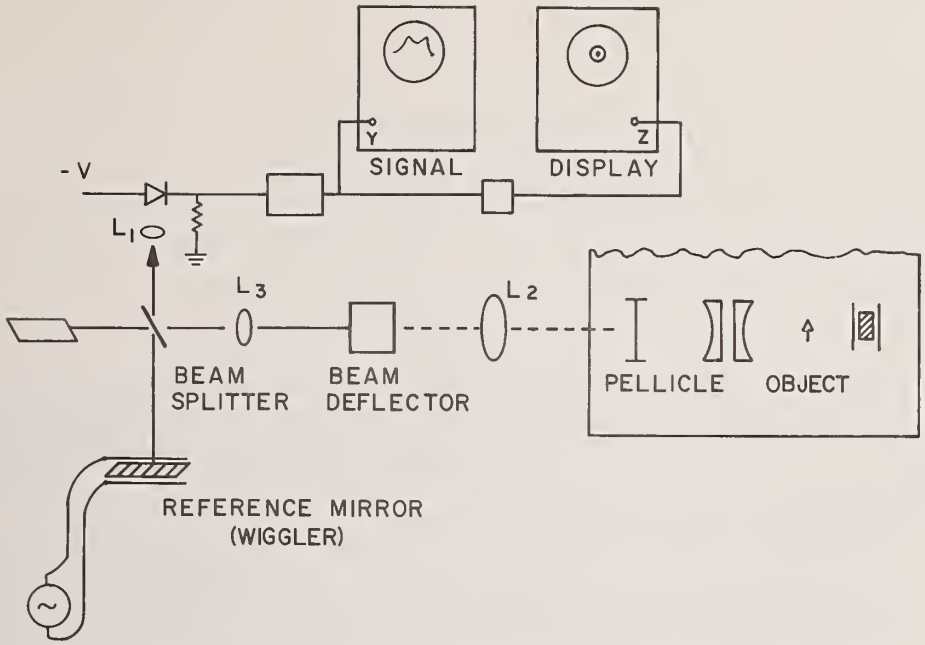

Figure 2. Schematic of practical interferometer for image display and measurement. Beam deflector, consisting of two-mirror galvanometers, is in one leg of the interferometer and "wiggler" (described below in text) is in the other leg. Current from photodiode, proportional to light intensity, is displayed and measured on signal scope and then processed to modulate the brightness of the display CRT.

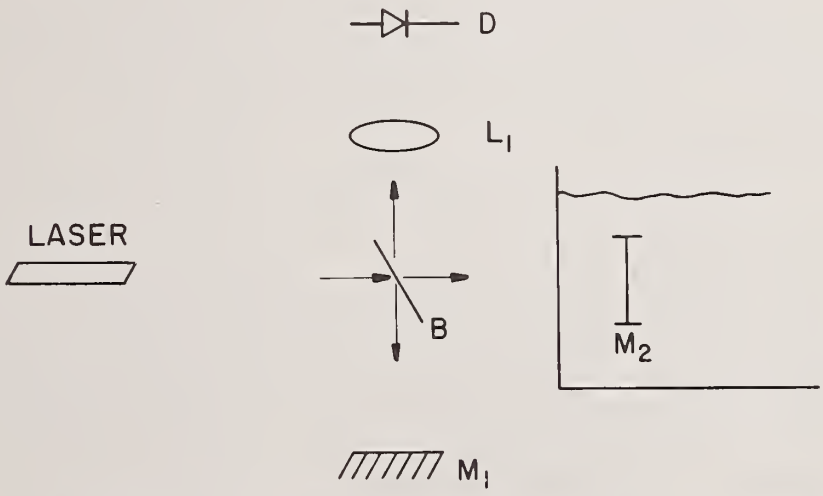

Figure 3. Michelson interferometer used to detect acoustic displacement amplitude. As pellicle (M_2) moves, the relative phase between M_1 and M_2 varies, causing intensity changes at photodiode (D). Laser beam is scanned to measure displacement at every point of pellicle (6 in diameter).

If the displacement amplitude of the acoustic wave at any point of the aperture is $\Delta \sin \omega t$ (which is related to the local acoustic intensity (I) by $I = \frac{1}{2}Z\omega^2\Delta^2$), then the motion of the pellicle at that point is also $\Delta \sin \omega t$. The phase of the light reflected from that point (the pellicle is gold coated and is one mirror of the interferometer) is

$$\phi_p = 2\Delta \cdot \frac{2\pi}{\lambda} \sin \omega t \tag{1}$$

and the amplitude of the light wave at the detector due to the pellicle is

$$A_p = A_{po} e^{j(\phi_{po} + 2\Delta \cdot \frac{2\pi}{\lambda} \sin \omega t)} \quad . \tag{2}$$

The amplitude of the light reflected from the reference mirror is

$$A_r = A_{ro} e^{j\phi_{ro}} \tag{3}$$

where ϕ_{ro} and ϕ_{po} are arbitrary phases which are measures of how far each mirror is from the beam splitter.

The light intensity at the photodiode, $I = |A_r + A_p|^2$, is

$$I = I_r + I_p + 2A_{ro}A_{po} \cos(\phi_{po} - \phi_{ro} + \frac{4\pi\Delta}{\lambda} \sin \omega t) \tag{4}$$

where I_r ($=|A_{ro}|^2$) and I_p ($=|A_{po}|^2$) are the average light intensities in each leg of the interferometer.

This intensity, which is related to the current in the photodiode by η (the quantum efficiency), is plotted as a function of $\phi_{po} - \phi_{ro}$ for the situation $\Delta \approx 0$ (fig. 4).

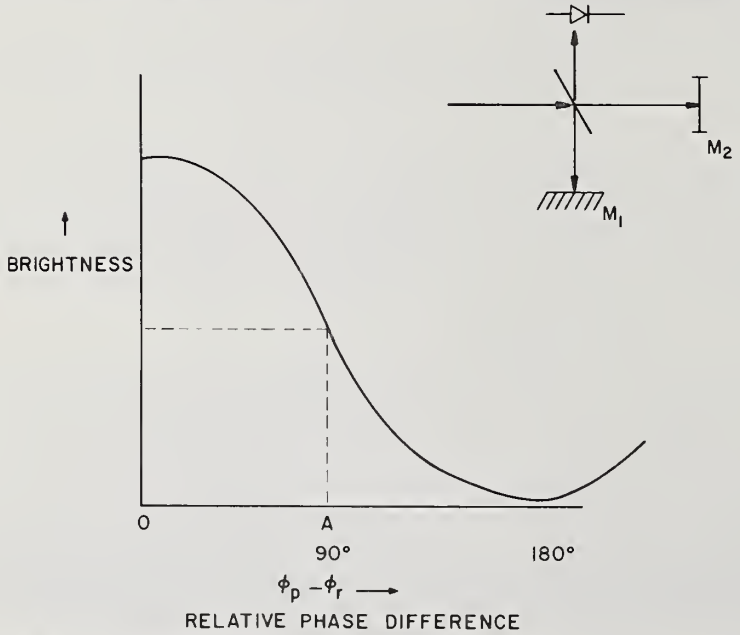

Figure 4. Interferometer response curve as function of relative mirror spacing. Maximum path difference for 180° phase shift is 1580Å for He-Ne laser. The slope of the curve is maximum at A (90° relative phase shift).

At the point $\phi_{po} - \phi_{ro} = 90°$, we note that the slope of the curve is linear and any change in phase, due to motion of the pellicle, causes a corresponding change in brightness and hence a change in photocurrent. The photocurrent at this point, neglecting the

contributions of the dc terms $I_r + I_p$ (which, in practice, are electrically filtered out), is

$$i_s = 2\eta A_{ro} A_{po} \sin\left(\frac{4\pi\Delta}{\lambda} \sin \omega_s t\right) \tag{5}$$

and for the situation $\Delta/\lambda << 1$ (*i.e.*, acoustic intensities less than 1 W/cm^2) this becomes

$$i_s = 8\pi\eta \frac{\Delta}{\lambda} A_{ro} A_{po} \sin \omega t \ . \tag{6}$$

The photocurrent is directly proportional to the displacement amplitude and can be easily calibrated by measuring the light intensity in each leg of the interferometer. As a check, the system accuracy was compared with a calibrated Navy reference transducer (NAL/USRD-E8) and the results agreed within ± 5%.

The sensitivity is proportional to the total light available and above about ¼ mW is limited by shot noise in the photocurrent. With a 15 mW He-Ne laser, the minimum detectable displacement is .07Å, corresponding to 5 nW/cm^2 acoustic intensity at 1.5 MHz, and with a 1 watt argon laser, acoustic intensity of 10^{-11}W/cm^2 should be detected. The upper limit of the linear range is determined by the linearity of the slope of the curve of figure 4, which is within 1% for pellicle motions as large as 100Å.

The accuracy of the system depends on the condition $\phi_{po} - \phi_{ro} = 90°$. At other values, the slope of the response curve varies, even going to zero at 0° or 180°. To prevent inaccuracies, a novel open-loop stabilization scheme was developed.

In this method, the reference mirror is mounted on a piezoelectric disc and vibrated, or "wiggled" so that the phase constantly varies between 0° and 180°. At least once per cycle (the mirror vibrates at about 50 kHz), the operating point of the system passes through the condition $\phi_{po} - \phi_{ro} = 90°$ and the response appears stable even in the presence of deleterious mechanical or thermal disturbances.

The signal at every point of the pellicle aperture (which can be as large as 6 in) is measured by scanning the laser beam over the pellicle. Once the signal is detected, it is amplified, measured, and processed for display on a CRT.

An example of the system operation, which illustrates the method by which measurements are made, is shown in figure 5. The object was a metal sheet with large (∿ 6 mm) and small (∿ 2.5 mm) holes which was insonified at 3 MHz and imaged onto the pellicle with F:2 acoustic lenses. The acoustic image is seen in A. B is the electrical signal from one scan along the image of the row of small holes, while C shows the same line but with the length of the scan reduced. Once the light is measured, the electrical signal is an accurate measure of the sound intensity at each point. Further details on the operation and construction of the system can be found in reference 5.

3. Transmission of Ultrasound through Biological Tissue

The system has been used to study acoustic properties of tissue sections, especially excised breast sections, with differing pathology. Figure 6 shows three such tissues (the optical and acoustic images are to the same scale), including a normal tissue, one with a benign fibrocystic structure, and one with a malignant structure. The acoustic attenuation (defined in dB/wavelength of ultrasound), measured as illustrated in figure 5, was 0.10 dB/Λ in the normal tissue, 0.8 dB/Λ in the benign fibrocystic tissue, and 1.4 dB/Λ and 0.15 dB/Λ in the cancerous and normal regions, respectively, of the malignant tissue.

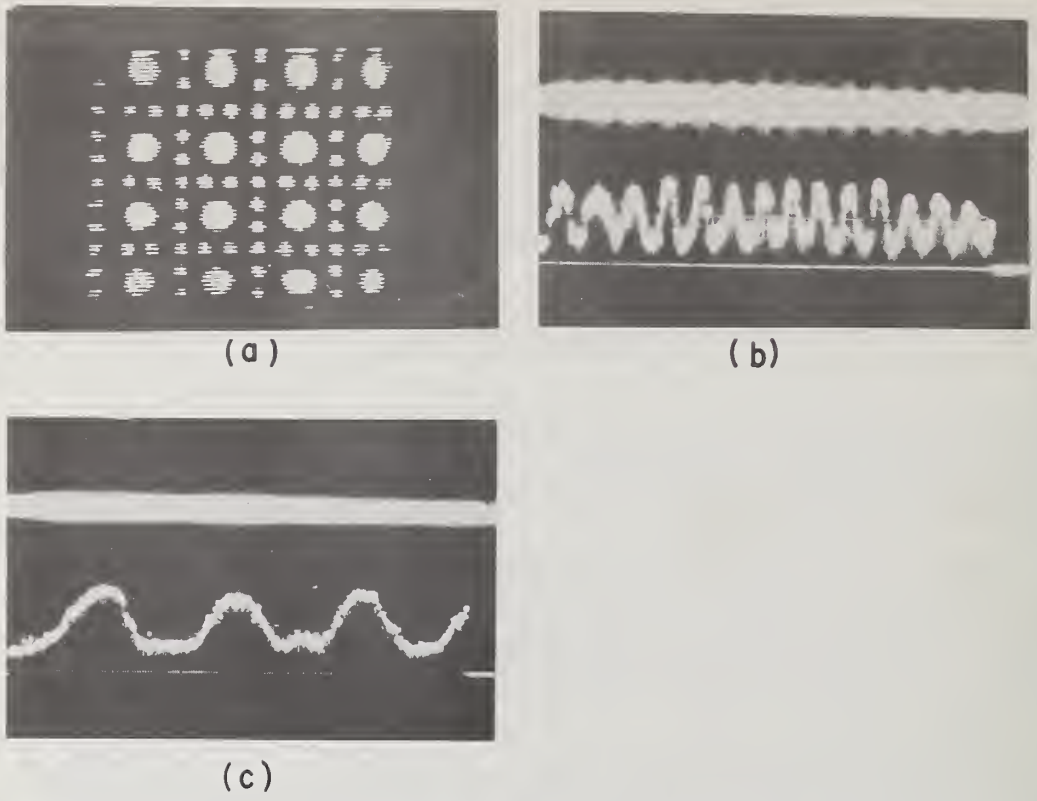

Figure 5. Acoustic image of test object with 2.7 mm diameter small holes and 6.4 mm large holes. Frequency was 3 MHz (0.5 mm wavelength) and lenses were F:2. A is picture on display CRT. B (lower trace) is amplified photocurrent signal from one scan through image of row of small holes. C is similar but with width of laser scan reduced. When system is calibrated (by measuring light), acoustic intensity at each point can be measured.

The tissues came from Hahnemann Hospital (Philadelphia, PA) and each tissue section was from similar patients. The tissues were examined by a pathologist (Dr. C. Calderone at Hahnemann) before and after our imaging experiments. The screws, seen in figure 6, were used as markers to identify particular structures of interest.

The results for a series of 18 tissue sections, prepared and measured as described above, are summarized in figure 7. (Details of the experiment are given in reference 6.) In this graph, the tissue transmissivity is normalized to the acoustic wavelength, as above.

The results fall in three clearly identifiable segments:

(1) Normal tissue, such as sample # 102 and sample # 109, had attenuation less than 0.25 dB/Λ.

(2) The attenuation of benign tumors, such as the dark region of sample # 103 in figure 6, was from 0.45 to 0.8 dB/Λ.

(3) The attenuation of the malignant tumors, with the exception of # 108, was between 1.1 to 1.6 dB/Λ.

There was only one case, a medullary carcinoma which has a soft cellular structure, where the acoustic attenuation fell in the range of benign tumor and led to an erroneous classification. This is a relatively rare tumor and we are trying to get some samples for further studies. In all other types, the results were unambiguous.

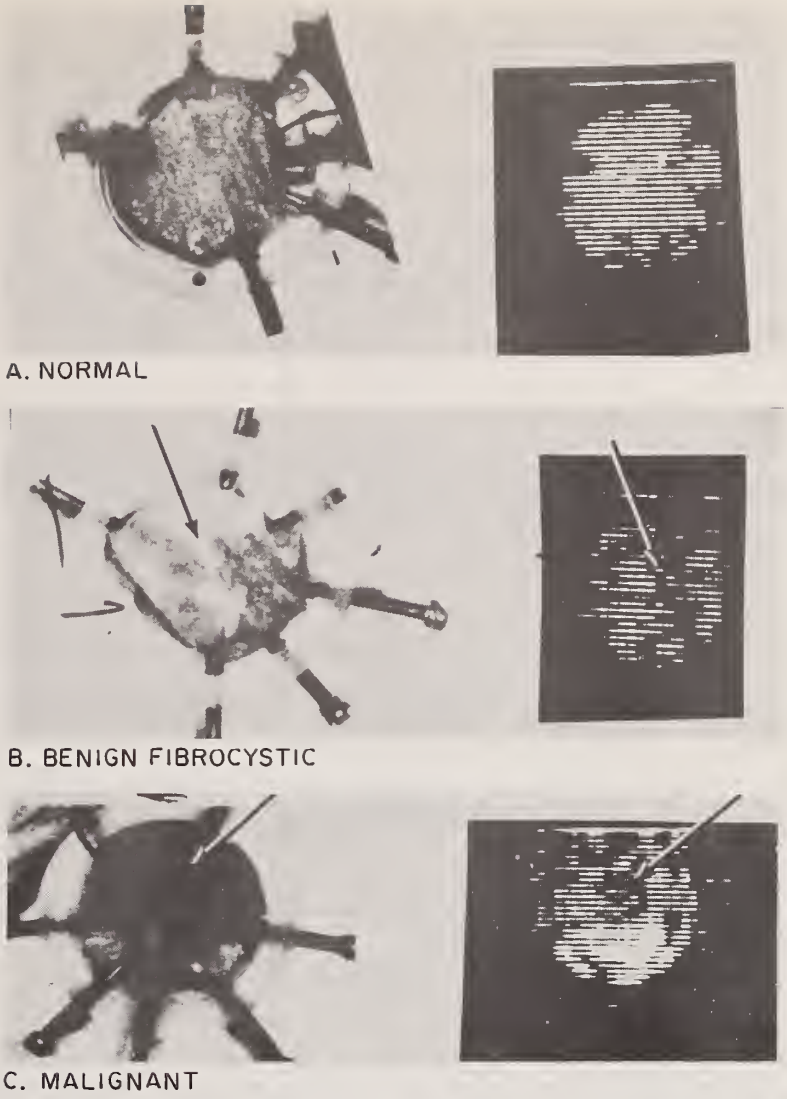

Figure 6. Optical and acoustic images, to same scale of breast sections, with normal, benign and malignant structures. Attenuation at 1.5 MHz was -2 dB in normal, -6 dB in benign fibrocystic structure, and -14 dB in malignant tumor.

Several theories have been proposed to explain the difference in acoustic transmission through such tissue. One, discussed in a paper by Fields and Dunn [7], is that any neoplasm triggers an inflammatory response resulting in the growth of fibrous connective tissue (as if the body were trying to wall off the cancerous cells). Cancer, an invasive neoplasm, stimulates greater fibrous tissue growth. As fibrous tissue is believed to be more strongly attenuating, benign tumors would show less attenuation than cancerous tumors, in agreement with our experimental results.

Regardless of the reason, the different tissue types interact differently with the acoustic wave, and these changes can be visualized and measured in detail with the ultrasonic imaging system. The important feature of the system is that it can measure such structures with high lateral resolution. In one instance, tumors as small as 2 mm were observed in the system and then verified as malignant by the pathologist.

These studies are being continued both with breast tissue and other structures. The system is also being adapted for reflective imaging, by using a "top lighting" technique as in optical microscopes, in order to more fully characterize the interaction of ultrasonic waves with tissues.

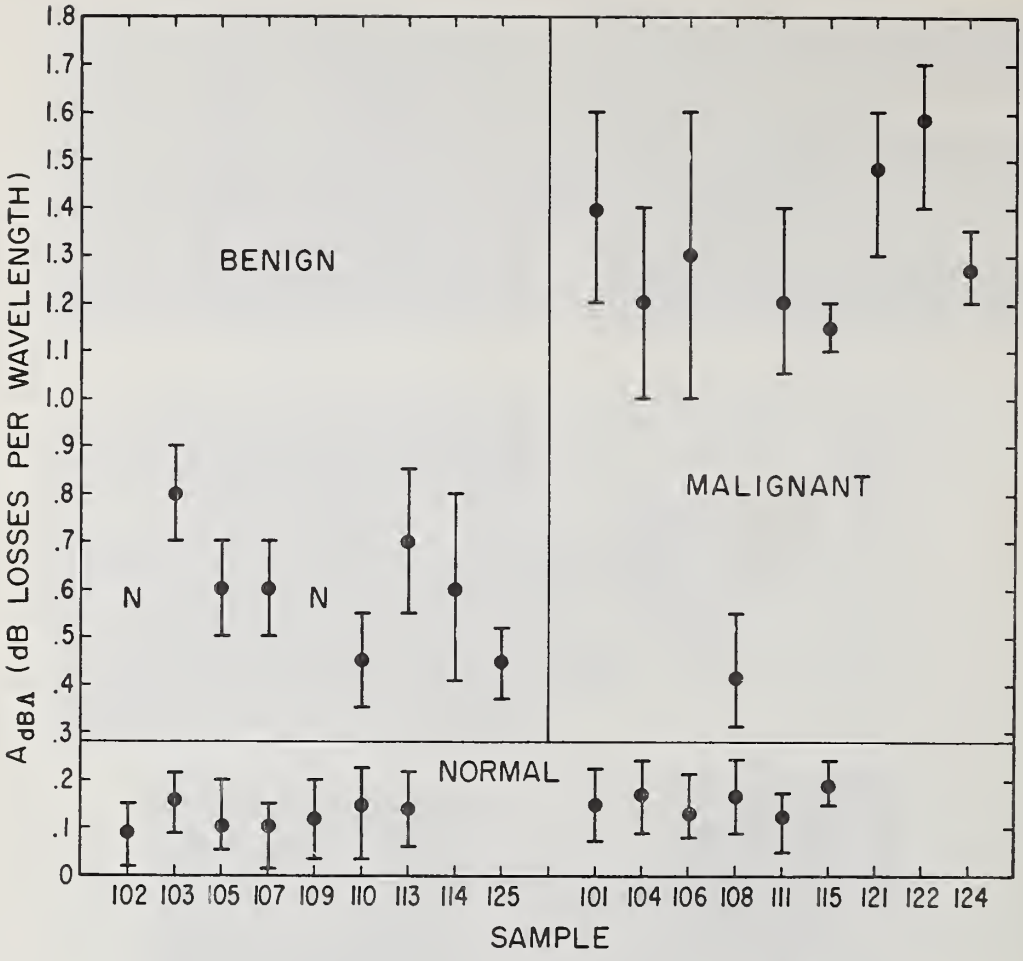

Figure 7. The transmissivity versus sample pathology. Table I lists the histological analysis of the samples. The transmissivity is defined here as the decibels loss, *i.e.*, -10 $\log_{10}$ Transmitted Intensity/Incident Intensity per wavelength of ultrasound, *i.e.*, if T_{dB} is 1, there is 10 dB loss in traversing 10 mm of tissue with 1 mm ultrasound. (The samples were numbered in chronological order starting with 101. Sample 112 is missing because of uncertainty in the records as to its pathology, and samples 116-120 were not cut as flat slices, so that the thickness was indeterminate and the data not included.)

4. Phase-Contrast Velocity Measurements

The preceding examples have been those where the amplitude of the acoustic wave was modified by the tissue. In many cases, the velocity of the wave passing through the tissue is also modified. Since the velocity is a function of tissue elasticity and density, and since both (especially the elasticity) can be modified by disease, the detection of velocity differences could be an aid to the determination of pathological state. Furthermore, many structures are either too thin, or have so little absorption that they do not substantially change the amplitude of the acoustic wave, but yet such tissues can show velocity differences. An important example is atherosclerotic plaque, which in the early stages of the disease consists of small (1-5 mm) fatty deposits on the interior wall of the artery. The fatty deposits have too little attenuation or reflectivity to be detected by normal acoustic techniques [8] (especially before they have calcified) but could be seen by a method sensitive to the phase of the transmitted ultrasound.

The phase-contrast method [9,10], initially developed to image optically-transparent biological specimens, can be applied to visualize and measure acoustic velocity differences in tissue.

The method can be explained by the following simple argument.

Consider an object (tissue) with some spatially-varying elasticity but with no absorption. An acoustic wave transmitted through it will propagate with differing velocities and as a result will have a spatially-varying phase. The amplitude of the wave as it leaves the tissue can then be written as

$$A_o = ae^{j\phi(x)} \tag{7}$$

where $\phi(x)$ is the spatially-varying phase and a is the wave magnitude (a = 1 for non-absorbing tissue). In a system sensitive to the wave intensity (as a light microscope) or magnitude (as our system is), the detected signal is proportional to

$$|A_o| = a \tag{8}$$

and will not directly show the effects of the phase variation.

Now consider the situation when the phase variation is small; then eq. (7) may be expanded as

$$A_o = ae^{j\phi(x)} \approx a(1 + j\phi(x)) \tag{9}$$

which consists of a nonvarying term which is in phase quadrature with the spatially-varying term.

If the phase of the nonvarying term is advanced or delayed by 90°, the amplitude becomes

$$A_o' = a(\pm j + j\phi(x)) \tag{10}$$

and the magnitude is

$$|A| = a(1 \pm \phi(x)) \tag{11}$$

and directly displays the phase variation.

In figure 8, we show a method for acoustic imaging. The acoustically-transparent object is insonified by a plane acoustic wave and imaged by acoustic lenses onto the pellicle. As the wave propagates through the object, some of it passes directly through, undisturbed, and is brought to a focus on the axis in the back focal plane of the first lens (the object lens). The remainder of the acoustic wave is scattered by the phase variations and is spread out over the back focal plane of the lens. It can be easily shown [10] that these two waves, the scattered and undisturbed, are in phase quadrature and that further, when they are combined at the pellicle by the second lens, they reproduce the wave that existed at the object, exhibiting phase variations but no contrast. Since the waves are in quadrature, they cannot interfere to produce amplitude variations.

The phase-contrast method takes advantage of the fact that the two waves are spatially separated in the object lens focal plane. By insertion of a phase plate (for example, a plastic disc of the proper thickness) over the focused "undisturbed"

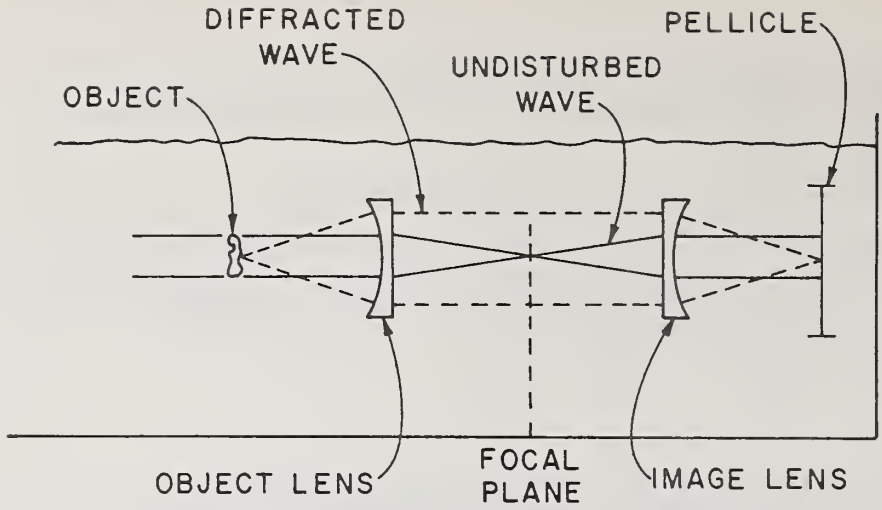

Figure 8. Arrangement for normal amplitude and phase-contrast imaging. "Undisturbed" wave is focused by object lens while scattered wave is spread over focal plane. Additional 90° phase shift can be obtained by inserting a plastic disc over focused "undisturbed" wave.

wave, the relative phase between the two waves can be adjusted so that they interfere at the pellicle. If the phase plate advances the undisturbed wave by 90°, the two waves will interfere constructively at the pellicle, giving a bright image. If the phase plate retards the phase by 90°, the two waves will interfere destructively, giving a dark image. Alternatively, the phase of the scattered wave could be modified giving similar results.

Figure 9 gives an example of the phase-contrast method. The object was a thin (0.5 mm) polystyrene strip which did not substantially absorb the sound (< 0.5 dB)

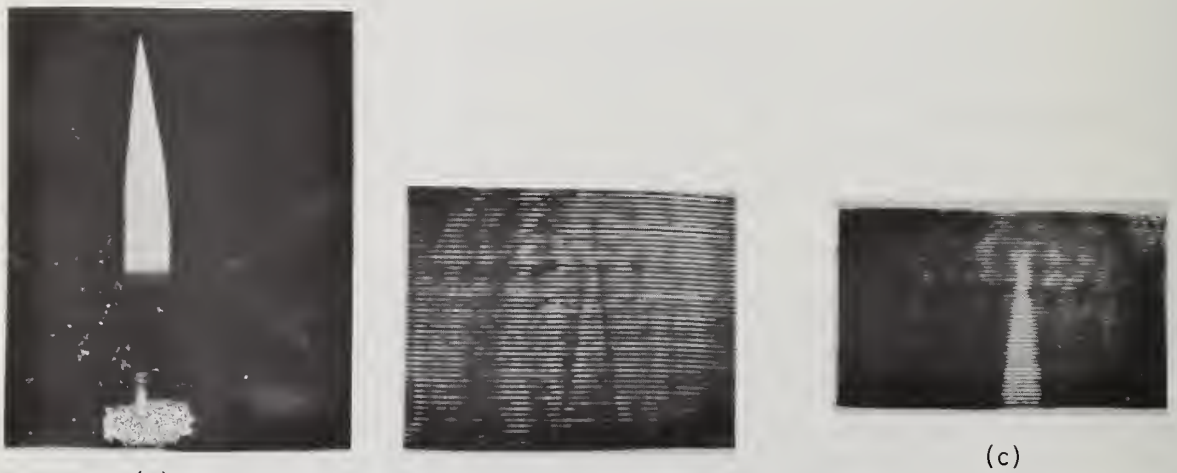

(a) (b) (c)

Figure 9. Phase-contrast image of test sample. Object (A) was 0.5 mm thick polystyrene with < 0.5 dB attenuation and 30° phase shift. Normal image shows edges (due to sound diffraction beyond edges) but no contrast. Phase-contrast image shows full detail, with brightness proportional to phase shift.

but did advance the phase, relative to water, by 36°. Part A shows an optical image and B a normal amplitude image of the object. Note that the edges of the object in the normal acoustic image are seen, due to sound diffracted beyond the lens aperture, but no detail is seen and there is no contrast against the background. Part C shows the phase-contrast image. The phase plate was 24 mil (0.6 mm) polyethylene placed over the focused "undisturbed" wave and at the frequency used (2.25 MHz) and at the temperature of the water bath (37°C) advanced the phase by 91°. The object is seen in detail and not just in outline.

This is an example of bright phase-contrast; the image is brighter than the background. By using a phase plate that retards the undisturbed wave, a dark image results. Alternatively, as mentioned above, the phase of the scattered wave can be modified. Figure 10 shows the results in this case, obtained using a polyethylene sheet with a hole in the acoustic axis. Part A shows the normal image, part B repeats the previous bright image and part C shows the dark image of the same object.

A B C

Figure 10. Bright and dark phase-contrast imaging. Also shown are processed acoustic signals from one line through image.

By a simple analysis [11], the change in amplitude at the image is

$$\Delta = \frac{[a^2 + 2\{1 + \cos\theta + a \sin\theta\}]^{\frac{1}{2}}}{a}$$

which, for small phase changes and a = 1, is (as in eq. (11))

$$\Delta \approx (1 + \theta) \ .$$

In polystyrene, the calculated phase change of the sound is 36°, which should give an amplitude change of $\sim$ 1.8. This agrees well with the measured values, measured as illustrated in figure 5.

A second example, with biological tissue, is seen in figure 11. The object, a section of calf liver containing several blood vessels, is seen in the photograph (A). (The sample was cut after the imaging experiments.) The normal acoustic image is seen in B and only the edges of the vessels can be seen, due to diffraction (the vessels were allowed to fill with water). The phase-contrast image is seen in C, where now the vessels can be seen in detail and with high contrast.

There is an important distinction between the phase-contrast method of velocity measurement and those methods that insert an electronic reference to detect phase variations. This becomes evident when considering a section to be examined surrounded by different

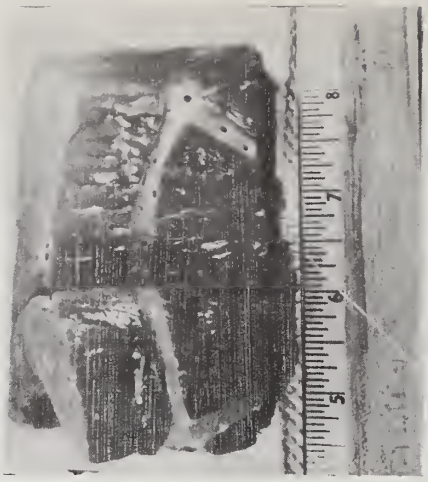

(a)

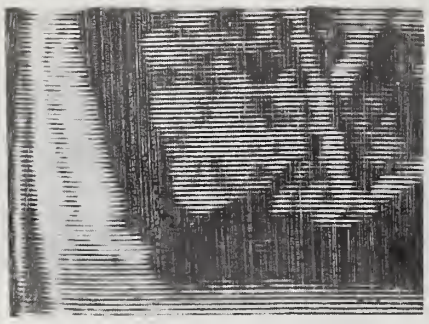

(b)

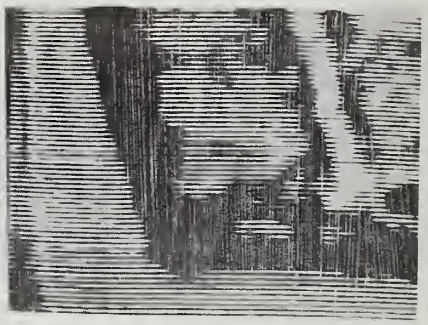

(c)

Figure 11. Phase-contrast image of calf liver section. A shows liver cross-section, cut after experiment, to show vessels. B is normal acoustic image with poor detail. C is phase-contrast image, and blood vessels are seen bright and in detail.

overlying tissues. When the wave propagates through the object, its phase is varied both by the section to be observed and by the overlying tissue, and the phase variation due to the region of interest alone cannot easily be identified by using an electronic reference. In the phase-contrast method, the reference (the "undisturbed" wave) and the scattered waves propagate through the tissue together and phase variations common to both cancel at the image. Unless the overlying tissue is very rough (rapid phase variation) or very far removed from the region of interest, it will have little effect on the image. (The situation is somewhat like looking through a shower glass; if the object is very close to the glass or if the glass is not too rough, the structure beyond the glass can be discerned.) By analogy to optical phase-contrast methods, it is expected that objects up to 10 cm thick can be examined.

With the addition of the phase-contrast method, it is expected that the ability of the technique to characterize and identify tissue will be extended. The study of atherosclerotic plaque is one example where phase-contrast may be applied, the visualization of tumors and fatty structure elsewhere in the body is another. The important feature is that with this method, as with the method used to display amplitude variations, the effect of the interaction of the tissue with ultrasound can be simultaneously displayed and accurately measured.

We have described a system to visualize and measure ultrasonic waves and given examples of its use in measuring and displaying ultrasonic tissue interactions, both amplitude and velocity. We hope that through continued use of this system, both by us and others, the ability to characterize tissue will be increased and more sophisticated devices based on a better understanding of the interaction of ultrasonic waves with tissue will become available for clinical use.

References

[1] Wild, J. J. and Reid, J. M., Other pilot echographic studies on the histologic structure of tumors of the lining intact human breast, *Am. J. Path.* 28, 839 (1952).

[2] Goldman, D. E. and Heuter, T. F., Tabular data on the velocity and absorption of high frequency sound in mammalian tissues, *J. Acoust. Soc. Am.* 28, 35 (1956).

[3] Freese, M. and Hamid, M. A. K., Lipid content in whole fish using ultrasonic pulse backscatter, in *Proc. IEEE Ultrasonics Symp.*, p. 69 (IEEE, New York, NY, 1974).

[4] Kossoff, G., Fry, E. K., and Jellins, J., Average velocity of ultrasound in the human female breast, *J. Acoust. Soc. Am.* 53, 1730 (1973).

[5] Mezrich, R. S., Etzold, K. F., and Vilkomerson, D. H. R., System for visualizing and measuring ultrasonic wavefronts, *RCA Rev.* 35, 483 (1974).

[6] Calderone, C., Vilkomerson, D., Mezrich, R., Etzold, K., Kingsley, B., and Haskin, M., Differing ultrasonic attenuation in normal, benign and malignant breast tissue. (Manuscript in preparation.)

[7] Fields, S. and Dunn, F., Correlation of echographic visualization of tissue with biologic composition and physiological state, *J. Acoust. Soc. Am.* 54, 809 (1973).

[8] Barber, F., Baker, D., Nation, A., Strandness, D., and Reid, J. M., Ultrasonic duplex echo-doppler scanner, *IEEE Trans Bio-Med. Eng.* BMR-21, 109 (1974).

[9] Zernike, F., Das phasen kontrastverfahren bei der mikroskopischen beobactung, *Z. Tech. Phys.* 16, 454 (1935).

[10] Bennett, A. H., Jupnik, H., Osterberg, H., and Richards, O. W., *Phase Microscopy*, (J. Wiley and Sons, New York, 1952).

[11] Born, M. and Wolf, E., *Principle of Optics*, p. 427 (Pergamon Press, Oxford, England, (1965).

National Bureau of Standards Special Publication 453. Proceedings of Seminar on Ultrasonic Tissue Characterization held at NBS, Gaithersburg, MD, May 28-30, 1975. (Issued Oct. 1976)

Paper 4.5: REFLECTION TECHNIQUES FOR MEASUREMENT OF ATTENUATION AND VELOCITY

G. Kossoff

Ultrasonics Institute
Sydney, Australia

Pulse reflection techniques may be used for *in vivo* measurement of attenuation and velocity. Measurement of the two-dimensional distribution of pulse attenuation may be obtained based on the equalization of internal echoes, while the differential pulse attenuation of encapsulated tissues is obtained by noting the difference in the echo from the posterior boundary at different frequencies. The average velocity in tissues may be measured by a simple technique if a reflector may be positioned at the posterior boundaries. A reflection technique for measurement of local values of velocity in heterogeneous tissues using two forward transducers separated by a known distance is suggested.

Key Words: Attenuation; breast; reflection techniques; ultrasound; velocity.

1. Introduction

Reflection techniques are based on the measurement of amplitude and time delay of echoes originating from discontinuities in acoustic impedance in the examined tissues. These echoes are also carriers of information about other acoustic parameters of tissue such as attenuation and velocity, and with suitable techniques, may be used to measure these parameters. Reflection techniques have the advantage that the measurements may be performed using only one transducer and in many instances are the only possible class of techniques for non-invasive *in vivo* measurement of these parameters.

2. Measurement of Average Velocity

If the tissues are such that it is possible to get access to their anterior and posterior boundaries, it is possible to use a reflection technique to measure the average velocity of propagation based on an analogous transmission measurement technique [1].[1] In this technique, a reflecting target is placed against the posterior boundary, replacing the opposing transducer in the transmission technique, and the average velocity is obtained by comparing the time of propagation in the tissues with the time taken for the energy to propagate in water, the distance between the transducer and the reflecting target being kept constant. As in the transmission method, the average velocity of propagation in the tissue v_b is given by

$$v_b = \frac{v_w}{1 \pm \frac{\Delta t}{t_w}} \quad , \tag{1}$$

where v_w is the known velocity of propagation in the water, Δt the time difference between the two measurements and t_w the total time taken to travel in water. A schematic of the method is illustrated in figure 1. In analogy with the transmission technique, the accuracy of the measurement is relatively high, being of the order of 0.5%. In practice, refractive processes limit the repeatability of the measurement, particularly in heterogeneous organs

[1]Figures in brackets indicate the literature references at the end of this paper.

such as the breast where the velocity of constituent tissues may vary by up to 15%. On repositioning, these affect the time of arrival of the pulse and in practice reduce the accuracy to approximately 2%.

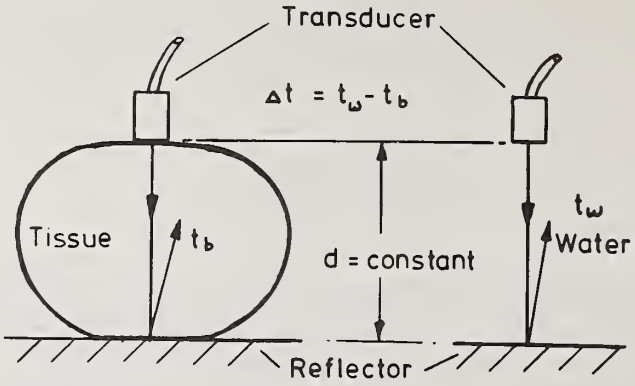

Figure 1. Technique for measurement of average velocity.

In theory, a similar technique based on the measurement of the amplitude of the echo from the reflecting target may be used for the measurement of average attenuation. In practice, refractive processes affect to a much greater degree the amplitude of the echo and make the technique unsuitable for this application.

3. Measurement of Attenuation

The measurement of attenuation may be made either from the echoes obtained from the internal structural organization of the tissues or the echoes obtained from the boundaries of the tissues [2].

3.1 Internal Echoes

The technique for measurement of attenuation from the A-mode, or unidimensional amplitude-versus-time delay presentation of data, is described in the paper "Quantitative A-scan Analysis of Normal and Cirrhotic Livers" (this volume, p. 61). It is also possible to measure attenuation from a special type of B-mode or two-dimensional presentation of the data. In this technique, the tissues are examined using simple scanning, such as linear or sector scanning, and the receiver gain is increased progressively step-wise by a known amount. If it can be postulated that the internal tissue distribution is homogeneous as, for example, in the case of a normal liver or a homogeneous tumor, then, after allowing for the transducer beam pattern variations, one may expect that the internal echoes should all be of the same strength and that the gradual decrease in the strength of the echoes with penetration is due only to attenuation. This is indeed the postulate made in the measurement of attenuation from the A-mode data. Therefore, if two echoes along the same line of sight in different penetration bands are displayed with the same intensity, then the known gain difference between the bands represents the loss of signal due to attenuation, since all the other factors such as receiver and display characteristics, photographic exposure, developing, etc., are constant. Thus, as illustrated in figure 2, the two-dimensional attenuation distribution is obtained by finding echoes of equal intensity in penetration bands with differing gains, the attenuation being given by the quotient of the gain difference and the distance between the echoes. The two-dimensional presentation of the data provided by the B-mode echogram has the advantage that it allows the selection of regions where the postulate of homogeneity of the tissues is most likely to be valid, while the intercomparison of echoes between different bands permits an averaging of the measurements.

The application of the method on a scan of a sponge target and a breast containing a small benign mass is illustrated in figure 3. In these examples, a stepped-gain function was approximated by superimposing a 3 dB gain reduction every second step on the normal

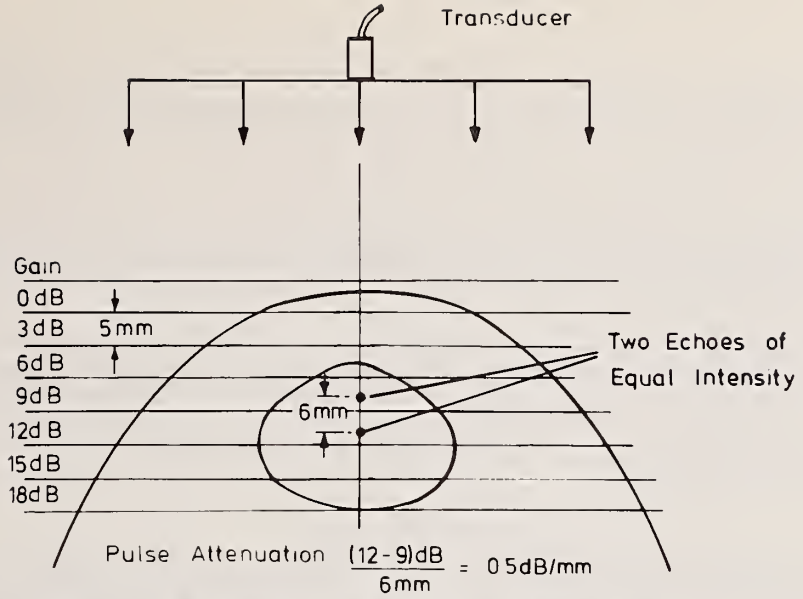

Figure 2. Principle for measurement of pulse attenuation.

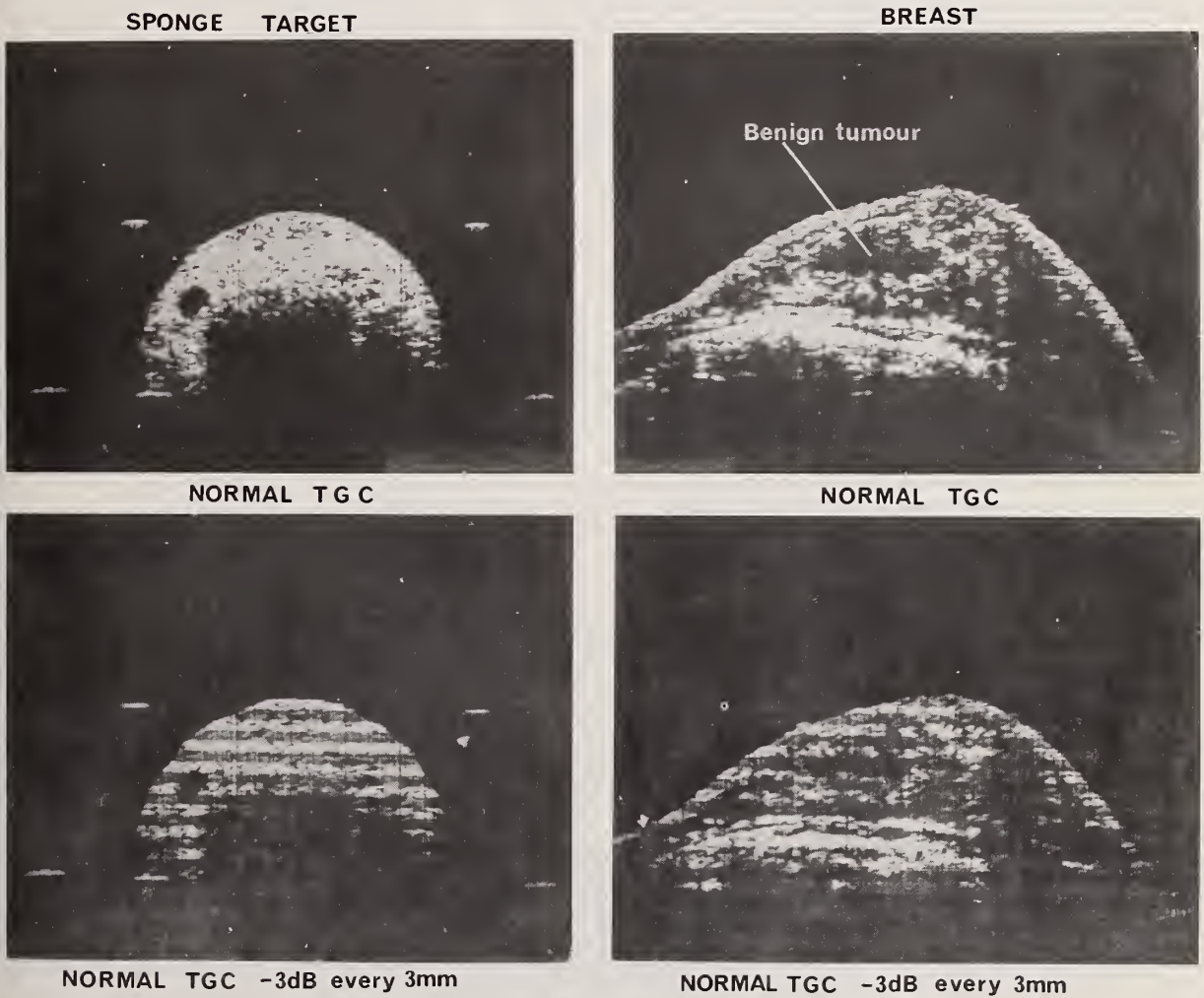

Figure 3. Normal and stepped-gain linear scan echogram for measurement of pulse attenuation.

gradually-increasing TGC (time-gain compensation) gain of the receiver. Although the size of the step, the grey scale range within the step and the frequency of operation of the equipment is not optimum for the application, the figure illustrates the typical striped appearance of the echogram and illustrates the applicability of the method. With the grey-scale presentation, the selection of echoes of equal strength may necessitate the use of a film densitometer since the human eye is not very effective in selecting regions of equal grey level. As the eye is more capable of selecting equal colors, color presentation could facilitate the recognition of echoes of equal strength and allow direct measurement from the echogram.

Generally, attenuation figures are specified at a single frequency. Since the echo pulse contains a relatively wide frequency spectrum, it is more appropriate to quote the reflection-based measurement as the "pulse attenuation" as it is to some extent dependent on the waveform of the pulse. Also, since in the reflection technique the energy has to go in both forward and backward directions, the figure corresponds to twice that obtained by a transmission measurement.

3.2 Boundary Echoes

The attenuation of encapsulated tissues cannot be determined by simple comparison of amplitude from the front and back boundaries. The amplitude depends on the geometry of the boundaries which, in general, are not similar, nor may it be assumed that the same impedance discontinuity exists at the two boundaries. A differential technique may be employed to obtain the differential pulse attenuation. In this technique, the examination is repeated at a different resonant frequency and the differential pulse attenuation is obtained by equating the amplitude of the echo from the front surface at the two frequencies and noting the difference in the amplitude from the back boundary. Theoretically, it is also possible to undertake this measurement with a single pulse by separating the frequency components of the pulse by filtering and comparing the amplitudes of the low and high frequency components of the pulse.

A schematic of the method is illustrated in figure 4, the differential pulse attenuation $\alpha_{f_2-f_1}$ being given by

$$\alpha_{f_2-f_1} = \frac{2}{d} \ell n \left[\frac{V^B_{f_1} V^F_{f_2}}{V^B_{f_2} V^F_{f_1}} \right], \qquad (2)$$

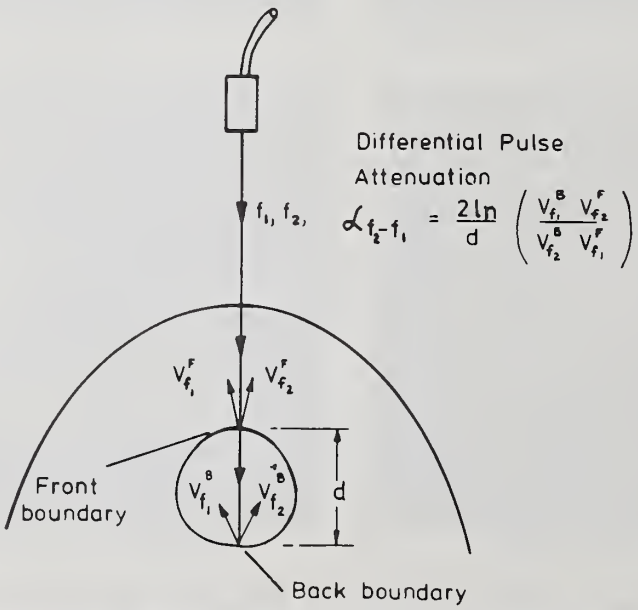

Figure 4. Principle for measurement of differential pulse attenuation.

where d is the distance between the boundaries, and $V^F_{f_1}$, V^B_f, $V^F_{f_2}$, $V^B_{f_2}$ the amplitudes of the echoes from the front and back boundaries at the resonant frequencies f_1 and f_2, respectively.

4. Measurement of Velocity

Theoretically, the value of velocity of the constituent tissues in a heterogeneous organ may be obtained by using two transducers separated by a known distance [2]. One transducer is used as the transmitter and the receiver while the other transducer is used as a receiver only and the measurement is obtained by noting the time delay of echoes received from the same internal reflectors by the two transducers. The principle of the method is illustrated in figure 5 which shows that the velocity in the first medium v_w is given by

$$v_w = \frac{d}{(t_2(t_2-t_1))^{\frac{1}{2}}}, \tag{3}$$

where d is the separation distance and t_2 and t_1 the respective time delays. If water is used as the coupling medium, then v_w is known and this equation may be used to calculate the separation distance d for the chosen transducer configuration and to check for any possible dependence on the penetration depth.

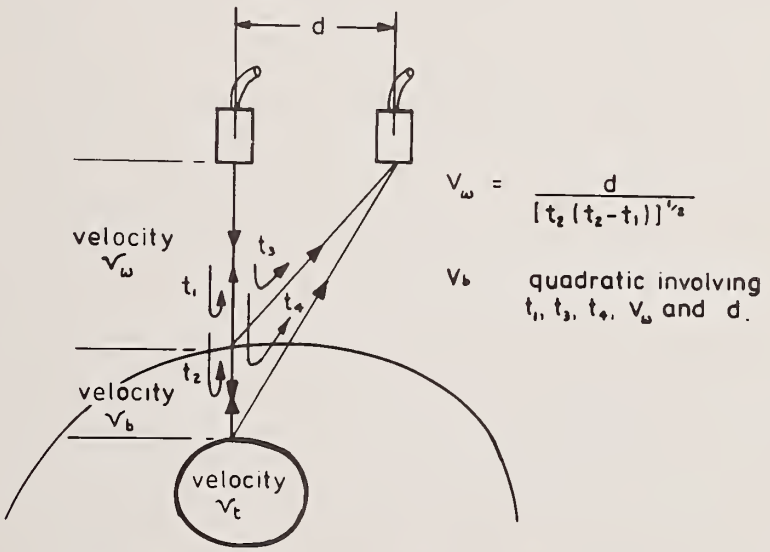

Figure 5. Principle for measurement of internal values of velocity.

Simple mathematical analysis shows that the velocity in the underlying layer in tissue v_b is given by a quadratic equation involving t_1, t_3, t_4, v_w, and d, and once v_b is determined, an iterative process may be used to determine the velocity in the distal tissues.

This paper is published with permission of the Australian Director-General of Health.

References

[1] Kossoff, G., Kelly Fry, E., and Jellins, J., Average velocity of ultrasound in the human female breast, *J. Acoust. Soc. Am.* 53, 1730 (1973).

[2] Kossoff, G., Progress in pulse echo techniques, in *Ultrasonics in Medicine*, M. de Vlieger, *et al.*, eds., p. 37 (Excerpta Medica, Amsterdam, 1974).

CHAPTER 5

ABSORPTION TECHNIQUES

National Bureau of Standards Special Publication 453. Proceedings of Seminar on Ultrasonic Tissue Characterization held at NBS, Gaithersburg, MD, May 28-30, 1975. (Issued Oct. 1976)

CHAPTER 5. ABSORPTION TECHNIQUES

Paper 5.1: ULTRASONICALLY-INDUCED TRANSIENT THERMAL GRADIENTS: THEIR POTENTIAL ROLE IN ACOUSTIC PARAMETER CHARACTERIZATION OF TISSUE

F. J. Fry

Fortune-Fry Laboratories
Indianapolis Center for Advanced Research
Indiana University Medical Center
Indianapolis, Indiana 46202

Induction of transient thermal gradients by ultrasonic means with concurrent detection by ultrasound offers the possibility of determining quantitatively some of the acoustic properties of live tissue. The transient thermal gradient is related to the inherent acoustic absorption property of the tissue. When used appropriately, this gradient can be used to determine acoustic absorption, attenuation, velocity, and to enhance acoustic impedance differences at certain interfaces. Additional work beyond that reported here is needed to explore essential application of this method in the area of acoustic parameter determination which could lead to an enhanced tissue differentiating capability.

Key Words: Absorption; attenuation; impedance gradient; transient thermal gradients; ultrasonics; velocity.

1. Introduction

The idea of using ultrasound to induce a transient temperature rise in tissue for the purpose of aiding in the identification of tissue types through ultrasonic interrogating means was first suggested in 1962 [1].[1] In its original form, advantage was to be taken of the fact that acoustic absorption in soft tissue has a much wider range of variation than does acoustic impedance which is the primary acoustic parameter used qualitatively or at most semi-quantitatively in present medical diagnostic regimes. This reliance on acoustic impedance differences is slowly changing as other acoustic properties permit ready presentation. It is anticipated that quantification of a spectrum of acoustic properties in tissue will lead to greater differentiation capability. One suggested mode of operation for the transient thermal gradient method was in the production of detectable and quantitatively-measurable acoustic impedance differences across tissue interfaces which normally would not have an acoustically-detectable difference. This effect would be operative if the tissues on either side of the interface had acoustic absorption differences which, if the tissue were acoustically irradiated at an appropriate intensity, would produce a temperature gradient resulting in an acoustic velocity gradient which would bring the interface into the detectable range. It is of course possible that there might be acoustic impedance differences which would be brought closer in value by this method. All of these temperature changes would, of necessity, need to be induced at acoustic intensity levels which produced no adverse biological effects in the tissue. It

[1]Figures in brackets indicate the literature references at the end of this paper.

was also recognized that irradiation in a homogeneous tissue itself would produce a temperature rise related directly to the intrinsic absorption property of the specific tissue and that this method could potentially be used to characterize a homogeneous tissue through appropriate interrogation means. An additional possibility arises which could lead to a tissue specific velocity determination since the thermal gradient induced by a focused transducer can be moved by accurate known amounts thereby permitting the determination of transit time measurements between targets of known separation. Conceivably, attenuation could be measured in a homogeneous tissue by observing the amplitude of the reflected signals from these known sites. This method requires a knowledge of the frequency-dependent character of attenuation in the tissue since for different path lengths the temperature-inducing beam will be absorbed differentially for the different sites. It would also be necessary that the reflection amplitude be quantitatively recorded. There are other ways in which thermally-induced changes can be potentially useful in acoustic interrogation for tissue parameter characterization which are covered by other authors in this volume.

2. Theoretical Analysis

In this section, we consider the magnitude of the induced temperature rise needed to produce an acoustically-detectable interface. Sensitive acoustic interrogating systems using focused transceivers will resolve acoustic impedance differences at interfaces of the order of 0.1%. Assuming that the temperature coefficient for sound velocity in tissue is substantially that of Ringer's solution (1% acoustic impedance change for a 10°C change: 30 to 40°C), it is apparent that a 1°C change would produce a detectable impedance change. The largest component of this impedance change is in the sound velocity rather than in the material density.

An approximation to the maximum temperature rise T (°C) in tissue produced by a short ultrasound exposure is given by:

$$T = \frac{\alpha I t}{\rho C} \tag{1}$$

where

α = acoustic intensity absorption coefficient (cm^{-1})
I = intensity at the site (W/cm^2)
t = sound pulse duration (seconds)
ρ = density
ρC = heat capacity/unit volume (joules/cm^3/°C).

The short exposure time (t < 1 sec) is used so as to insure substantially no heat conduction loss in the tissue.

Computation of the temperature rise in brain tissue is shown in Table I for a given set of acoustic parameters. The resultant temperature rise of approximately 5°C or 10°C

Table 1. Computed Temperature Rise in White and Grey Matter of Brain after 0.1 sec Irradiation with Ultrasound

Intensity at Site (W/cm^2)	Frequency (MHz)	Time On (sec)	Temperature Rise (°C)	
			White Matter	Gray Matter
1,000	1.0	0.1	5.0	3.0
2,000	1.0	0.1	10.0	6.0

is presumably a safe increment [2] under the conditions of the 0.1 sec. pulse duration. Additionally, the 1 MHz ultrasonic beam used for raising the tissue temperature by 5°C would be delivering an ultrasonic dose which is an order of magnitude below that which has been identified as the threshold for lesion production in brain [3]. Since brain

white matter has an intensity absorption coefficient approximately 50% higher than that of grey matter, a temperature difference of approximately 2°C or 4°C (depending on the acoustic intensity values used as shown in Table I) would appear across a grey-white matter interface. On the basis of these computations, it would appear possible to produce approximately 1% acoustic impedance discontinuity in homogeneous brain tissue for a 10°C rise and an enhancement of grey-white matter interface of about 0.4% for a 10°C rise in the white matter.

All of the above considerations involve the concept of an abrupt discontinuity in the acoustic impedance induced by a temperature rise. An idea of the abruptness of the temperature transition in the tissue can be obtained by considering the temperature distribution following induction of a one-dimensional unit temperature step function. This temperature distribution (T(x)) centered at the plane X = 0 can be expressed as [2]

$$T(x) = \frac{1}{2}\left\{1 + \phi\left(\frac{X}{2a\sqrt{t}}\right)\right\} \tag{2}$$

where ϕ is the error function defined by

$$\phi\left(\frac{X}{2a\sqrt{t}}\right) = \frac{2}{\pi}\int_0^{\frac{X}{2a\sqrt{t}}} e^{-y^2}\,dy \tag{3}$$

and

X = space coordinate
t = time
s = heat capacity per unit mass
K = thermal conductivity coefficient
a^2 = diffusivity = $\frac{K}{\rho s}$.

For a value of $a^2 = 0.001$ cm^2/s, the normalized temperature distribution is shown in figure 1 for time intervals measured in seconds after unit-temperature step-function application.

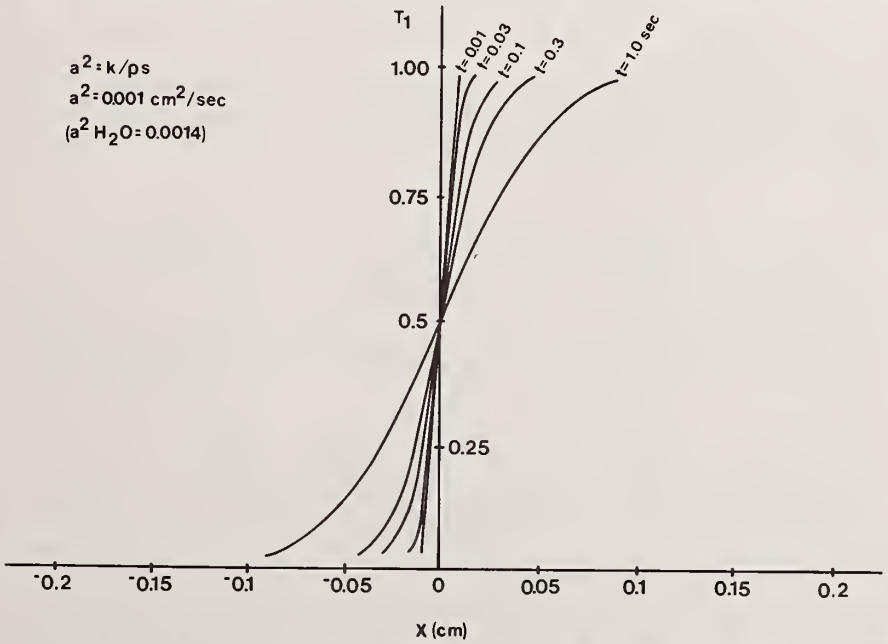

Figure 1. Temperature distribution as a function of distance from the X = 0 plane for various time intervals after unit-temperature step-function induction centered at X = 0.

From the curves of figure 1, it is possible to estimate a structural resolution capability assuming that an appropriate acoustic-sensing frequency is used. In this case, we take the plane X = 0 as either the interface between two tissues of different acoustic absorption coefficients and the surface corresponding to the center of the heating beam or as representing a plane in a homogeneous tissue in which a step function temperature rise has been produced. More sophisticated approaches to this problem of temperature rise in tissue undergoing ultrasonic irradiation have been considered by others [4].

Resolution in the X direction is assumed as approximately the incremental X distance for the time intervals on the specific curve. In a homogeneous tissue at t = 0.1 s, resolution would be of the order of 0.4 mm.

In order to see that these resolution values are achievable, it is necessary to select an interrogating frequency such that the magnitude of reflected energy at the thermally-induced transition will approximate that from an abrupt acoustic impedance change. A previous analysis [2] of the approximate relationship between the reflection from an abrupt transition and a graded transition of the type delineated by the curves of figure 1 indicates that a transition zone of the order of 1/4 wavelength or less of the interrogating beam will be a good approximation to the abrupt transition. This means that an interrogating frequency of 2 MHz is adequate, since $\lambda/4$ in soft tissue is approximately 0.2 mm which is in the range of the structural resolution referred to previously.

The magnitude of the acoustic pressure reflection coefficient r at an interface between two media (with acoustic impedances of $\rho_1 c_1$ and $\rho_2 c_2$) is described by

$$r = \frac{\rho_1 c_2 - \rho_2 c_2}{\rho_1 c_2 + \rho_2 c_2} \quad . \tag{4}$$

If a change is induced in c_1 and c_2 due to a thermal gradient and if $\rho_1 = \rho_2$, then the reflection coefficient becomes

$$r_{\Delta t} = \frac{c_1 - c_2 + (\Delta c_1 - \Delta c_2)}{c_1 + c_2 + (\Delta c_1 + \Delta c_2)} \quad . \tag{5}$$

Depending on the initial velocities, assuming generally a positive coefficient of velocity with increasing temperature, and depending on which media has the larger velocity coefficient, it is possible to increase or decrease the reflection coefficient (Table II shows several examples).

Table II. Reflection Coefficient Change due to Temperature Modification*

Case	Relative Velocity		Relative Velocity Change		Reflection Coefficient
	c_1	c_2	Δc_1	Δc_2	r
1	1.5	1.6	--	--	.0323
2	1.5	1.6	0.5	.10	.0462
3	1.5	1.6	0.10	.05	.0154

*The densities in both tissues are assumed to be equal. In case 2, the thermal perturbation provides an increased reflection while in case 3, it provides a decreased reflection.

3. Experimental Results

A first observation of an ultrasonically-induced transient effect which was presumably thermal in nature was made in an experimental animal brain [1] (adult cat). The experimental arrangement used for this observation is shown in figure 2. A 1 MHz focused beam was used to irradiate the brain and a 5 MHz unfocused transceiver was used for detection of the effect. Results of this first experiment are shown in figure 3. For this and all subsequently mentioned observations, a skull bone section was removed for the acoustic interrogation implementation. If the high intensity irradiating beam remained on until a permanent effect was observed, the results appear as in figure 4. Figure 5 shows a series of three pictures taken on an excised human brain which has been fixed in formalin. In figure 5A, the reflections are shown before transient heating induction. The effect of transient heating can be seen in figure 5B. After cessation of the heating beam irradiation, the additionally observed reflection completely disappeared. If the duration of the

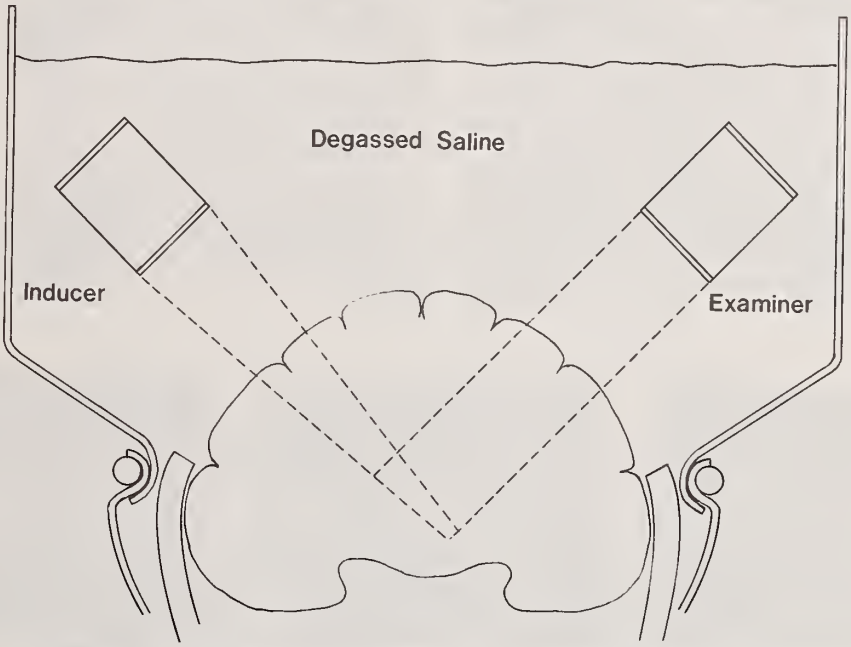

Figure 2. Schematic diagram of arrangement for ultrasonically inducing and detecting a transient thermal gradient in a cat brain.

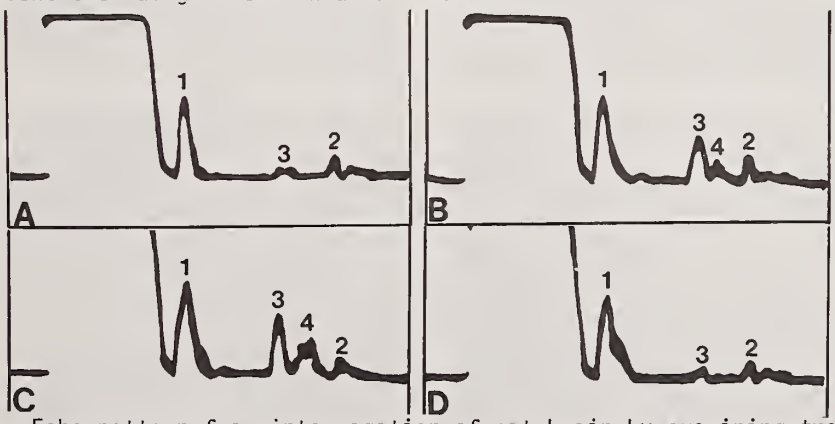

Figure 3. Echo pattern from interrogation of cat brain by examining transducer: (A) preceding induction of transient-temperature distribution caused by 1.0 second pulse of focused ultrasound; (B) two seconds after focused sound pulse; (C) five to six seconds after focused sound pulse; (D) one and one-half minutes after focused sound pulse. Echo 1 is from the near surface of cat brain and echo 2 is from the far surface of the brain. Echo 3 is transiently modified and echo 4 is transiently induced.

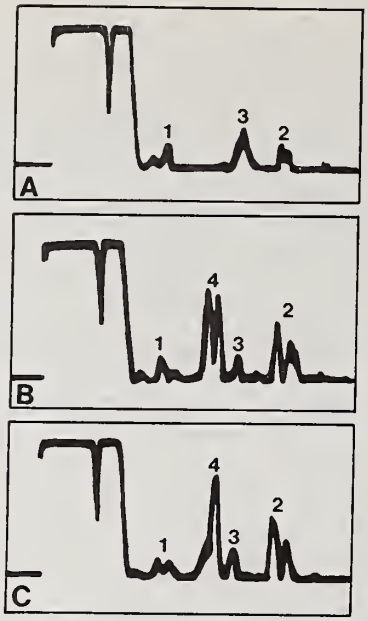

Figure 4. Echo pattern from interrogation of cat brain by examining transducer: (A) preceding induction of a lesion caused by a 6 s pulse of focused ultrasound; (B) fifteen seconds after lesion induction (echo 4 is induced); (C) persisting echo pattern.

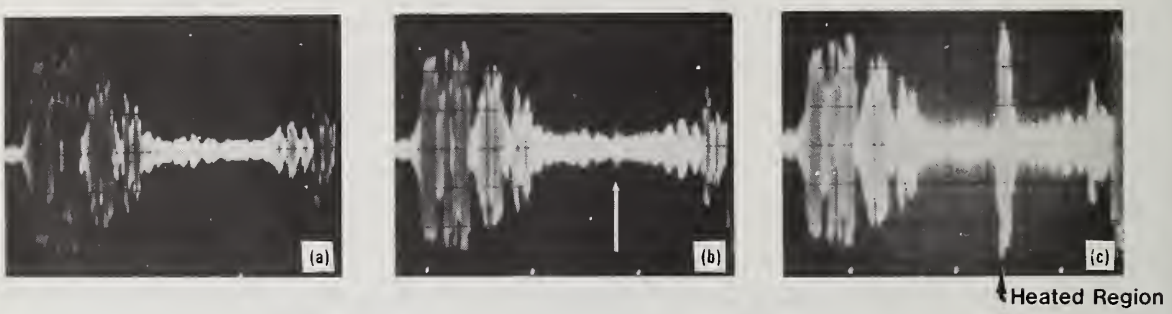

Figure 5. Ultrasonic induction and detection of both transient-heating effect and permanent-reflecting region in a formalin-fixed human brain.

heating beam was further increased, a permanent effect could be produced as shown in figure 5C. Another experimental observation involved ultrasonic visualization of a transiently-cooled region in the occipital lobe of the Rhesus monkey brain. A cryoprobe used for cryosurgery was placed in contact with the dura in the occipital area and the brain tissue was slowly cooled (over a several minute time period). The two-dimensional cross section images of the brain region before, during and after cooling are shown in figure 6. This cooling was sufficient to produce a subsequently observed brain lesion.

Physical model studies involving thermal heating in lucite with focused ultrasound have shown that transient and permanent acoustically-detectable effects can be observed [2]. The setup for observing these effects is rather similar to that used for the tissue observations shown in figure 2. An example of an acoustic transiently-observable effect in lucite is shown in figure 7. Figure 8 shows the echogram of a transient acoustically-observable effect in lucite in which the opposite sides of the heated region can be separated into two echoes. The peak-to-peak spacing distance for this picture is approximately 3.5 mm. These lucite observations of a transient nature are in general associated with a permanently-observable optical effect.

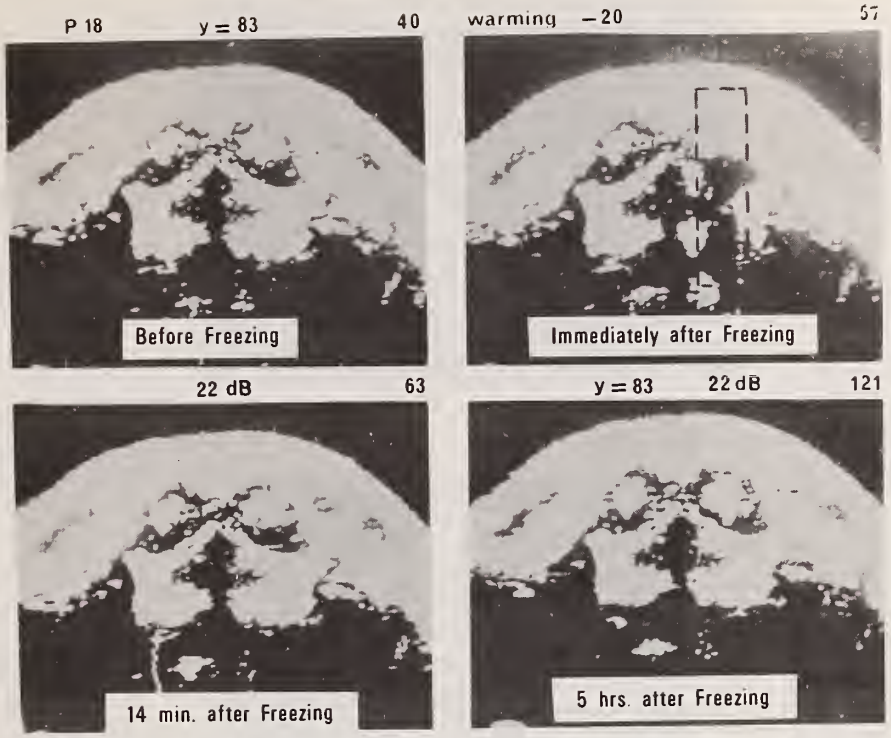

Figure 6A. Ultrasonic visualization of live Rhesus monkey brain subjected to cryoprobe cooling sequence.

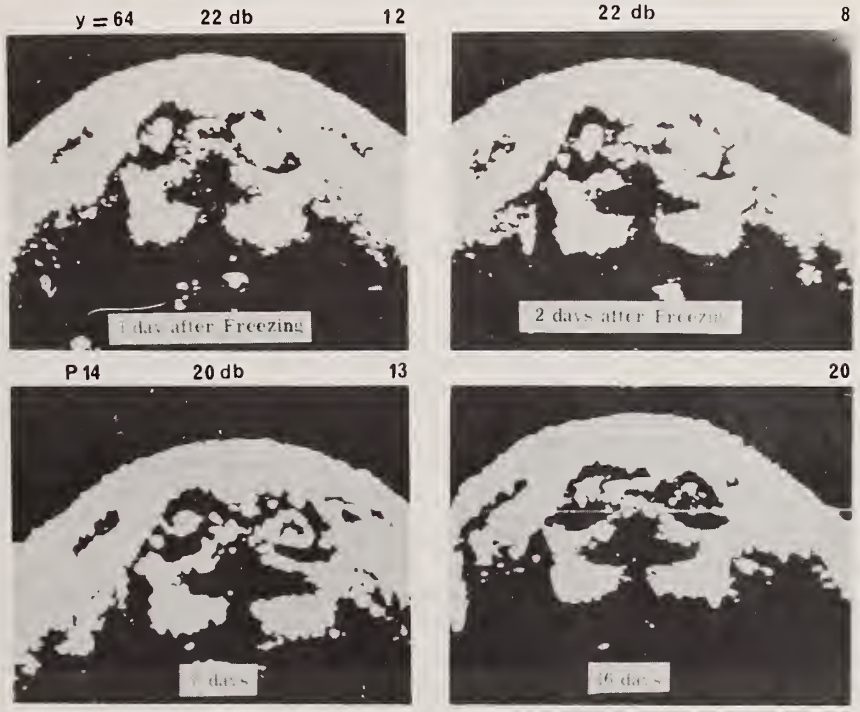

Figure 6B. Ultrasonic visualization of live Rhesus monkey brain subsequent (1-16 days) to cryoprobe cooling sequence.

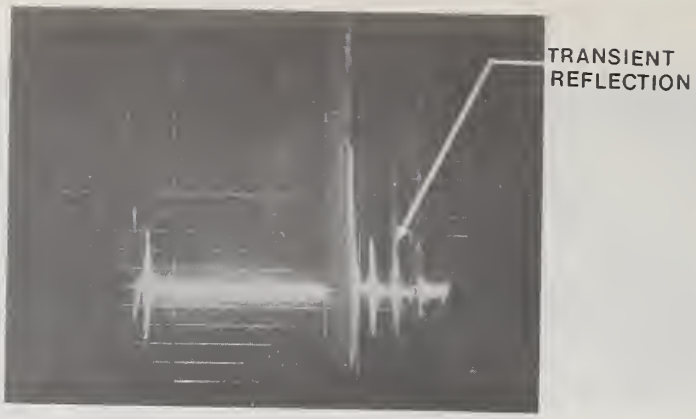

Figure 7. Ultrasonic detection of transiently-induced thermal gradient in lucite block.

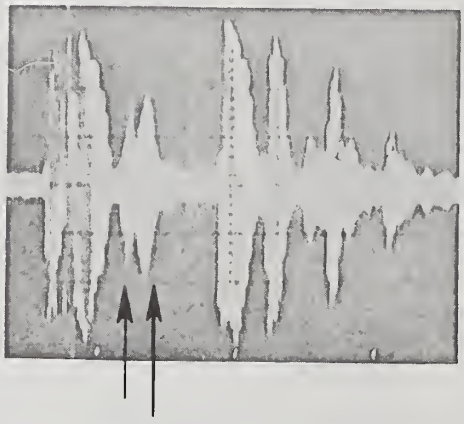

Figure 8. Ultrasonic detection of transiently-induced thermal gradient in lucite block in which echoes appear from both sides of the cylindrically-heated region.

4. Conclusion

A number of acoustically-induced thermal effects having a transient or permanent character (as determined acoustically) have been studied in physical models and in experimental animal tissues. For tissues, the possibility exists of using these effects to differentiate tissue types based on acoustic absorption spectra. Naturally, it would be ideal if all this could be accomplished in a totally reversible manner from a physiological perspective. It does not seem unreasonable to suggest the additional possibility of using focused ultrasound even if it involved a small modified tissue volume, provided a definitive tissue differentiation could be accomplished. Biopsy by mechanical means is a medically-acceptable procedure which could find perhaps a less traumatic counterpart in either reversible or irreversible ultrasonic biopsy.

Implementation of velocity determination or attenuation loss based on interrogation of multiple thermal gradient sites would of course require additional experimental investigation before any definitive statements can be made about its utility in tissue differentiation.

References

1] Fry, W. J. and Fry, F. J., Ultrasonic visualization of soft-tissue structure based on gradients in absorption characteristics, *J. Acoust. Soc. Am.* 35, 1788 (1963).

2] Fry, W. J., Fry, F. J., Kelly, E., Fry, T.A., and Leichner, C. H., Ultrasound transmission in tissue visualization, in *Diagnostic Ultrasound*, p. 13 (Plenum Press, New York, 1966).

3] Dunn, F. and Fry, F. J., Ultrasonic threshold dosages for the mammalian central nervous system, *IEEE Trans. Biomed. Eng.* BME-18, 253 (1971).

4] Robinson, T. C. and Lele, P. P., Analysis of lesion development in the brain and in plastics by high intensity focused ultrasound at low megahertz frequencies, *J. Acoust. Soc. Am.* 5, 1333 (1972).

National Bureau of Standards Special Publication 453. Proceedings of Seminar on Ultrasonic Tissue Characterization held at NBS, Gaithersburg, MD, May 28-30, 1975. (Issued Oct. 1976)

Paper 5.2: TAST: A NON-INVASIVE TISSUE ANALYTIC SYSTEM

T. D. Sachs, P. T. Anderson, R. S. Grimes
S. J. Wright, Jr., and R. M. P. Donaghy

University of Vermont
Burlington, Vermont 05401

The Thermo-Acoustic Sensing Technique (TAST) uses two intersecting sound fields to measure the acoustic absorption of cerebral tissues at the point of intersection. A resolution of better than 1/8 inch was achieved in initial scans through the coronal plane of a fixed human brain. The sylvian and cortical fissures, basal ganglia, and ventricular boundaries appeared to be profiled by the TAST values. Conceivably, TAST may provide numerical tissue characteristics in 0.002 cubic inches of selected cerebral tissue. Should predictions based on current theory and data prove correct, TAST may become a repeatable non-invasive means of establishing intracerebral diagnosis.

Key Words: Absorption; attenuation; brain; neoplasm; TAST; thermal effects; tissue; tumor; ultrasonic; velocity.

1. Introduction

Present day methods of obtaining biological information by means of ultrasound have in general three principal difficulties: (1) the information obtained is not as closely related to the biological function of the tissue as one might wish; (2) the measurements are subject to severe interference and; (3) information can be obtained only where interfaces exist. The Thermo-Acoustic Sensing Technique (TAST) technique described here appears to have advantages in all problem areas.

1.1 Velocity Versus Attenuation

Most present-day ultrasonic systems obtain their information through the measurement of either the acoustic attenuation or impedance discontinuties in the tissue being examined. Attenuation is composed of two components, absorption and scattering. The absorption part of the attenuation exhibits a much larger percentage change in its value for a given biological difference than does the impedance, [1][1] and thus would appear to be the parameter of preference in biological analysis. To date, however, the emphasis has been on the measurement of impedance discontinuties rather than on attenuation or absorption.

1.2 Attenuation

Hueter and Bolt [2] measured transmission losses through the head. They scanned the transmitter and receiver together so as to produce a map comparable to an x-ray picture. Thus, their technique measured the total attenuation along the beam, comprising the superimposed effects of transmission through bone, having a high attenuation coefficient, and soft tissue, whose coefficient is far lower. They found eventually that most of the measured effect was due to bone and that little useful information was obtained on the soft tissue of interest.

Fry and Fry [3] studied absorption gradients in tissues. They used a focused sound field to heat the tissue of interest. This heating changed the sound velocity and thus the acoustic impedance of the tissue. Where the heating field focus crossed a

[1]Figures in brackets indicate the literature references at the end of this paper.

boundary between two media of differing absorption coefficients, the media are heated differently and a reflecting surface is generated. If a reflecting surface is already present, its characteristics will be modified. These surfaces can be detected by normal echography apparatus. Thus, the Fry technique is sensitive to interfaces between tissues having different absorption coefficients.

Fry and Fry were able to pinpoint the position of an absorption gradient but were unable to determine the direction of the gradient. Hueter and Bolt's transmission system could achieve high signal-to-noise ratios in the received signal in contrast to echography even while working through the head, but was unable to localize the point of interest or to distinguish its effects from those of the skull.

The extension of computerized axial tomography to acoustic attenuation measurements such as those of Hueter, *et al.*, was reported at this meeting by Greenleaf and Johnson [4]. Such a procedure would appear to eliminate many of the problems associated with the Hueter technique.

2. The Thermo-Acoustic Sensing Technique

2.1 Principle

TAST [5-7] has the ability to sense tissue characteristics at a point by making use of the acoustic absorption and the temperature coefficient of velocity. Two sound fields are utilized. One, referred to as the "thermometer beam," is a parallel beam which is propagated into the tissue from one side and on its emergence from the other side is picked up by a receiver. The other field, referred to as the "heating field," is a focused sound field whose focal volume falls along the thermometer beam's path.

In operation, a burst of thermometer beam sound is passed through the tissue and its transit time recorded. The heating field is then activated and warms the tissue in its focal volume which is in the path of the thermometer beam. A second thermometer beam burst is then passed through the tissue and its transit time subtracted from the transit time of the first thermometer beam burst. The resulting difference in transit times is the output parameter of the system. This difference occurs because the sound velocity is dependent on the tissue temperature, which increased. The temperature rise is proportional to the intensity of the heating field as well as to the acoustic absorption coefficient of the tissue. The measured transit-time difference thus depends on the tissue's acoustic absorption coefficient for the heating field frequency, its temperature coefficient of velocity, and the intensity of the heating field along the thermometer beam's path.

2.2 System Geometry

The basic system is shown in figure 1. Thermometer beam transmitting-transducer A propagates a wavefront through the tissue D to the receiver B. In the process of going through the tissue, the wavefront will be greatly distorted and become the perturbed plane wave which arrives at the receiver and acts as a transit-time reference for the system. The heating-field transmitting transducer with its focusing lens C produces a cigar-shaped focal volume along the path of the thermometer beam. The temperature changes within the tissue are dependent on both the geometry of the heating field and the absorption coefficient distribution in the tissue.

2.3 Theory of Measurement

The transit-time difference between the two thermometer beam bursts is directly proportional to the acoustic absorption coefficient of the tissue, the intensity of the heating field where it interacts with the thermometer beam, the temperature coefficient of velocity in the tissue; and is inversely proportional to the specific heat of the tissue, its mass density, and the distance the thermometer beam travels through the focal volume. It is convenient to divide the parameters which affect the difference in thermometer beam transit times into three groups: one having to do with the type of tissue, another having to do with the parameters of the system used for making the measurement. It can be shown that the transit time difference t_d between thermometer beam bursts before and immediately after the heating field burst is given by:

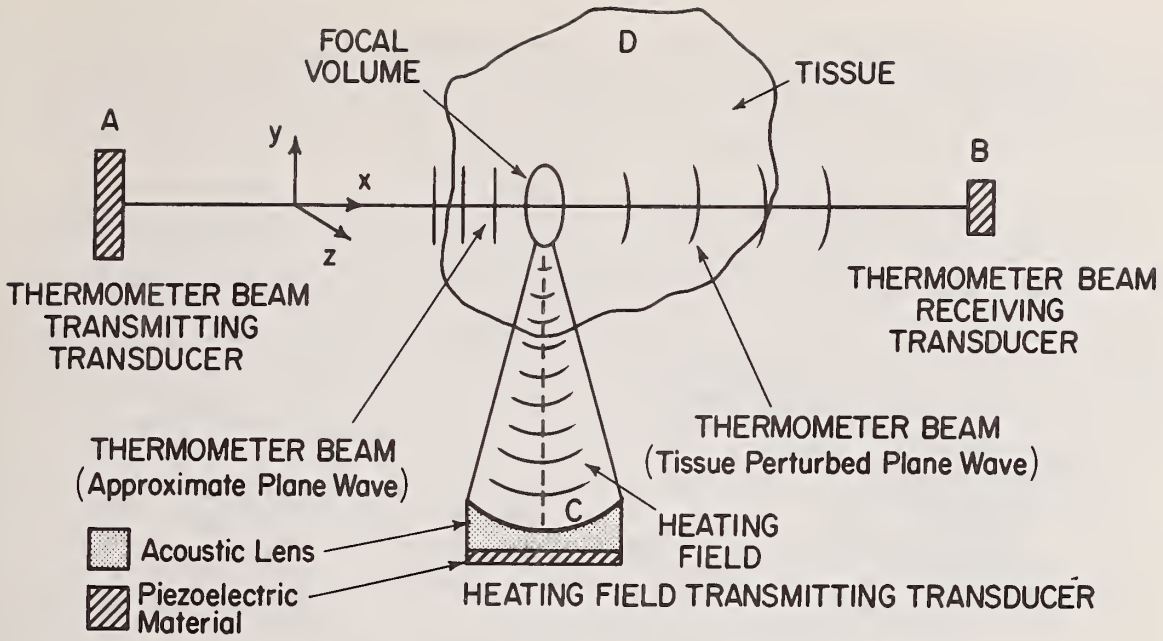

Figure 1. TAST System Geometry.

$$t_d = K \int_{-\infty}^{+\infty} I \cdot P \cdot dx \qquad (1)$$

where

$$K = \tau / J, \qquad (2)$$

and

$$P = (\partial V/\partial T) 2\alpha / V^2 \rho C \ . \qquad (3)$$

K contains the constants of the system, including the heating beam burst length τ, and the mechanical equivalent of heat J. I is the intensity of the heating field which is assumed to be a function of the distance x along the thermometer beam. P is the perturbation factor containing the tissue characteristics which are the temperature coefficient of velocity ($\partial V/\partial T$), the acoustic amplitude absorption coefficient α, the mass density ρ, the specific heat C of the tissue, and the velocity of propagation V at the tissue temperature T.

TAST's insensitivity to intervening structures arises from the nature of the integration which is carried out along the path of the thermometer beam. Only those portions of its path which have been modified by the energy input from the heating beam contribute to the arrival time difference which is the output parameter of the system. Those portions of the thermometer beam which lie outside the volume affected by the heating field make identical contributions to the total transit time before and after the heating field burst and thus the difference between the two contributions, and their contribution to the integral, is zero. The only spatial points that contribute to the transit time difference are those which are heated by the heating field. Thus, since the integrand is zero wherever the intensity is zero, namely outside the influence of the heating field, the limits of integration can be extended to infinity in both directions without affecting the result. Because the tissue outside the focal volume does not contribute to the output, it would appear that the system should be capable of working through heavily-interfering tissues such as skull. Stated another way, the initial thermometer beam burst of each measurement cycle is used as a reference which takes into account all of the diffraction and scattering effects on the thermometer beam and cancels them out of the system output.

2.4 Differential Transit-Time Measurement Electronics

The *difference* in transit time between two successive thermometer beam bursts is taken, and no attention need be paid to the absolute value of the transit time. Because the difference in transit times of the two bursts is so small, one may make the measurement by performing a phase comparison resulting in an analog signal which is then analog-to-digital converted. The differences are taken digitally.

The *phase-measurement system* is shown in figure 2, where the master oscillator signal is shown being fed to the phase comparator by two different paths. One is a direct electrical path, the other makes use of the thermometer beam as a transmission element. The output of phase comparators such as double-balanced mixers are harmonic functions of the phase-angle difference. In order to linearize the output of the phase comparator, we make the output of the comparator a sine function of the phase difference and utilize the small angle approximation in which we assume that the output is proportional to the angle itself rather than to the sine of that angle. This is done by adjusting the phase shifter until the output of the phase comparator is zero.

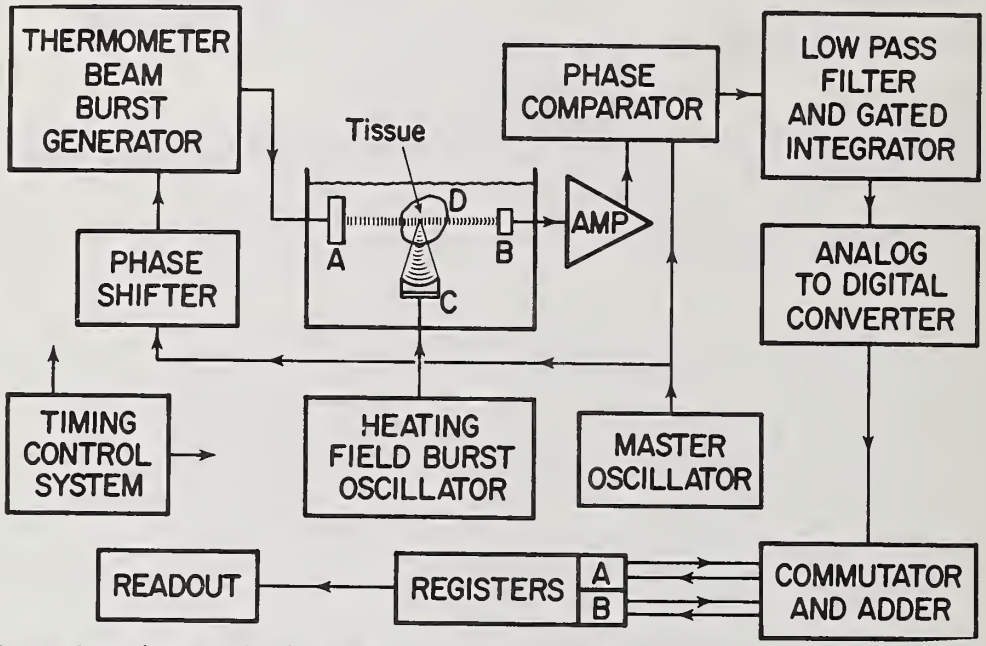

Figure 2. TAST block diagram.

The *micro-timing diagram* figure 3 indicates the details of phase evaluation of a single thermometer beam burst. Since the thermometer beam burst is generated by digital techniques, the output of the transmitter contains harmonics. This mode of generation insures phase coherence between the burst envelope and the reference rf signal and is necessary to avoid stop and start transients. The received signal contains no visible trace of the harmonics present in the transmitter waveform after it undergoes transmission through two transducers and experiences frequency-discriminatory transmission through the intervening medium. The comparator output consists of a pulse having the shape of the burst envelope with some additional components at the acoustic frequency and harmonics of that frequency. The amplitude of the pulse is proportional to the phase angle, in the small angle approximation. The high frequency components are first removed by a low-pass filter and the remaining signal is integrated over the period of the "sample" time slot. The integrator cannot keep up with the high frequency signals, but it does collect an appropriate charge at its input terminal. After the signal ends, it requires a few tens of microseconds to reach its final value and damp out the transients generated by this abrupt signal. The defects in the signal are greatly exaggerated in the figure for the sake of visibility. The analog-to-digital conversion takes place after the signal has stabilized. Since the time slots are synchronous with the master oscillator, the period of integration will always be synchronous with the received signal for a given measurement with a given amount of tissue in the thermometer beam's path.

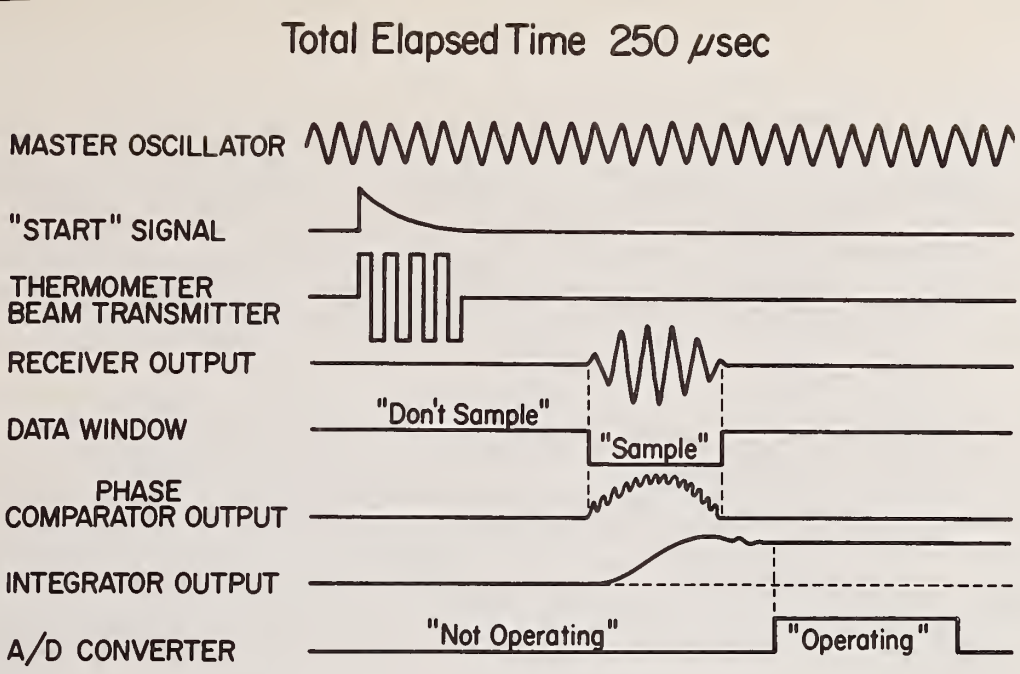

Figure 3. Micro-timing diagram.

The *macro-timing diagram* of figure 4 covers a period of time approximately 500 times that shown in the micro-timing diagram of figure 3. Each of the thermometer beam bursts shown as a single vertical line represents the entire cycle shown in figure 3. It is seen that the micro-timing activities are repeated eight times before the heating field is turned on, during a total elapsed time of 3 milliseconds. Then the heating field is turned on for 100 milliseconds, and after that, the micro-timing activities are again repeated eight times. The digital result from the eight thermometer beam bursts which precede the heating field burst, labelled A, are added to a register, while the result from the eight bursts which occur after the heating field burst, labelled B, are subtracted from that register. The difference remaining is the time-averaged representation of the time difference t_d caused by the TAST interaction described above.

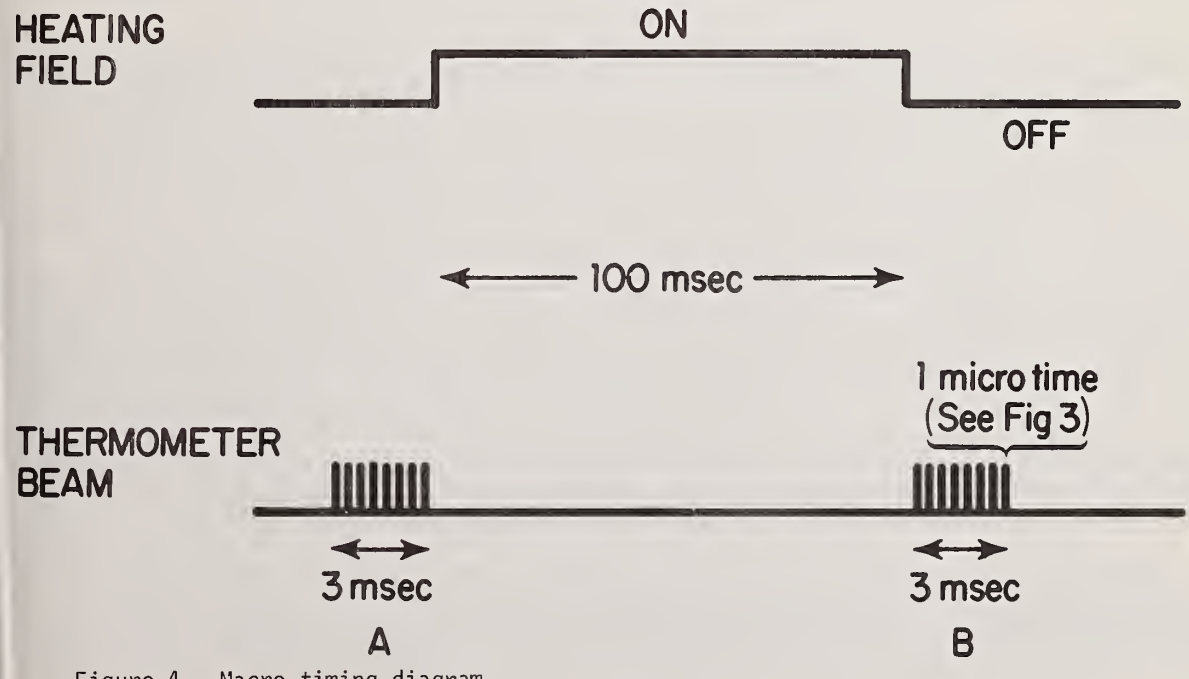

Figure 4. Macro-timing diagram.

3. P Factor, Absorption, and Temperature Coefficient of Velocity

The perturbation factor P (eq. (3)) is the product of the temperature coefficient of velocity ($\partial V/\partial T$) times the acoustic absorption coefficient α, divided by the density ρ, the specific heat C, and the velocity of propagation V. We expect the density, specific heat and velocity to be reasonably constant in tissues. The temperature coefficient of velocity on the other hand could be expected to vary considerably from one material to another. Further, the temperature coefficient of velocity of water is known to vary over a three to one range from 0°C to 37°C [8], and thus it would not be surprising if it varied from tissue to tissue.

The absorption coefficient is known to be extremely sensitive to tissue types. Thus, the temperature jump caused by the heating field varies widely between tissues and in a different fashion for different tissues. For example, the ratio of temperature rises in water and bone, both exposed to the same ultrasonic field intensity, is of the order of 1:2800. Even various types of brain tumors exhibit greatly differing absorption coefficients. For example, [1] a meningioma has some 2.5 times the absorption coefficient of an oligodendroglioma. The degree of heating in the focal volume is thus a very good indication of tissue types. It is presently uncertain as to whether the temperature coefficient of velocity does vary from tissue to tissue, but even if this is not the case, the P factor can be expected to exhibit such variation [6], and therefore should be useful in the characterization of tissues.

5. Normal Anatomy

Of the three major body cavities, the intracranial cavity seemed desirable as an experimental subject because of: (1) the lack of interfering gas pockets; (2) the potential of limiting motion of the head by fixation; and (3) TAST's differential nature which allows it to operate through interfering structures such as the skull. This is not to imply that motion problems would not be a serious complication in the TAST system.

Readily-available formalin-fixed human brain was used in initial experiments. The experiences of Hueter, Bolt and Ballantine [2] seem to indicate strongly that our thermometer beam would pass through *in vivo* skull when the next stage of experimentation was reached. Fry [3] indicated that energy can be deposited in a localized volume of tissue by a focused sound beam penetrating the *in vivo* skull as required for our heating field.

5.1 Experiment

This intial work was concerned only with the measurement of normal structures along a line passing through cortical and Sylvian fissures, internal capsule, basal ganglia, and ventricles, as shown in figures 6-8, to determine if these structures were distinguishable. We placed an intact fixed human brain in the brain holder shown in figure 5. This was in turn enclosed in a plastic box to protect the transducer system from biological fluids. The thermometer beam passed through the brain coronally in a side-to-side fashion. The heating field penetrated through the top portion of the inverted brain. The scan was produced by moving the focus of the heating field along the path of the fixed thermometer beam. The point of measurement was always the intersection of the two fields. The heating field focus was moved in 0.1 in steps through the brain. These increments were deliberately chosen because they were smaller than the Airy circle (0.150 in) for the 940 KHz field, formed by our f/2 lens. It will be seen below, that this predicted limit of resolution for our system may have been too conservative. *Interfering phenomena* are of several types. A sound field passing through a fluid carries momentum. When the sound intensity decreases due to absorption, the sound momentum cannot be lost and appears as a flow of fluid in the same direction as the sound beam. If this flow pattern is perpendicular to the thermometer beam, as in this case, the interference takes the form of a slight second-order Doppler shift of the type often described in connection with the Michaelson-Morley experiment.

When such a flow occurs, two different phenomena arise. One effect takes place when the heating field is focused in fluid, and streaming *through the focal point* occurs. Such streaming is sensed by the thermometer beam and results in large TAST numbers. These numbers permit us to identify *large fluid-filled cavities*. Another effect occurs when an even *larger-scale streaming pattern* is generated by the heating field in the fluid *outside*

the tissue. This pattern may extend into the path of the thermometer beam far from the focal point inside the tissues. These flow patterns disrupt the stability of the thermometer beam's path and may completely obscure TAST data. The second effect can easily be prevented by enclosing the thermometer beam in an undisturbed medium. This is the purpose of the streaming shield tubes shown in figure 5. The flow patterns inside the box have been found to be much more serious than those outside. An internal streaming shield appears to provide adequate protection for the thermometer beam.

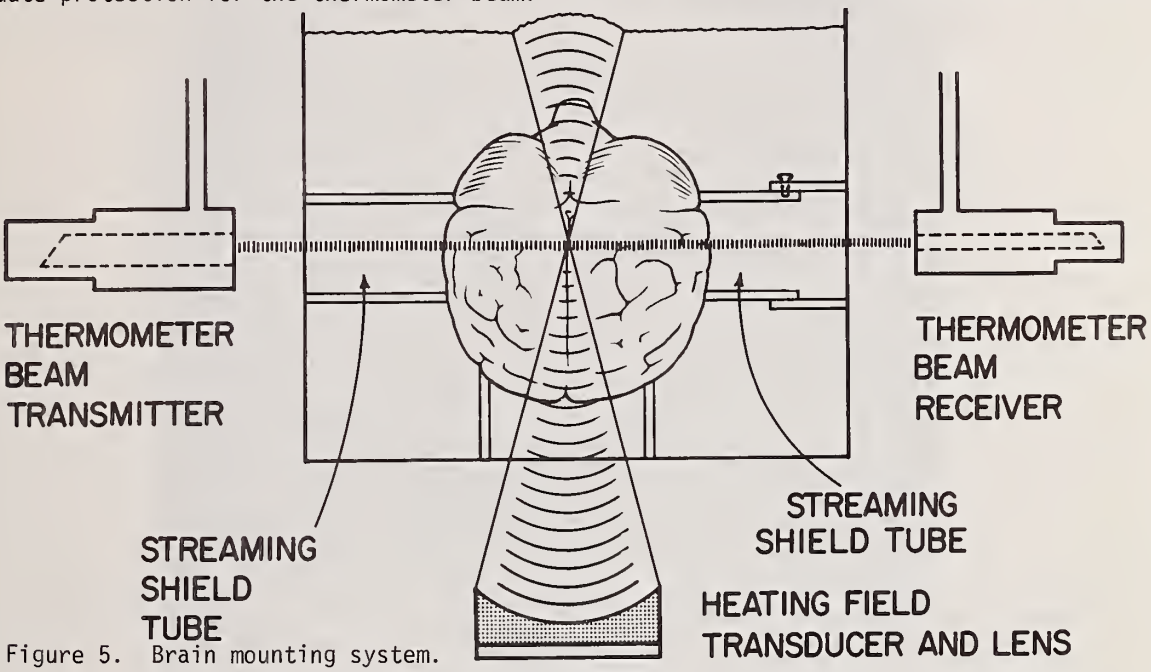

Figure 5. Brain mounting system.

Streaming phenomena which occur near bubbles also cause very serious interference when they are excited in the heating field [10]. In addition, excited bubbles vibrate the tissue and introduce interfering Doppler shifts.

In this preliminary experiment, the brain was not as rigidly secured as it might have been and probably moved during the measurements. On this basis alone, it is to be expected that the TAST values and brain structure will not correspond perfectly in all areas. The validity of brain structure-TAST relationships is inferred by two observations: (1) the close correlations of the two successive TAST measurements at given points in the same run; and (2) the fact that only minor displacements of the TAST curve are required to make large segments of that curve correspond very closely to brain structures.

Data analysis of three runs (figs. 6-8) through the same brain loci and comparison of TAST data and brain structure are facilitated by a composite representation. Superimposed on top of the pertinent coronal section of brain are the measured relative values of time delay t_d plotted vertically. The best estimate of where the thermometer beam passes is shown by the heavy black line drawn across the coronal section. Variations of cerebral anatomy are intended to lie perpendicularly below the TAST profile. Several aspects of the data suggested this correspondence.

The expected streaming artifacts are seen. Streaming effects at the edge of the brain are seen at the left side of the first run (fig. 6) and again on the right side of the brain in the second run (fig. 7). Additional streaming phenomena show up in the ventricles and give large peaks in all three runs.

A bubble artifact may also have been present. In each of the three runs, a large peak was seen 1-1/2 to 1-3/4 in from the left. These peaks were over four times the height of the ventricular peaks and therefore were truncated for scaling reasons in the profile. A reasonable explanation for these peaks would be a bubble lodged in the Sylvian fissure near

the heating focus. Since water has a calculated P factor of about 1/300th that of brain, it is not surprising that the slit-like water filled portions of the same fissure exhibited low TAST values. This is in contrast to the situation in the ventricles where sufficient volume exists for streaming phenomena.

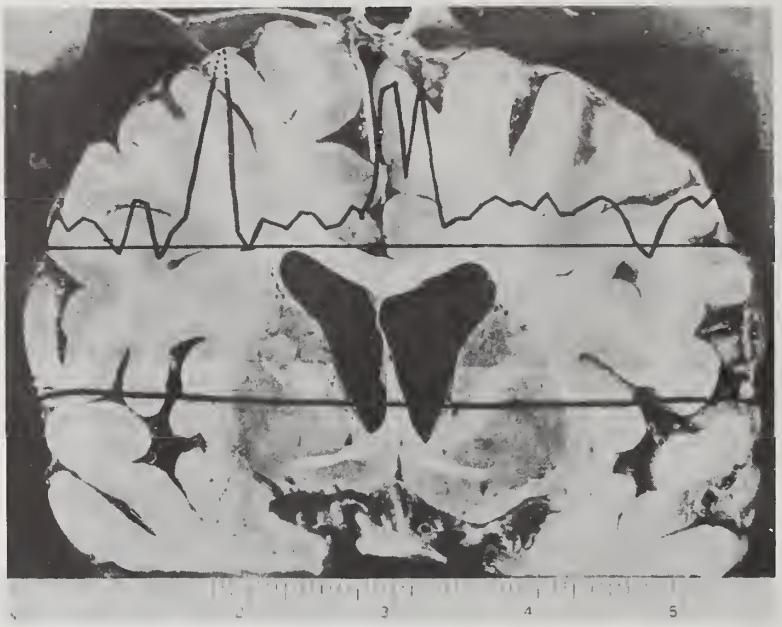

Figure 6. Coronal section of fixed human brain. Dark line through basal ganglia indicates thermometer beam path, and superimposed curve with zero reference line represents TAST measured values during run #1.

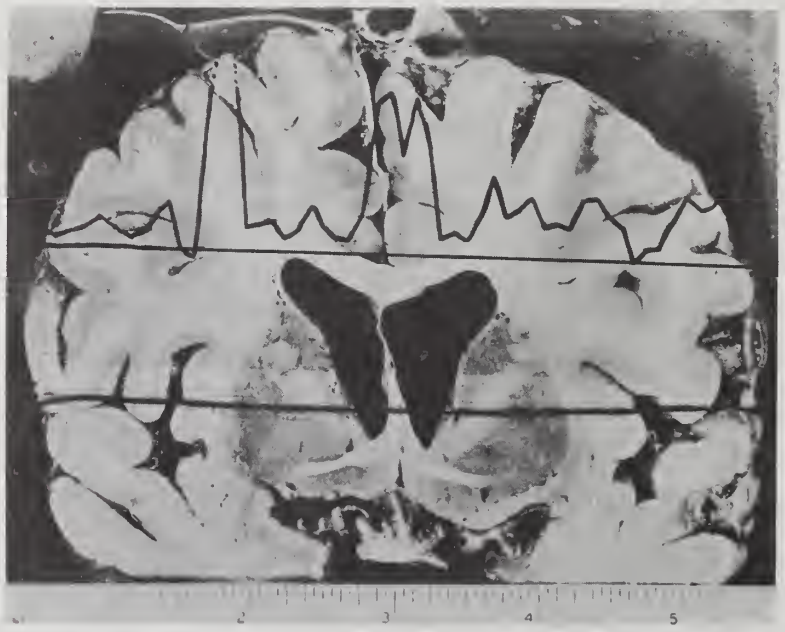

Figure 7. Coronal section of fixed human brain. Dark lines through basal ganglia indicates thermometer beam path, and superimposed curve with zero reference line represents TAST measured values during run # 2.

The most obvious correlation between the TAST profile and the coronal brain structure would appear to be the large notched central peak, surely representing the ventricles. The interhemispheric cleft would seem to be too narrow and asymmetrical to account for this symmetrical peak. Also the interhemispheric cleft is nowhere near the supposed focus of the system. The total width of the lateral ventricles where crossed by the thermometer beam was 5/8 in. This correlates well with the large central peak in the TAST profile. First inflection points were used in figures 7 and 8 and second inflection points in figure 6. At the present time, it is not clear why the second inflection points corresponded to ventricle edges in the latter case.

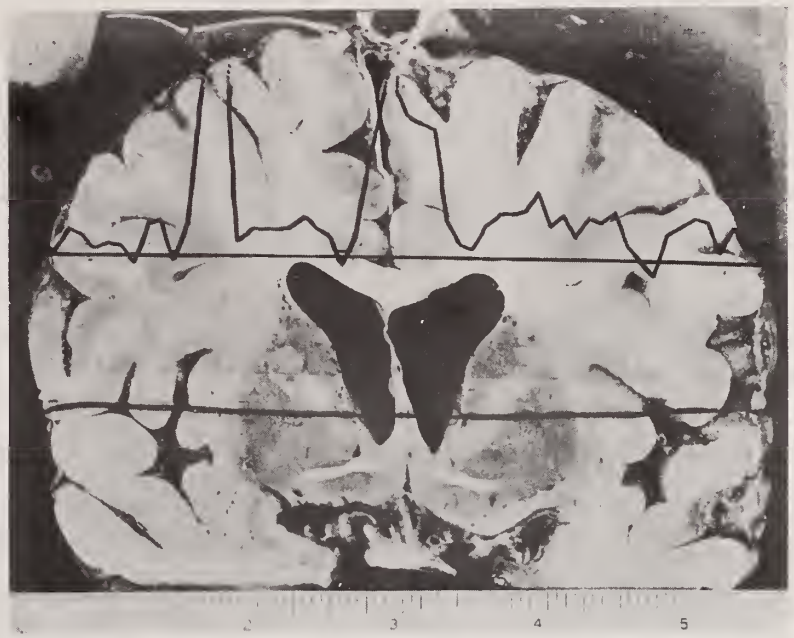

Figure 8. Coronal section of fixed human brain. Dark line through basal ganglia indicates thermometer beam path, and superimposed curve with zero reference line represents TAST measured values during run # 3.

The distance from the midpoint of the septum to either ventricular wall measured 5/16 in, placing the septum in the center of the lateral ventricles as expected. Within an error of 1/32 in, the dip in the ventricular peak measured 5/16 in from the first inflection points in figures 7 and 8 or the second inflection points of figure 6. Therefore, the dip, centrally placed in the ventricular peak, corresponds to the septum. It is theorized that TAST has the resolution to see the septum which is a little less than 3/16 in wide. This corresponds to a volume of 0.002 in^3. Since the midpoint of the interhemispheric cleft is 1-3/4 in above the presumed focus in the septum, it most likely does not account for this dip. Furthermore, the thermometer beam is located well below the cleft.

The lateral boundary of the internal capsule was 3/8 in from the lateral wall of the lateral ventricle. Three-eights of an inch to either side of the first inflection point in figures 7 and 8 and the second inflection point in figure 6 are a depression and rise. Sharp peaks are seen within these bounds in figure 7. Whether the capsule is represented by the low point or the higher shoulder is not clear.

The lateral boundary of the putamen (part of the basal ganglia) was 1-1/8 in from the septum. This corresponds on the left side to a segment of the profile extending from the lateral margin of the capsular boundary to the initial rise of the off-scale peak thought to be associated with the hypothetical bubble mentioned earlier. A mid-segment peak is more prominent in figures 6 and 7 than in figure 8. The comparable TAST segment on the right side encompasses one distinct peak in figures 6 and 7 and possibly a smaller one in figure 8.

These findings are of sufficient symmetry to suggest that capsular/putaminal and putaminal/insular boundaries are recognized. From the data regarding internal capsule and adjacent putamen, it is unclear as to which has the greater TAST value. To settle this point, the signal-to noise-ratio of the system has been reduced and separate slices of grey and white matter from a formalin-fixed brain are in the process of being evaluated.

The 3/8-in width of the insular and subinsular structures on the left are encompassed by the off-scale peak thought to represent a bubble in recesses of nearby fissures. The 1/2-in width of insular and subinsular structures on the right, when superimposed on the TAST profile, singles out a hump that is smoothest in figure 6, less so in figure 7, and somewhat bimodal in figure 8.

There are three dips below the baseline in the TAST profile that correspond in width to the two recesses of the sylvian fissure on the left and the larger recess on the right. Although the matching is not perfect, the 5/16-in and 1/2-in gyri on the left are associated with prominent peaks in the TAST profile of about the same width. The more medial peak in each of these instances is higher than the more lateral bimodal peak. On the right, the 1/4-in gyrus matches the first rise and fall of the TAST profile superimposed above it. Whether the final and most lateral TAST peak represents the dura or the dura/water effect is unclear.

In all these profiles, the TAST baseline was increasing from left to right. Whether this represents acoustical or electronic drift, is unclear. It might also represent an altered condition of the brain. However, with regard to either hemisphere of the brain, the different tissue peaks do seem to have reproducible absolute and relative TAST values.

Throughout this analysis, it has been assumed that the superficial gyri pattern does not account for the TAST profile because the focus of the system was on the average two inches or more within the brain substance. Refraction of the heating field entering the convex surface of the brain is not thought to be a major consideration at this time.

Reviewing the TAST profile/coronal brain correlation, certain points seem tenable: (1) the ventricles are readily identifiable and measurable; (2) the septum is discernible, suggesting the resolution of the system to be at least 1/8 in or an equivalent volume of 0.002 in^3; (3) intracerebral boundaries between grey and white matter can be distinguished; and (4) a suggested difference in TAST values between putaminal grey and capsular white matter was at the limit of resolution of the apparatus.

6. Abnormal Anatomy

TAST-obtained information may be particularly useful in the management of stroke, head injury and tumors, and in the identification of lacunar infarcts in basal ganglia. In view of TAST's theoretical and tentatively demonstrated ability to differentiate tissue types, detection of edema and infarction is conceivably within reach. Absence of cerebral infarction in the first few hours following hemiparesis or aphasia would be particularly valuable in deciding whether to do emergency cerebral revascularization--such as carotid endarterectomy or superficial temporal-middle cerebral anastomosis. The effectiveness of such procedures is thought to be less [11] if true infarction is underway. At the earliest, brain scans do not turn positive until late in the first week following stroke. This is too late in many instances to be helpful in making this early surgical decision.

In head injuries, evaluation of the seriousness of the insult by current measures has many inaccuracies. Intracranial pressure measurements alone, pressure/volume curves, and cerebrospinal fluid biochemical determinations might be augmented by a numerical value for the degree of injury at selected sites. TAST may supply such data.

In managing patients with tumors, it would be advantageous to distinguish the malignant glioblastoma from the benign meningioma, and thus save operations in hopeless cases. P factors have been calculated (without regard to the variation of the temperature coefficients of velocity [6]) indicating that various tumor types may well be identifiable. No information on glioblastomas *per se* is available.

TAST may also be able to identify radiologically-invisible lacunar infarcts in basal ganglia.

7. Summary

TAST measures a tissue property proportional to the product of the absorption coefficient and the temperature coefficient of velocity, both of which appear to be highly sensitive to tissue types. Initial measurements strongly suggest the system's ability to identify and differentiate between normal tissues in brain, and possibly to make identifications in volumes as small as 0.002 in^3. Intracranial uses for the system may include the analysis of stroke, head injury, tumor, and perhaps identification of lacunar infarcts.

The authors should like to express their appreciation to the Sloan Foundation for its partial support of this work.

References

[1] Yukishita, K., Tanaha, K., Ito, K., Ehara, K., and Watanabe, H., Ultrasonic diagnosis of brain tumors, in *Proceedings In Echo-Encephalography*, Proceedings of the International Symposium on Echo-Encephalography, Erlangen, Germany, 1967 (Springer-Verlag, 1967).

[2] Hueter, T. F. and Bolt, R. H., An ultrasonic method for outlining the cerebral ventricles, *J. Acoust. Soc. Am.* 23, 160 (1951).

[3] Fry, W. J. and Fry, F. J., Ultrasonic visualization of soft-tissue structure based on gradients in absorption coefficients, *J. Acoust. Soc. Am.* 35, 1788 (1963).

[4] Greenleaf, J. F. and Johnson, S. A., Algebraic reconstruction of spatial distributions of acoustic velocity and attenuation in tissues from time-of-flight and amplitude profiles, this volume (p. 109).

[5] Sachs, T. D., Welt, A. J. and Slayton, P. W., Thermo-acoustic sensing technique-TAST, in *Proceedings of IEEE Ultrasonics Symposium*, P. 54, (IEEE, Cat. No. 72 CHO 708-8 SU, New York, 1972).

[6] Sachs, T. D., Potential of TAST for measurements of perfusion, ultrasonic absorption and intensity at a point, in *Proceedings 1973 IEEE Ultrasonic Symposium*, p. 52 (Cat. No. 73 CHO 807-8 Su, IEEE, New York, 1973).

[7] Patents: U.S. 3,771,355, French 2, 155,465; other U.S. and foreign patents pending.

[8] McSkimmin, H. J., Velocity of sound in distilled water for the temperature range 20° - 75°C, *J. Acoust. Soc. Am.* 37, 325 (1965).

[9] Fry, W. J., personal communication (April 1973).

[10] Devin, C., Jr., Survey of thermal, radiation, and viscous damping of pulsating air bubbles in water, *J. Acoust. Soc. Am.* 31, 1654 (1959).

[11] Crowell, R., personal communication (April 1975).

CHAPTER 6

SCATTERING TECHNIQUES

National Bureau of Standards Special Publication 453. Proceedings of Seminar on Ultrasonic Tissue Characterization held at NBS, Gaithersburg, MD, May 28-30, 1975. (Issued Oct.1976)

CHAPTER 6. SCATTERING TECHNIQUES

Paper 6.1: TISSUE CHARACTERIZATION BY ULTRASONIC FREQUENCY-DEPENDENT ATTENUATION AND SCATTERING[1]

P. P. Lele, A. B. Mansfield, A. I. Murphy, J. Namery, and N. Senapati

Laboratory for Medical Ultrasonics
Massachusetts Institute of Technology
Cambridge, MA 02139

Studies conducted in this laboratory to explore the feasibility of utilizing acoustic impedance, attenuation, and scattering characteristics of tissues for enhancing the diagnostic capabilities of ultrasound are described. Frequency-dependent ultrasonic attenuation is found to be sufficiently greater in infarcted or otherwise necrotized tissues than in normal controls to permit their positive identification. Superficial and internal scattering properties of tissues hold the promise of being significant for diagnostic applications. The difficulties that will have to be overcome to successfully utilize these properties are discussed.

Key Words: Acoustic impedance; Bragg diffraction; computer processing; frequency-dependent attenuation; internal scattering; myocardial infarction; scattering; surface scattering; tissue characterization; ultrasound diagnosis; ultrasonic spectroscopy.

1. Introduction

This paper summarizes the work conducted in this laboratory on the utilization of the acoustical impedance, attenuation and scattering properties for tissue characterization. Differences in the acoustic impedance and attenuation of various normal and abnormal tissues were studied under a variety of known and controlled ultrasonic field conditions. These were found to be quantitatively significant and could be correlated with differences in tissue structure and pathological changes. Differences in scattering from the surface as well as the interior of normal and pathological tissues indicate that studies of acoustical scattering could provide important information on tissue structure in a non-invasive manner.

Different amphibian and mammalian organ samples were studied *in vitro* and *in vivo*. Heat, vascular occlusion and chemicals were used for induction of controlled pathological changes in different experiments.

2. Acoustic Impedance

Fresh specimens of normal and infarcted myocardium were obtained from the heart of thoracotomized dogs 20 to 30 minutes after the ligation of the circumflex branch of the left coronary artery. Pieces of myocardium were excised and placed in a bath of normal saline. Damped ultrasonic transducers with resonant frequencies of 1 to 5 MHz were coupled to the specimens with a column of degassed normal saline which also acted as a delay line. By means of conventional pulse-echo techniques, the orientation of the transducer with respect to the specimen was adjusted to obtain the maximum echo amplitude from the saline-myocardium interface. The echoes thus obtained were compared with echoes obtained from targets of known acoustic impedance, *e.g.*, glass, plexiglass, and soft polyethylene. Comparison of figures 1a and b, typical of the results obtained, shows that the acoustic impedance of infarcted myocardium is consistently lower than that of the normal myocardium.

---

[1]This work was supported in part by the U.S. Public Health Service (grants FD-00680, CA-16111, GM-19706 and contract NO1-HV 22017).

These differences were also found to remain unchanged over a period of approximately 30 minutes during which observations were continued. The absence of progressive change in the acoustic impedance over periods of 30 minutes at temperatures of 37° C or lower is consistent with previous observations in the cat brain *in vivo* [1].[2]

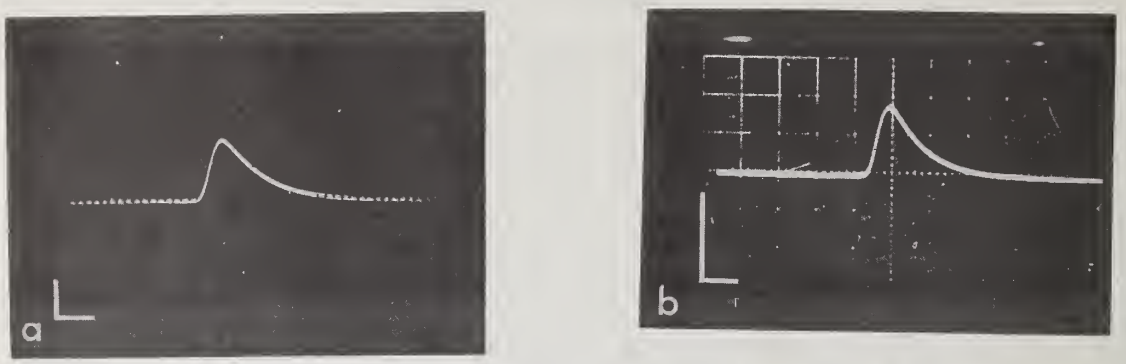

Figure 1. Maximized echo (rectified envelope of the RF pattern) from front surface of excised canine myocardium in saline: (a) normal myocardium, (b) infarcted myocardium. Vertical bar = 5 volts; horizontal bar = 2 μs. Note that the amplitude of the echo from the infarcted myocardium is 3.8 volts compared with 7 volts from the normal myocardium.

Since echo amplitude is highly dependent on target orientation [2], differences in the amplitudes of the echoes from the normal and infarcted myocardium are indicative of the differences in the acoustic impedance of the tissues only when both are measured under identical conditions of transducer-tissue surface orientation. In diagnostic situations *in vivo*, the orientation of the interface with respect to the transducer will vary with cardio-respiratory movements from point to point and even at the same point. Simple, direct measurement of the echo amplitude from the accessible surfaces of organs *in vivo*, *e.g.*, the myocardium, thus cannot be of diagnostic significance in clinical applications.

3. Acoustic Attenuation

3.1 Rationale

Ultrasonic attenuation in biological tissues has previously been shown to rise precipitously on heat necrotization or thermal denaturation [1,3,4] and a similar but slower increase in attenuation was found to occur with sustained anemic damage in the cat brain. It is, therefore, plausible that measurement of acoustical absorption or attenuation may help to differentiate abnormal from normal tissues. The absorption coefficients of tissues are also known to increase with frequency, the slope of this dependence varying with the type of tissue [5]. In a previous study, the curves for absorption at different frequencies were found to be significantly different in astrocytomas than in normal brain, the absorption at any frequency being higher in the astrocytoma than in the normal brain [6,7]. Thus, the frequency-absorption slope may be expected to change significantly when the tissue is necrotized and thus permits the differentiation of this tissue from normal tissue.

3.2 Broadband Ultrasonic Technique

In the field of nondestructive evaluation (NDE) of materials, frequency-domain analysis of a single broadband ultrasonic echo before and after its passage through a specimen has been shown to contain enough information on the frequency-dependent attenuation properties of the specimen to permit its characterization [8,9]. Since with this technique, the entire curve of the frequency-attenuation characteristics can be obtained with a single

[2]Figures in brackets indicate the literature references at the end of this paper.

interrogation, it should permit differentiation *in vivo* of normal from infarcted myocardium, provided that the angle of incidence of the interrogating ultrasound is not a critical factor and that the single echo could be captured and analyzed in the frequency domain. Experiments were first conducted on "stationary" samples of skeletal and cardiac muscles *in vitro*, using a slowly-sweeping spectrum analyzer. On finding that the technique, in fact, does permit differentiation of infarcted from normal myocardium, a computer-based data acquisition system for capturing and analyzing a single echo was developed.

The instrumentation used initially was basically that of a pulse-echo, A-scope ultrasonograph. A highly-damped (Q≈1) broadband transducer (10 MHz bandwidth) was shock-excited by a pulser (300 volts step, 10 ns rise time). The echoes received by the same transducer were fed into a wideband, low-noise amplifier (-3dB at 50 kHz and 17 MHz; 40dB gain). The transducer loop response was measured in the conventional manner by using a standard reflector, consisting of a flat, thick glass plate placed parallel to the face of the transducer to ensure normal incidence of the interrogating beam of ultrasound. The echoes were gated repetitively into a slowly-sweeping spectrum analyzer as well as into an oscilloscope. The A-scope display thus provided information on the echo amplitude or on the target impedance, whereas the spectrum analyzer displayed the spectral energy content, or the Fourier transform, of the echo signal, *i.e.*, the loop response of the system (figs. 2a, b). It should be emphasized that the reference reflector (or any other target) has to remain stationary over approximately 2000 interrogations by the ultrasonic pulse for the spectrum analysis to be performed.

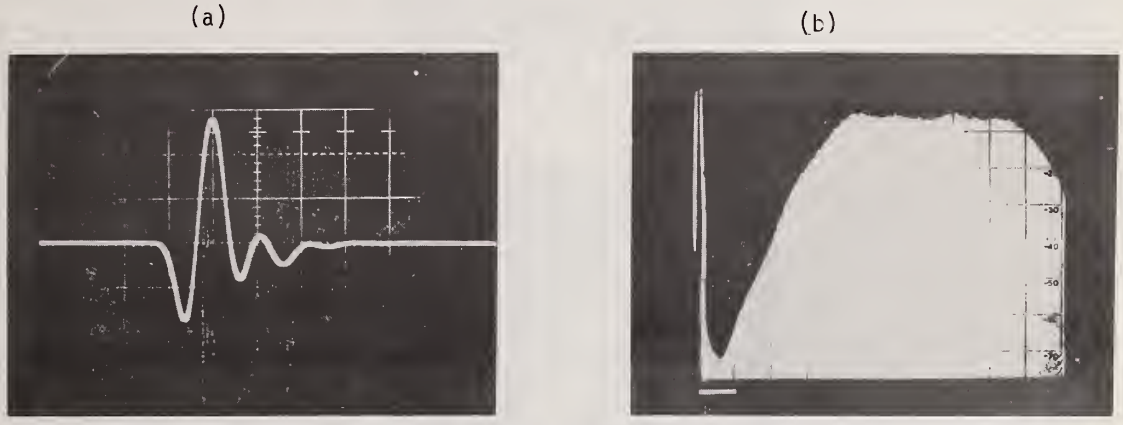

Figure 2. (a) Characteristic echo of broadband transducer (10 MHz bandwidth) received from the first surface of a flat reflector (aluminum in saline). Vertical, 100 mv/div; horizontal, 100 ns/div. (b) Fourier transform of calibration echo in (a) measured by repetitively gating the above echo into a slowly-sweeping, analog spectrum analyzer. Total sweep time is 2 seconds. Vertical scale, linear amplitude; horizontal scale, linear frequency (bar = 1 MHz; vertical marker at left is DC or 0 MHz).

Introduction of a tissue specimen (*e.g.*, muscle) between the transducer and reflector leads to frequency-dependent attenuation of ultrasonic energy and hence, to a change in both the amplitude and the shape (spectral energy content) of the echo from the reflector. Figure 3 is the spectrum of the echoes through a freshly-excised, healthy, mammalian skeletal muscle (approximately 1 cm thick). Figure 4 shows the spectrum obtained under comparable experimental conditions from a freshly-excised muscle, the vascular supply of which has been occluded 24 hours earlier. For comparison, figure 5 shows the spectrum from a normal muscle stored in normal saline for three hours after excision. Note the faster high-frequency roll-off in both figures 4 and 5. Comparable results were obtained in similar experiments on skeletal muscles with localized areas of heat necrotization and infarction by vascular occlusion and from *in vitro* experiments on specimens of normal myocardium and anemic infarcts. The slope of the frequency-dependent attenuation (*i.e.*, the slope of the roll-off) characteristically is steeper for the infarcted tissue than in the normal control specimens. Thus, basically, the frequency spectrum of the ultrasonic signal contains enough information on the tissue it has traversed to permit characterization

of the tissue as normal or necrotic. Additionally, it was observed that specimens of skeletal muscle obtained 4 to 8 hours after vascular occlusion did not show attenuation slopes characteristic of necrotization (compared to control specimens), whereas specimens obtained 10 hours or later after vascular occlusion, invariably did so. This correlates well with the results of Moore, *et al.*, [10] and Stenger, *et al.*, [11]. Again, in the heart, changes in attenuation slopes (and in the ECG) were absent or negligible with a low L.A.D. ligation (which is known to cause a diffuse infarct) even after 6 hour survival, whereas a high circumflex ligation (which produces a solid infarct) caused obvious changes in the attenuation slopes (and ECG) even with relatively short survival times (2 to 3 hours). The ultrasonic diagnosis was confirmed by histological and ultrastructural examination in each of these cases.

Figure 3. Spectrum of reflector echo after traversing 1 cm thick normal skeletal muscle, freshly excised. Same scales as figure 2b.

Figure 4. Spectrum of reflector echo after traversing same thickness of infarcted muscle, excised 24 hours after ligation. Same scales as figure 2b.

It is germane to point out here that the power density spectrum and pulse shape are analogous and that frequency-doman analysis does not generate new information that is not contained in the (time-domain) pulse itself. Frequency-spectrum analysis or Fourier transformation, however, is the most effective and simplest way to study pulse shape details and to differentiate between two almost identical pulse shapes. Differentiation can be attempted - and was - by waveform pattern recognition (*i.e.*, location of pulse maxima, minima, zero crossing and slopes) which is much more complex than Fourier analysis. Furthermore, comparison of the power density spectra yields a direct measurement of the frequency-dependent attenuation which correlates well with histopathological changes in tissues.

3.3 Target Orientation: Effect of Off-Normal Angles of Incidence of the Interrogating Beam

With the interrogating beam of ultrasound incident on the reflecting interface at off-normal angles, not only does the amplitude of the echo diminish markedly [2] (to 1/10 with 6°, 1/100 with 12°), but also its shape (and Fourier transform) changes drastically (fig. 6). The magnitude of this change is directly proportional to both the ultrasonic

Figure 5. Same as figure 3, but muscle was stored for 3 hours in 20 °C saline.

beamwidth and the degree of off-normal angulation and is due to phase cancellations resulting from different path lengths between the transducer and target. Reduction of the ultrasonic beamwidth at the target by the use of focused transducers effectively eliminates this problem (fig. 7), extending the usefulness of the technique to off-normal target orientation. Use of a focused beam also substantially improves the lateral resolution of the system which is proportional to the diameter of the ultrasonic beam at the interface. Dynamic tracking of a moving interface with a concentric annular-ring phased-array transducer [12] to retain the interface at the focus can be expected to yield a lateral resolution of approximately 1 wavelength.

In more than 50 skeletal muscles and 16 dog hearts with induced infarctions used in these studies, the results obtained were very similar to those in skeletal muscle shown in figs. 2 to 5. From measurements made on the photographs of the spectral energy content of the second surface echo (*i.e.*, after attenuation by 2 transits through the sample) as displayed on the spectrum analyzer, graphs of the energy content of the echo at different frequencies were plotted. From figure 8, which is typical of results obtained in cardiac as well as skeletal muscle, it can be seen that the amplitude, at 7 MHz, of the echoes that had passed through an infarct is less than half that of the echo through the normal tissue. The difference between the echoes through the infarcted and normal muscle becomes less pronounced as the frequency decreases, being negligible at frequencies below 2 MHz. However, it should be noted that the energy content in the interrogating pulse itself falls off rapidly below about 3.5 MHz, (see fig. 2b). This is presently corrected in the software. A frequency-sweep (chirp) technique and amplitude modulation has been employed in order to equalize the energy content at all frequencies above 1 MHz. It is planned to interrogate the tissue by paired bursts (approximately 5 μs in duration) at two frequencies. The first burst, at about 2 MHz, will be used to compare successive targets and normalize data; the energy in the echo at the higher frequency (∿6 MHz) will characterize the target as normal or necrotic. Matched filtering of the echoes will be digitally implemented to preserve the axial resolution - as is commonly done in other signal detection techniques.

3.4 Instrumentation for *in vivo* Applications

The application of this technique to tissues *in vivo*, however, presents several problems due to the continual cardio-respiratory movements. As stated above, real-time spectrum analysis requires that the same signal is fed repetitively (approximately 2,000 times which under normal operating conditions requires approximately 2 s) into the slowly-sweeping spectrum analyzer. The motions of the body structures preclude the possibility of obtaining a stable, repetitive signal. A digital, on-line, signal acquisition and processing system has therefore been developed. The single, gated echo signal is directly digitized, and fed into a computer for processing and into a disc for storage. The computer performs a fast-Fourier-transform (FFT) of the echo and calculates the frequency-dependent attenuation, taking into account the loop response characteristic of the transducer and the specimen thickness at the focus of the interrogating ultrasonic beam in the tissue specimen. To minimize electronic variability, FFT's of 16 consecutive echoes are averaged in the computer for stationary targets. Various interrogation methods have been developed

for rapidly-moving structures, *e.g.*, the heart; some of these have been described in a previous paper [13]. The results yielded by these techniques are the same as those yielded by analog spectrum analyzers with repetitive interrogation.

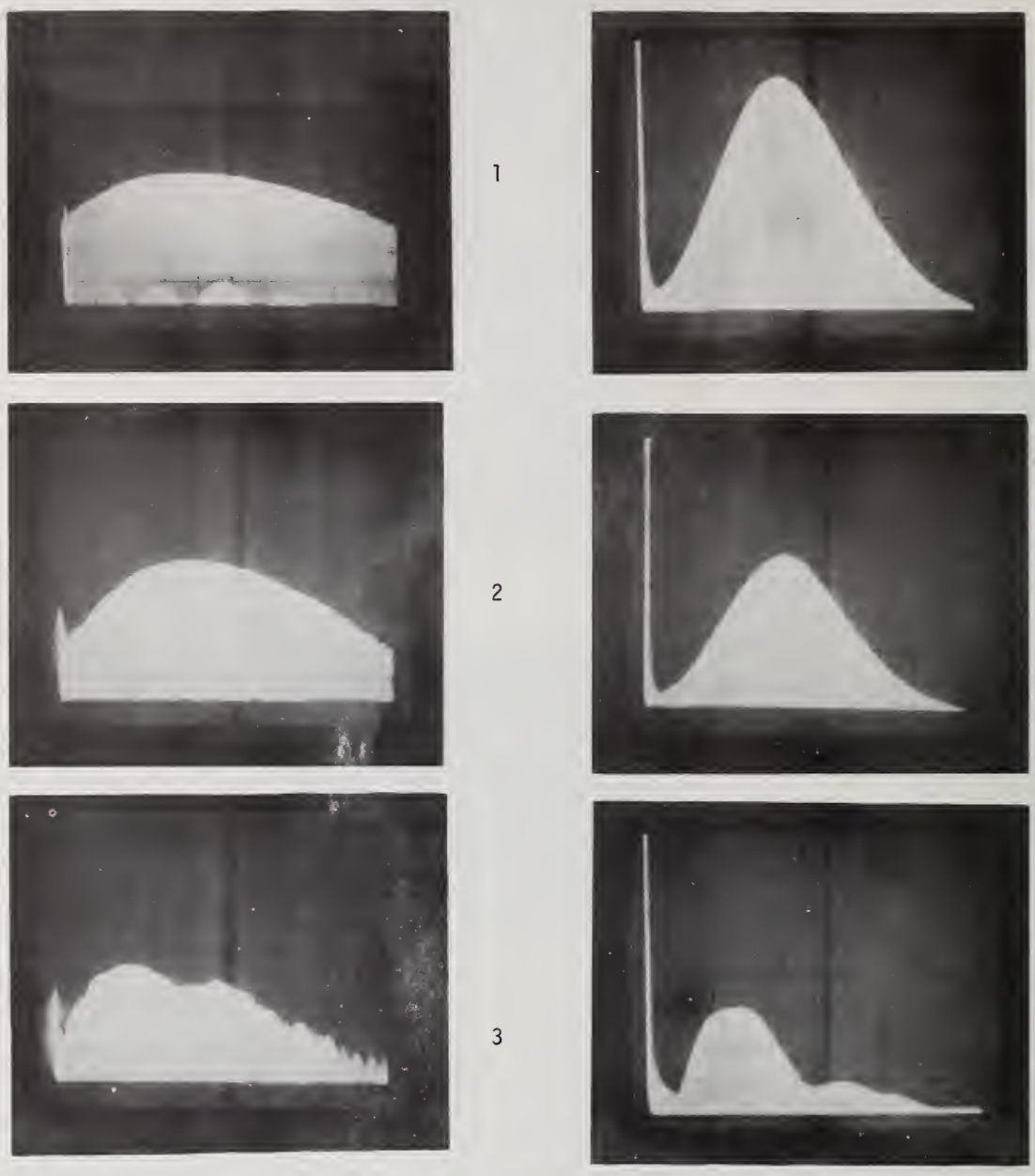

Figure 6. Effect of off-normal angles of incidence of unfocused interrogating beam on Fourier transform of the echoes. The ultrasonic beam was incident normal to the target in records a1 and b1. Records 2 and 3 were obtained when the angle of incidence was increasingly off-normal.

3.4 Results in other Tissues

Results of some *in vitro* studies on bovine liver, kidney, skeletal muscle, and cardiac muscle are shown in fig. 9. Each of the organs, obtained from freshly-killed animals, was

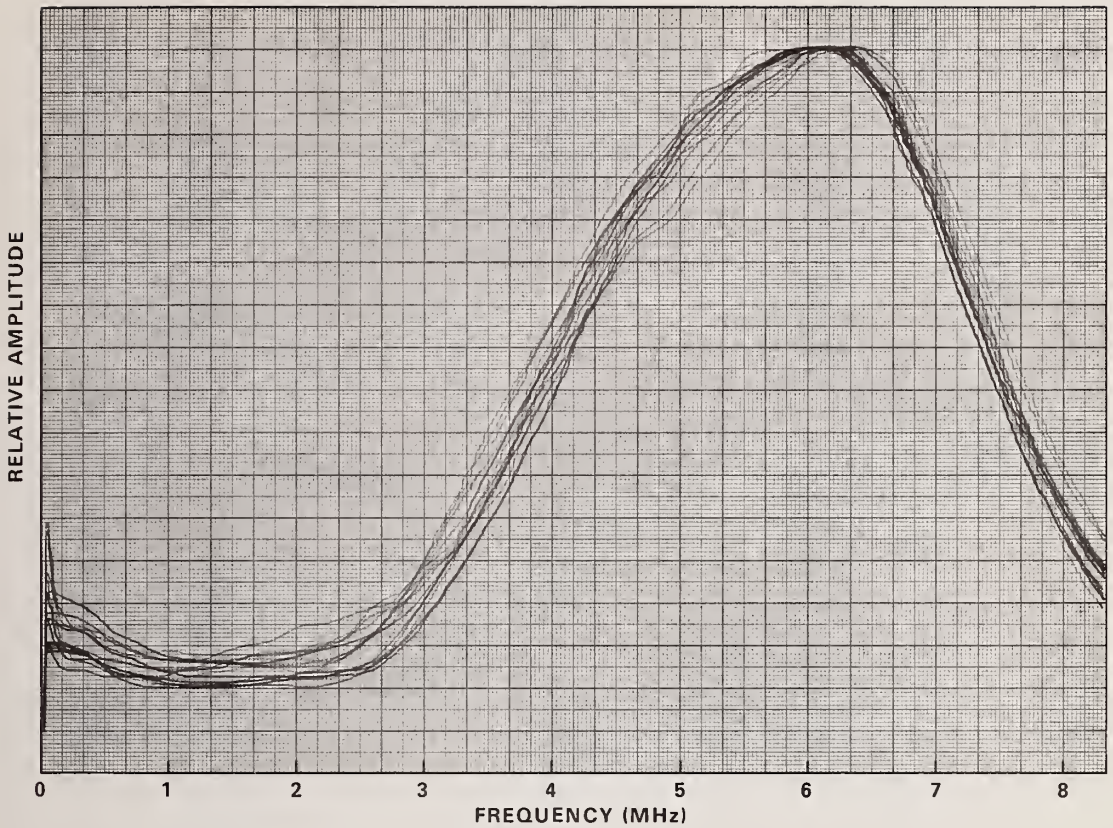

Figure 7. Effect of off-normal incidence of a focused beam for ten different angles. Target angulation, similar to that in figure 6, has relatively little effect on the Fourier transforms.

cut into several (6 to 10) blocks, 5 to 20mm in thickness and with parallel surfaces. These were placed on glass block sample holders immersed in a controlled temperature bath of normal saline. Attenuation curves were obtained at graded (15 to 30 minutes) intervals over periods of up to 30 hours. Necrotization of tissues was effected by immersion into normal saline at 55° C for 1 hour or by formalin-fixation. The results obtained showed remarkable consistency and were not affected by time, provided the temperatures were below 40° C. In fig. 9, note that although the attenuation coefficients for each of the normal tissues are different from each other at the lower frequencies, they increase markedly at higher frequencies. The slope of the frequency-dependent attenuation is also different for different tissues. The slopes are also markedly steeper for necrotized tissue as compared to the same normal tissue.

Comparable results have recently been obtained in measurements of the absorption coefficients by the thermo-electric method. As discussed below, heat-necrotization or formalin-fixation of tissues does not lead to an increase in the amount of energy scattered internally. The increased attenuation in necrotized tissues thus appears to be primarily due to an increase in absorption.

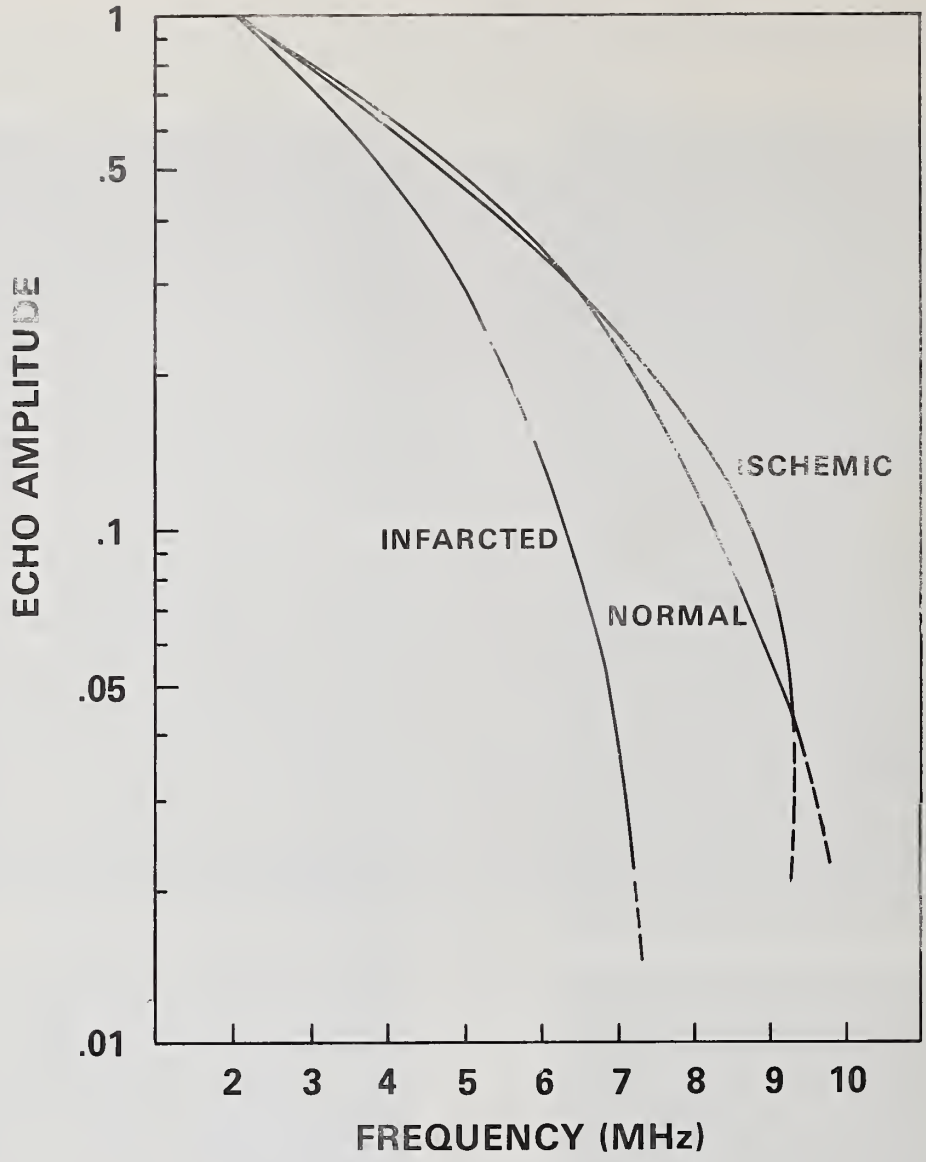

Figure 8. Typical results showing the frequency-dependence of the amplitude of echoes that have made two passes through normal, ischemic and infarcted muscle of equal thickness. Infarction was produced by vascular occlusion. The curves are obtained by dividing the observed spectra (such as those in figures 3 and 4) by the calibration spectrum (as in figure 2b).

These studies are being extended to tissues *in vivo*, in animals with induced pathology. Hardwired, stand-alone instrumentation for the detection of the differences in slopes of frequency-dependent attenuation in relatively stationary targets is also under development. Measurements on dynamically-moving structures, *e.g.*, the heart, require the use of a computer. The design of such a computer-based system has been described previously [13].

4. Acoustical Scattering

Current ultrasonic techniques of tissue visualization are based on specular reflection of ultrasound from tissue interfaces. At frequencies of 5 MHz and above, the wavelength of ultrasound in the tissue is of the order of the tissue surface undulations. Hence, a significant amount of ultrasonic energy may undergo Rayleigh scattering. Detection of such

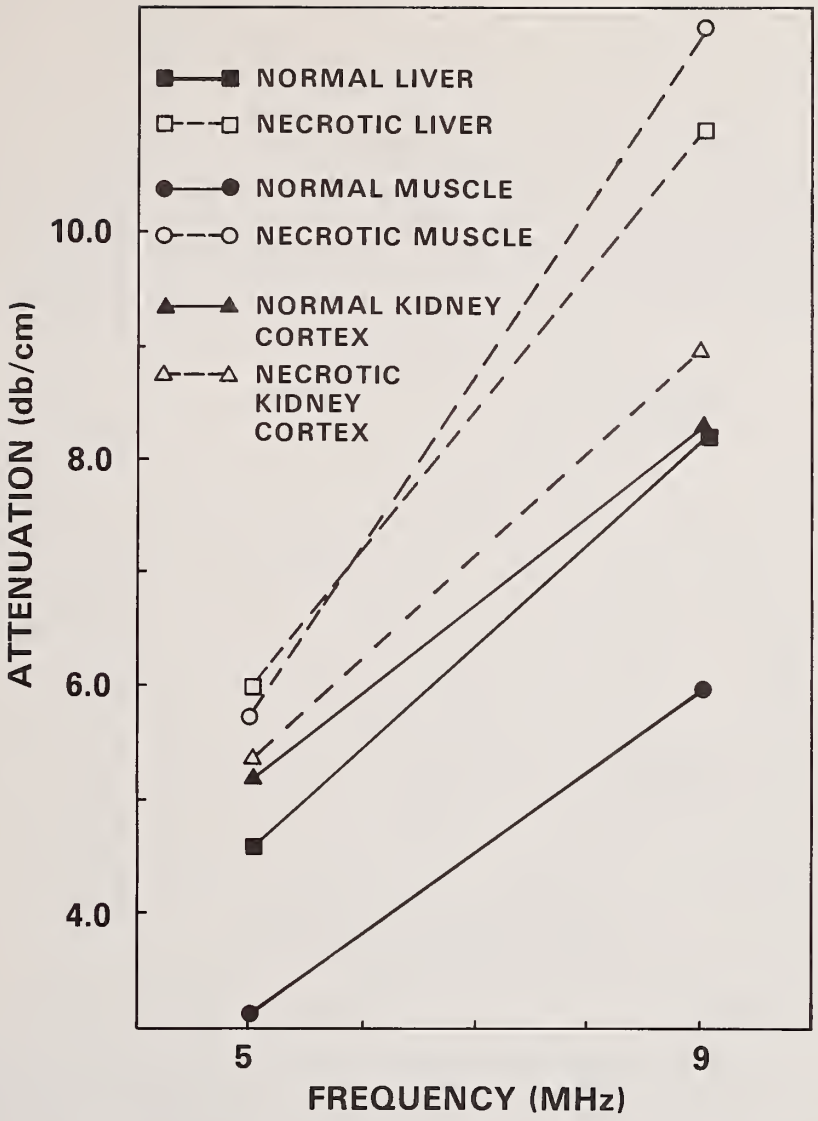

Figure 9. Frequency-dependent attenuation in normal and necrotized mammalian liver, muscle, and kidney. Each line represents the results obtained in 750 or more measurements made in 15-20 specimens in each type of tissue. The data were obtained using the computerized acquisition and processing system described in the text. The variance in the results was small and is omitted for clarity.

scattered radiation and knowledge of its functional dependence may yield information on tissue interface or organ surface characteristics that is not currently obtained from pulse-echo techniques. Similarly, internal inhomogeneity in an organ, due to its microstructural organization, normal or pathological, may lead to internal scattering. Both of these phenomena have been studied in this laboratory over several years.

4.1 • Surface Scattering

A theoretical model of the ultrasonic surface scattering was developed based on a statistical formulation of the rough surface as a function of the surface undulation parameters [14, 15]. The functional dependence of ultrasonic scattering intensity from rough surfaces on frequency, scattering angle, and surface root-mean-square roughness was

studied semi-empirically. The validity of the theoretical model was verified by experimental studies of ultrasonic scattering from aluminum surfaces of known roughness parameters (figs. 10, 11). Experiments were then conducted on fresh, isolated muscles (gastrocnemius, rectus abdominis) and liver of the frog. The results showed a characteristic angular dependence and a distinct increase in scattered intensity with frequency as predicted by the model and could be correlated with the differences in the surface texture of different muscles (figs. 12, 13) and liver (figs. 14, 15a). In contrast, the surface scattering from a specimen of a liver with red-leg disease, which leads to pitting of its surface, showed diffuse scattering (fig. 15b), varying randomly, irrespective of the scattering angle. Microscopically, liver with red-leg disease displays the presence of numerous irregularly-dispersed micro-emboli on the surface as well as in the parenchyma (fig. 16). This randomly-distributed pitting is believed to lead to diffuse scattering. Details have been presented elsewhere [14, 15]. Mountford and Wells [16] also found it possible to differentiate between normal and cirrhotic liver by processing A-scope echoes.

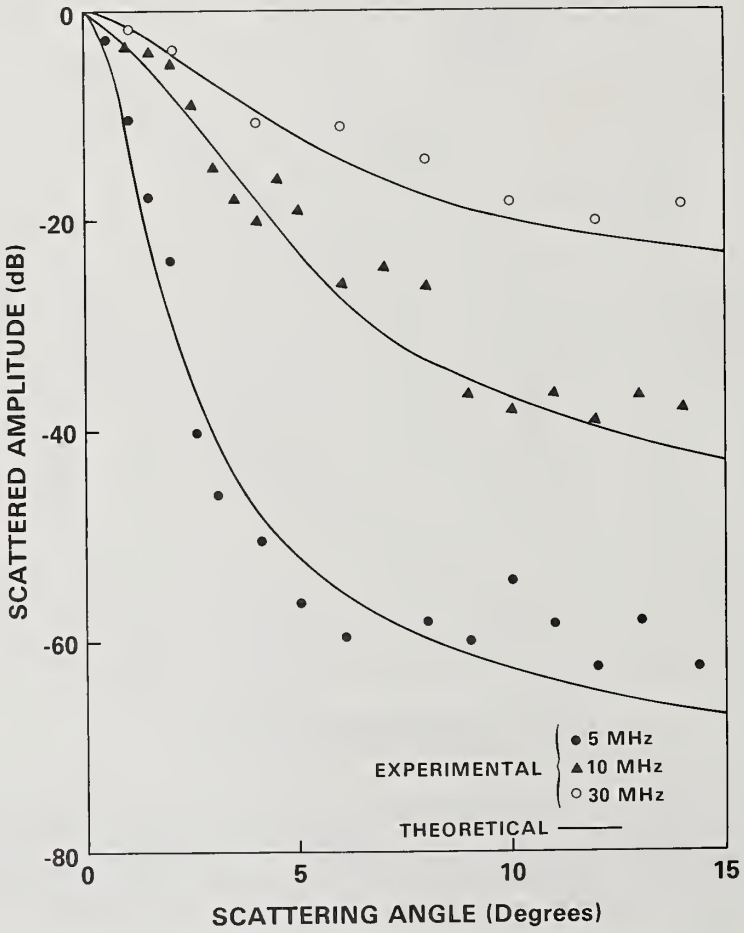

Figure 10. Ultrasound scattering from a rough (0.0025 in rms) aluminum surface.

4.2 Internal Scattering

4.2.1 Introduction and Theory

In contrast to the irregular spacing of the micro-emboli in the frog liver with red-leg disease, the microscopic structures of normal as well as many pathological tissues show characteristic patterns of organization. From an acoustic point of view, these patterns may be regarded as exhibiting characteristic spacings of acoustically-different targets, which will behave as diffuse scatterers due to their small size relative to the ultrasonic wavelength.

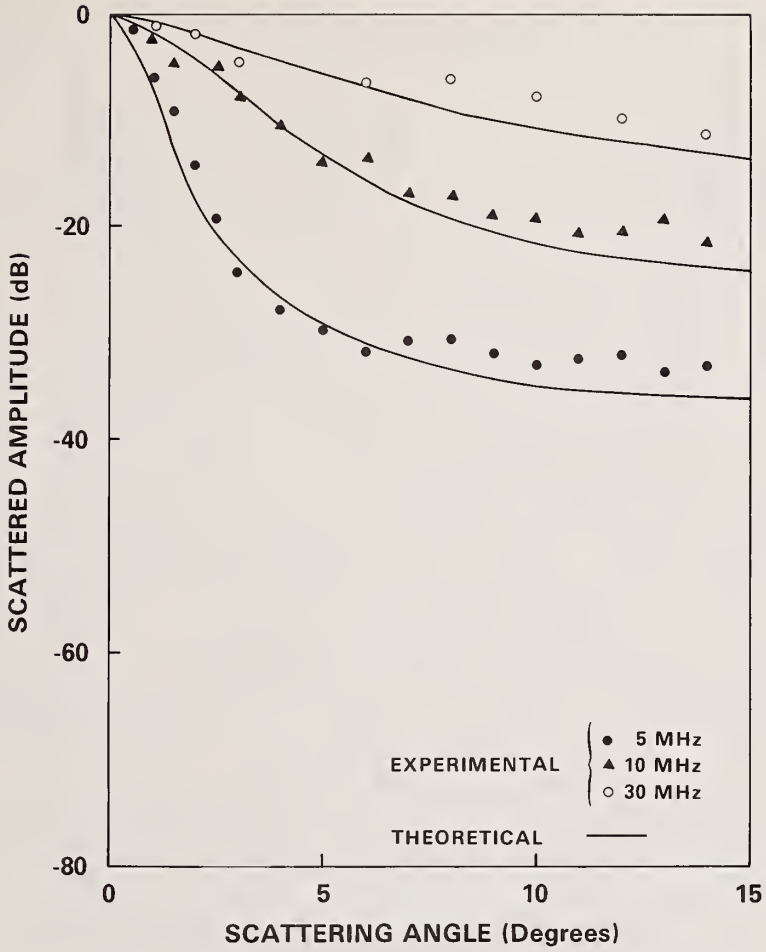

Figure 11. Ultrasound scattering from a rough (0.005 in rms) aluminum surface.

Very little research has been aimed at characterization of tissue on the basis of its scattering interactions with ultrasound. Scattering has been considered a nuisance which blurs the images obtained in echo techniques, especially B-scan, but not as a useful diagnostic parameter.

If changes in scattering characteristics could be correlated with specific tissue structure and pathologies, this property could become a valuable diagnostic aid. Preliminary to *in vivo* studies, tissue samples were examined *in vitro* to determine the feasibility of detecting tissue structure differences on the basis of the internal scattering properties of the various tissue samples investigated. The samples chosen exhibited great structural differences which could cause a variation of scattering patterns, each characteristic for the tissue under study. If these rather gross differences could be detected, it may prove possible to investigate the smaller differences in scattering which occur in certain pathological states, and correlate these with the specific disease processes.

The prediction that differences in scattering will be apparent for different tissues, both normal and pathological, is based upon a physical theory of scattering and diffraction of waves which has been used to great advantage in x-ray crystallography. Wavefronts impinging upon a regular array of small reflecting surfaces produce interference patterns which depend quite specifically upon the physical parameters, such as the spacing of the array. Beam components are selectively reinforced or cancelled according to the relative spacing and orientation of scatterers in the beam.

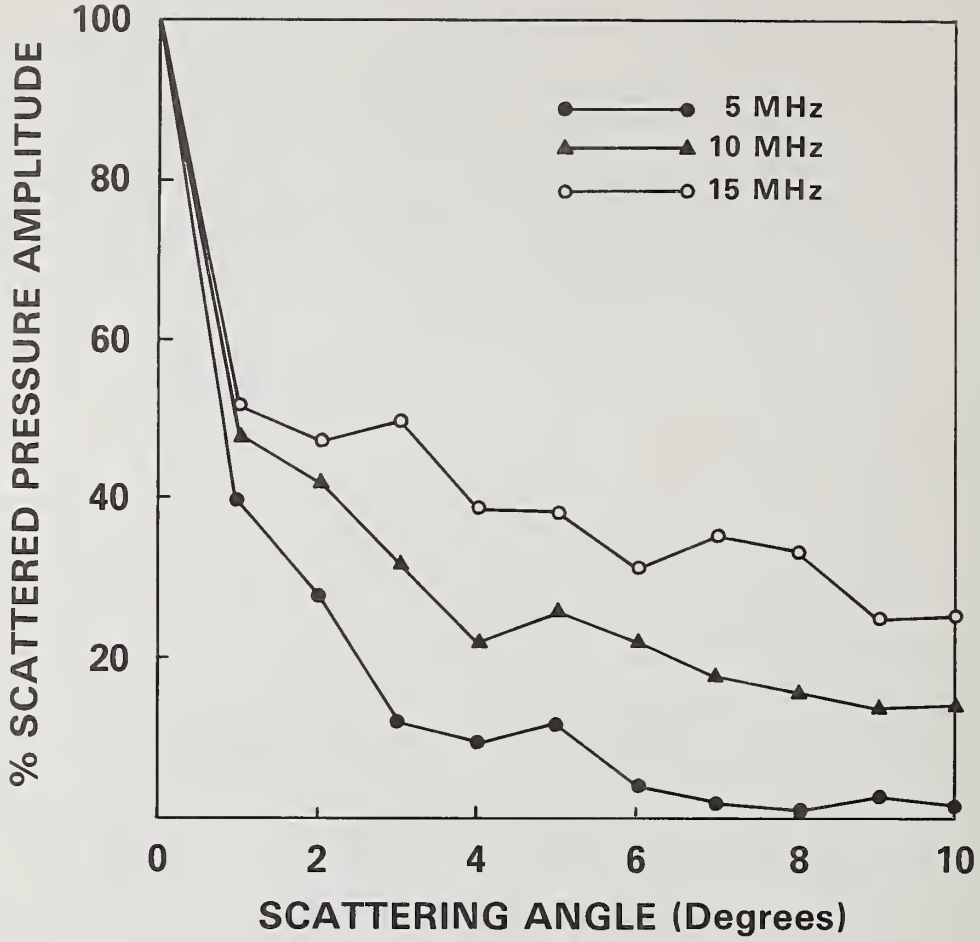

Figure 12. Ultrasound scattering from surface of gastrocnemius muscle of frog.

Ultrasound may be used to determine the acoustical structure of tissue, on a scale corresponding to the wavelengths employed, in a fashion completely analogous to x-ray crystallography. The underlying concept is the relation between the spacing of tissue elements, the ultrasonic wavelength, and the scattered signal. There is a selective reinforcement of certain frequencies, such that the Bragg scattering condition,

$$n\lambda = 2d \sin \theta,$$

where λ = ultrasonic wavelength
n = integer
d = distance between adjacent scatters
θ = angle from the horizontal to the scattered signal,

is met. Integral multiples of the wavelength are required for constructive interference to occur.

The formula is derived by considering path length differences such that the scattered waves are exactly in phase, yielding maximum constructive interference. This relationship is illustrated in figure 17.

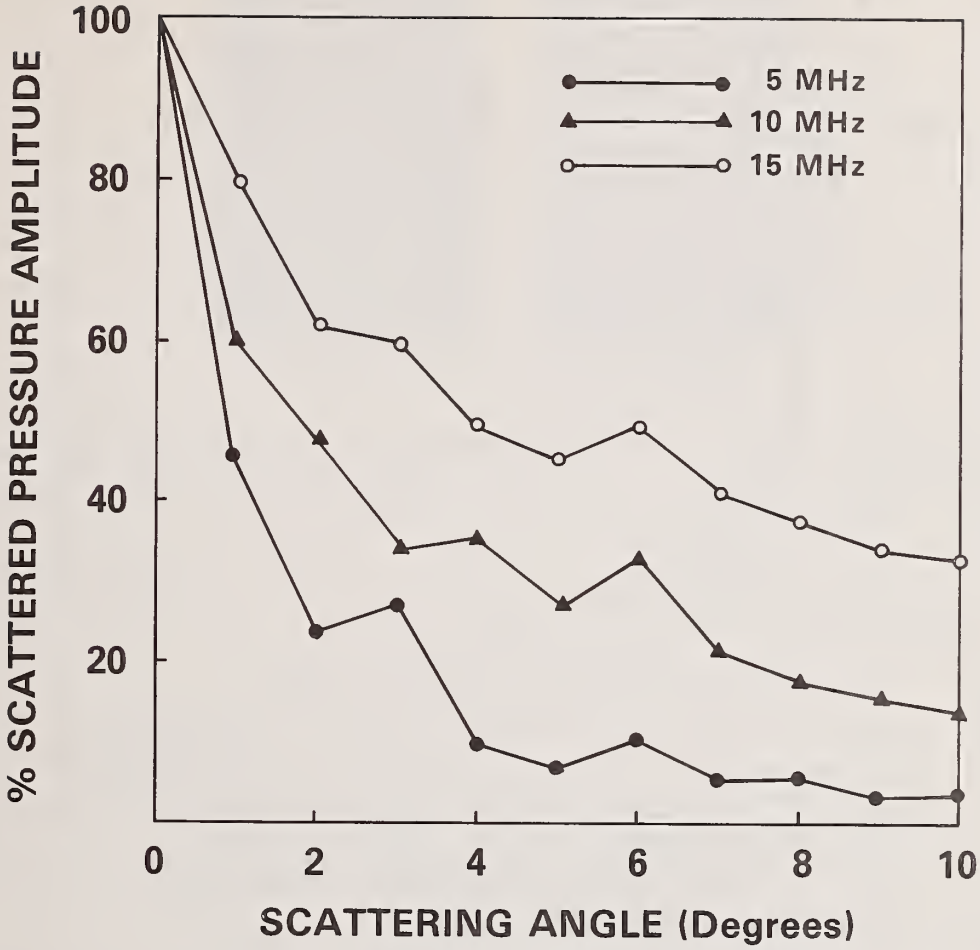

Figure 13. Ultrasound scattering from surface of rectus-abdominis muscle of frog.

The tissue may be characterized by either fixing the frequency (and hence λ), and then varying the angle, or by fixing the angle Θ and sweeping the frequency so that differences in path length vary over a number of wavelengths. Theoretically, either technique should yield a succession of signal amplitude peaks whose spacing is indicative of the target's internal structure.

If one considers a perfect lattice in which the acoustical variations are a series of uniformly-spaced impedance discontinuities, the scattered signal will exhibit a periodic series of maxima as either the incident angle or the frequency is changed; each maxima corresponds to a path length difference of an integral number of wavelengths. With this single uniform reflector spacing, a sinusoidal variation of signal amplitude occurs. The Fourier transform of this yields a single peak, whose location is a measure of reflector spacing, and whose amplitude is a measure of the scatter number n.

In biological tissue, changes in acoustic impedance are expected to occur randomly. In any particular tissue, the spacings between scatterers may vary widely, but still fall within certain limits that can be statistically specified by the scattering profile shape. In disease processes, when the structure is altered, the statistical values of d obtained from the scattering profile should also be altered correspondingly.

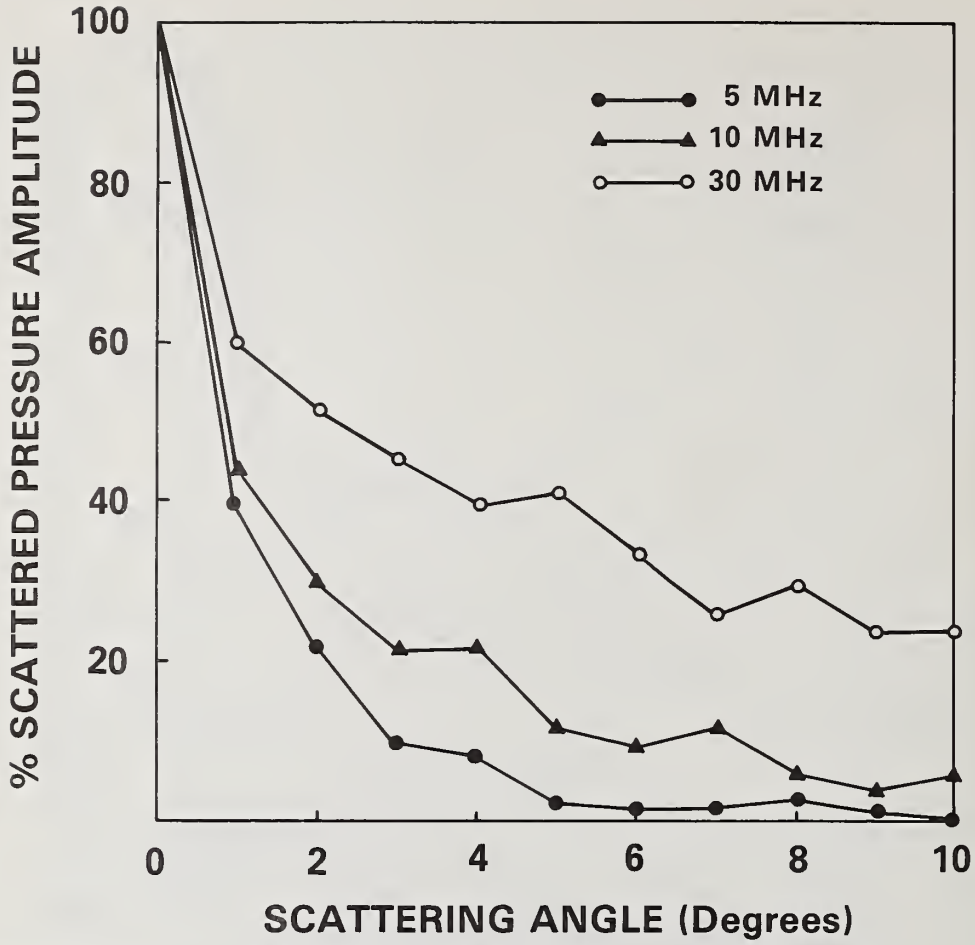

Figure 14. Ultrasound scattering from frog liver.

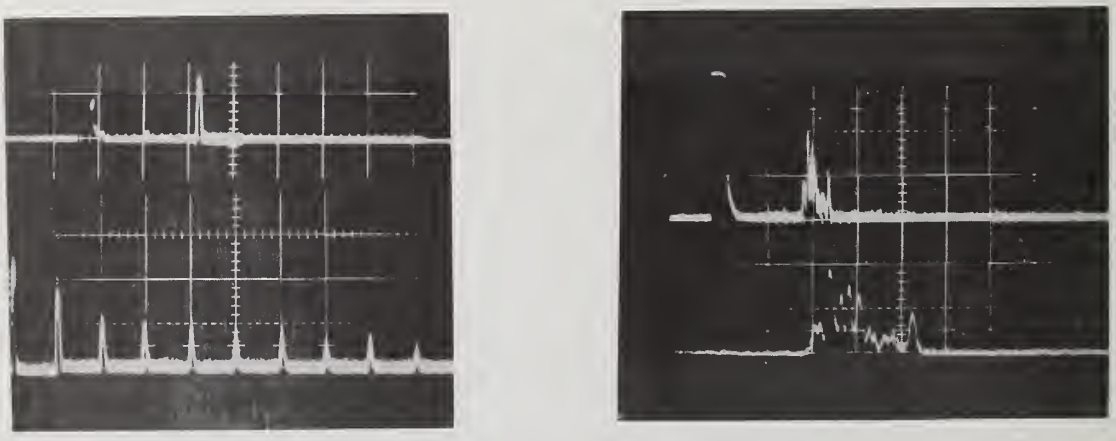

(a) (b)

Figure 15. Surface scattering from liver at 15 MHz (a) Normal tissue. Vertical scale, 5 v/div; horizontal scale-top, 20 μs/div, bottom, 1°/div. (b) Diseased tissue. Vertical scale, 5 v/div; horizontal scale-top, 20 μs/div, bottom, 5 μs/div.

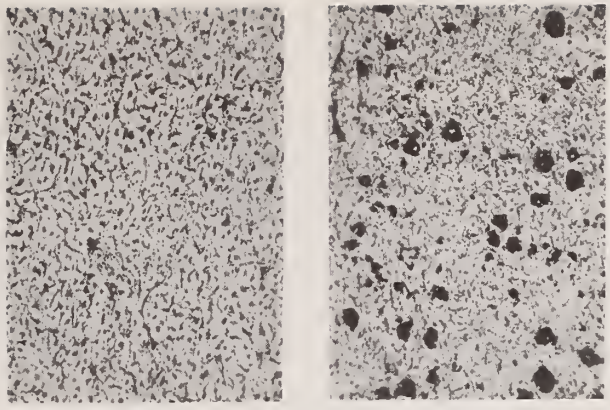

Normal Red-leg disease

Figure 16. Photomicrographs of specimen of frog liver, hematoxylin and eosin-stained. Magnification is 150X.

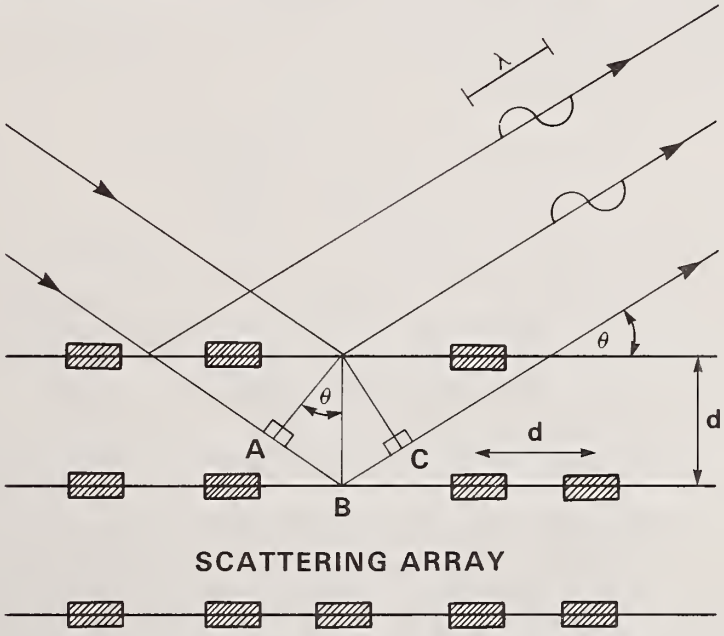

$$\text{ABC} = \text{PATH LENGTH DIFFERENCE} = d\sin\theta + d\sin\theta$$

$$\text{FOR CONSTRUCTIVE INTERFERENCE:}$$

$$2d\sin\theta = n\lambda$$

Figure 17. Geometry for Bragg diffraction.

The effects of randomness introduced into a regular pattern are well described in x-ray crystallography, which operates on the same Bragg diffraction principle. An "imperfect" lattice structure produces diffracted radiation which is not well-localized. There are strong peaks corresponding to the average ideal lattice, but in other directions the wavelets reflected by the individual scatters do not cancel perfectly by interference. The peaks are broadened, and weaker diffuse scattering is seen in many directions not specified by the Bragg formula. Thus, there is a corresponding decrease in the intensity of the

selective peaks specified by the Bragg law. This is, in general, the type of scattering expected from structures such as seen in highly-organized tissues and organs, where there exists a structural order which is marked by small perturbations, and statistical fluctuations of inter-scatterer distance occur around a certain mean value.

From the earlier studies in this laboratory cited above [14, 15], as well as from the work of Chivers, Hill and Nicholas [17-20] and of Waag, Gramiak and Lerner [21], it appears likely that scattering and diffraction-based probing techniques can be used to characterize the acoustical variations in tissue for medical diagnosis. It is not yet possible to know how much information about a tissue sample may be obtained in this manner. The differences in the densities of many tissues constituents, *e.g.*, collagen, elastogen, etc., are very small, although the differences in their bulk moduli are believed to be large [22]. Whether these differences yield sufficiently different ultrasonic signals at the wavelengths involved to be of diagnostic value remains yet to be determined. Therefore, the dependence of the scattered signal on angle was studied at several discrete frequencies in phantoms and tissues of known structure.

4.2.2 Experimental Apparatus and Procedures

The specimen tank is shown in Figure 18. A cylindrical anechoic tank, with two rotating arms for the transmitting and receiving transducers, respectively, was used. The tank and each of the arms could be rotated independently around the vertical axis to permit angle-sweep scanning as well as specimen rotation. The bottom and sides of the tank were lined with soft polyethylene. The specimens were placed in the center and coupled to the transducers through degassed saline (or water) and a thin film of polyethylene.

The tissue specimens were carefully-cored cylindrical plugs 3 cm in diameter, which permitted adequate separation of surface echoes from internally-scattered signals without excessive attenuation of the latter in the sample itself.

Matched pairs of unfocused transducers, 1 to 4 MHz in frequency, were used. The transmitting transducers were driven in a c.w. burst mode of 20 μms duration over the frequencies used. This burst width was considered to be sufficiently long for the continuous wave approximation to be valid, yet short enough for the signal to remain distinct from any reflections from the walls of the specimen tank. The experiments were conducted with specimens situated in the near field of the transducers since it was not feasible to fabricate a tank large enough to enable the measurement to be made in the far field.

The signals from the receiving transducer were amplified in a tuned amplifier in order to maximize the signal-to-noise ratio, then rectified and time-gated to eliminate the echoes from the front surfaces of the specimen and the tank. The gated, internally-scattered signals were integrated in an operational amplifier and displayed on an oscilloscope (fig. 19). The magnitude of the integrated signal which, for a constant gating time, was proportional to the average amplitude of the internal scattering signal, was recorded as a function of the transducer angle. This averaging process, as well as the averaging due to the finite ultrasonic beamwidth, served to compensate for the intensity variations in the near field as well as for any local inhomogeneity in the tissue specimens.

4.2.3 Angle-Scanning Procedure

Two different scanning procedures were used in the course of this experiment. The first method tried was an arc scan and involved holding one transducer fixed and moving the other in a large arc around the tank. Many problems were encountered in this approach, the most important of which was the detection of the unmodified transmitting beam by the receiving transducer, thus masking out the much smaller scattered signal. This procedure failed to give very reproducible results, and the profile of amplitude vs. angle was very random and erratic, with very large amplitude fluctuations occurring for small angular changes.

If one considers the physics of Bragg scattering, the reason for the failure of arc scanning becomes apparent. As shown in figure 20a, there are various planes of scattering elements which can serve as the basic "reflecting surface." Each of these has a different value of d (distance between adjacent array elements), and therefore a different requirement for fulfillment of the Bragg condition.

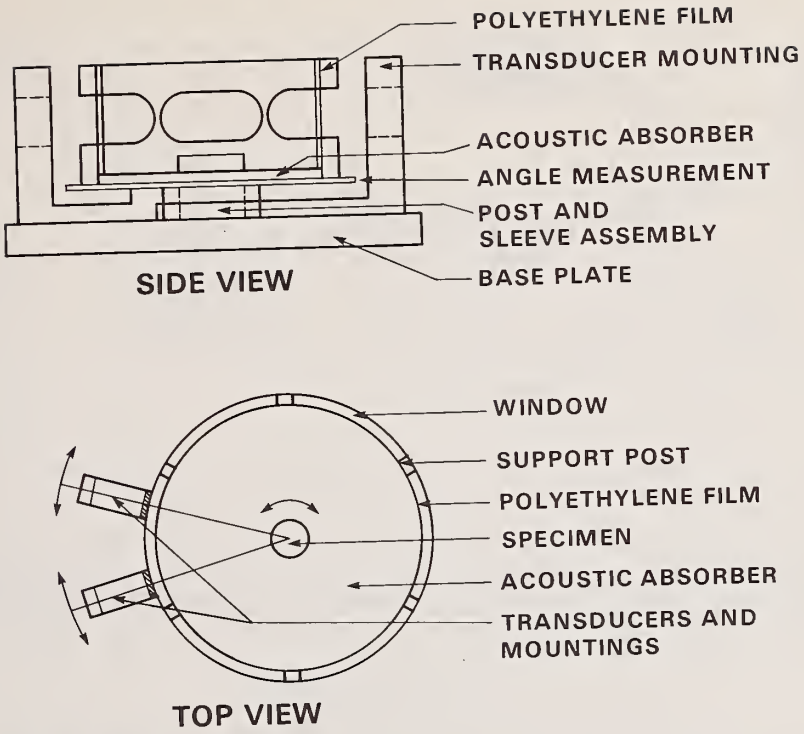

Figure 18. Specimen tank design (side and top views)

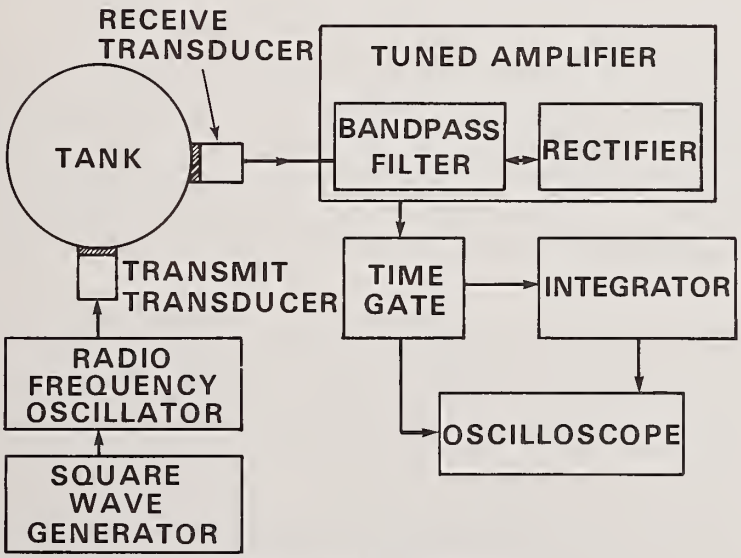

Figure 19. Schematic of experimental apparatus.

The second method of conducting the angle-sweep scan involved moving both the transmitting and receiving transducers, each by an equal amount. Thus, the line of scatterers from which the reflection and interference phenomena occur will be the same for the entire scan, and there should be some values of θ for which the Bragg condition is met. This "double-angle scan" method is illustrated in figure 20b.

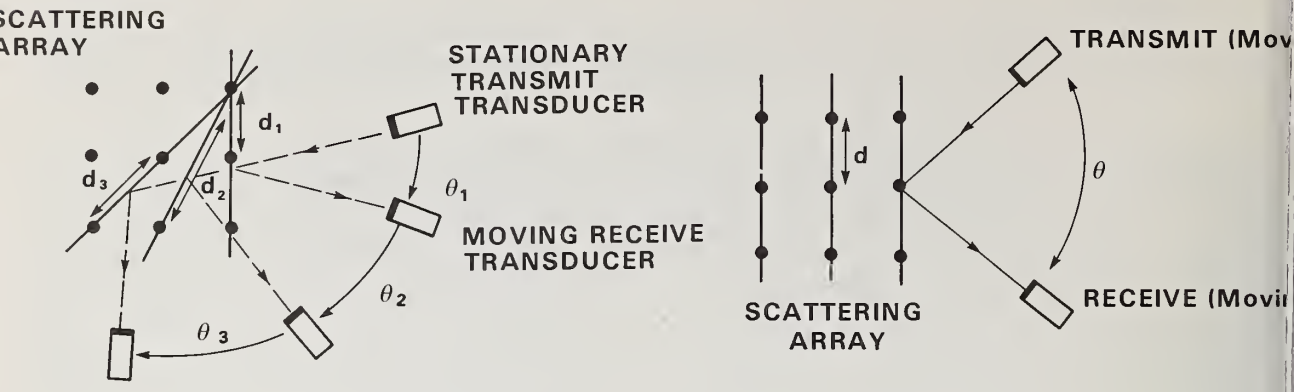

Figure 20. (a) Arc scanning and the Bragg formula. (b) Double-angle scanning method.

Several double-angle scans were made to characterize various specimens, and the results were plotted as amplitude vs. total transducer angle (2Θ in the Bragg Law). These scans were repeated at various frequencies to assess the effect of wavelength upon the internal-scattering profile.

4.2.4 Results

4.2.4.1 Results Obtained from Phantom Targets of Known Geometry

To test the feasibility of making these internal-scattering measurements and the correlation of the results with Bragg diffraction theory, phantom scattering targets of precisely-known geometry were used. A target was made of steel pins (diameter 0.026 in) spaced in a square grid with a distance of 0.10 inches between adjacent pins. If an ultrasonic frequency of 2.25 MHz is used, the Bragg formula predicts maxima at approximately 15°, 30°, 45°, 62°, 81°, 102° and 131° total transducer angle (2Θ). These predicitons correlate very well with the experimental result obtained by a double-angle scan, as shown in figure 21. The values obtained were highly reproducible, with most of the fluctuations being accountable on the basis of uncertainty in positioning the two transducers. The values plotted are the mean of 5 separate runs, and the relative range of values obtained was approximately 7% of the total signal amplitude. The scattered signals obtained were very strong due to the large acoustic impedance mismatch between the steel pins and the water surrounding them.

In order to better simulate the gross acoustic properties of biological tissues, a second phantom target was made of soft polyethylene with holes drilled through it in a regular array. The water-filled holes were 0.026 inches in diameter, and the spacing between them was 0.05 inches. According to Bragg's law, the angular locations of expected maxima are approximately 35° and 70° of total transducer angle, if these measurments are taken at a frequency of 2.25 MHz. The experimental results correlated very well with theory, and were very reproducible, as seen in figure 22. The points plotted are the mean values of 5 experimental runs, and the average range of values was approximately 8% of the total signal amplitude. The magnitude of the scattered signal was significantly reduced from the values obtained with the pin-scatterer phantom, due to the fairly small acoustic impedance difference at the water/polyethylene interface, as well as to the increased absorption of ultrasonic energy by the polyethylene. In both of these respects, the polyethylene phantom appeared to be a good model of an idealized tissue sample. As a control, a cylindrical plug of soft polyethylene without any holes drilled into it was used as the target. The oscilloscope recorded an echo from the front and back surfaces, but no evidence of any scattering signal from the interior was found, even at very high gain. This indicated that inhomogeneity is indeed the source of the internally-scattered echoes, and the phenomenon which we wish to investigate was directly responsible for the signals which we were measuring.

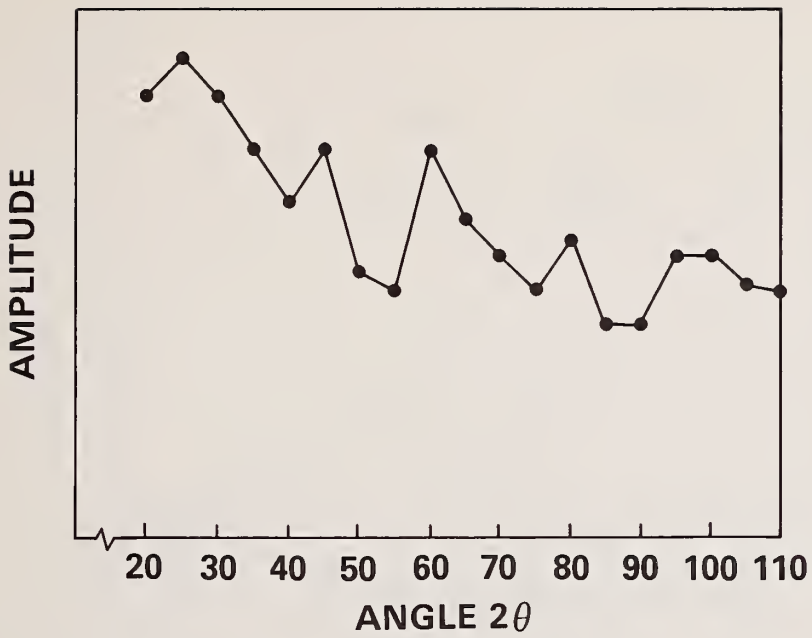

Figure 21. Scattering profile of pin-scatterer phantom target. Average of 5 runs. Frequency is 2.25 MHz.

4.2.4.2 Results Obtained from Various Biological Tissue Samples

Double-angle scans were performed with many different samples of mammalian tissue from various organs and from various species. Samples of calf liver, pig liver, calf skeletal muscle, and calf cardiac muscle were investigated to determine their characteristic internal-scattering profiles. The most striking result was the periodicity of maxima and minima which was evident in the angular dependence of the amplitudes of the scattered signals. The precise values of the signal strength appear not to be important, and were noted to change as the tissue was rotated. However, the average periodicity, the angular distance by which maxima are separated, remained constant for a given tissue at a given incident frequency. For example, at 2.25 MHz, calf liver produced a scattering profile with an average angular separation of approximately 20° of arc (figs. 23, 24). There was a fairly large spread of values for the average periodicity of the scatter profiles, due largely to biological variations from one tissue sample to another. However, when statistical analysis was done on the data (student's t-test [23], calculated at the 5% significance level), the range of periodicity values evident in calf liver could be demonstrated to be a separate population from the values obtained from other tissue samples.

The important parameter to consider in analyzing the scattering profiles appears to be the average periodicity, and not the relative heights of the maxima. This is evident in figures 23 and 24, which show two characteristic scans obtained from calf liver tissue. Although the profiles may appear to be different due to the change in sample orientation, the average angular separation of maxima remains roughly constant.

These double-angle scans were performed on many other different tissue samples, each yielding a characteristic scattering profile with a certain average intermaximal separation at the operating frequency of 2.25 MHz. Although these average periodicities were statistically recognizable as several significantly-different populations, it was often difficult to tell by eye which type of tissue sample was under study, given the resulting scattering profile. A more reliable method of discriminating tissue type based upon internal-scattering properties utilized the frequency dependence of the angular profile patterns.

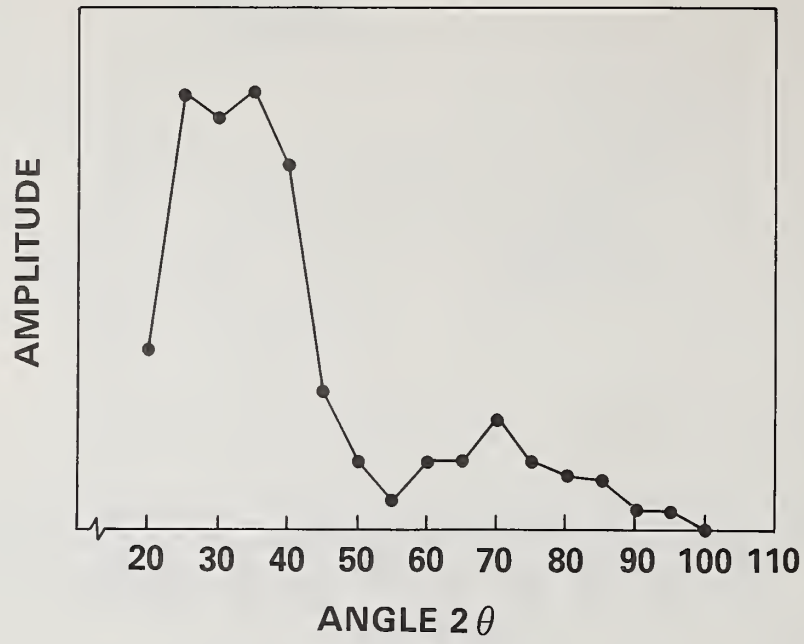

Figure 22. Scattering profile of polyethylene phantom target. Average of 5 runs. Frequency is 2.25 MHz.

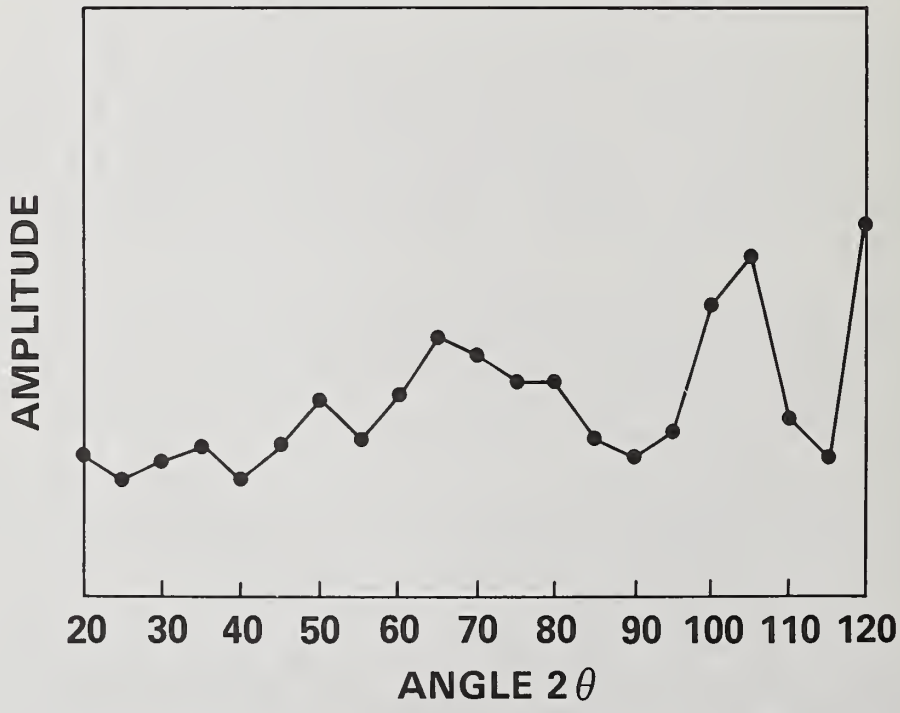

Figure 23. Double-angle scan at 2.25 MHz of fresh calf liver in degassed saline. (Trial 1) Average of 5 runs. Average periodicity equals 20° of arc.

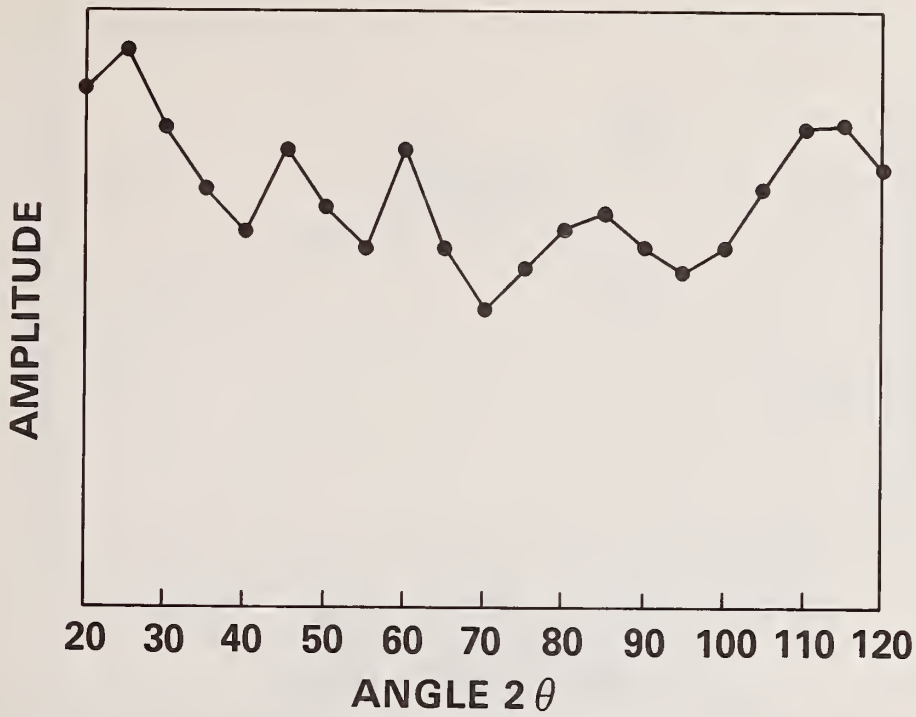

Figure 24. Double-angle scan at 2.25 MHz of fresh calf liver in degassed saline. (Trial 2) Average of 5 runs, average periodicity equals 21.875° of arc.

4.2.4.3 Frequency-Dependent Characterization of Tissue Type

Double-angle scans were performed with various tissue samples as scattering targets, and after each scattering profile was determined and its average periodicity calculated, the ultrasonic frequency was changed and the test repeated. Thus, we were able to correlate ultrasonic frequency with average peak separation. Orientation of the tissue appeared to affect the results very little, except in cases of marked tissue anisotropy. Again, the scatter of the data was larger than can be expected purely on the basis of the instrumentation and experimental design; the large variations appeared to be due entirely to natural variations within tissue samples from different regions of one organ, or from different animals.

The most evident trend exhibited by the frequency plots is the linearity of the relationship between angle and frequency. This is seen in figure 25, which shows the frequency dependence of fresh calf liver in degassed saline. The best linear fit to the experimental data was determined by a least-squares regression analysis. The closeness of fit can also be calculated by finding the coefficient of determination which is a direct measure of accuracy of fit [24].

Almost all of the frequency-dependent plots which were made correlated very well with the least-squares line, with coefficients of determination (r^2) ranging in value from 0.80 to 0.93, all indicating excellent agreement of data and empirical line fit. There were some exceptions, however; certain frequency plots correlated rather poorly with a linear fit, with values in the vicinity of 0.50.

Frequency plots of pig liver and calf heart muscle are shown in figures 26 and 27, respectively. The raw data points as well as the best line fits are shown. The frequency dependencies of the tissues under study were quite characteristic. For example, calf liver and pig liver may be differentiated easily by comparison of both slope and axial intercept values, as can calf skeletal muscle and calf cardiac muscle. Thus, these two parameters may prove to be an accurate method of cataloguing tissue scattering properties.

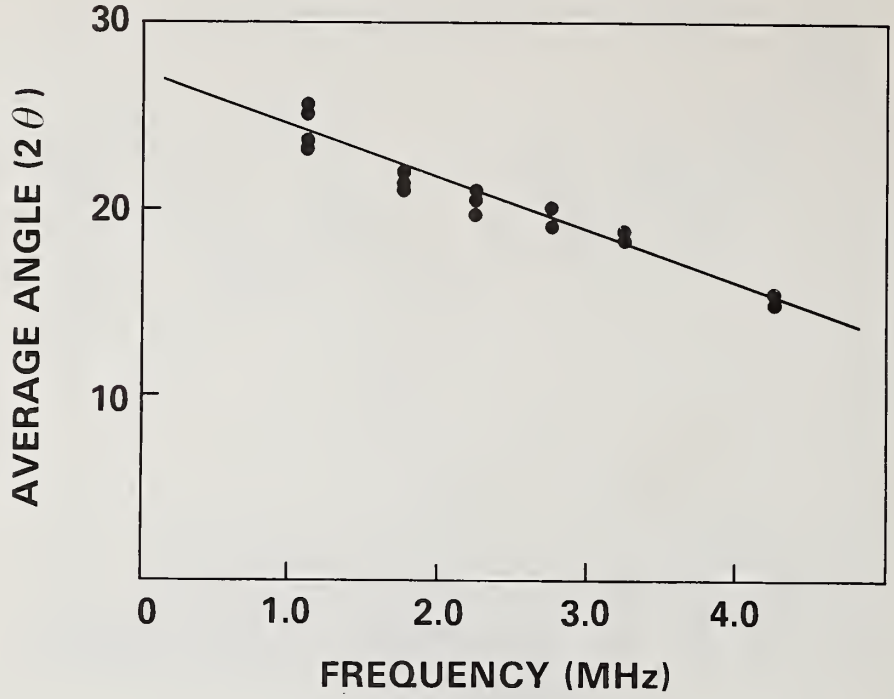

Figure 25. Frequency dependence of fresh calf liver in degassed saline.

4.2.4.4 Effect of Tissue State and Tissue Anisotropy

Calf liver tissue was used in a study of the effects of freezing and formalin-fixation upon the scattering profile and the frequency dependence of biological tissues. Calf liver that had been frozen and thawed and then examined in a series of double-angle scans at various ultrasonic frequencies is not significantly different in its internal scattering properties than the freshly-excised calf liver specimens. A trend may be seen toward a general lowering of the angular values obtained, but this difference is not statistically significant at the 5% level of the t-test. Since the formation of ice crystals can produce tissue structure changes, this may appear to be a surprising result; however, the only changes observed when a histological examination was made were the breakage of cell membranes and destruction on the scale of microns. The ultrasonic scattering phenomenon measured in this experiment does not approach this level of resolution. The ultrasonic wavelengths used were in the submillimeter to millimeter range, and could not detect the damage occuring on a cellular and subcellular level. However, as stated earlier, such damage does result in an increase in frequency-dependent acoustical attenuation (and absorption).

Similar results were obtained when formalin-fixed tissues were studied. Formalin-fixation was not expected to change the tissue structure, but it could change the tissue elasticity, and therefore the acoustic impedance. Scattered signal strength increased in the angle-scanning of formalin-fixed tissues, but the change in the frequency dependence remained insignificant. Figure 28 compares the results for fresh, frozen, and formalin-fixed calf liver samples.

Certain tissues exhibit structural anisotropy which was detectable by characterization of the scattering. Calf skeletal muscle displays different frequency-dependent behavior related to the direction at which the ultrasonic wavefront impinges upon the sample. If the cylindrical tissue plug was cut such that the muscle fiber bundles ran parallel to the cylinder height (cut "across" the grain), the resulting angular separation was higher than that of muscle cut longitudinally ("along" the grain). The differences are statistically significant and readily recognizable, as shown in figures 29 and 30. This structural anisotropy and the resulting dependence of scattering characteristics upon fiber orientation,

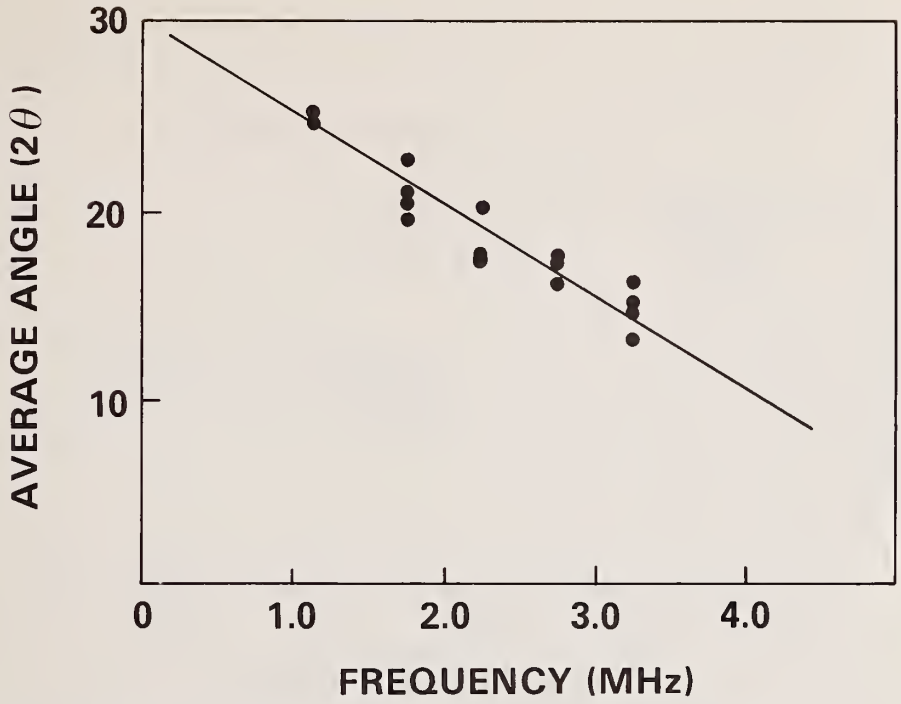

Figure 26. Frequency dependence of pig liver in degassed saline.

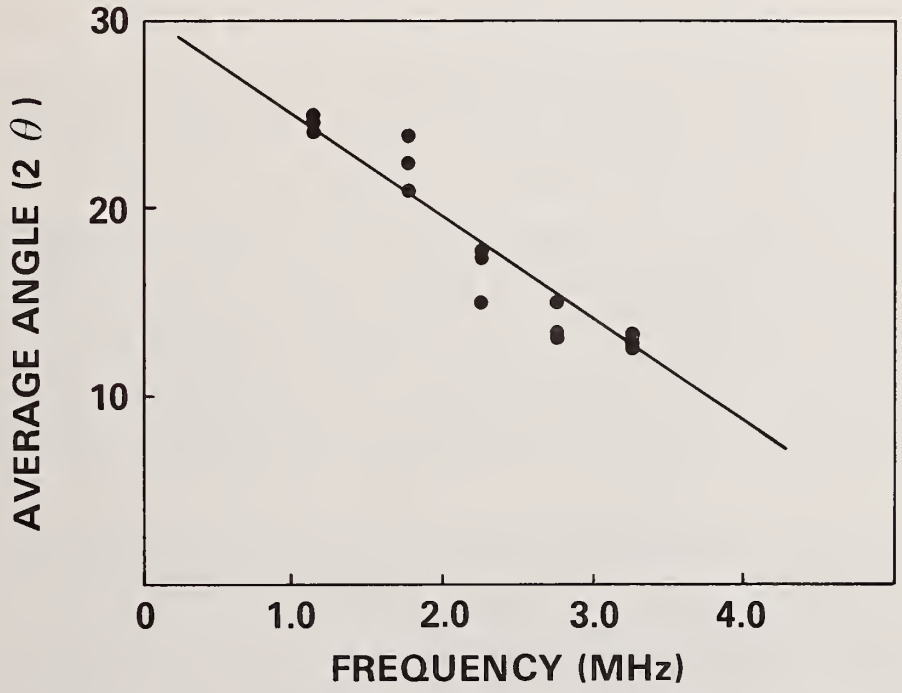

Figure 27. Frequency dependence of calf heart muscle in degassed saline.

were not seen in cardiac muscle samples, where no single predominant fiber orientation exists. Cutting heart muscle specimens at varying planes resulted in the same frequency dependence in all cases.

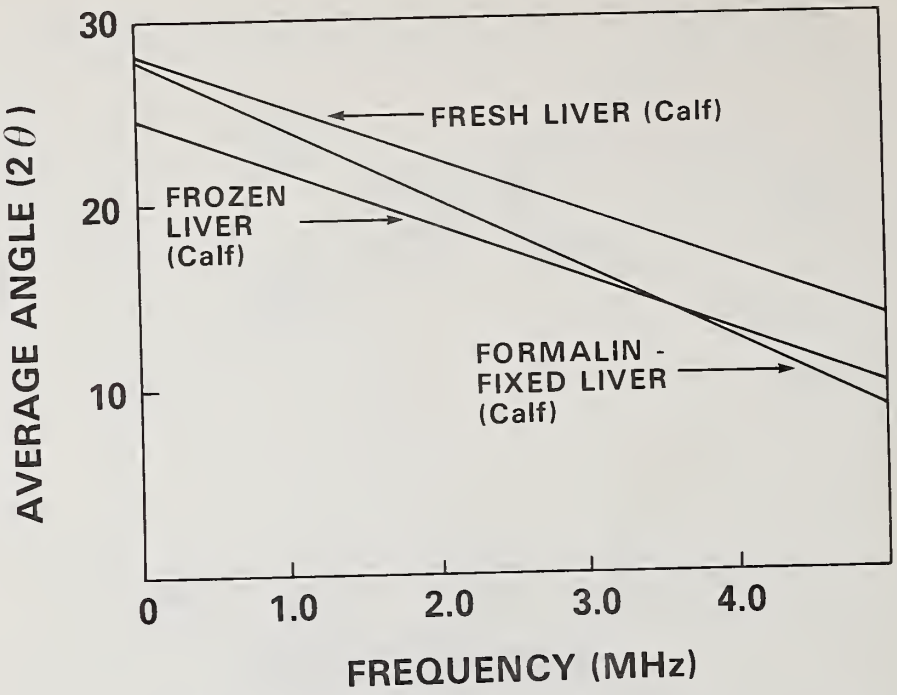

Figure 28. Frequency dependence comparison for fresh, frozen, and formalin-fixed calf liver.

4.2.5 Statistical Comparison of Experimental Data and Bragg Diffraction Theory

The experimentally-determined frequency dependence, as previously stated, appears to be linear. However, if one plots the expected dependence, predicted by Bragg's law, the result is a hyperbolic curve. Some tissue samples appear to follow this dependence more closely than others, with calf heart muscle providing the closest correlation between experiment and theory, and calf liver being the most divergent.

To facilitate the analysis of experimental data and its correlation to Bragg theory, a second type of plot is more useful: the sine of the average periodicity angle vs. ultrasonic wavelength. On such a plot, Bragg diffraction theory predicts a straight line passing through the origin. The fit obtained from a least-squares regression analysis is not very good, with coefficient of determination values (r^2) being less than 0.65 for all tissue samples under study. Thus, the phenomenon is not what might be expected from simple Bragg diffraction theory, yet it shows an apparent periodicity which varies with frequency in a very linear manner. Although one cannot directly attribute the scattering to a regular array of small reflectors, the tissues under study exhibited strong differences in the frequency-dependent scattering behavior which may well be of future diagnostic use.

By examining the best theoretical line fit to the experimental data, one can calculate the best value of d, the interscatterer array distance, by substitution back into the Bragg formula. One can also define limits for the possible values that d can assume so to encompass the existing experimental data. Such an analysis was done for all the tissues studied, and the ranges of d values obtained are shown in figures 31 through 35. The sine of the average angular separation is plotted vs. wavelength, and the best theoretical fit is demonstrated for calf liver, pig liver, calf cardiac muscle, and calf skeletal muscle.

The possible reasons for the discrepancy between Bragg theory and experimental observations are many. The most probable explanation is that biological tissue samples may not be ordered in an array which is regular enough at the submillimeter to millimeter scale. Observation of histological slides of the tissues investigated tends to confirm this. There exists a great deal of order on a smaller scale, and order is apparent even at the

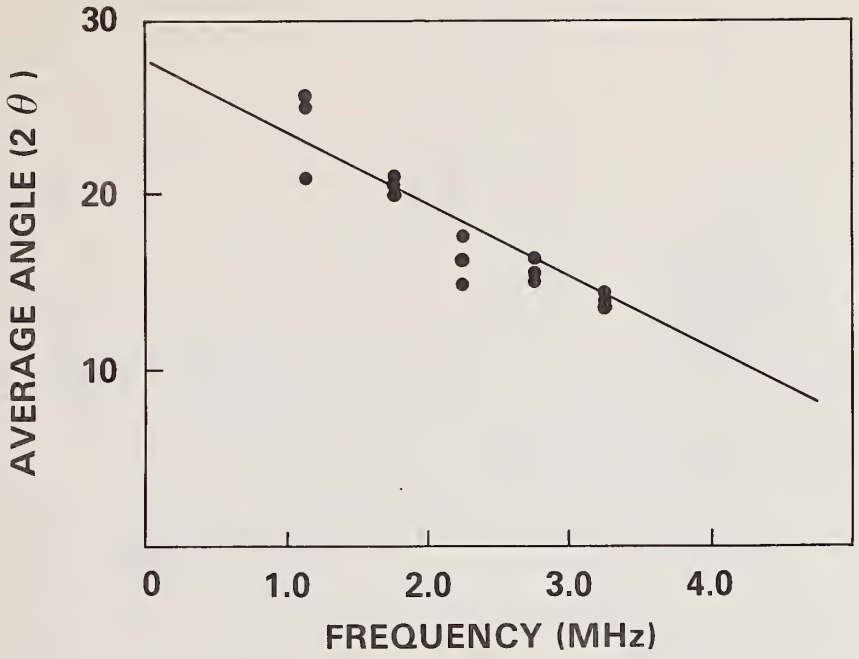

Figure 29. Frequency dependence of calf skeletal muscle cut longitudinally.

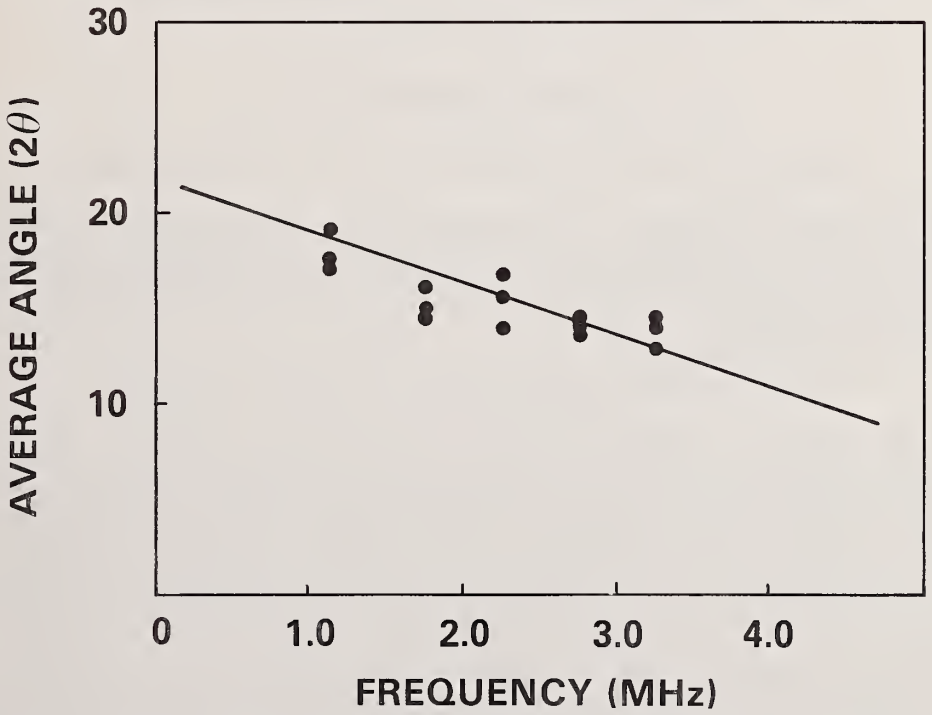

Figure 30. Frequency dependence of calf skeletal muscle cut across-grain.

scale which is resolved by the ultrasonic scattering measurement apparatus; however, the regularity with which the clusters of ordered elements are arranged is very slight. For example, muscle fibers are very well ordered, have the same orientation, and are grouped together into bundles surrounded by sheaths of connective tissue. These bundles of fibers

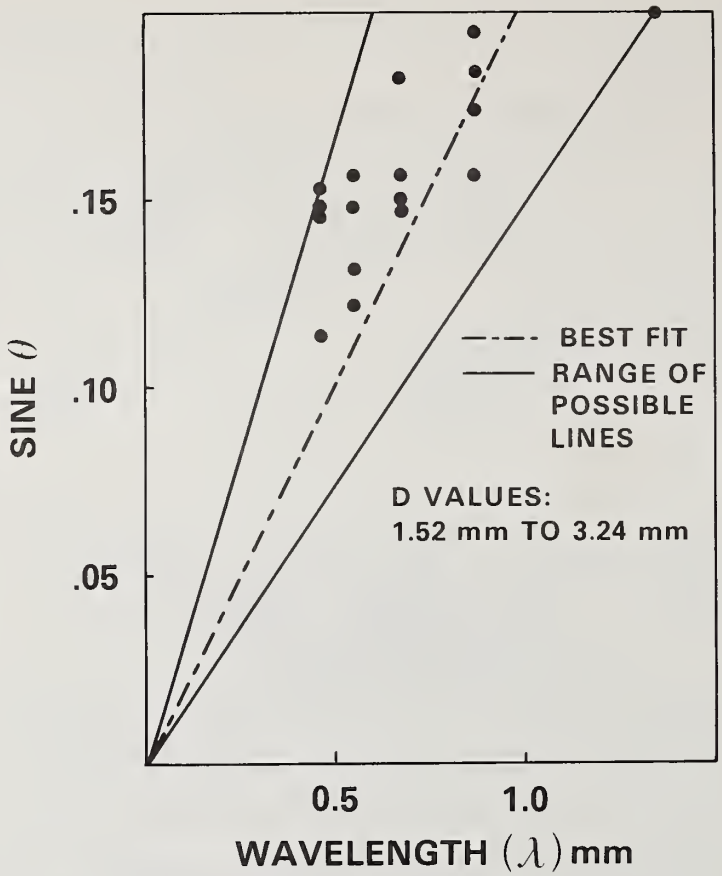

Figure 31. Comparison of theory and experimental results for calf liver.

are not very consistent in diameter, and the ordered array which is seen is composed of bundles of many varying diameters. It seems possible that enough regularity exists to give rise to the periodicity evidenced in the ultrasonic internal scattering profiles, but perhaps not enough strict matrix ordering is present to give the full manifestations of Bragg diffraction phenomena.

4.2.6 Diagnostic Implications of the Scattering Data

Despite the apparent disagreement between the experimental results and the predicted values for Bragg diffraction, the internal scattering properties of biological tissues hold the promise of being significant for diagnostic applications. Tissues which have structural differences that occur within the resolving power of the ultrasound (limited by the wavelength) are easily distinguished by means of their characteristic frequency-dependent scattering. For example, calf and pig liver are structurally different in their organization of cells into clusters. Pig liver, even with the unaided eye, appears to have a honeycombed, hexagonal organizational unit, which is probably the theorized scattering element. These clusters, like the muscle fiber bundles, appear to vary in diameter. Calf liver has far less obvious a unit of structural regularity. The cell clusters are present, but are not as well defined in shape as are those of pig liver. It is interesting to note that the most regular and organized of the tissue samples, cardiac muscle, also exhibited the closest correlation to the ideal Bragg theory. The muscle fiber bundles were very regular in diameter despite the lack of one predominant orientation direction. Another factor that may lead to the non-ideal results is the irregularity introduced into the array by the presence of blood vessels dispersed throughout the tissue, leading to discontinuities in the array structure.

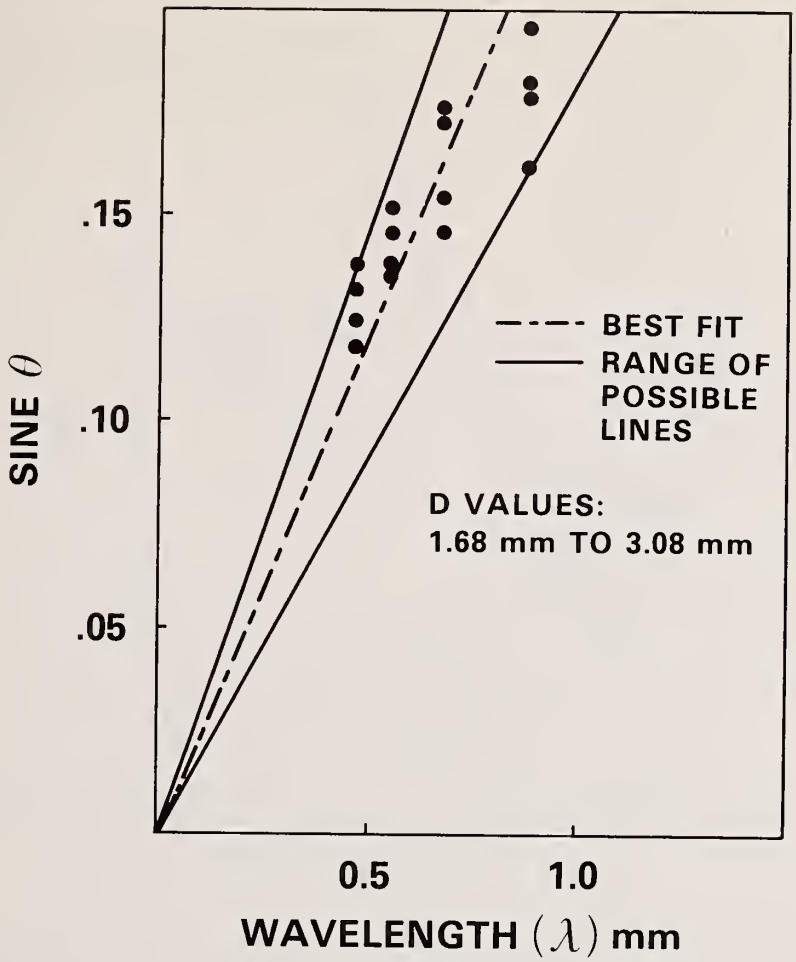

Figure 32. Comparison of theory and experimental results for pig liver.

Work with tissue specimens of known pathology is necessary to determine more precisely the diagnostic utility of scattering characterizations. An interesting extension of this experiment might involve the scattering changes which occur in cirrhotic liver and in fatty necrosis, both of which disrupt the structure by introducing fat globules and many randomly-oriented fibers. Such pathologies can be induced in experimental animals by the feeding of certain toxic substances, such as alcohol or CCl_4, to overload the liver's detoxification apparatus. A study of the progression of the disease with time can then be correlated to the changes in ultrasonic scattering properties.

Observation of the frequency-dependent phenomena exhibited by various tissues seem to be the best method of characterizing tissue type. It is superior to looking at either the double-angle scan or at the surface scattering properties. From a diagnostic standpoint, the best method might be to keep the transducers at a fixed angle, and to do a continuous sweep of frequency to measure the amplitude vs. frequency profile. A scan such as this should take less time, and could be performed using existing B-scan diagnostic equipment with minor modifications.

It is still too early to assess the possible impact of frequency-dependent attenuation and internal scattering measurements as new diagnostic tools. Certain limitations are already apparent: resolution and accessibility. As previously discussed, the resolving power is limited by the ultrasonic wavelength. Use of higher frequencies would produce a system with increased tissue resolution; however, at higher frequencies, tissue absorption becomes a problem, and there is also the related technical problem of a decreased signal strength to be measured. Design of instrumentation to overcome these difficulties should prove challenging.

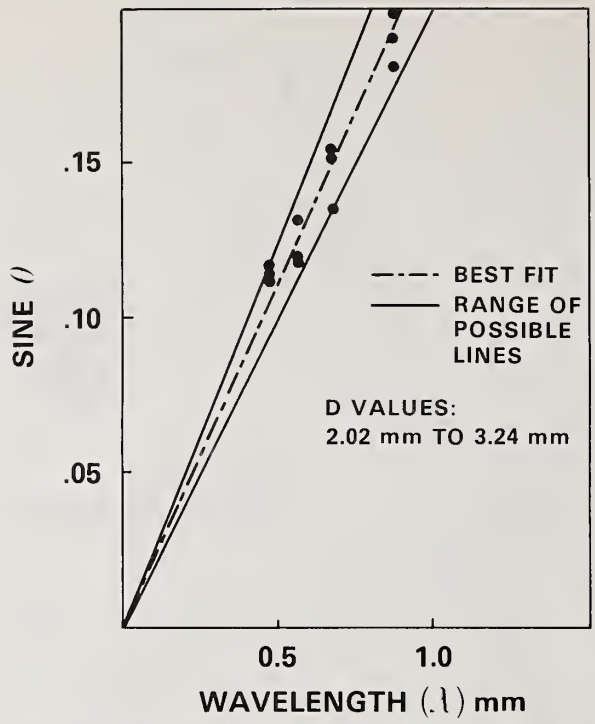

Figure 33. Comparison of theory and experimental results for calf cardiac muscle.

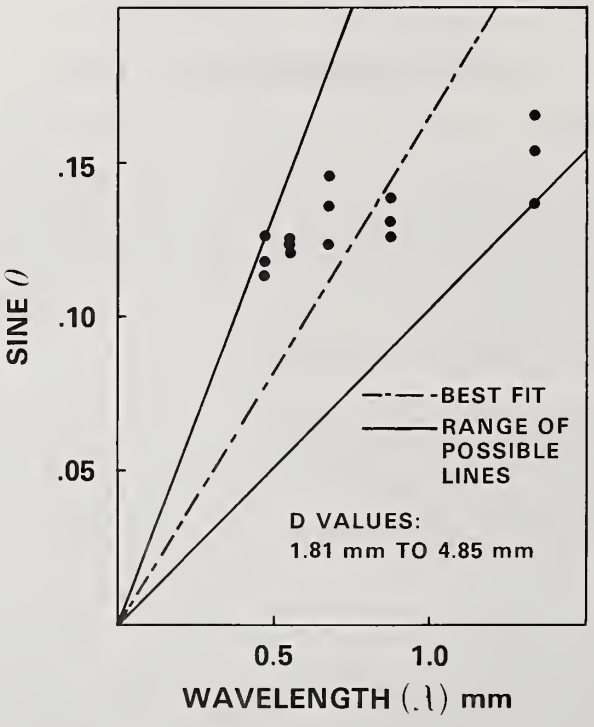

Figure 34. Comparison of theory and experimental results for calf skeletal muscle, cut across-grain.

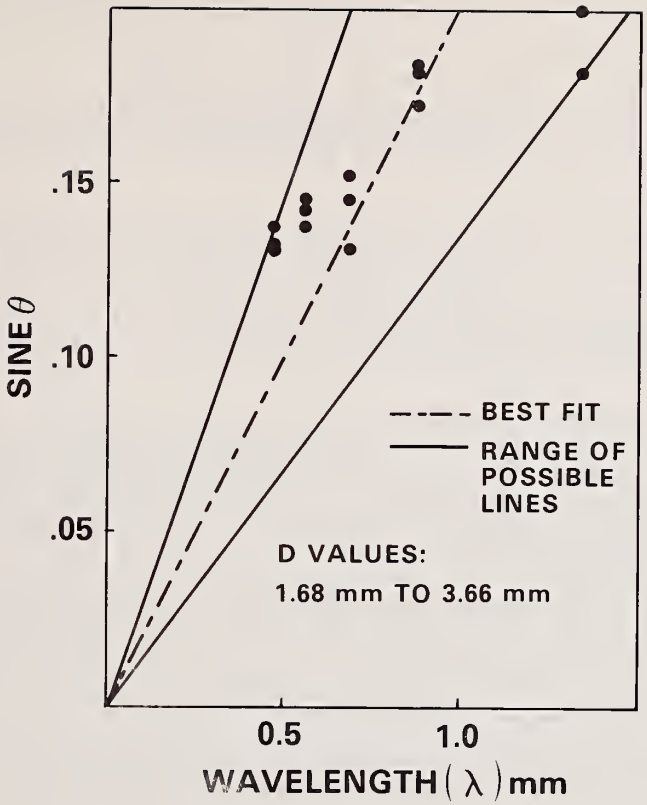

Figure 35. Comparison of theory and experimental results for calf skeletal muscle, cut longitudinally.

References

[1] Robinson, T. C. and Lele, P. P., An analysis of lesion development in the brain and in plastics by high intensity focused ultrasound at low megahertz frequencies, *J. Acoust. Soc. Am.*, 51, 1333 (1969).

[2] Howry, D. H., Techniques used in ultrasonic visualization of soft tissues, in *Ultrasound in Biology and Medicine*, E. Kelly, ed., p. 49 (Am. Instit. of Biolog. Science, Washington, DC, 1957).

[3] Robinson, T. C., An analysis of lesion development in plexiglas and nervous tissue using focused ultrasound, Ph.D. Thesis, M.I.T. (1968).

[4] Pauly, H. and Schwan, H. P., Mechanism of absorption of ultrasound in liver tissue. *J. Acoust. Soc. Am.*, 50, 695 (1971).

[5] Hueter, T. F., Viscoelastic losses in tissues in the ultrasonic range, WADC Tech. Rept. 57-706 (1958).

[6] Lele, P. P., Unpublished data reported to the U.S. Army Medical Research and Development Command (1963).

[7] Kikuchi, Y., Present aspects of ultrasonotomography for medical diagnostics, in *Ultrasonic Imaging and Holography*, G. W. Stroke, W. E. Kock, Y. Kikuchi, and J. Tsujiuchi, eds., p. 229 (Plenum Press, New York, 1974).

[8] Gericke, O. R., Ultrasonic spectroscopy, in *Research Techniques in Nondestructive Testing*, R. S. Sharpe, ed., Chapter 2 (Academic Press, New York, 1970).

[9] Papadakis, E. P. and Fowler, K. A., Broadband transducers: radiation field and selected applications, *J. Acoust. Soc. Am.*, 50, 729 (1969).

[10] Moore, D. H., Ruska, H., and Copenhaver, W. M., Electron microscopic and histochemical observations of muscle degeneration after tourniquet, *J. Biophys. Biochem. Cytol.*, 2, 755 (1956).

[11] Stenger, R. J., Spiro, D., Scully, R. E., and Shannon, J. M., Ultrastructural and physiological alterations in ischemic skeletal muscle, *Am. J. Path.* 40, 1 (1962).

[12] Conner, E. S., Hubelbank, M., and Lele, P. P., Acoustic field patterns of a digitally programmed five-element, concentric ring phased array, in *Proc. Third New England Bioeng Conf.*, p. 342 (Tufts Univ., 1975).

[13] Lele, P. P. and Namery, J., A computer-based ultrasonic system for the detection and mapping of myocardial infarcts, in *Proc. San Diego Biomed. Symp.*, 13, 121 (1972).

[14] Senapati, N., Lele, P. P., and Woodin, A., A study of the scattering of sub-millimeter ultrasound from tissues and organs, in *Proc. IEEE Ultrasonics Symp.*, p. 59 (IEEE Cat. No. 72 CH0708-8SU, IEEE, New York, 1972).

[15] Senapati, N., Some studies on scattering of ultrasonic waves by rough surfaces simulating body organs and tissue surfaces, M.S. Thesis, M.I.T. (1971).

[16] Mountford, R. and Wells, P. N. T., Ultrasonic liver scanning: the A-scan in the normal and cirrhosis, *Phys. Med. Biol.*, 17, 261 (1972).

[17] Hill, C. R. and Chivers, R. C., Investigations of backscattering in relation to ultrasonic diagnosis, in *Conf. Proc. UBIOMED 70* (Warsaw, 1970).

[18] Chivers, R. C., Hill, C. R., and Nicholas, D., Frequency dependence of ultrasonic backscattering cross-sections: an indicator of tissue structure characteristics, in *Ultrasonics in Medicine*, M. deVlieger, D. N. White, and V. R. McCready, eds., p. 300 (Excerpta Medica, Amsterdam, 1974).

[19] Hill, C. R., Interactions of ultrasound with tissues, in *Ultrasonics in Medicine*, M. deVlieger, D. N. White, and V. R. McCready, eds., p. 14 (Excerpta Medica, Amsterdam, 1974).

[20] Chivers, R. C. and Hill, C. R., A spectral approach to ultrasonic scattering from human tissue: methods, objectives, and backscattering measurements, *Phys. Med. Biol.*, 20 799 (1975).

[21] Waag, R. C., Gramiak, R., and Lerner, R. L., Ultrasonic determination of cardiac macrostructure, in *Cardiac Ultrasound*, R. Gramiak and R. C. Waag, eds., p. 277 (C. V. Mosby, St. Louis, MO, 1975).

[22] Harkness, R. D. and Harkness, M. L. R., Some mechanical properties of collageneous frameworks and their functional significance, *Biorheology*, 1, 1 (1963).

[23] Snedecor, G. W., *Statistical Methods*, 4th edition (Iowa State College Press, Ames, Iowa, 1946).

[24] Draper, N. R. and Smith H., *Applied Regression Analysis* (John Wiley, New York, 1968).

National Bureau of Standards Special Publication 453. Proceedings of Seminar on Ultrasonic Tissue Characterization held at NBS, Gaithersburg, MD, May 28-30, 1975. (Issued Oct. 1976)

Paper 6.2: FREQUENCY AND ANGULAR DEPENDENCE OF ULTRASONIC SCATTERING FROM TISSUE

C. R. Hill

Physics Division
Institute of Cancer Research
Royal Marsden Hospital
Sutton, Surrey, U.K.

This paper reports on an ongoing program of work that, commencing in 1969, has been aimed at elucidating, and ultimately applying in clinical investigation, the processes by which ultrasound is scattered by volumes of human tissue. The report covers two related aspects of the work, concerned with the specific patterns of dependence of volume backscattering cross-sections on, respectively, acoustic frequency and the relative orientation between the axis of the interrogating ultrasonic beam and the backscattering structure. These two aspects of the subject have been treated from both theoretical and experimental points of view and both aspects show promise as possible bases for practical tissue characterization. Particular interest has centered in the orientation analysis approach, which constitutes an acoustic analog of Bragg diffraction of x-rays and has been shown to be capable of quantitatively significant differentiation between different human tissue types. The feasibility of applying this approach to *in vivo* tissue characterization has been demonstrated.

Key Words: Bragg diffraction; diagnosis; frequency dependence; orientation dependence; scattering; tissue characterization; ultrasound.

This paper reports on an ongoing program of work that, commencing in 1969, has been aimed at elucidating, and ultimately applying in clinical investigation, the processes by which ultrasound is scattered by volumes of human tissue. This is a report on two aspects of this work, which is a group activity to which major contributions have been made by a number of individuals, and particularly by R. C. Chivers, D. Nicholas, R. W. Huggins, and J. Milan. Furthermore, it is work that has been carried out in close liaison with a parallel program of development and clinical application of grey-scale imaging methods for tumor diagnosis [1-3],[1] and the scatt ring work has thus been carried out with the dual aim of extending fundamental knowledge and evolving clinically-useful analytical techniques complementary to tissue imaging.

At the time of commencement of this project, no significant published data were available on the ultrasonic scattering properties of human tissues. Even in other branches of acoustics, reference to the literature yielded little of direct relevance [4,5] although a possibly productive line of work was suggested by the interest, in the field of non-destructive testing, in target characterization by ultrasonic spectroscopy.

[1]Figures in brackets indicate the literature references at the end of this paper.

A full understanding of the processes of ultrasonic scattering by human tissues will only come about by a combination of theoretical description and experimental measurement. In practice, the structural complexity of real human tissues is such that achievement of exact theoretical descriptions will be out of the question, but a promising method of bridging this gap between theory and experiment will be to work with tissue models of various kinds, for example, suspensions of spherical or cylindrical particles in liquid or gel matrices. This type of synthesis between theory and experiment has been an ideal at which we have felt it is appropriate to aim.

Conceptually, the early stages of our work were concerned with the frequency dependence of scattering. Our basic experimental system for this work, shown here in figure 1 as originally described in 1970 [6] and later elsewhere [5,7,8], has subsequently been modified

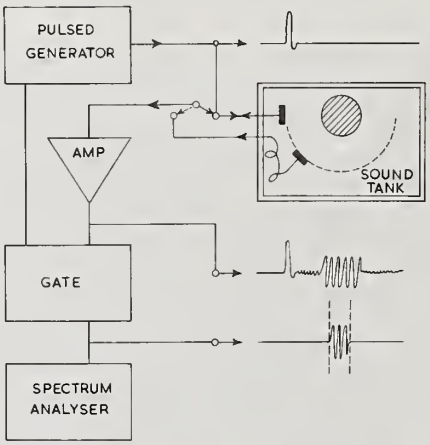

Figure 1. Basic block diagram of system for measurement of frequency dependence of ultrasonic scattering by human tissue [6].

only in detail as, for example, by being connected on line to a PDP 8E computer for data storage and processing. As we pointed out earlier [6], there is a basic choice open between using a broad or a narrow band system. For reasons of convenience and compatibility with conventional pulse-echo techniques, we chose to use the broad band (short pulse) approach, with spectrum analysis of a resulting time-gated echo packet, but there may well be ultimate advantages in the alternative of narrow band (tone-burst) methods. The influence of time-gating on information derived by spectral analysis has been examined elsewhere [4,9,10].

There is also an important choice to be made between limiting investigations to 180° backscattering and covering a significant range of angles, as envisaged in our 1970 paper [6] In the light of some of our recent findings, outlined below, it seems likely that useful information may be yielded by the multiple angle approach but, on analysis, it appears that the geometry of the situation will place severe difficulties in the way of any exact quantitative analysis of the resulting data [5,10].

Initial experimental measurements of the frequency dependence of volume backscattering by human tissues have been reported elsewhere [8,10] and some examples are shown here in figure 2. Each spectrum contains considerable detail and, visually, there appear to be some characteristic differences between different tissues. However, without further analysis, objective characterization by this approach does not appear to be possible and an important and fundamental feature of the situation is illustrated by the changes in spectral detail obtained by repositioning of the tissue specimens within the beam (compare the two columns of spectra in figure 2). Evidently, this is the consequence of a diffraction phenomenon corresponding to the existence of a complex array of scattering centers within the interrogated volume.

Possibilities for further analysis and useful exploitation of frequency spectra of this type appear to lie in two related directions, both calling for statistical treatment

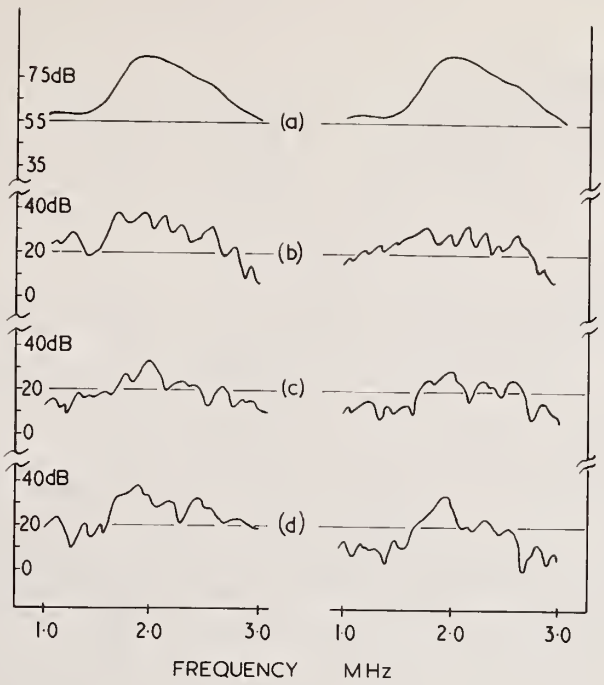

Figure 2. Frequency spectra of ultrasonic backscattering from three types of human soft tissue (two samples of each type) compared with the interrogating spectrum: (a) transducer reference spectrum, (b) fat, (c) liver, (d) spleen. IF filter width, 30 kHz; gate length, 8 μs [5].

of the data. On the one hand, this involves examining and looking for significant changes in the envelope shape of the spectra, such as might be expected in the presence of a significant component of Rayleigh-type scattering. The complementary approach is to look for characteristic properties of the spectral fine structure.

An interesting extra dimension to this situation can be obtained by systematizing the process of repositioning the tissue with respect to the interrogating beam. Specifically, this can be done by arranging for relative rotation between the tissue structure and beam axis about a line intersecting the beam axis normally and passing through the center of the interrogated volume. This technique and its application have already been described [5,11,12] and are illustrated here in figures 3 and 4. The measurements originally reported (fig. 4) were carried out on nominally normal tissues obtained at autopsy from two different subjects (identified as LF and ML) and it is quite clear from these and subsequent data that it is possible on this basis to obtain objective remote characterization of tissues. Evidently, this technique is an acoustical analog of the classical x-ray crystallography of Bragg and von Laue and, as discussed below, the implications of its results as to the mechanical-acoustical structure of human soft tissues seem quite intriguing.

Presentation of data in the form of the crude "Bragg traces" of figure 4 is visually interesting but lacking in objectivity. For the purposes of practical tissue characterization, it will be desirable to obtain a method for categorizing data in a statistically-objective manner. A number of possible approaches exist, but one that seems attractive is to derive the Fourier transforms of the basic Bragg traces. With the data in this form, it appears practicable to place confidence limits on the range of variations in data measured for tissues of various types [13]. Examples of characteristically different measured Bragg traces and their corresponding Fourier transforms have been published [5,12,14] and are reproduced here as figures 5 and 6.

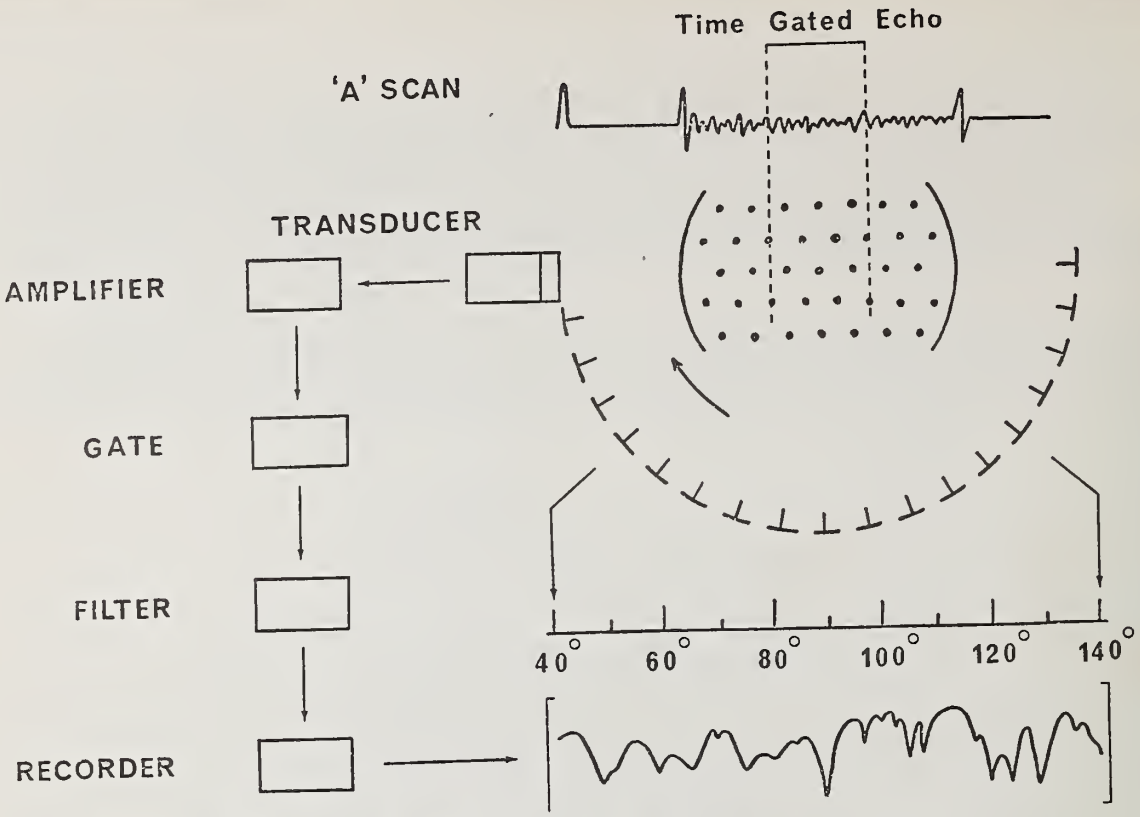

Figure 3. Experimental arrangement for investigation of the backscattered Bragg diffraction characteristics of human tissues [5].

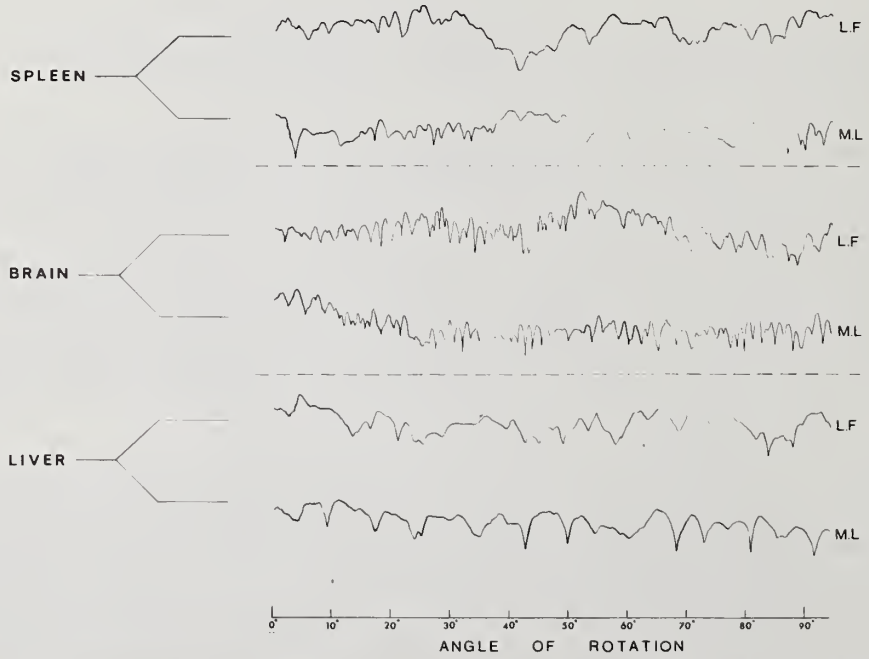

Figure 4. Angular dependence of backscattering amplitude at 1 MHz for fresh human spleen, brain, and liver, obtained from two different subjects, identified as LF and ML [11].

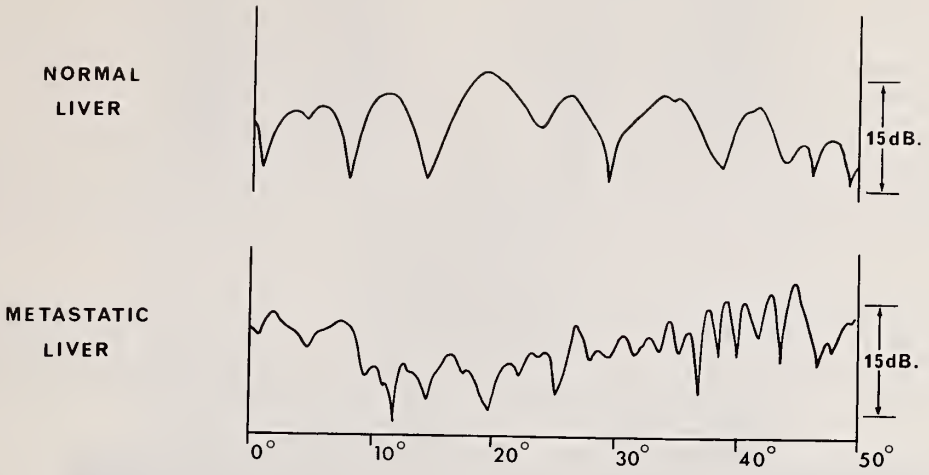

Figure 5. Observed backscattered Bragg diffraction patterns, taken at 1 MHz from normal and cancerous liver. Upper trace: normal liver parenchyma. Lower trace: secondary liver tumor [5].

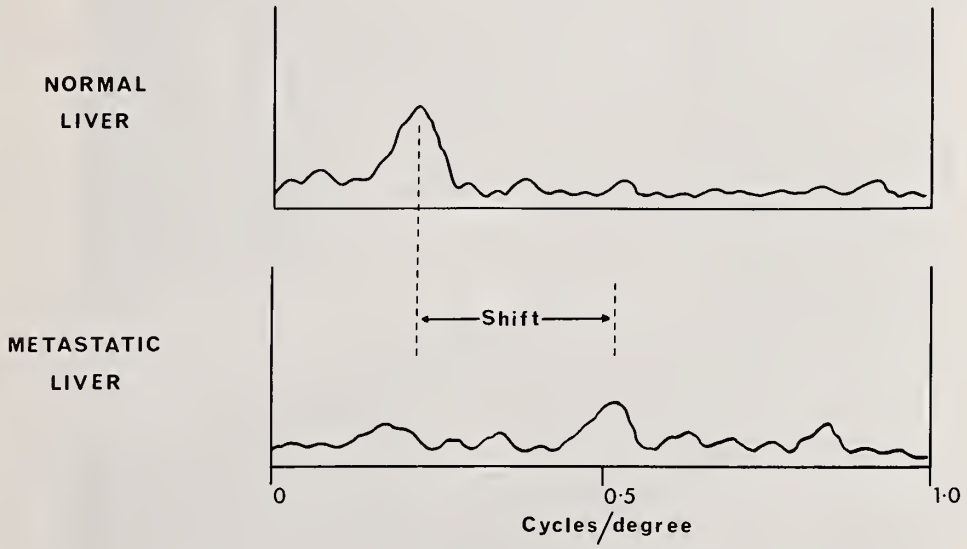

Figure 6. Power spectra derived from the Bragg diffraction records of figure 5. Upper trace: normal liver parenchyma. Lower trace: secondary liver tumor.

As mentioned at the outset, it has been the aim of our work not only to elucidate the volume scattering properties of human tissues, but also to evolve clinically practicable methods of tissue characterization. An advantage of working with 180° backscattering and broad band pulses is that the experimental system is compatible with pulse-echo imaging equipment. On this basis, it is possible to build compatible, and even hybrid, imaging/analysis systems. For superficial sites, such as the breast, this can fairly readily be

achieved in a water bath configuration. It is also possible, however, to instrument this idea in a skin-contact mode of operation and we have recently constructed and commenced trials on a machine of this kind intended for liver investigations. Technical details of this device are described elsewhere [15] and it is illustrated here in figure 7. Simultaneously-obtained B-scans and Bragg traces obtained with this device for a normal human liver are shown in figure 8. It is anticipated that this device will be interfaced to a small computer and will enable both orientation- and frequency--dependence data to be derived from selected tissue volumes within, for example, a liver, under conditions compatible with conventional clinical B-scan investigations. Ultimately, the development of a two-dimensional (acoustic Laue pattern) interrogation system is an interesting possibility here and, as Greguss has recently pointed out, such an approach would lend itself well to information analysis by coherent optical techniques.

The interpretation of experimental observations in this field, in terms of their relationships to the mechanical-acoustical properties of the echogenic tissue volumes, is a formidable problem that calls for work on several fronts. One of these is theoretical understanding of the acoustic scattering properties of complex three-dimensional matrices.

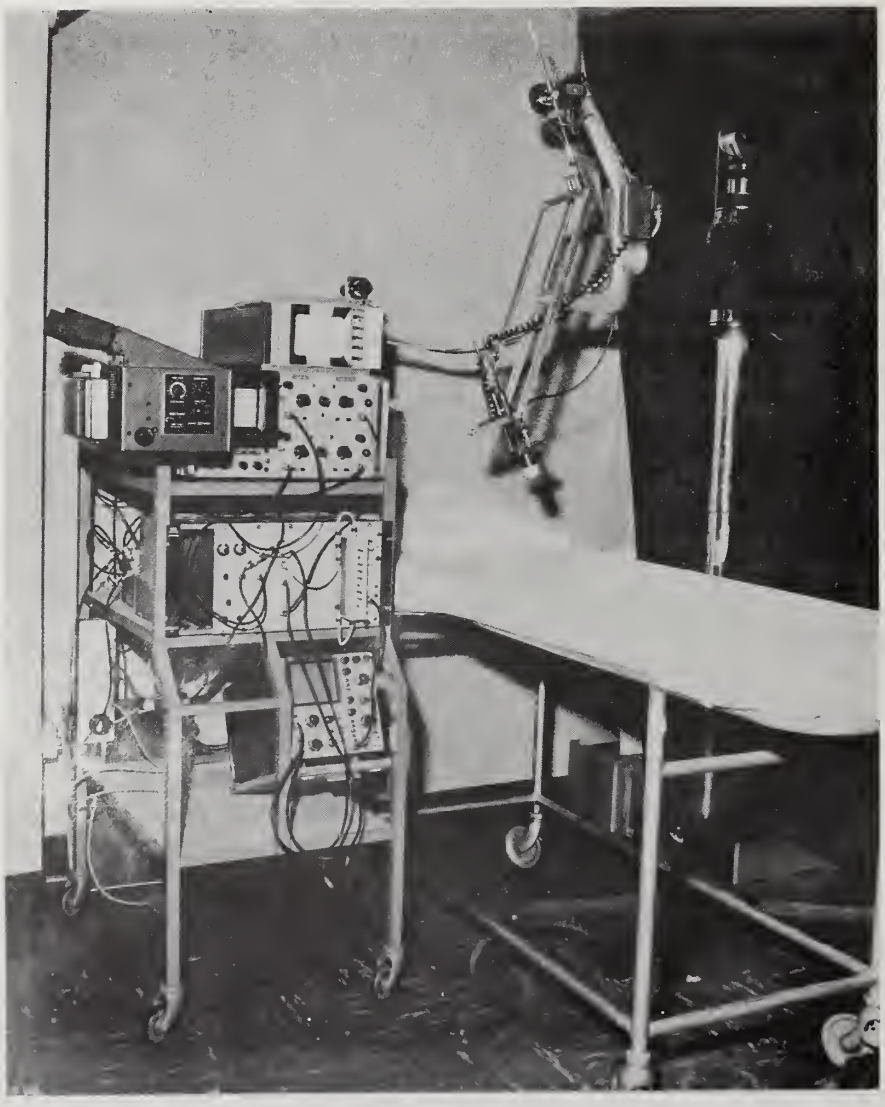

Figure 7. Skin-contact scanning device for simultaneous section scan imaging and Bragg analysis.

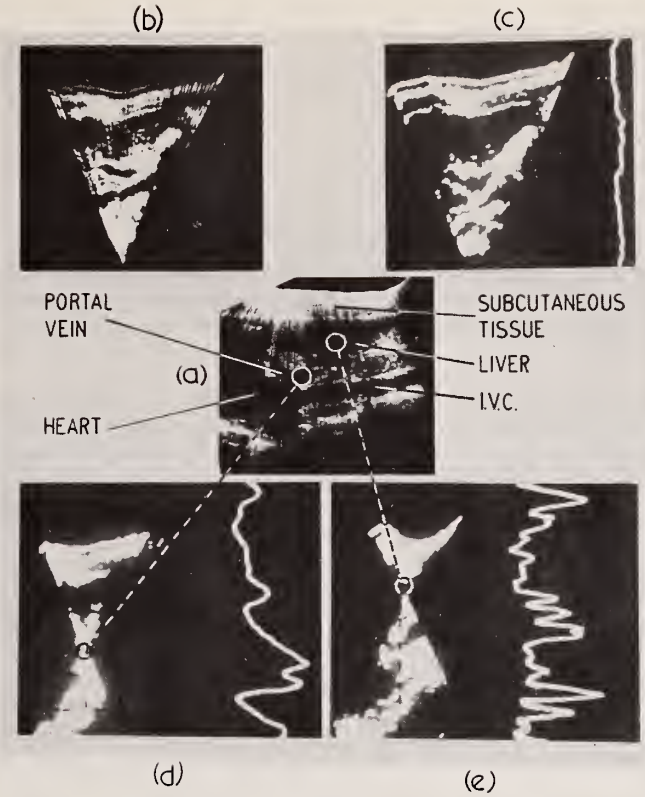

Figure 8. *In vivo* Bragg traces and corresponding section scans of normal human liver: (a) conventional B-scan (saggital section), (b) and (c) the same section imaged using the Bragg scanner with its focal point at its lowest position, (d) section image and Bragg trace derived from echoes from the region of the portal vein, (e) the same for a region of liver parenchyma.

Here, a number of results are available, either directly or in modified form, from work in other areas of scattering physics and there is a possibility, partly from these various existing strands and partly from original extensions, to synthesize a satisfactory theoretical structure for the tissue scattering situation. Some work on this has already been completed [4,5] and a further extension is in preparation [16].

The theoretical description of scattering by a complex three-dimensional matrix such as a human tissue can be approached from the viewpoint of two different models, that of a multiple array of discrete scatterers and that of an inhomogeneous continuum. Both models have been quite extensively studied in other contexts and both may have a role to play in the present situation. In particular, analysis of the multiple scatterer model suggests that it may be useful to distinguish between coherent and incoherent components of the scattered energy. Of these, the former apparently corresponds to that fraction of the echo signals that arise from refraction and specular reflection and which are exploited in conventional organ outline imaging techniques, while the latter may comprise the volume scattering that is of importance in grey-scale imaging of tissues.

The inhomogeneous continuum model has been developed in relation to hydroacoustics but the results can be appropriately modified for application in this field. In cases where the scale of the inhomogeneities is much greater than the wavelength, this model can be shown to lead to the classical ray approximation while, for a scale of homogeneities of the order of a wavelength, diffraction theory will hold. One interesting result of our investigations has been to show that Rayleigh's original analysis of diffraction phenomena due to discrete scatterers is much more generally applicable than was originally realized and holds also for inhomogeneous continua. A practically interesting consequence of such theoretical analysis is that it leads to predictions, which may be experimentally tested, for the form of the frequency dependence of scattering by various matrix configurations.

Theoretical analyses of this kind are generally based on the assumption of time waveforms being continuous. The extent to which results may be carried over to the case of interrogation by short pulses is open to question, although there are arguments in favor of the validity of such a step [16].

As has already been suggested, the particular experimental results described above in relation to the orientation dependence of backscattering (figs. 4, 5, and 6) invite theoretical consideration along lines applicable in x-ray crystallography. The relationship of this approach to general scattering theory is now under investigation [16] and certain specific attempts at interpretation of the findings have already been reported [5,12]. Support for the usefulness of the crystallographic hypothesis is provided by the very good agreement found between experiment and computations from the theory for simple physical models [12].

Such findings lead to renewed interest in the question of the identity of the discontinuities in tissue properties that constitute the acoustic scattering centers. The suggestion made by Fields and Dunn [17] that this may specifically involve connective tissues, seems plausible and can be applied usefully in testing the acoustic crystallography hypothesis. Specifically, if one considers the known histology of two human tissues, skeletal muscle and liver parenchyma, one finds that they consist of fibers and lobules, respectively, whose boundaries are, in each case, defined by connective tissue structures. These structures thus may constitute arrays which, in practice, exhibit an appreciable degree of short range order. By assuming reasonable values for the parameters describing such arrays, one may construct computational models for them and thus again compare experimental observation with theoretically predicted crystallographic behavior [5]. The results of such a comparison, illustrated here for skeletal muscle in figure 9, lend considerable support to the general validity of the underlying hypothesis.

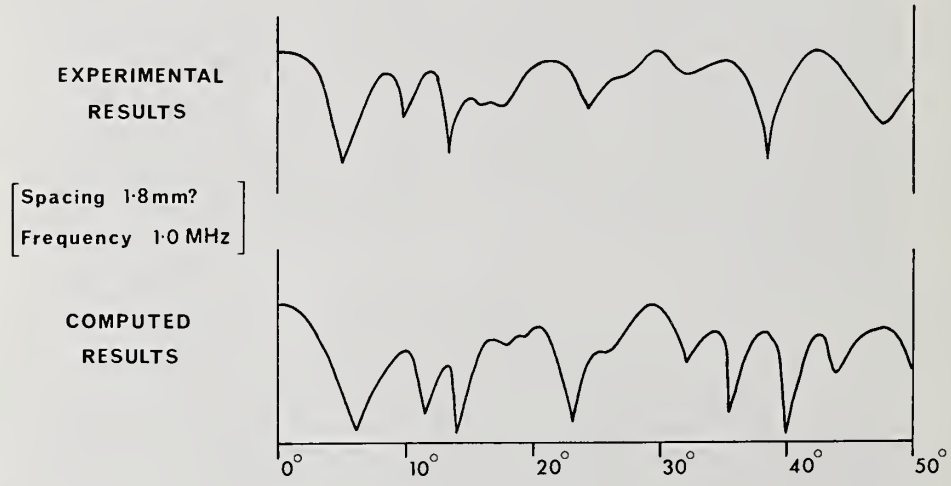

Figure 9. Acoustic Bragg diffraction records for skeletal muscle at 1 MHz (log scale). Upper trace: measured. Lower trace: computed from parallel filament array model with 1.8 mm spacing [5].

Experience in our hospital, over the past two years, of carrying out more than 3000 grey-scale ultrasound examinations on cancer patients, has served to emphasize the need for complementary analytical techniques which will provide additional information, on pathology and histo-anatomy, over and above that directly available from the grey-scale images. The science of acoustic tissue characterization is a new one but our own limited experience indicates that there are a number of interesting possibilities for applications that are likely to be both practicable and clinically relevant. The present paper has

been concerned with only two aspects of tissue characterization involving frequency and angular dependence of scattering, respectively, but there are evidently a number of other possibilities, several of which are being actively investigated by our own research group [18].

This is a report of a group effort to which contributions have been made by numerous individuals. Financial support has been provided by the Medical Research Council and Cancer Research Campaign.

References

[1] Hill, C. R. and Carpenter, D. A., Ultrasonic echo imaging of tissues: instrumentation, *Brit. J. Radiol.* (in press).

[2] Taylor, K. J. W. and McCready, V. R., A clinical evaluation of grey-scale ultrasonography, *Brit. J. Radiol.* (in press).

[3] Taylor, K. J. W., Carpenter, D. A., and McCready, V. R., Grey-scale echography in the diagnosis of intrahepatic disease, *J. Clinical Ultrasound*, 1, 284 (1973).

[4] Chivers, R. C., *The scattering of ultrasound by human tissues*, Ph.D. thesis, (University of London, 1973).

[5] Hill, C. R., Chivers, R. C., Huggins, R. W., and Nicholas, D., Scattering of ultrasound by human tissue, in *Ultrasound: Its Applications in Medicine and Biology*, F. J. Fry, ed., Ch. 9 (Elsevier, in press).

[6] Hill, C. R. and Chivers, R. C., Investigations of backscattering in relation to ultrasonic diagnosis, in *Proceedings of Conference on Ultrasound in Biology and Medicine; UBIOMED-70*, L. Filipczinski, ed., p. 110 (Polish Academy of Sciences, 1972).

[7] Hill, C. R., New uses and developments: diagnosis, in *Interaction of Ultrasound and Biological Tissues*, J. M. Ried and M. R. Sikov, eds., p. 251, DHEW Publication (FDA) 73-8008 (U. S. Government, 1972).

[8] Chivers, R. C., Hill, C. R., and Nicholas, D., Frequency dependence of ultrasonic backscattering cross-section: an indicator of tissue structure characteristics, in *Ultrasonics in Medicine*, M. de Vlieger, *et al.*, eds., p. 300 (Excerpta Medica, Amsterdam, 1974).

[9] Chivers, R. C., Ultrasonic scattering properties of human tissues: some theoretical considerations, in *Proceedings of 8th International Congress of Acoustics*, p. 359 (1974).

[10] Chivers, R. C. and Hill, C. R., A spectral approach to ultrasonic scattering from human tissue: methods, objectives and backscattering measurements, *Phys. Med. Biol.* 20, 799 (1975).

[11] Hill, C. R., Interactions of ultrasound with tissues, in *Ultrasonics in Medicine*, M. de Vlieger, *et al.*, eds., p. 14 (Excerpta Medica, Amsterdam, 1974).

[12] Nicholas, D. and Hill, C. R., Tissue characterisation by an acoustic Bragg scattering process, in *Proceedings of the 1975 Ultrasonics International*, (Iliffe, London, in press).

[13] Nicholas, D. and Hill, C. R., Acoustic Bragg diffraction from human tissues, *Nature*, 257, 305 (1975).

[14] Hill, C. R. and Nicholas, D., Ultrasonic scattering characteristics of human tissues: experimental investigations, in *Proceedings of 8th International Congress of Acoustics*, p. 357 (1974).

[15] Huggins, R. W. and Phelps, J. V., Bragg diffraction scanner for ultrasonic tissue characterisation *in vivo* (manuscript in preparation).

[16] Nicholas, D., *Ultrasonic scattering and the structure of human tissues*, Ph.D. thesis, (University of London, in preparation).

[17] Fields, S. and Dunn, F., Correlation of echographic visualizability of tissue with biological composition and physiological state, *J. Acoust. Soc. Am.* 54, 809 (1973).

[18] Hill, C. R., Echoes from human tissues, in *Proceedings of the 1975 Ultrasonics International*, (Iliffe, London, in press).

National Bureau of Standards Special Publication 453. Proceedings of Seminar on Ultrasonic Tissue Characterization held at NBS, Gaithersburg, MD, May 28-30, 1975. (Issued Oct. 1976)

Paper 6.3: THE SCATTERING OF ULTRASOUND BY RED BLOOD CELLS

K. K. Shung, R. A. Sigelmann,[1] and J. M. Reid

Providence Hospital
Seattle, Washington 98122

This paper reviews the experimental results obtained on the measurement of ultrasonic scattering properties of erythrocytes. The scattering is proportional to the fourth power of the frequency, as predicted by Rayleigh's scattering theory, for frequencies below 15 MHz. The scattering is not linearly dependent upon the hematocrit as would be expected for a single scattering process. Twersky's wave scattering theories are therefore applied to describe this result. The magnitudes of the monopole scattering due to compressibility and of the dipole scattering due to density are in good agreement with theory. Blood is the first tissue for which a nearly complete experimental and theoretical characterization of scattering exists.

Key Words: Angular dependence; blood; compressibility; density; distribution function; erythrocytes; hematocrit; scattering; ultrasound.

1. Introduction

Because it is easier to characterize physically, the scattering of ultrasonic waves by red blood cells is a unique problem compared with the ultrasonic scattering by other biological tissues such as muscle, lung, etc. Blood can be considered as a suspension of red blood cells in plasma as far as the mechanism of the scattering is concerned. The scattering of ultrasound by other blood corpuscles was experimentally shown to be insignificant [1].[2]

The scattering of acoustic waves by suspensions of particles has been studied by many investigators both theoretically and experimentally [2-4]. However, most of these studies have been concentrated on sparse concentrations of scatterers. Few investigations were reported on dense media such as normal whole blood. This is probably due to the complexity of this problem. A complete solution requires the knowledge of multiple-particle distribution functions. Unfortunately, these are not available. Twersky solved this problem in terms of a one-particle distribution function [5-7]. Beard, *et al.* [8] performed a series of measurements on the dependence of wave scattering upon concentration of the scatterers. A serious discrepancy exists between their results and Twersky's theories. They therefore resort to a heuristic "hole" approach. Similar results can also be acheived by a "two-phase" approximation [9]. In this approximation, some of the scatterers are considered randomly distributed, the others fixed in position. Only the random particles contribute to the incoherent scattering. In a dense medium like blood, the blood cells are so close to each other that the motion of the cell may be affected by the presence of other cells. Thus, it is highly possible that some of the cells can no longer be considered randomly located and the division of particles into random and non-random populations is comprehensible.

---

[1]University of Washington, Seattle, Washington 98105.

[2]Figures in brackets indicate the literature references at the end of this paper.

The objective for pursuing this research is that the information obtained can be used to improve existing diagnostic instruments such as the Doppler flowmeter or to develop new methods for clinical use. See "The Scattering of Ultrasound by Tissues," this volume (p. 29) for details of application.

2. Experimental Results and Theoretical Analysis

The experimental technique and arrangement employed in our measurements have been described elsewhere [10-12]. Thus, they will not be repeated here. Essentially, in this method, the scattering coefficient (scattering cross-section per unit volume of scatterers) can be measured by comparing the RMS value of the gated backscattered wave from a specified volume of blood with that of a stainless steel flat reflector.

Outdated citrated bank blood cells were suspended in Ringer's Injection solution in our measurements. Additional anticoagulant (Sodium Heparin) was added whenever necessary. Great care was taken to prevent hemolysis during the experiment. Clumping and settling of the red blood cells were prevented by pumping. All measurements were done at 37°C. We envisioned that results using outdated blood obtained *in vitro* may be different from those using fresh blood obtained *in vivo*. We intend to repeat these measurements *in vivo* in the near future.

Our experimental data indicate that for frequencies below 15 MHz the scattering is proportional to the fourth power of the frequency and this relation is not affected by the hematocrit (percentage packed-cell volume occupied by blood cells) of the blood (fig. 1). This is predicted by Rayleigh's scattering theory because the ultrasonic wavelength is much longer than the dimension of the scatterer.

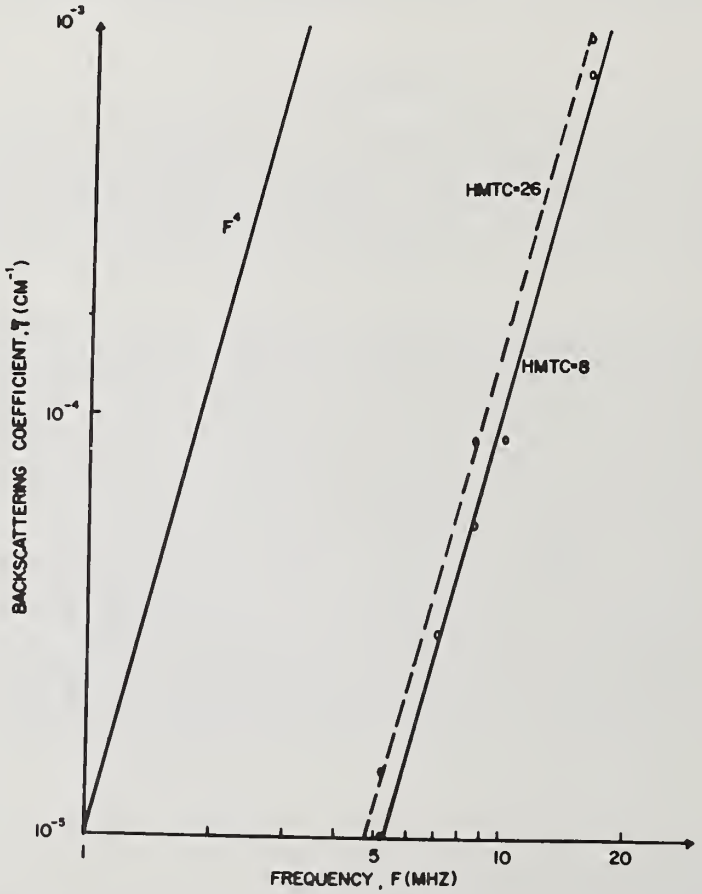

Figure 1. Volumetric backscattering coefficient versus frequency.

The scattering of ultrasound by blood was found to increase approximately linearly with the number of red blood cells present in the blood sample for hematocrits less than 8%. After this point, the scattering process becomes more complicated. It reaches a maximum around a hematocrit of 26%, then decreases as the hematocrit increases (fig. 2).

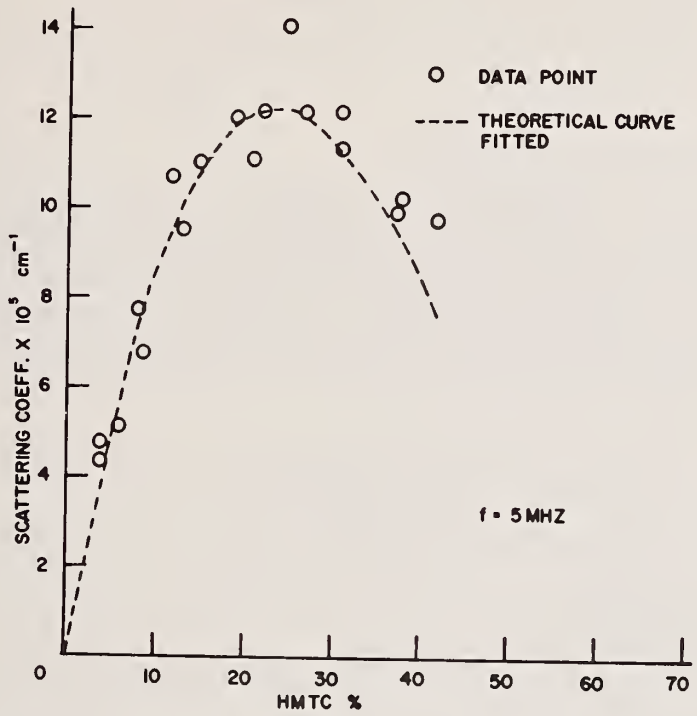

Figure 2. Volumetric scattering coefficient versus hematocrit at 5 MHz.

The physical significance of these phenomena can be explained as follows: at low hematocrits (less than 8%), the red blood cells behave as incoherent, randomly-distributed scattering centers. The total scattered intensity is the sum of the intensities from each cell, *i.e.*, a single scattering mechanism will suffice to describe the scattering process. At very high hematocrits (greater than 58% or so),[3] the blood resembles a perfect crystalline solid. There would be no wave scattering if all cells were regularly spaced at very small distances from each other. Although the cells can be considered as scattering centers, the waves scattered from them will interfere destructively at any point of observation. The reason for this is that the cells can be so paired that the waves from each pair traveling in a particular direction are exactly out of phase. For intermediate hematocrits, some of the cells can be considered in a random state while the others are in a crystalline state. Only the random cells will contribute to incoherent scattering. Coherent scattering by the crystalline cells contributes only to scattering in the forward direction.

Twersky [5-7] expressed the pair distribution function by the product of two one-particle distribution functions and solved the problem of wave propagation in a dense medium. For the case of ka much less than 1, he obtained the following result:

$$d_s = 0.21k^4a^3w_o(1-w_o)\left|\frac{\beta_e - \beta}{(1-w_o) + w_o\beta_e}\right| + \left|\frac{\rho_e - \rho}{\rho_e}\right|^2 \qquad (1)$$

[3]Beard *et al.* found that the maximum volume concentration that can be obtained without the deformation of the scatterers is between 59% and 64% [14].

where α_s = scattering coefficient

k = wave number

a = radius of the scatterer

β_e = adiabatic compressibility of the scatterer

β = adiabatic compressibility of the imbedding medium

ρ_e = density of the scatterer

ρ = density of the imbedding medium

w_o = volume concentration of scatterers.

It should be noted that for this expression to be valid the scatterers must be point scatterers and independent of each other. This is physically unrealizable. To modify this result, he therefore introduced two heuristic approximations [8,9]. In the so-called "two-phase" system, he divided the scatterers into two phases, N_r of them in gas phase and N_x of them in crystal phase such that $N_r+N_x = N$ (the total number of scatterers in the system). In the "hole" approach, the scattering was thought to occur at the cavity sites (space not occupied by the scatterers) in the very dense situation, and the volume of each "hole" was assumed to be

$$V_h = V_o(1-bw_o) \tag{2}$$

where V_h = volume of the hole

V_o = volume of the scatterer

b = a fitting constant.

Using our experimental data and introducing the "hole" approximation, we obtained the following theoretical result:

$$\alpha_s = 0.21k^4a^3w_o(1-w_o)(1 - 1.72w_o)\left|\frac{\beta_e - \beta}{(1-w_o) + w_o\beta_e}\right| + \left|\frac{\rho_e - \rho}{\rho_e}\right|^2 \tag{3}$$

Equation (3) is also shown in figure 2 as a dotted line. We can also obtain the theoretical curve for the volumetric scattering cross-section by dividing eq. (3) by w_o. Both the data points and the theoretical curve for the scattering cross-section are shown in figure 3. This figure indicates that the scattering contributed by each scatterer decreases as hematocrit increases. The agreement between results at low hematocrits and the value calculated from Morse and Ingard's formula [13], assuming the volume of a red blood cell to be 87 μm [3], is good. Our result is slightly larger than the theoretical value. However, it should be pointed out that the volume of the red blood cell increases with age.

The angular scattering of ultrasound by blood was measured from 60° to 150° (fig. 4). The theoretical curve based on Morse and Ingard's formula [13] and Ahuja's result [15] are also plotted in figure 4. It should be noted that the scattering angle in this figure is the angle between the direction of incidence and the direction of observation. In the theoretical calculations, we have assumed that the angular dependence is independent of the number of the scatterers present in the medium. This may not be true [7] in dense media. However, in the hematocrit range of our measurements, this effect seems to be so small that it may be neglected. Comparing the experimental data with the theoretical curves, we can see that very good agreement exists between our result and Ahuja's expression, which includes the effects of viscosity.

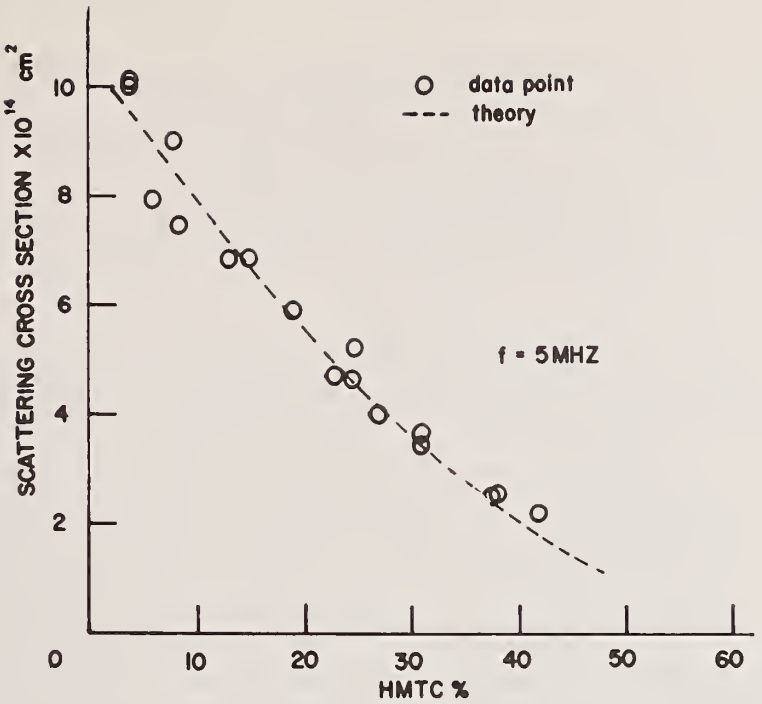

Figure 3. The scattering cross-section per cell versus hematocrit at 5 MHz.

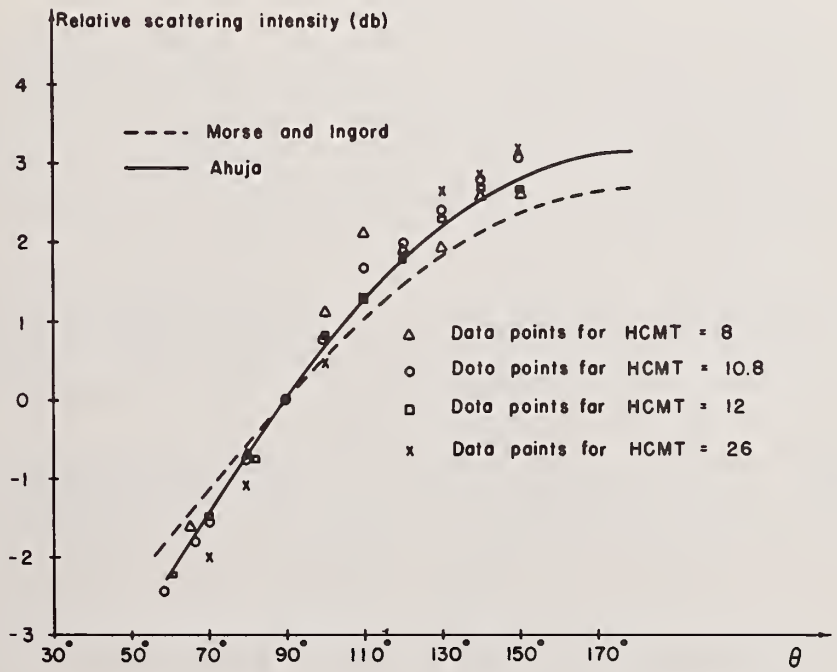

Figure 4. Measured angular scattering intensity normalized with respect to I(90°). Theoretical predictions are given by the curves.

3. Conclusion

This paper reviews the experimental data obtained so far on the scattering properties of ultrasound in blood. We showed the frequency and angular dependence of the scattering and the relation between the scattering and the volume concentration of the red blood cells. However, most of our experiments have been limited to hematocrits below 45%. This is because, in the present experimental arrangement, effects other than the scattering due to blood cells may be present in the scattered signal at very high hematocrits. For instance, the scattering is found to be heavily dependent upon the flow rate for samples with hematocrits greater than 45%. To eliminate this effect, some of the apparatus should be redesigned such that a clear relation between the scattering and flow rate can be established.

References

[1] Reid, J. M., Sigelmann, R. A., Nasser, M. G., and Baker, D. W., The scattering of ultrasound by human blood, in *Proceedings 8th ICMBE* (1969).

[2] Rayleigh, L., *Phil. Mag.* 41, 107, 274 (1871); 47, 375 (1899).

[3] Kol'tsova, I. S. and Mikhailov, I. G., Scattering of ultrasonic waves in heterogeneous systems, *Sov. Phys. Acoust.* 15, 390 (1970).

[4] Allegra, T. R. and Howley, S. A., Attenuation of sound in suspensions and emulsions, *J. Acoust. Soc. Am.* 51, 1545 (1972).

[5] Twersky, V., On scattering of waves by random distribution; I. free space scatterer formalism, *J. Math. Phys.* 3, 700 (1962).

[6] Twersky, V., On scattering of waves by random distribution; II. two space scatterer formalism, *J. Math. Phys.* 3, 724 (1962).

[7] Twersky, V., Acoustic bulk parameters of random volume distributions of small scatterers, *J. Acoust. Soc. Am.* 36, 1314 (1964).

[8] Beard, C. I., Hays, T. H., and Twersky, V., Scattering by random distributions of spheres versus concentrations, *IEEE Trans. Antennas Propag.* AP-15, 99 (1967).

[9] Twersky, V., Multiple scattering of waves in dense distributions of large tennuous particles, in *Electromagnetic Scattering*, M. Kerker, ed. (1962).

[10] Sigelmann, R. A. and Reid, J. M., Analysis and measurement of ultrasound backscattering from an ensemble of scatterers excited by sine wave bursts, *J. Acoust. Soc. Am.* 53, 1351 (1973).

[11] Shung, K. P., Sigelmann, R. A., and Reid, J. M., The angular dependence of the scattering of ultrasound by blood, *IEEE Trans. Biomed. Engr.* (to be published).

[12] Shung, K. P., Sigelmann, R. A., and Reid, J. M., The scattering of ultrasound by blood, *IEEE Trans. Biomed. Engr.*, (September, 1976).

[13] Morse, P. M. and Ingard, K. U., *Theoretical Acoustics* (McGraw-Hill Book Co., New York, 1968).

[14] Hawley, S. W., Hays, T. K., and Twersky, V., Comparison of distribution functions from scattering data on different sets of spheres, *IEEE Trans. Antennas Propag.* AP-15, 118 (1967).

[15] Ahuja, A. S., Effect of particle viscosity on propagation of sound in suspensions and emulsions, *J. Acoust. Soc. Am.* 51, 182 (1972).

National Bureau of Standards Special Publication 453. Proceedings of Seminar on Ultrasonic Tissue Characterization held at NBS, Gaithersburg, MD, May 28-30, 1975. (Issued Oct. 1976)

Paper 6.4: SWEPT-FREQUENCY ULTRASONIC DETERMINATION OF TISSUE MACROSTRUCTURE[1]

R. C. Waag, R. M. Lerner, and R. Gramiak

University of Rochester
Rochester, New York 14627

Ultrasound may be used to determine the acoustic structure of tissue on a scale corresponding to the wavelengths employed by using scattered signal to infer the organization of tissue elements. The underlying concept is the selective reinforcement or cancellation of certain frequencies depending on the relation of wavelength, reflector spacing, and orientation. A Fourier analysis of the received signal as a function of frequency or scattering angle reveals the acoustic variations corresponding to structure. By employing a swept-frequency ultrasonic signal, data similar to that obtained by angle scanning at a fixed frequency in x-ray diffraction has been obtained. Predicted deterministic interference patterns have been demonstrated for aluminum plates. Random scattering for two different sizes of dextran particles has also demonstrated predicted differences in scattering spectra. Pilot studies of liver specimens have shown marked variations in intensity-frequency distributions for individual disease processes.

Key words: Diffraction; Fourier transform; scattering; tissue characterization; ultrasound.

1. Introduction

There has been a long-standing interest in characterizing tissue remotely by its ultrasonic properties. Evidence that there is considerably more information than simply amplitude and time-of-arrival in ultrasonic echoes exists from studies of animals such as bats and dolphins [1].[2] One of the first medical demonstrations of tissue characterization with ultrasound was by Wild and Reid [2], who distinguished malignant and normal breast tissue through analysis of the area under A-mode echoes.

The ultrasonic properties of tissue can be determined in various ways. Bulk measurements have been made of impedance [3] and also of acoustic absorption and speed of propagation as functions of frequency [4]. Experience has shown that variations in these parameters due to disease processes are difficult to assess. However, it appears that characterization of local variations of tissue properties can provide important information about tissue structure and, therefore, pathology.

Recent research has been directed at a quantitative analysis of echo amplitude, signal frequency analysis, and hitherto unexplored acoustic concepts. For example, Baum [5] and Ossoinig [6] have both shown how echo amplitude can be used to distinguish various eye lesions. Namery and Lele [7] have observed differences in absorption as a

[1]This work was supported in part by NIH Grant No. 5 R01 150106 and NSF Grant No. APR75-14890.

[2]Figures in brackets indicate the literature references at the end of this paper.

function of frequency between diseased and normal heart muscle. Among the new concepts have been measurement of backscatter amplitude as a function of angle [8] and also impediography [9].

Our approach to tissue characterization with ultrasound involves the adaptation of the concepts used in x-ray diffraction and atmospheric probing. It has begun with the use of ultrasonic frequency scanning [10] to determine the acoustic properties of tissue on a scale corresponding to the wavelengths employed. It is expected that additional frequency scan studies will, with angle scan data, reveal optimal combinations of frequency and angle interrogation for tissue characterization.

2. Theoretical Basis

Biological tissue is extremely complex and has many levels of organization progressing upwards in size from DNA through organelles, cells, groups of cells in a connective tissue matrix, and finally, organs.

The model we postulate relates scattering parameters of tissue to the acoustic structure and indicates that the different levels of organization may be studied with ultrasound by appropriate choice of frequency and geometry. The resulting acoustic characterization can then be compared to microscopic determinations of structure to establish tissue pathology. The theory we develop is analogous to that used in x-ray diffraction of amorphous materials and allows the structure of the medium to be inferred from measurements of the scattered acoustic wave.

Our analysis begins with consideration of a plane wave propagating through a lossless unbounded medium which has small variations in refractive index. Tissue absorption unnecessarily complicates the analysis and will be incorporated later. Our theory deals with refractive index rather than impedance variations because there is evidence [11] that the density variations in tissue are very small compared to variations in the speed of sound and, therefore, refractive index variations are a direct indication of tissue structure.

The refractive index, which is the ratio of the average bulk speed of sound in the medium to the speed at a specific point in the medium, may be written as

$$n(\underline{r}) = \frac{c}{c(\underline{r})} = n_0 + n_1(\underline{r}) \qquad (1)$$

where n_0 is the average refractive index and assumed to be 1 in this treatment and $n_1(\underline{r})$ is the variation of $n(\underline{r})$ at a point $\underline{r}$ in space.

The equation governing the time harmonic motion of a pressure field in a weakly inhomogeneous medium is conveniently expressed in terms of a velocity potential[3] as

$$\Phi(\underline{r},t) = \mathrm{Re}[\phi(\underline{r})e^{-i\omega t}] \ .$$

---

[3]Acoustic pressure is proportional to this velocity potential and can be determined in terms of the velocity potential by the relation

$$p(\underline{r},t) = \rho_0 \frac{\partial}{\partial t} \Phi(\underline{r},t)$$

in which ρ_0 is the average bulk density of the medium.

The spatial component of this velocity potential satisfies the equation

$$\nabla^2\phi(\underline{r}) + k^2(\underline{r})\phi(\underline{r}) = 0 \tag{2}$$

where

$$k(\underline{r}) = \frac{\omega}{c(\underline{r})} \ , \ c(\underline{r}) = \frac{1}{(\rho_r \kappa_r)^{\frac{1}{2}}} \ ,$$

ρ_r is the medium density and κ_r is its compressibility. This is the well-known Helmholtz equation with a spatially-varying wave number. Using the expression for refractive index given in eq. (1), this equation becomes

$$\nabla^2\phi(\underline{r}) + (1 + n_1(\underline{r}))^2 k^2 \phi(\underline{r}) = 0 \tag{3}$$

where k^2 now refers to average medium properties. For $n_1(\underline{r}) << 1$, eq. (3) may be approximated by

$$\nabla^2\phi(\underline{r}) + k^2\phi(\underline{r}) = -2n_1(\underline{r})k^2\phi(\underline{r}) \tag{4}$$

which is the Helmholtz equation with a forcing term.

The total velocity potential may be written

$$\phi(\underline{r}) = \phi_i(\underline{r}) + \phi_1(\underline{r}) \tag{5}$$

where

$\phi_i \equiv$ incident velocity potential
$\phi_1 \equiv$ first-order scattered velocity potential.

Substituting this expression into the Helmholtz equation yields

$$\nabla^2\phi_1(\underline{r}) + k^2\phi_1(\underline{r}) = -2n_1(\underline{r})k^2[\phi_i(\underline{r}) + \phi_1(\underline{r})] \tag{6}$$

because

$$\nabla^2\phi_i(\underline{r}) + k^2\phi_i(\underline{r}) = 0.$$

This inhomogeneous Helmholtz equation may be solved by using the Green's function for unbounded space. The result is

$$\phi_1(\underline{r}) = \frac{k^2}{4\pi} \int_{V'} [\phi_i(\underline{r}') + \phi_1(\underline{r}')]2n_1(\underline{r}') \frac{e^{ik|\underline{r}-\underline{r}'|}}{|\underline{r}-\underline{r}'|} dV' \tag{7}$$

where the geometry is defined in figure 1. Since the variations in refractive index give rise to relatively small scattered waves, this equation may be approximated by

$$\phi_1(\underline{r}) = \frac{k^2}{2\pi} \int_{V'} \phi_i(\underline{r}')n_1(\underline{r}') \frac{e^{ik|\underline{r}-\underline{r}'|}}{|\underline{r}-\underline{r}'|} dV' \tag{8}$$

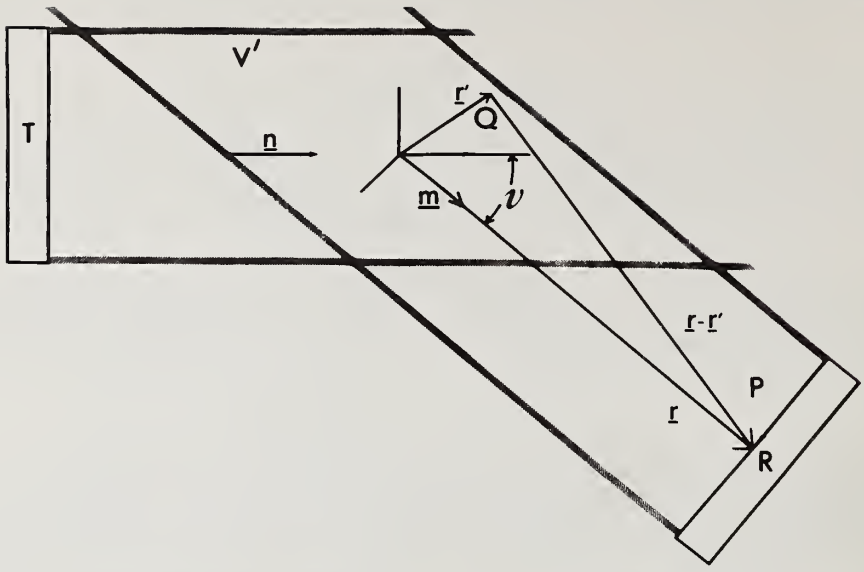

Figure 1. Scattering model geometry. The scattering volume, V', is illuminated by a plane wave traveling in the $\underline{n}$ direction and emitted from transducer T. The scattered signal traveling in direction $\underline{m}$ is received at point P by transducer R. The angle between the direction of incidence and reflection is ν.

This expression gives the velocity potential $\phi_1(\underline{r})$ at the point P due to variations in refractive index in a source volume V'.

If the point P is far from the scattering volume with dimension d and the Fraunhofer condition holds, *i.e.*,

$$\frac{kd^2}{2r} << 1 \tag{9}$$

the expression

$$|\underline{r} - \underline{r}'|$$

may be replaced by

$$\underline{r} - \underline{r}' \cdot \underline{\hat{m}}$$

in the exponent of the equation and

$$|\underline{r} - \underline{r}'|$$

may be replaced by r in the denominator. The result is

$$\phi_1(\underline{r}) = \frac{k^2 e^{ikr}}{2\pi r} \int_{V'} \phi_i(\underline{r}')n_1(\underline{r}')e^{-ik\underline{m}\cdot\underline{r}'}\, dV' \tag{10}$$

Now, if $\phi_i(\underline{r})$ is taken as a plane wave,

$$\phi_i(\underline{r}') = A_o e^{i\underline{k}\cdot\underline{r}'} = A_o e^{ik\underline{n}\cdot\underline{r}'}$$

and

$$\phi_1(\underline{r},k) = \frac{A_o}{2\pi}\frac{k^2 e^{ikr}}{r}\int_{V'} e^{ik(\underline{n}-\underline{m})\cdot\underline{r}'}\, n_1(\underline{r}')dV' \tag{11}$$

Defining

$$\underline{K} = k(\underline{n}-\underline{m})$$

where

$$|\underline{K}| = 2\,k\,\sin\,\frac{\nu}{2}$$

the velocity potential for the received scattered wave becomes

$$\phi_1(\underline{r},k) = \frac{A_o}{2\pi}\frac{k^2 e^{ikr}}{r}\int_{V'} e^{i\underline{K}\cdot\underline{r}'}\, n_1(\underline{r}')dV' \tag{12}$$

Thus, the pressure at point P is defined by the product of the factor

$$-\frac{i\omega\rho_o A_o k^2 e^{ikr}}{2\pi r}$$

and the three-dimensional Fourier transform of $n_1(\underline{r})$ with respect to the wave vector $\underline{K}$.

If the acoustic properties of $n_1(\underline{r})$ are isotropic with respect to $\underline{K}$, eq. (12) may be further simplified by allowing $\underline{K}$ to be the azimuthal axis for a spherical coordinate system. Then,

$$\underline{K}\cdot\underline{r}' = |\underline{K}||\underline{r}'|\cos\psi$$

and

$$\phi_1(\underline{r},k) = \frac{A_o k^2 e^{ikr}}{2\pi r}\int_{\theta=0}^{2\pi}\int_{\psi=0}^{\pi}\int_{r'=0}^{d} n_1(r')e^{ikr'\cos\psi}\, r'^2\sin\psi dr' d\psi d\theta$$

which, for elastic scattering, reduces to

$$\phi_1(\underline{r},k) = \frac{A_o k e^{ikr}}{2\sin(\frac{\nu}{2})r}\int_o^d r' n_1(r')\sin(Kr')dr' \tag{13}$$

Equation (13) shows that the velocity potential or pressure at $\underline{r}$ is proportional to the finite Fourier sine transform of $r'n_1(r')$ when the scattering volume is spherical and the structure of $n_1(\underline{r}')$ is isotropic.

Many structures of interest are random and require statistical approaches to characterize them. Statistics of the medium may be taken into account by considering the scattered wave intensity instead of the amplitude. In terms of eq. (12), the scattered wave intensity is

$$|\phi_1(\underline{r},k)|^2 = \frac{A_o^2 k^4}{4\pi^2 r^2}\int_{V'}\int_{V'} e^{i\underline{K}\cdot(\underline{r}'_1-\underline{r}'_2)}\, n_1(\underline{r}'_1)n_1(\underline{r}'_2)dV'_1 dV'_2 \tag{14}$$

This expression may be simplified by taking the ensemble average of both sides, interchanging the order of averaging and integration, and defining a medium correlation

function,[4]

$$\overline{n_1(\underline{r}_1)n_1(\underline{r}_2)} = B_{n_1}(\underline{r}_1,\underline{r}_2) \tag{15}$$

The result is

$$\overline{|\phi_1(\underline{r},k)|^2} = \frac{A_o^2k^4}{4\pi^2r^2}\int_{V'}\int_{V'} e^{i\underline{K}\cdot(\underline{r}'_1-\underline{r}'_2)}B_{n_1}(\underline{r}'_1,\underline{r}'_2)dV'_1dV'_2 \tag{16}$$

If the statistics of $n_1(\underline{r}')$ are independent of spatial origin, then the correlation function B_{n_1} becomes only a function of the difference $\underline{r}_1 - \underline{r}_2 = \underline{\rho}$ and eq. (16) can be written

$$\overline{|\phi_1(\underline{r},k)|^2} = \frac{A_o^2k^4}{4\pi^2r^2}\int_{2V'} e^{i\underline{K}\cdot\underline{\rho}}\, B_{n_1}(\underline{\rho})\left[\int_{V'(\underline{\rho})} dV'\right] dV'_\rho$$

The correlation function is windowed by the bracketed volume integral which depends on $\underline{\rho}$. When the volume of integration is rectilinear and the integration is carried out in a Cartesian coordinate system with axes originating at the volume centroid and parallel to the volume edges, the window takes the form

$$\prod_{\ell=1}^{3} L_\ell\left(1 - \frac{|\rho_\ell|}{L_\ell}\right)$$

where L_ℓ (ℓ = 1, 2, and 3) are the dimensions of the volume.

If the correlation length is small compared to the dimensions of the scattering volume so that the correlation function becomes small before the window variation becomes appreciable, the average received intensity expression reduces to

$$\overline{|\phi_1(\underline{r},k)|^2} = \frac{A_o^2k^4V}{4\pi^2r^2}\int_{V'} e^{i\underline{K}\cdot\underline{\rho}}\, B_{n_1}(\underline{\rho})dV'_\rho \ . \tag{17}$$

This shows that the average intensity of the scattered wave pressure is equal to the product of the frequency dependent factor

$$\frac{\omega^2\rho_o^2A_o^2k^4V}{4\pi^2r^2}$$

and the 3-dimensional spatial Fourier transform of the correlation function of the refractive index fluctuations. If the correlation function is independent of direction, eq. (17) takes the form

$$\overline{|\phi_1(\underline{r},k)|^2} = \frac{A_o^2k^3V}{4\pi\sin(\frac{\nu}{2})}\int_0^d \rho B_{n_1}(\rho)\sin(K\rho)d\rho \tag{18}$$

which is analogous to the well-known relation developed for x-ray diffraction studies of materials [12].

[4]The bar represents an ensemble or statistical average.

Our analysis permits measurements of $\phi_1(\underline{r},k)$ or $|\phi_1(\underline{r},k)|^2$ to be interpreted in terms of the refractive index variations and is based on volume scattering. Although specular reflections which are usually much larger than volume echoes can mask volume signals arising from near interfaces, the method can, in principle, be applied to regions where the scattering volume does include interfaces. In addition, principles discussed here may also be applied to the measurement of surface roughness.

The transform relation between the velocity potential and acoustic refractive index fluctuations enables us to relate measurements of scattered ultrasound signal to tissue structure in a way analogous to x-ray crystallography. Since the wave vector $\underline{K}$ can be varied by changing angle or wavelength, measurements of the scattered wave potential obtained either by varying angle or by frequency scanning can be used to deduce structure. For example, in the classic flat plate x-ray diffraction experiment from isotropic materials such as liquid metals [13], circular ring patterns appear on film as a result of interference of x-rays scattered by nearby centers. Measurements of ring diameters and knowledge of geometry and x-ray wavelength allow computation of scattering center separations and, thus, a determination of material structure. In the acoustic case, it is convenient to use a single transducer as a point detector instead of film to map out the scattering pattern. This mapping can be accomplished in a way directly analogous to the film detector by moving the transducer around the sample or, alternatively, by sweeping frequency with the transducer fixed.

The foregoing theory can be extended to show the effect of absorption, which is known to be appreciable in tissue [3]. The development of expressions for velocity potential and average intensity considers the Helmholtz equation with a complex wave number, *i.e.*,

$$\frac{\omega^2}{c_c(\underline{r})} = k_c^2(\underline{r}), \qquad k_c(\underline{r}) = k_R[1+n_1(\underline{r})] + ik_I[1+n_2(\underline{r})] \tag{19}$$

$$\overline{n_1} = \overline{n_2} = 0 \ ,$$

where n_1 and n_2 are variations in the real and imaginary parts of the complex index of refraction. The imaginary part of the wave number produces attenuation and allows absorption to be taken into account. The Helmholtz equation when the wave number is complex becomes

$$\nabla^2\phi(\underline{r},k) + [k_R^2-k_I^2+i2k_rk_I]\phi(\underline{r},k) = \{-2n_1(\underline{r})k_R^2+2n_2(\underline{r})k_I^2-i2k_Rk_I[n_1(\underline{r})+n_2(\underline{r})]\}\phi(\underline{r},k) \tag{20}$$

where

$$k_R^2 - k_I^2 + i2k_Rk_I$$

represents bulk average properties. Proceeding as in the lossless case, the following expressions for scattered wave potential and intensity result for unit amplitude:

$$\phi_1(\underline{r},k) = \frac{k_R^2 e^{-k_I r} e^{ik_R r}}{2\pi r} \int_{V'} f(\underline{r}') e^{-\underline{K}_I\cdot\underline{r}'} e^{i\underline{K}_R\cdot\underline{r}'} \, dV' \tag{21}$$

$$|\phi_1(\underline{r},k)|^2 = \frac{k_R^4 e^{-2k_I r}}{4\pi^2 r^2} \int_{V'} \int_{V'} f(\underline{r}'_1) f^*(\underline{r}'_2) e^{-\underline{K}_I \cdot (\underline{r}'_1 + \underline{r}'_2)} e^{i\underline{K}_R \cdot (\underline{r}'_1 - \underline{r}'_2)} dV'_1 dV'_2 \tag{22}$$

where

$$f(\underline{r}') = n_1(\underline{r}') - \left(\frac{k_I}{k_R}\right)^2 n_2(\underline{r}') + i\left(\frac{k_I}{k_R}\right)[n_1(\underline{r}') + n_2(\underline{r}')]$$

and

$$k_R(\underline{n}-\underline{m}) = \underline{K}_R, \; k_I(\underline{n}-\underline{m}) = \underline{K}_I$$

Since

$$k_R >> k_I$$

and the real fluctuations in acoustic refractive index are expected to be on the order of those in the imaginary part, eqs. (21) and (22) may be approximated as

$$\phi_1(\underline{r},k) = \frac{k_R^2 e^{-k_I r} e^{ik_R r}}{2\pi r} \int_{V'} n_1(\underline{r}') e^{-\underline{K}_I \cdot \underline{r}'} e^{i\underline{K}_R \cdot \underline{r}'} dV' \tag{23}$$

and

$$\overline{|\phi_1(\underline{r},k)|^2} = \frac{k_R^4 e^{-2k_I r}}{4\pi^2 r^2} \int_{2V'} e^{i\underline{K}_R \cdot \underline{\rho}} B_{n_1}(\underline{\rho}) \times \left[e^{-2\underline{K}_I \cdot \underline{r}} \int_{V'(\underline{\rho})} e^{-i\underline{K}_I \cdot \underline{\rho}} dV' \right] dV'_\rho \tag{24}$$

where $B_{n_1}(\underline{\rho})$ again represents the correlation of the real part of the acoustic refractive index variations and the correlation function is windowed by the bracketed function which contains the effects of absorption on the Fourier integral. Evaluation of the window for a rectilinear scattering volume in a Cartesian coordinate system chosen as in the lossless case yields

$$\prod_{\ell=0}^{3} \frac{1}{K_{I_\ell}} \sinh\left[K_{I_\ell} L_\ell \left(1 - \frac{|\rho_\ell|}{L_\ell}\right)\right]$$

which decays faster than the window in the lossless case and also has a rate of decay that increases with frequency.

Equations (23) and (24) show that, to within the approximation of $|k_I|/|k_R| << 1$, only the real variation in refractive index gives rise to scattering. The effects of absorption are to reduce high frequency components of the scattered waves and to give more weight to scattering from closely-spaced centers. The real negative exponential terms outside the integrals represent attenuation through the medium.

3. Experiments

The relations that have been developed in the preceding section show that measurement of the scattered pressure as a function of the scattering vector $\underline{K}$ can be processed to yield tissue structure information. Although $\underline{K}$ can be varied either by changing angle or frequency, frequency scanning appears more advantageous for clinical use because the same transmission path is always used and path variations are avoided.

A system (fig. 2) that permits frequency scanning of tissue specimens has been assembled (fig. 3). The transmitter consists of a variable frequency oscillator, adjustable

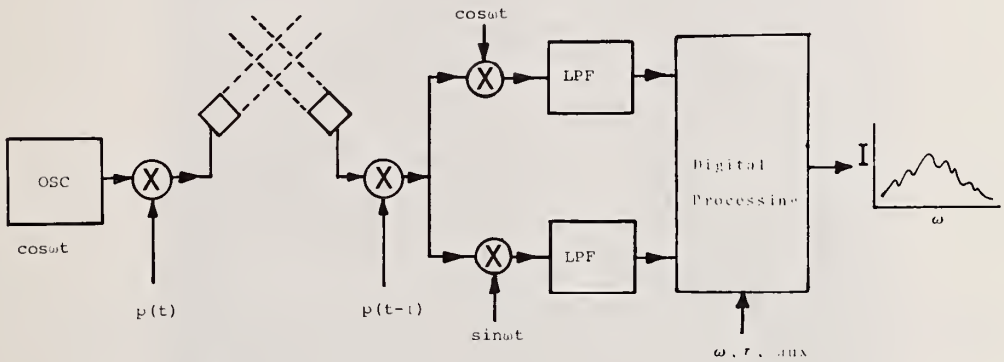

Figure 2. Instrumentation block diagram. The transmitter (left) consists of a variable frequency oscillator (OSC) which is gated to the transducer by a variable length pulse, p(t). The received signal is range-gated by p(t-τ) and its quadrature components are envelope detected and recorded digitally along with range (τ), frequency (ω), and target identification information (aux) for the computation of swept-frequency spectra, I (right).

pulse width gate, and a power amplifier. The center frequency, which is essentially constant over several pulses, is slowly swept from 1 MHz to 10 MHz. The receiver employs a wideband, high-gain RF amplifier, a range gate with variable width and delay, and a quadrature detector. The two output signals of the quadrature detector along with range and frequency information are sampled by high speed A/D conversion equipment under computer control and are recorded on disk or magnetic tape. The form of the data is thus convenient for subsequent digital processing and analysis. The tissue sample is mounted on a stage that can be moved laterally and vertically between two supports holding the transducers. Data was collected using wideband 1/2" diameter transducers. The distance between transducers and scattering target was always about 10 cm.

Aluminum plates were employed to demonstrate that structure information on the order of a wavelength can be obtained by frequency scanning. Sound reflecting from the front and back surfaces of the plates produced interference effects (fig. 4) from which plate thickness could be calculated using the known geometry and speeds of propagation. These highly-reproducible patterns may be used for calibration of instrumentation before data is obtained from randomly-organized scatterers.

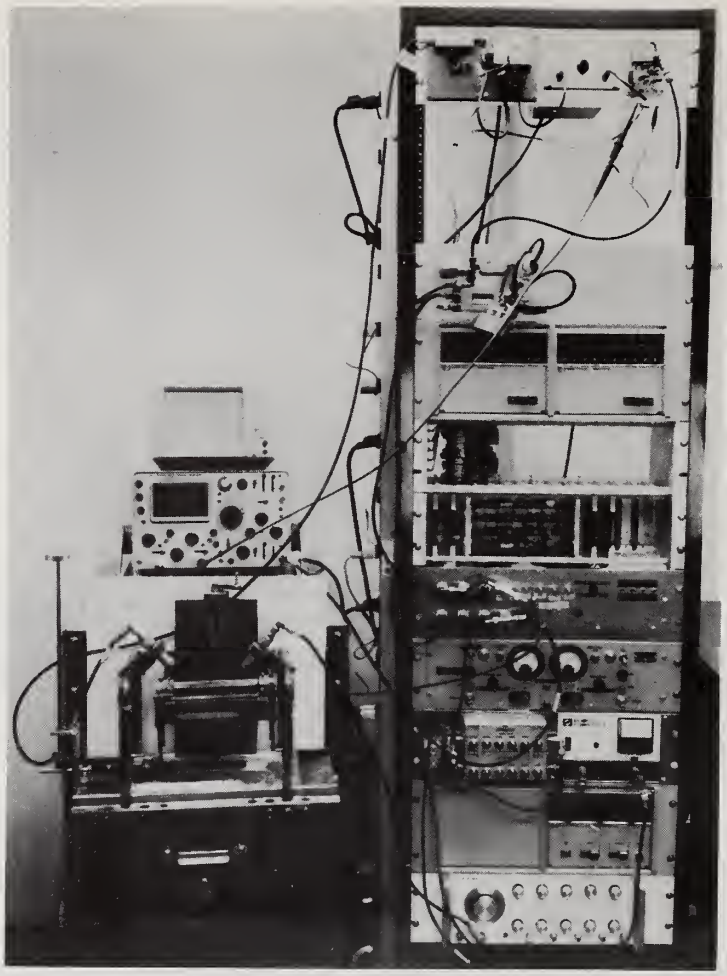

Figure 3. Swept-frequency hardware. The rack of instrumentation generates, amplifies, and detects swept-frequency ultrasound. It develops range, frequency, and quadrature received signals for digital processing and recording. A tissue handling stage, ultrasound transducers, and monitor oscilloscopes are displayed on the left. (Reproduced from Gramiak, R., and Waag, R. C.: *Cardiac Ultrasound*, The C. V. Mosby Co., St. Louis Mo., 1975).

Swept-frequency scattering data was also obtained from Sephadex[5] suspensions. Whereas individual spectral sample functions are highly random (fig. 5), averages of frequency scans (fig. 6) from two different sizes of particles clearly demonstrate the effects of particle size on the frequency spectrum.

Both normal and diseased liver specimens have been examined with swept-frequency ultrasound. Liver was chosen because of its clinical importance and because its relatively large homogeneous size permits frequency scanning of many independent sample volumes. Uniform slices from the right lobe were obtained at autopsy and mounted on the movable stage. The transducers were oriented to give a $\underline{K}$ vector direction 4 degrees from normal and minimize surface scattering. The common volume of transmit and receive beams was set at 1.0 cm below the tissue surface by means of a 10 μs wide receiver gate beginning

[5]Sephadex consists of cross-linked dextran particles which absorb water and scatter weakly.

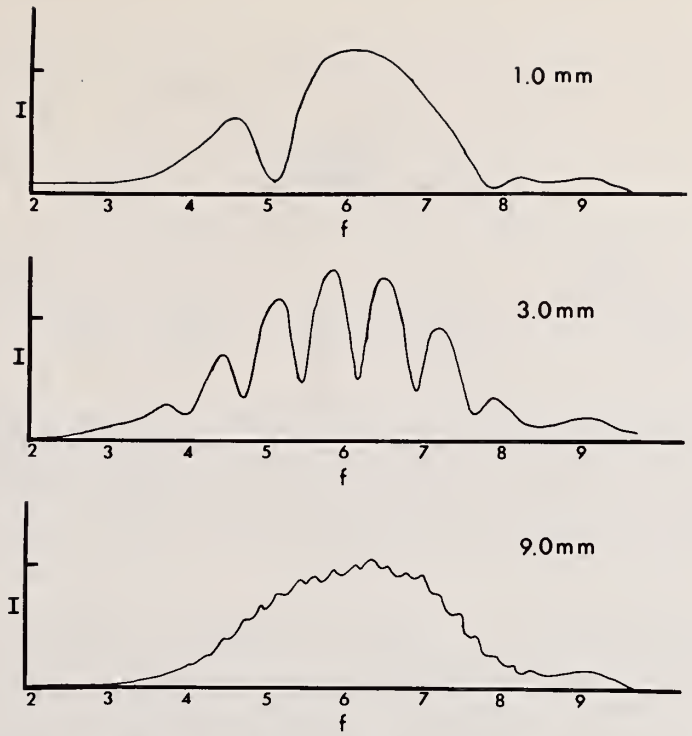

Figure 4. Scattering from aluminum plates. Received pressure intensity, I, as a function of frequency (in MHz) for 1.0 mm, 3.0 mm, and 9.0 mm thicknesses. The absolute values of nulls and the spacings closely conform to predictions obtained using the velocity of shear waves in aluminum.

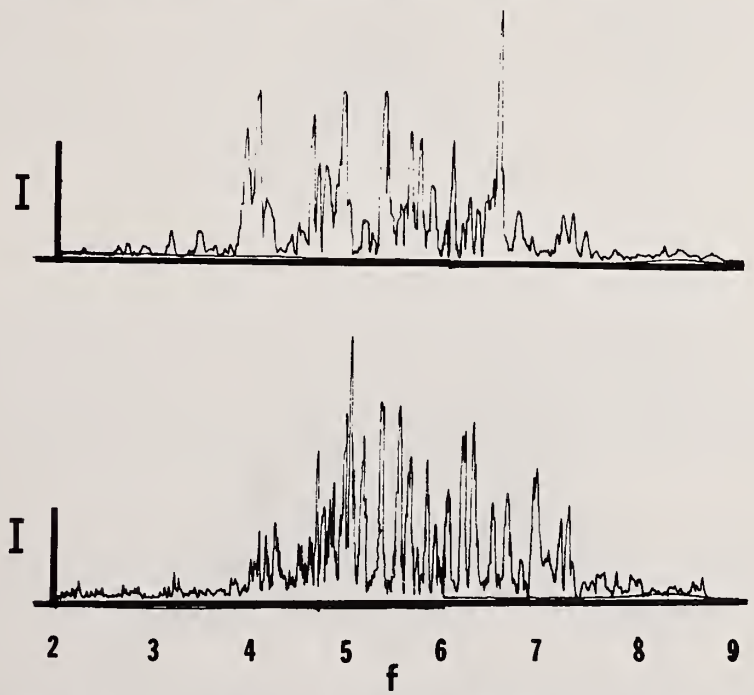

Figure 5. Sample scattering spectra from random media. Scattered intensity, I, as a function of frequency (in MHz) for a single statistical realization of 200 micron (upper) and 60 micron (lower) Sephadex particles. Intensity fluctuations obscure the increased scattering at higher frequencies by smaller particles that is revealed by ensemble averaging.

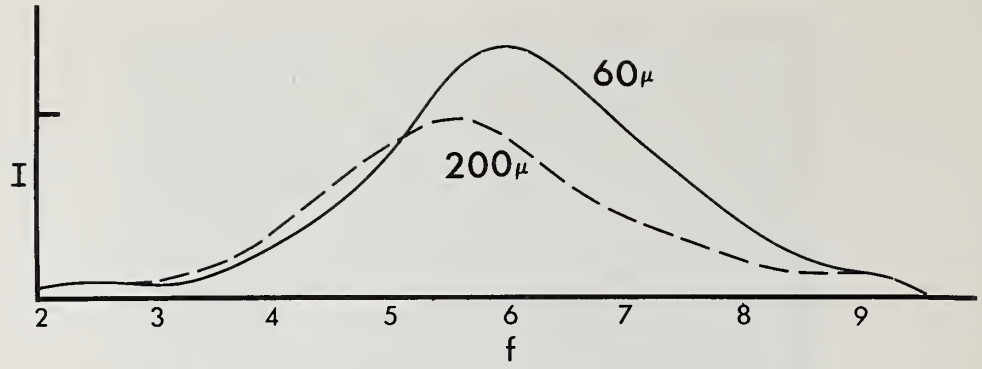

Figure 6. Size-dependent scattering in random media. Average received intensity, I, as a function of frequency (in MHz) for scattering from two different Sephadex sizes. The data, which was obtained by averaging 6 swept-frequency runs for each particle size, has a variance of about 15% of the distance from the horizontal scale to the vertical scale mark. The predicted increase in intensity for smaller scatterers at high frequency is evident.

at 108 μs after a transmitted pulse. The stage was adjusted vertically so that surface scattering occurred at a delay of 100 μs from the emission of a pulse. A 6 μs transmitted pulse length was chosen to avoid surface effects while maintaining maximum power. A typical experiment consisted of recording swept-frequency spectra at 28 horizontal positions spaced 1.4 mm apart. Swept-frequency data from normal liver and livers showing cirrhosis and infiltration with myelogenous leukemia have revealed marked differences in spectra from both single (fig. 7) and averaged (fig. 8) scans.

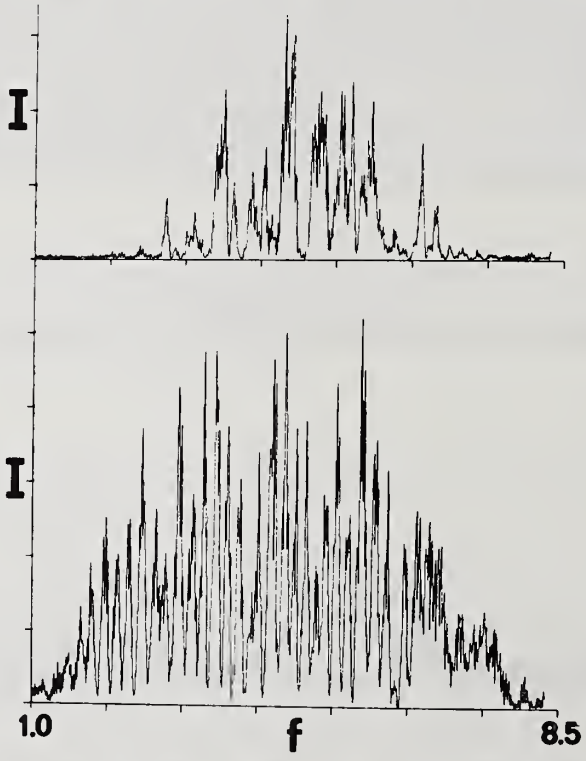

Figure 7. Sample scattering spectra from liver. Single normalized scattered intensity spectra realizations obtained from a normal (upper) and cirrhotic (lower) liver. The differences in periodicities in the spectra suggest that the cirrhotic liver contained scattering centers which were more regular and more widely spaced than in the normal liver.

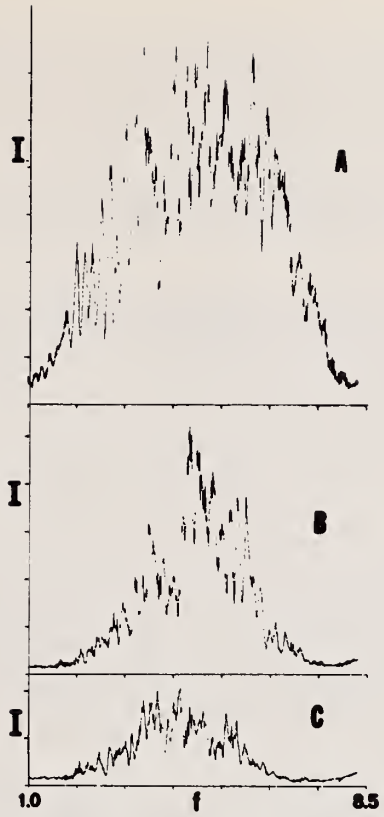

Figure 8. Averaged scattering spectra from liver. Scattering from a cirrhotic liver is shown in A while B represents scattering from a normal specimen and C is scattering from a liver infiltrated by myelogenous leukemia cells. In each display, the spectra is plotted on the same intensity (I) scale and is the result of averaging 28 runs in which the frequency (f) was swept from 1.0 to 8.5 MHz. The three curves differ in both relative signal level as well as distribution of peaks as a function of frequency.

4. Discussion

4.1 Experimental Results

The measured spectra obtained from aluminum plates demonstrate the inverse relationship between plate thickness and interference periodicity in the frequency or K domain. The data from the aluminum plates is in close agreement with predictions from an optical model developed for wave interference in thin films [14] when the locations of peaks and spacings are computed using the speed for shear wave propagation in aluminum. Longitudinal waves did not propagate in the experimental configuration because the incident wave arrived at greater than the critical angle.

The data from the Sephadex experiments agrees qualitatively with the predictions of an expression describing scattering from a cloud of particles [15]. The expression predicts that smaller particles will scatter more power at higher frequencies than larger particles. This is evident in the smoothed spectra which do not contain the fluctuations present in a single swept-frequency run.

Volume scattering data from various livers indicates structural differences which may be related to pathology. Scattered power from the one specimen of cirrhotic liver that we examined was significantly greater than that from the one normal. This wideband finding is consistent with A-mode results obtained by others [16]. The higher collagen content of cirrhotic liver may be responsible for increased scattered power since elasticity increases locally with collagen infiltration. Individual frequency scans of the cirrhotic liver

showed significant periodicities which are different from those observed in normal tissue. The cirrhotic liver data implies a mean scatterer spacing considerably greater than for the normal liver tissue. Additional studies are needed to correlate acoustic structural differences with histological determinations of structure.

The one liver with myelogenous leukemia cells that we examined scattered less power than the normal liver. This reduced scattering is probably due to invasion of leukemia cells altering the structure.

Further investigation is required to determine the specific structural changes observed acoustically and establish the reproducibility of the results that we have obtained from these studies of three individual liver specimens.

4.2 Theoretical Limitations

There are a number of constraints which may affect the experimental determination of tissue structure with ultrasound. Angle scanning and frequency scanning yield equivalent information only when the medium is isotropic. Thus, in studies of anisotropic media, knowledge of structure orientation is needed to relate angle and frequency scanning results.

A far-field approximation is made in the model, but experimental conditions may not always satisfy this approximation. In our experimental configuration, the Fraunhofer condition was not satisfied at the high end of the frequency scans. However, even though our data was not strictly from the far-field, the results obtained from aluminum plates showed good agreement with far-field predictions. This implies that the far-field condition which simplifies analysis may be more stringent than necessary to obtain meaningful tissue characterization with ultrasound.

The finite extent of a physical receiver produces a signal that is a summation of the incident spherical wave over its surface area, while the Fourier-transform relations between scattered signal and variations in index of refraction have been derived for a point receiver. It is therefore desirable to choose the receiver aperture in conjunction with its distance from the scattering volume so that phase variations across the receiver face are negligible. Although this can be achieved in practice, our aluminum plate data showed good agreement with point receiver analysis even though significant cancellation was expected at the high frequency end of the scan. This implies that a point receiver requirement may also be unnecessarily restrictive for ultrasonic characterization of tissue.

Finite scattering volumes always exist in practice so that the interpretation of scattered pressure as a Fourier integral of the variations in index of refraction requires assignment of values over an infinite region. However, the assignment of zero values to refractive index outside the common volume may result in a smearing of the $\underline{K}$ value which is negligible for the dimensions of interest. For example, a typical $|\underline{K}|$ value at the midpoint of a scan is

$$\frac{2\pi}{\lambda} \sin\left(\frac{\nu}{2}\right) = 150 \text{ cm}^{-1}.$$

This value is broadened by convolution with a sinc function resulting from the common volume window. The widening is approximately given by the reciprocal beamwidth and, for the beams we used which are about 1 cm wide, the smearing is less than 1 part in a hundred.

Fourier inversion of the spectral data requires knowledge of the scattered pressure for all values of $|\underline{K}|$. The highest usable frequency is limited by tissue absorption which increases linearly with frequency, while resolution limits the lowest frequency for scanning. Although increased range of $|\underline{K}|$ may be achieved by altering the scattering angle in addition to sweeping the frequency, data covering only a finite range of $|\underline{K}|$ can be obtained in practice. This data may be inverted using a known functional dependence to extend it outside the measurement range or by assuming zero values which may smear the transform function. Laboratory studies employing angle and frequency scanning are necessary

to determine important ranges of $\underline{K}$ for tissue characterization and identification of various abnormal structures resulting from disease processes.

In the analytical model, sine wave excitation was assumed for convenience. However, finite length pulses are used in experiments to provide more control of scattering volume. The error introduced by finite pulse duration is a spectral broadening resulting from convolution with the transform of the gate function and can be made small. For example, at a carrier frequency of 5 MHz, spectral broadening due to a gate length of 10 μs is about 100 kHz and introduces less than 2% uncertainty in the frequency.

Pulse-to-pulse averaging employed to increase signal-to-noise ratio with swept-frequency measurements introduces a slight error because all the pulses in the averaging window do not have exactly the same frequency. This is not a fundamental limitation because frequency can be changed in steps with the averaging window or the sweep can be made slow enough to maintain the error below any specified limit. For a sweep rate of 1 MHz/s and an averaging time of 100 ms, the frequency shift is 100 kHz over the averaging interval and results in an error of less than 2% at 5 MHz.

5. Conclusion

A general theory has been developed to characterize tissue structure from data obtained in ultrasound scattering experiments. The basic relation is that the scattered pressure at a given scattering vector is the Fourier component of the refractive index fluctuation. Thus, by sweeping frequency, the magnitude of the scattered wavevector is varied and a spectrum of the refractive index fluctuations may be obtained for statistically-isotropic tissue. Angle scanning may also be used to vary the scattering wavevector and this may give useful information for anisotropic tissue.

Swept-frequency experiments with known deterministic and random media have shown the promise of the concept. Preliminary data from swept-frequency experiments with normal and diseased liver tissue show that this technique may lead to a useful diagnostic tool. However, additional data is needed to characterize tissue more completely and thus point the way to optimum parameters for clinical determinations of tissue structure with ultrasound.

References

[1] *Animal Sonar Systems: Biology and Bionics*, Vols. I & II, G.-G. Busnel, ed., (Jony-en-Josas-78, France: Laboratoire de Physiologie Acoustique, 1966).

[2] Wild, J. J. and Reid, J. M., Further pilot echographic studies on the histologic structure of tumors of the living intact human breast, *Am. J. Path.* 28, 829 (1952).

[3] Gregg, E. C. and Palagallo, G. L., Acoustic impedance of tissue, *Invest. Radiol.* 4, 357 (1969).

[4] Dunn, F., Edmonds, P., and Fry, W., Absorption and dispersion of ultrasound in biological media, in *Biological Engineering*, H. Schwan, ed. (McGraw-Hill, Inter-University Electronic Series, Vol. 9, 1969).

[5] Baum, G., Quantized ultrasonography, in *Recent Advances in Diagnostic Ultrasound*, E. Rand, ed. (C. C. Thomas, Springfield, Ill., 1971).

[6] Ossoinig, K. C., Quantitative echography - the basis of tissue differentiation, *J. Clin. Ultrasound*, 2, 33 (1974).

[7] Namery, J. and Lele, P. P., Ultrasonic detection of myocardial infarction in dog, in *Proceedings of 1974 Ultrasonics Symposium*, p. 491 (IEEE Cat. No. 72 CHO 708-8 SU, 1974).

[8] Chivers, R. C., Hill, C. R., and Nicholas, D., Frequency dependence of ultrasonic backscattering cross-section: an indicator of tissue structure characteristics, in *Ultrasonics in Medicine*, M. de Vlieger, D. N. White, and V. R. McCready, eds., p. 300 (Excerpta Medica, Amsterdam, 1974).

[9] Jones, J. P., Impediography: a new ultrasonic technique for diagnostic medicine, presented at the Nineteenth Annual Conference of the American Institute of Ultrasound in Medicine, 5-10 October 1974, Seattle, Washington.

[10] Waag, R. C. and Lerner, R. M., Tissue macrostructure determination with swept-frequency ultrasound, in *Proceedings of 1973 Ultrasonics Symposium*, p. 63 (IEEE Cat. No. 73 CHO 807-8 SU, 1973).

[11] Fields, S. and Dunn, F., Correlation of echographic visualizability of tissue with biological composition and physiological state, *J. Acoust. Soc. Am.* 54, 809 (1973).

[12] Azaroff, L. V., Kaplow R., and Kato, N., *X-Ray Diffraction*, p. 85 (McGraw-Hill, Inc., New York, 1974).

[13] Kakudo, M. and Kasai, N., *X-Ray Diffraction by Polymers*, (American Elsevier Publishing Co., New York, 1972).

[14] Jenkins, F. A. and White, H. E., *Fundamentals of Optics*, 3rd edition, p. 273 (McGraw-Hill, Inc., New York, 1957).

[15] Morse, P. M. and Ingard, K. U., *Theoretical Acoustics*, p. 439 (McGraw-Hill, Inc., New York, 1968).

[16] Mountford, R. A. and Wells, P. N. T., Ultrasonic liver scanning: the A-scan in the normal and cirrhosis, *Phys. Med. Biol.* 17, 261 (1972).

CHAPTER 7

IMPEDANCE PROFILE TECHNIQUES

National Bureau of Standards Special Publication 453. Proceedings of Seminar on Ultrasonic Tissue Characterization held at NBS, Gaithersburg, MD, May 28-30, 1975. (Issued Oct. 1976)

CHAPTER 7. IMPEDANCE PROFILE TECHNIQUES

Paper 7.1: ACOUSTIC IMPEDANCE PROFILING: AN ANALYTICAL AND PHYSICAL MODEL STUDY*

A. C. Kak

School of Electrical Engineering
Purdue University
West Lafayette, Indiana 47906

and

F. J. Fry

Fortune-Fry Laboratories
Indianapolis Center for Advanced Research
Indiana University Medical Center
Indianapolis, Indiana 46202

Qualitative measurements of the acoustic impedance of tissue have been extensively exploited for medical diagnosis. In this paper, we report on an analytical and physical model study directed towards quantifying this parameter. The model selected is a medium having plane-parallel impedance interfaces which is insonified at normal incidence. Analytical expressions and computer algorithms are given for determining the impulse response of the medium and the impedance profile from this impulse response. Experimental data are presented which shows the accuracy with which the method can presently be applied.

Key Words: Attenuation; computer; deconvolution; impedance; impulse response; layer model; lucite; ultrasound.

1. Introduction

Acoustic characterization of living tissue in a quantitative manner should be of considerable significance to diagnostic medicine. The ability to accurately classify tissue types in a non-invasive atraumatic manner is the sought-after goal. A variety of acoustic techniques offer possibilities for tissue characterization, hopefully leading to precise identification. Since no one acoustic parameter is likely to qualify as a unique determinant in tissue characterization, it is important to assess a number of acoustic properties in an attempt to identify indices which may be definitive. Under the circumstances presented in clinical diagnostic medicine, as differentiated from laboratory measurements on excised specific tissue types, it is apparent that considerable problems exist if an attempt is made to uniquely define only one specific acoustic parameter. Acoustic impedance profiling is an example typifying this difficulty. In order to derive this parameter, we consider a physical model of a lossless medium having acoustic impedance transitions associated with discrete plane-parallel interfaces and an interrogating acoustic pulse normally incident on these interfaces. The theory of linear systems implies applicability of the superposition integral which operationally convolves the impulse response of the system with the input interrogating waveform to yield the output waveform. Thus, we can derive the impulse response from a knowledge of the input and output waveform. From this impulse response, the impedance profile for the idealized model can be derived in a rigorous manner.

*Work supported by National Institute of Health Contract NO1-NS-3-2319.

In any tissue or organ system, however, the medium is always lossy. This attenuation loss is composed generally of a number of components (*viz.*, intrinsic absorption, scattering). An average value of absorption loss of soft tissues of the human body is 1 dB per centimeter of path length at 1 MHz frequency. Soft tissues also show an approximately linearly-increasing absorption loss as a function of frequency. Since there is a characteristic frequency dependence of attenuation in tissue, it is apparent that the temporal character of the acoustic interrogating pulse will be modified depending on its bandwidth as it passes through the tissue. Thus, in order to arrive at an appropriate acoustic impedance profile for medically-relevant systems, practical methods must be developed which will permit the simultaneous determination of the attenuation profile and the impedance profile. In this work, the attenuation losses have been inserted in an *a priori* fashion and the impedance values computed for the model material. Individual layer thickness variations with variable amounts of insertion loss are computed from a determination of the transit time between interfaces after an *a priori* insertion of sound velocity for individual layers.

Another approximation made in the idealized model is to ignore higher-order reflections. This approximation would be valid for tissues and organs which possess sufficient absorption to highly attenuate such reflections. The rationale for using an idealized layer model is based on a number of factors including the fact that, to the present, substantially all medical diagnostic procedures using ultrasound have relied heavily on a qualitative interpretation of acoustic impedance differences at tissue interfaces. Conceptually, the individual layer methodology can be extended to include any number of reflective targets in a tissue or organ system. It seems appropriate to perform the necessary research leading to a more quantitative description of acoustic impedance as it seems apparent that this will be one of the parameters of significance in a quantitative approach to differential diagnosis of disease.

Methods of signal processing and computer technology have been applied to acoustic interrogating pulses in this study so that ultimately real time, or near real time, quantitative descriptions of acoustic impedance profiles will be possible. Detailed descriptions of the analytic approach to the layered model, specific algorithm considerations and computer simulation studies are discussed later. The algorithm implemented for impulse response determination for the experimental studies uses the matched filtering technique which is applicable to a large class of acoustic waveforms.

The first major subdivision presents the analytical descriptions, from a physical acoustics viewpoint, signal processing methods and computer simulations. Experimental results are presented in the second major subdivision.

2. Relationship between the Impedance Profile and the Impulse Response

2.1 No Multiple Reflections and Lossless Media

Let us consider a target interrogated by a plane acoustic wave. In the linear regime of operation, the reflected wave can be considered to be a convolution of the input signal and an impulse response associated with the medium. (This is also true for the transmitted wave for some different impulse response.) This impulse response is strictly a property of the medium in the direction of propagation of the incident wave. Relationships between the impulse response and the impedance profile of a medium have been a matter of investigation in the past [1,2][1]. The relationships that have been developed in these investigations are iterative in nature. By this we mean a medium is considered to be composed of a large number of layers, each of constant acoustic impedance, and one calculates the impedance of one layer at a time starting from the first. The accuracy of the calculation at each step depends upon how accurately the previous impedance values have been calculated. In practice, these techniques cannot often be used because their recursive iterative nature is a source of instability.

Non-recursive relationships are a topic of current research. In a recent paper by Jones [3], one such relationship was presented for the restricted case of monotonically-

[1]Figures in brackets indicate the literature references at the end of this paper.

increasing or decreasing impedance profiles in the absence of multiple reflections. We will now show that the same relationship holds for any arbitrary impedance profile. We will first rederive the non-iterative relationship for the monotonically-increasing profile by a method different from that given by Jones. The derivation given here provides insight for the general case of arbitrary impedance profiles, which will be presented later.

Let a monotonically-increasing or decreasing profile be approximated by discrete layers of constant impedance. Evidently, as the number of layers in such an approximation approaches infinity for an acoustic target of finite extent, the impulse response calculated from the discrete approximation should approach that from the continuous profile. The discrete approximation may be constructed in such a way that the reflection coefficient at each impedance boundary is the same; let this value be denoted by r. It is easily seen that the impulse response of such a discrete profile is a train of impulses. Let the time instances at which the reflected impulses are received be denoted by t_1, t_2, t_3, ... If $h(t_m)$ denotes the strength of the reflected impulse at t_m, then it can be shown that

$$h(t_m) = r(1-r^2)^{m-1} \quad . \tag{1}$$

Let us integrate the impulse response from 0 to a time t with $t_m \leq t < t_{m+1}$. Then

$$s(t) = \int_0^t h(t)\, dt = \sum_{k=1}^{m} r(1-r^2)^{k-1} \quad . \tag{2}$$

Substituting (1) in (2), we get

$$s(t) = \frac{1-(1-r^2)^m}{r} \quad . \tag{3}$$

For a given t as $m \to \infty$ and $r \to 0$, the discrete impedance profile will approach the continuous profile. As $m \to \infty$, the time intervals between successive reflections from the impedance discontinuities approaches zero, so that t_m approaches t. Also, as $m \to \infty$, r must approach zero in such a way that the following is always satisfied [4]

$$m = \frac{\log z_m}{\log \frac{1+r}{1-r}} \tag{4}$$

where $Z_m = Z_m/Z_o$, Z_m being the impedance of the mth layer in the discrete profile, and Z_o the impedance of the water bath in which the target is immersed. Substituting (4) in (3) and taking the limit $r \to 0$, we get the following result (for details see [4])

$$s(t) = \int_0^t h(t)\, dt = \frac{1}{2} \log \frac{Z_t}{Z_o} \tag{5}$$

where Z_t is the acoustic impedance of the medium at a point where the acoustic impulse arrives in t/2 seconds (we assume the medium to be non-dispersive).

In deriving the impulse response-impedance profile relationship given by (5), we assumed in the discrete approximation that all reflection coefficients are equal. This assumption constrains the impedance profile to be either monotonically-increasing or decreasing. We will now show that the equation (5) is valid even when the impedance profile does not satisfy this condition. We will continue to assume the absence of multiple reflections. In the discrete approximation of a continuous medium, let r_k be the reflection coefficient at the kth step, the kth step being a transition from impedance Z_{k-1} to Z_k.

By definition,

$$r_k = \frac{Z_k - Z_{k-1}}{Z_k + Z_{k-1}} \tag{6}$$

Clearly,

$$z_m = \frac{Z_m}{Z_o} = \prod_{k=1}^{m} \frac{1+r_k}{1-r_k} . \tag{7}$$

As the continuous medium is approximated by increasingly finer steps, each $r_k \to 0$. In such a limit, each $\log (1+r_k)/(1-r_k) \to 2r_k$ and, therefore, from eq. (7), we get

$$\left(\log z_m\right)_{r_k \to 0} = 2 \sum_{k=1}^{m} r_k . \tag{8}$$

Again, in the absence of multiple reflections, each

$$h(t_k) = r_k \prod_{\ell=1}^{k-1} (1-r_\ell^2) . \tag{9}$$

As each $r_\ell \to 0$, we get from (9) and (7)

$$\log h(t_k) - \log h(t_{k-1}) = \log\left[\frac{1}{2} (\log z_k - \log z_{k-1})\right] - \log\left[\frac{1}{2} (\log z_{k-1} - \log z_{k-2})\right] - \frac{1}{4}\left[\log z_k - \log z_{k-1}\right]^2 .$$

The normalized impedance z is a function of distance. It can also be considered to be a function of time, in the sense z(t) is the impedance of the medium at a position which the incident wave takes t/2 seconds to arrive at. In fact, in the absence of any knowledge of acoustic velocities in the medium, the best one can do is to find the impedance profile as a function of time. Let $\Delta t = t_k - t_{k-1} = t_{k-1} - t_{k-2} = \ldots$; then

$$\Delta t \frac{\log h(t_k) - \log h(t_{k-1})}{\Delta t} = \log\left[\frac{\log z_k - \log z_{k-1}}{\Delta t}\right] - \log\left[\frac{\log z_{k-1} - \log z_{k-2}}{\Delta t}\right] - \frac{(\Delta t)^2}{4}\left[\frac{\log z_k - \log z_{k-1}}{\Delta t}\right]^2 . \tag{11}$$

As $t \to 0$, we get from the above equation

$$h(t) = C \frac{d}{dt} \log z(t) \tag{12}$$

where C is a constant of integration. To evaluate this constant, we make use of the boundary condition that for some non-zero distance near the first change in impedance, the impedance variation is increasing or decreasing, making eq. (5) valid for times t that correspond to reflections from such regions. This implies C = 1/2. Substituting this in eq. (12)

and integrating, we get

$$\int_0^t h(\tau)\, d\tau = \frac{1}{2} \log \frac{Z(t)}{Z_o} \tag{13}$$

which completes the proof.

2.2 Multiple Reflections Included

In the derivations in the preceding subsections, we assumed that multiple reflections made negligible contributions to the reflected waveform at the receiver. There are experimental situations where such an assumption would be justified. For illustration, consider a medium in which the impedance changes in discrete steps, and let all these changes be of equal magnitude. The reflection coefficients at each impedance change will then be the same and let r denote their value. It is easily seen that the ratio of third-order reflections to first-order reflections is proportional to r^2, the ratio of fifth-order to first-order reflections is r^4, and so on. Evidently, if r is equal to, let us say, 0.1, all the reflections higher than the first order can be neglected. By extending this argument, one concludes that so long as the total impedance change is small, and so long as its rate of change is small, neglecting higher-order reflections would introduce negligible error. In biological experiments, soft tissue with tumors would often satisfy this condition. But if the interrogation is made through bone, this assumption would be grossly violated.

We will now derive a relationship between the impulse response and the impedance profile for the case in which, in a discrete approximation to a continuous medium, all the reflection coefficients can be considered to be equal.

To find the effect of third-order reflections on $\int_0^t h(\tau)d\tau$, consider the pulse bounce diagram in figure 1. Each $I_{\tau,j}$ represents the amplitude of a positive traveling impulse through section $Z_{j-\tau-1}$ between times t_i and t_{i+1} where i is the largest integer less than or equal to $(j+\tau-1)/2$. From the pulse bounce diagram, it can be shown that $I_{j-k,j}$ has k-1 second-order reflections. Therefore, each $h(t_j)$ has $L(j) = 1 + 2 + \ldots + \ldots + (j-3) + (j-2) = ((j-2)(j-1))/2$ third-order reflection components, each component having an amplitude proportional to $-r^3(1-r^2)^{j-2}$. It is easily shown that each $h(t_j)$ is now given by

$$h(t_m) = r(1-r^2)^{m-1} - L(m)\, r^3(1-r^2)^{m-2} \tag{14}$$

where

$$L(m) = \frac{(m-2)(m-1)}{2} . \tag{15}$$

Therefore,

$$\int_0^t h(\tau)d\tau = \sum_{k=1}^{m} r(1-r^2)^{k-1} - \sum_{k=1}^{m} L(k)\, r^3(1-r^2)^{k-2} \tag{16}$$

where $t_m \leq t < t_{m+1}$. In the limit as the discrete profile becomes continuous, $r \to 0$ and $m \to \infty$ in such a way that eq. (4) is satisfied. The first term on the R.H.S. in (16) is the same as the expression in (2). The problem of finding the limit of this expression was rigorously solved earlier, the result being eq. (5). The result for this expression could also be obtained by a not-so-rigorous method by recognizing that as $r \to 0$ and $m \to \infty$, $(1-r^2)^{m-1} \to 1$. This makes the first term in (16) equal to mr. Now as $r \to 0$, we get from (4), $m \to 1/2r \log z_m$. This implies that as $r \to 0$ and $m \to \infty$, $mr = 1/2 \log z_m$, which when substituted in

$$\int_0^t h(\tau)\, d\tau = mr,$$

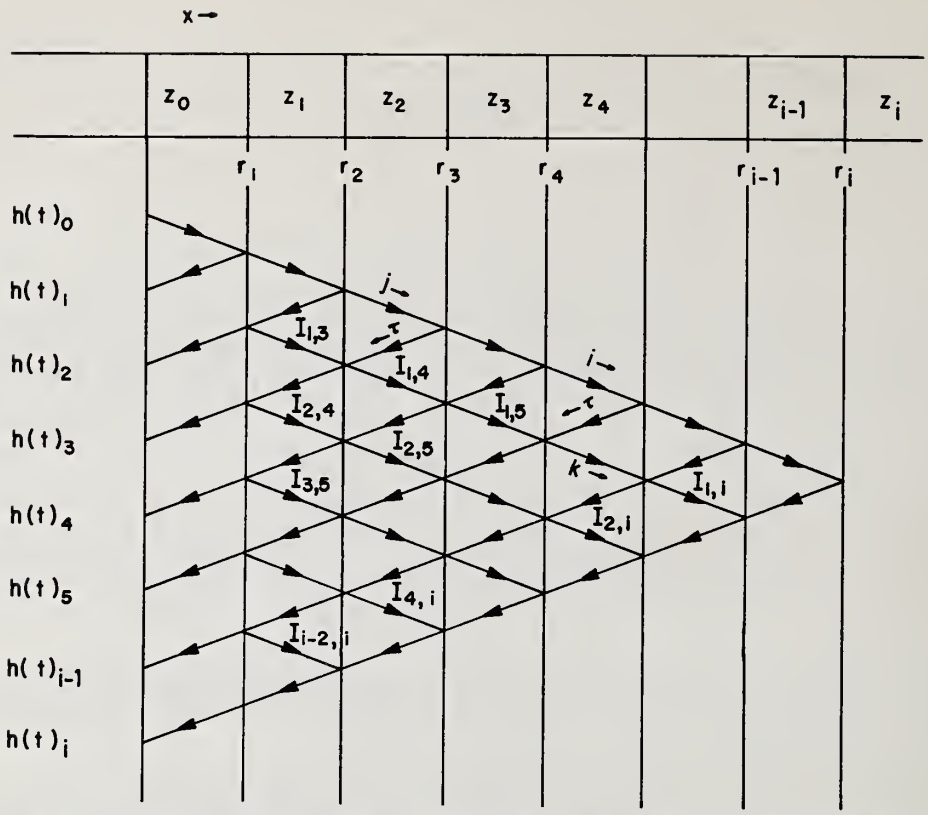

Figure 1. Pulse-bounce diagram for multiple reflections in a parallel-plane target of i layers.

leads to the same result as in (5). We will use this line of reasoning to find the limit of the second term. We can write in the limit $m \to \infty$ and $r \to 0$,

$$\int_0^t h(\tau)d\tau = mr - r^3 \sum_{k=1}^{m} L(m)$$

$$= mr - r^3 \frac{m(m-1)(m-2)}{6} \qquad (18)$$

where we have made use of (15). Since $m \to \infty$, the above expression becomes

$$\int_0^t h(\tau)d\tau = mr - \frac{(mr)^3}{6} \quad . \qquad (19)$$

Substituting (17) in (19) and recognizing that in the limit $t_m \to t$, we get

$$\int_0^t h(\tau)d\tau = \frac{1}{2} \log \frac{Z(t)}{Z_o} - \frac{1}{6}\left(\log \frac{Z(t)}{Z_o}\right)^3 \quad . \qquad (20)$$

It is immediately clear that in the presence of third-order reflections, the impedance profile is not uniquely related to the integral of the impulse response. We refer to uniqueness in the sense that eq. (20) is a cubic equation in log Z(t), therefore, in general, it has three roots for every t.

One can similarly derive non-recursive relationships of the type (20) which would include reflections of, say, nth order, the right-hand side in such a case being an nth

order polynomial in log Z(t). The futility of such an effort is clear from the fact that for any value of t, $\int_0^t h(\tau)d\tau$ would not yield a unique value for Z(t) because of reasons mentioned above.

Limitations such as above should not reduce the importance of eq. (13) which holds in the absence of multiple reflections. As had been mentioned, experimental situations of importance do exist which satisfy this condition.

3. Determination of the Impulse Response

If a treatment of the subject of the impedance profile determination was to be done in the order in which the data is processed, then the first topic to be discussed should be the calculation of the impulse response from the reflected waveforms. Our reason for first presenting the relationships between the impulse response and the impedance profile was to provide the reader with motivation for the material to be presented in this section.

If the incident and the reflected ultrasound waveforms in a given direction through a medium are considered an input and output, respectively, of a linear system, then by the theory of such systems the medium can be characterized by an impulse response in that direction. Let x(t) and y(t) denote the input and output waveforms, respectively. And let h(t) be the impulse response of the medium along the path of propagation. Then by the theory of linear systems,

$$y(t) = \int h(\tau)\, x(t-\tau)\, d\tau \ . \tag{21}$$

Evidently, given a knowledge of x(t) and y(t), the above integral equation can be solved for h(t). Depending upon the extent of *a priori* information available, the above equation can be solved by one of a large number of techniques that have been developed to date [5].

Let us consider the case in which the target can be assumed to be composed of a countable number of parallel layers. (In practice, for a focused transducer, this assumption need to be strongly satisfied only in the region of the focus.) The impulse response of such a target can be written as

$$h(t) = \sum_i A_i\ \delta(t-\tau_i) \tag{22}$$

where $\delta(t-\tau_i)$ represents an impulse located at $t = \tau_i$, and where, in the absence of multiple reflections, τ_i is the time at which the reflection from the ith discontinuity arrives at the receiver, the strength of this reflected impulse being A_i. Substituting (22) in (21), we get for the received waveform y(t):

$$y(t) = \sum_i A_i\ x(t-\tau_i) \ . \tag{23}$$

Given the received waveform, the aim is to estimate the values of the coefficients A_i. The waveform y(t) is in practice recorded in the presence of noise. Also, in the digital calculation of the impedance profiles, further noise is introduced by the sampling and quantization of the waveforms. If the noise can be considered to be white Gaussian, the following correlation technique yields the maximum likelihood estimate for the coefficients A_i. In the presence of colored noise, the optimality of the estimate can be preserved by using a prewhitening filter [6]. However, this case will not be treated here.

Multiplying both sides of (23) by $x(t+\tau)$ and integrating over the entire time axis, we get

$$R_{xy}(\tau) = \sum A_i R_{xx}(\tau-\tau_i), \tag{24}$$

where $R_{xy}(\tau)$ and $R_{xx}(\tau-\tau_i)$ are the cross-correlation and autocorrelation functions, respectively. If the cross-correlation function is sampled at $\tau = \tau_1', \tau_2', \tau_3', \ldots$, we can then generate a set of simultaneous equations given by

$$R_{xy}(\tau_1') = \sum A_i R_{xx}(\tau_1' - \tau_i)$$

$$R_{xy}(\tau_2') = \sum A_i R_{xx}(\tau_2' - \tau_i) \; . \qquad (25)$$

In practice, it is useful to take the sampling instant τ_i' equal to the corresponding τ_i. Substituting this in eq. (25), we get

$$\begin{bmatrix} R_{xy}(\tau_1) \\ R_{xy}(\tau_2) \\ \vdots \\ R_{xy}(\tau_N) \end{bmatrix} = \begin{bmatrix} R_{xx}(0) & R_{xx}(\tau_1 - \tau_2) & \cdots & R_{xx}(\tau_1 - \tau_N) \\ R_{xx}(\tau_1 - \tau_2) & R_{xx}(0) & \cdots & R_{xx}(\tau_2 - \tau_N) \\ \vdots & \vdots & & \vdots \\ R_{xx}(\tau_1 - \tau_N) & \cdots & & R_{xx}(0) \end{bmatrix} \begin{bmatrix} A_1 \\ A_2 \\ \vdots \\ A_N \end{bmatrix} . \qquad (26)$$

The coefficients A_i can thus be determined provided the τ_i are known. An analysis of the reflected waveform for the case of weakly-damped oscillatory inputs shows that the times τ_i correspond to the maxima of the envelope of the cross-correlation function $R_{xy}(\tau)$ with an uncertainty of a half a cycle. This is also true for non-oscillatory waveforms provided the smallest-layer transit time in a multilayer target is much greater than the effective duration of the incident waveform. (By oscillatory waveform, we mean narrow-band waveforms that take non-zero values over many cycles of oscillations. On the other hand, the term non-oscillatory waveform is not restricted to unipolar pulses but includes highly-damped waveforms one or two cycles in duration.) For target layer thicknesses large compared to a wavelength, the errors caused in the calculation of A_i by this assumption is negligible. In this case, the diagonal term in the matrix of coefficients in eq. (26) is much larger than the non-diagonal terms. (It is perhaps intuitively clear that as the ratio of the product of the diagonal terms in a matrix to the total determinant approaches unity, the calculations become more insensitive to the noise in the non-diagonal terms.) For illustration, we have shown in figure 2 an example of an oscillatory waveform,

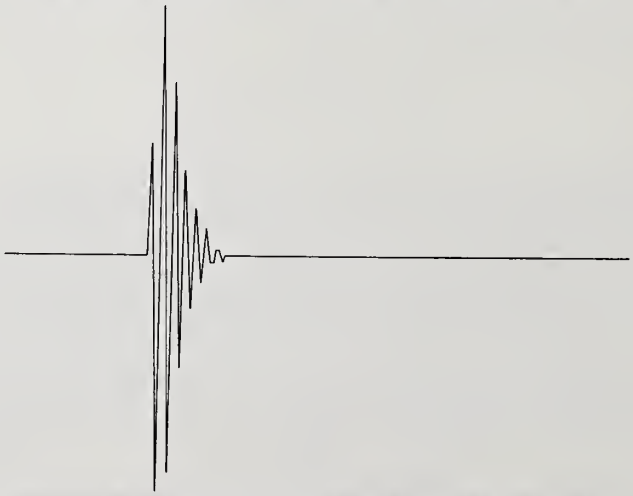

Figure 2. Incident waveform used with lucite-water-glass target.

x(t), that was used to interrogate targets for tissue profiling. In figure 3, we have shown the reflected waveform, y(t), from a lucite-water-glass target. Figure 4a shows the cross-correlation function $R_{xy}(\tau)$ for the waveforms in figures 2 and 3. The τ_i's required in eq. (24) were determined by first rectifying the cross-correlation function and then locating the peaks of the envelopes of the resulting function. The envelope function is shown in figure 4b.

Figure 3. Reflected waveform from lucite-water-glass target.

Figure 4a. Representation of $R_{xy}(\tau)$, the cross-correlation function.

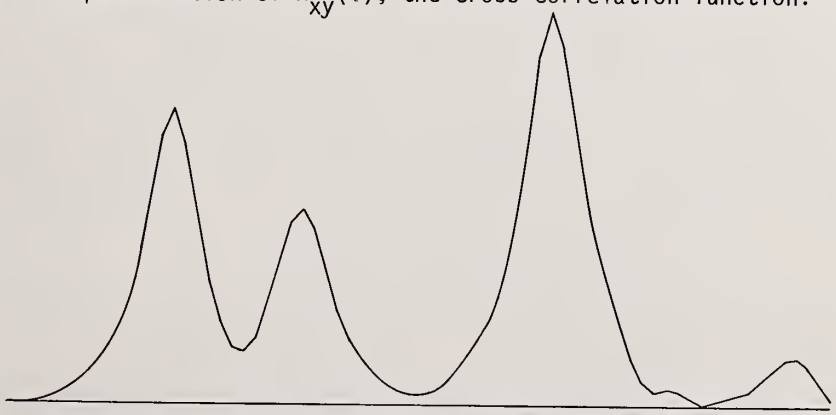

Figure 4b. Representation of $|R_{xy}(\tau)|$, the magnitude of the cross-correlation function.

For non-oscillatory waveforms, we have developed a new deconvolution procedure that appears very promising. This technique is essentially a modification of the direct deconvolution techniques to reduce their extreme sensitivity to noise.

Let the input waveforms be digitized and let the samples of the waveform be represented by x_1, x_2, x_3, ..., as shown in figure 5 where the sample value 1 is the maximum at the first peak and occurs for the Nth sample. The z transform of this waveform can be written as*

$$X(z) = x_1 + x_2 z + x_3 z^2 + \ldots \tag{27}$$

if Y(z) denotes the z transform of the received waveform. If y_1, y_2, ... denote the samples of the reflected waveform, then

$$Y(z) = y_1 + y_2 z + \ldots + \ldots \quad .$$

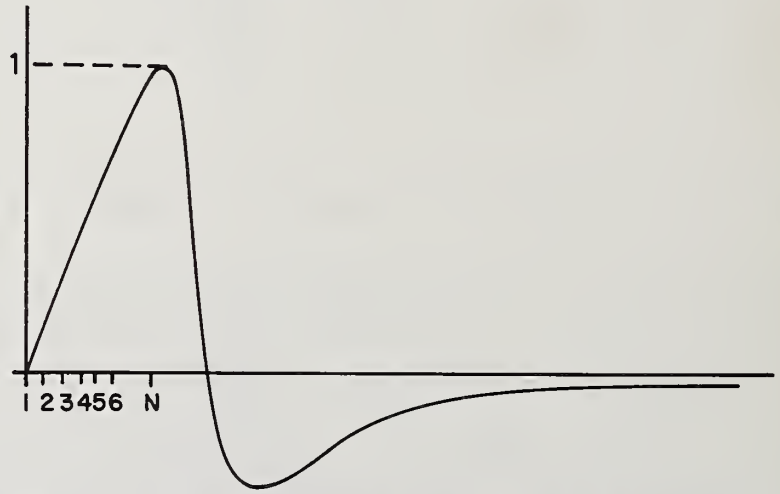

Figure 5. Broadband non-oscillatory waveform used for the determination of acoustic impedance profile.

Then H(z), the z transform of the impulse response, is given by

$$H(z) = \frac{Y(z)}{X(z)} = \frac{y_1 + y_2 z + \ldots + \ldots}{x_1 + x_2 z + \ldots + \ldots} \tag{28}$$

or

$$H(z) = \frac{1}{x_1}\left[(y_1 + y_2 z + \ldots) - H(z)(x_2 z + x_3 z^2 + \ldots)\right]. \tag{29}$$

If h_1, h_2, ... denote the samples of the impulse response, then from the above equation, the recursive relationship for the calculation of the samples h_i from the input and the output waveforms is

$$h_i = \frac{1}{x_1}\left[y_i - (x_2 h_{i-1} + x_3 h_{i-2} + \ldots)\right] . \tag{30}$$

*Note that in eqs. (27) through (33), the symbol z does *not* stand for the normalized acoustic impedance.

Note that x_1 is the first sample of the incident waveform, and because of the way it appears in the above recursive relationship, the calculation of all h_i is critically dependent upon the accuracy of this sample and also the sensitivity of the calculation to noise is dependent upon the magnitude of x_1.

To get around the difficulties mentioned above, some researchers take the first sample of the incident waveform at the first maximum. For either unipolar or bipolar waveforms, this usually means neglecting a significant portion of the waveform, leading to inaccuracies.

We are currently developing techniques that use the *a priori* knowledge about the waveform to modify the above procedure in order to eliminate the difficulties mentioned there. An explanation of some of the concepts that we have developed follows.

Let us assume that the first maximum occurs at the Nth sample and up to this sample the incident waveform obeys the following relationship

$$x_i = kx_{i+1} \qquad \begin{cases} k < 1 \\ i < N \end{cases} \tag{31}$$

which really means an exponential growth up to the first maximum. Therefore,

$$X(z) = k^{N-1} + k^{N-2}z + \ldots + z^{N-1} + x_{N+1}z^N + x_{N+2}z^{N+1} + \ldots , \tag{32}$$

where we have assumed that the waveform is normalized so that the first maximum has a value of unity. By substituting eq. (32) in the relationship $H(z) = Y(z)/X(z)$, it can be shown that the recursive relationship for the samples of the impulse response can be written as

$$h_i = \frac{1}{1-x_{N+1}k} \left\{ y_{i+N-1} - ky_{i+N} - [(x_{N+1} - kx_{N+2})h_{i-1} + (x_{N+2} - kx_{N+3})h_{i-2} + \ldots] \right\} . \tag{33}$$

Note that $x_{N+1}k$ will never be equal to 1 because: (i) $x_{N+1} \simeq x_N = 1$, since x_{N+1} and x_N are adjacent samples of the incident waveform, and, (ii) since $k^N \simeq 0$ for N not very large, so k will, in practice, be much less than 1.

4. Experiments

Essentially all experimental data collected has been on physical models involving layered media having plane-parallel faces, which can be considered of essentially infinite extent in the direction perpendicular to the incident longitudinal acoustic wave propagation. This wave is at normal incidence to the interfaces of the model. The exception to the plane-parallel face structures involves acoustic wave transmission through excised sections of human skull bone which can considerably modify the amplitude and temporal character of the acoustic pulse.

Acoustic interrogation of the models has involved both damped oscillatory and non-oscillatory pulse type waveforms, as will be expanded on subsequently.

4.1 Instrumentation and Technique

A block diagram of the system components used for this study is shown in figure 6 and a photograph of the equipment is shown in figure 7. For the damped oscillatory wave interrogation, a focused transceiver is used. Non-oscillatory type pulses are generated by an unfocused plane-face one-inch diameter disc, and input and output waves from the model are received on a small probe. Each of these schemes is presented in figure 8.

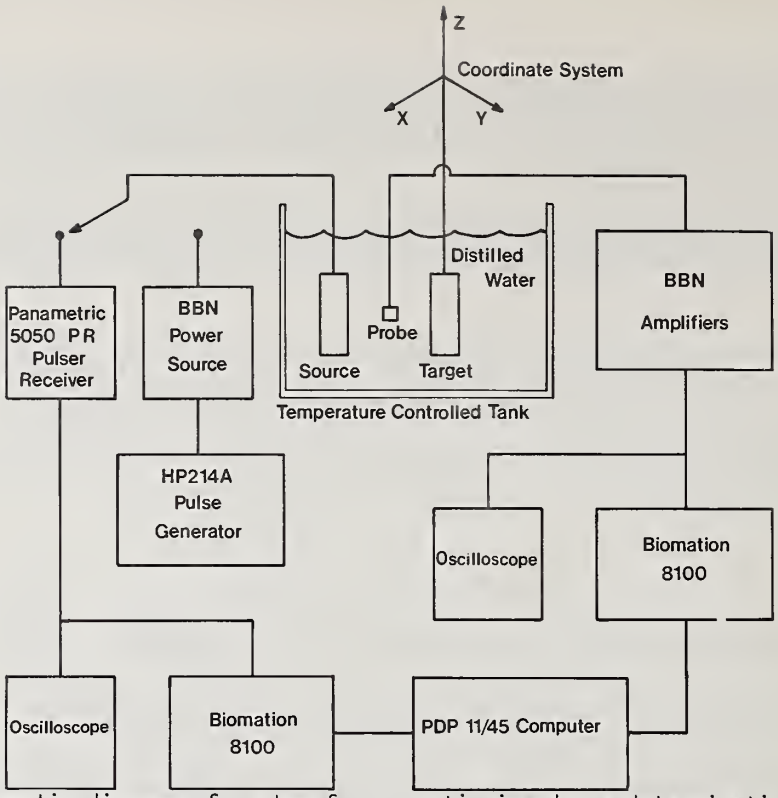

Figure 6. Schematic diagram of system for acoustic impedance determination.

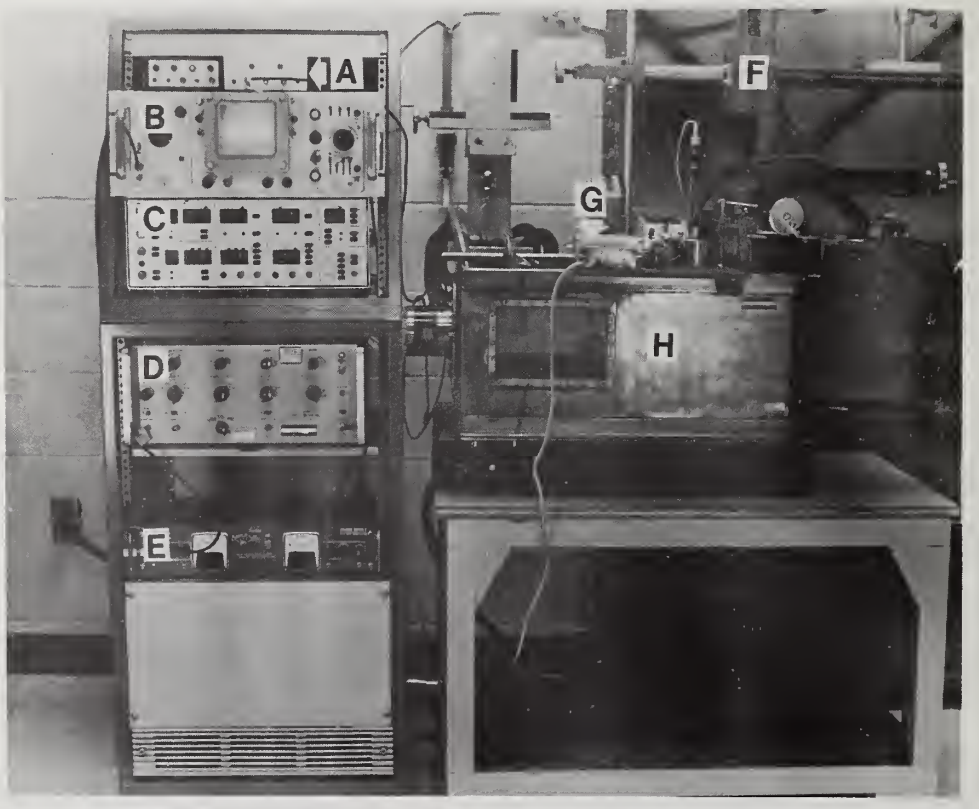

Figure 7. Acoustic interrogating system: (A) Panametrics 5050PR; (B) oscilloscope; (C) Biomation 8100; (D) pulse generator; (E) power supply for BBN Unipolar Pulse Generator; (F) coordinate system; (G) amplifiers for use with BBN style probe; (H) interrogating tank. (see also figure 11.)

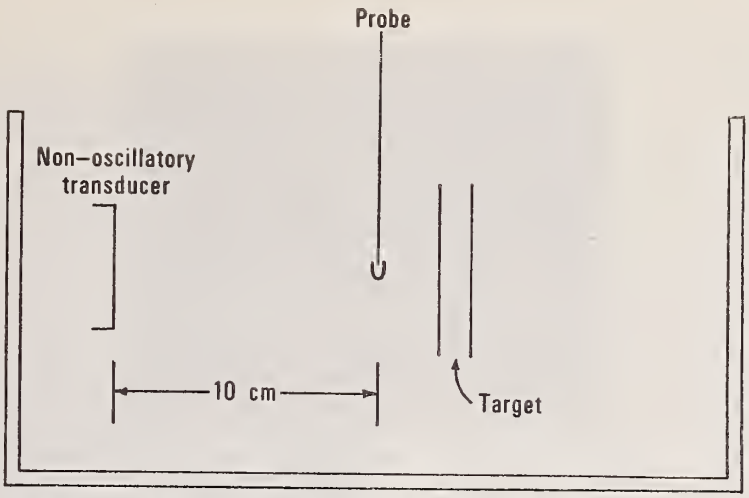

Figure 8a. Schematic diagram of non-oscillatory pulse interrogation.

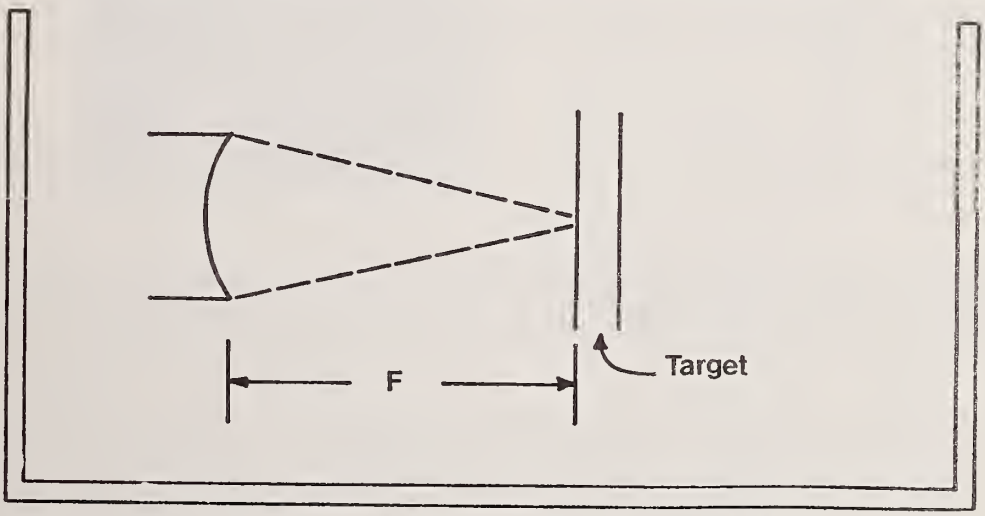

Figure 8b. Schematic diagram of focused-transceiver interrogation.

When the non-oscillatory pulse system is used for interrogation, the system configuration involves the non-oscillatory transducer source driven by an appropriate ramp voltage. The small piezoceramic probe records the input wave before entering the target and the received reflected wave from the target. An example of these waveforms for a single layer lucite target is shown in figure 9. Transceiver operation involved a transducer having an on-axis longitudinal beam plot (taken by recording reflections from a 1.0 mm diameter steel ball target) and a lateral beam plot recorded with the same ball in the focal plane. These plots are shown in figure 10. The resonant frequency of this particular transceiver is 1.7 MHz, and the focal plane is 20 cm from the transceiver face, with a total aperture angle of 14 degrees. No programs have been implemented correcting for amplitude drop in the longitudinal direction, angulation variations across the beam profile for planar targets and out-of-phasing occurring as the targets move out of the focal zone for the focusing transceiver. Of necessity, interrogated thin layered targets will yield data with the greatest absolute accuracy under these circumstances.

Digitized waveforms are stored in the digitizer (8-bit with 10 ns minimum sample interval) in 2,000 word lengths. This word sequence is transferred to DEC tape on the dedicated PDP-11/45 computer. Two waveforms, the input waveform to the target and the received waveform, are separately recorded. For the non-oscillatory pulse, the input waveform is recorded on the probe with no target in place, while for the transceiver arrangement, the input waveform is recorded from an essentially perfectly reflecting target placed at the focal plane. In either case, the target is then placed in position for the received

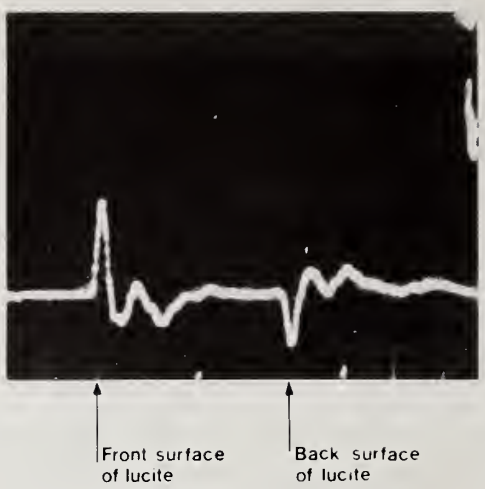

Figure 9. Probe output for signals from a single-layer-lucite target in water with non-oscillatory acoustic interrogatory pulse.

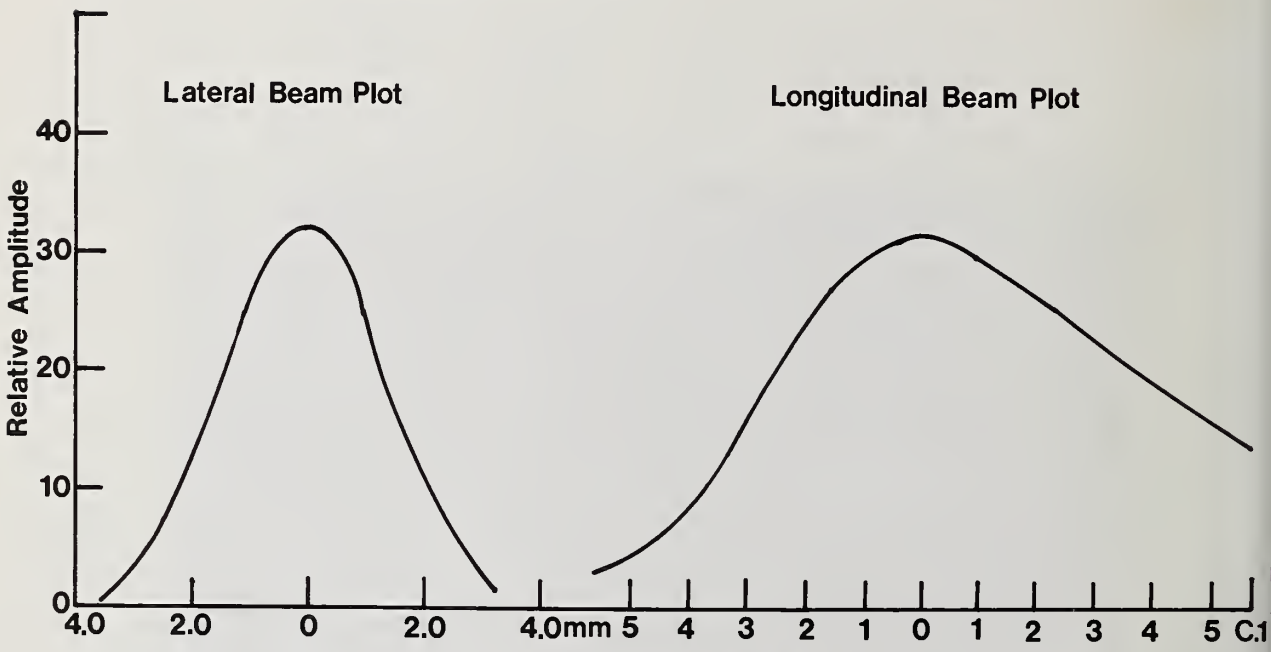

Figure 10. Field plot of the interrogating beam from the focused transceiver.

waveform recording. This recording method facilitates the program methodology which performs a cross-correlation as discussed previously. From this correlation function, the impulse response of the system is computed. Subsequent processing, as discussed previously, yields the impedance profile.

In order to project from the present status of these analytical and experimental considerations to the realm of human tjssue parameter characterization, questions of spatial resolution and sensitivity require discussion. Focused transceivers of the type used for this experimental program have a lateral resolution which is substantially equal to one wavelength at the transceiver resonant frequency operation. This resolution capability is demonstrated in figure 11. Two converging monofilament nylon threads (0.010 in diameter) are scanned by the transceiver and the position of coalescence of two separate target delineations into one single reflection is taken as a meaningful indication of

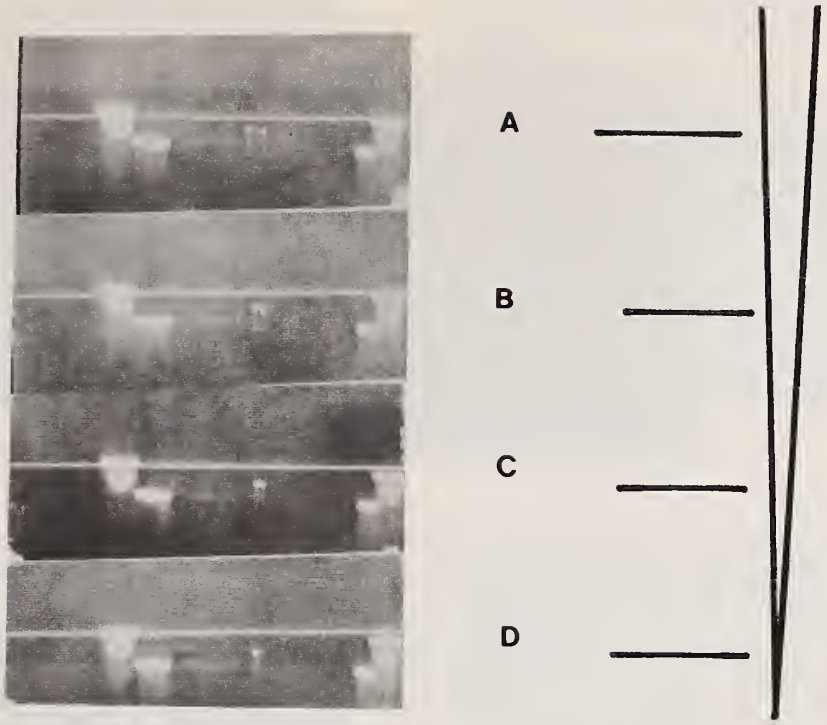

Figure 11. Reflections from V configuration of 0.005 in diameter nylon filaments. The two white dots in the middle of the left hand photographs just below the white horizontal focus maker line correspond to the echoes received from the V element shown on the right. (A) 3.5 mm nylon element spacing; (B) 2.0 mm spacing; (C) 1.2 mm spacing; (D) 0.8 mm spacing.

lateral resolution. Depth resolution is determined by using a similar target. An indication of depth resolution capability can be obtained from figure 12. With the electrical output wave shown, it is evident that, depending on the type of target, spacing distances of one or two wavelengths can be resolved.

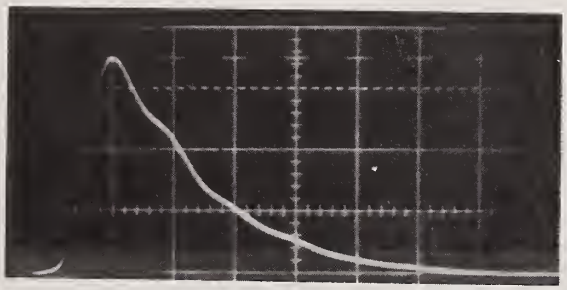

Figure 12a. Electrical driving pulse to transducer. Spacing of vertical lines is 0.5 μs.

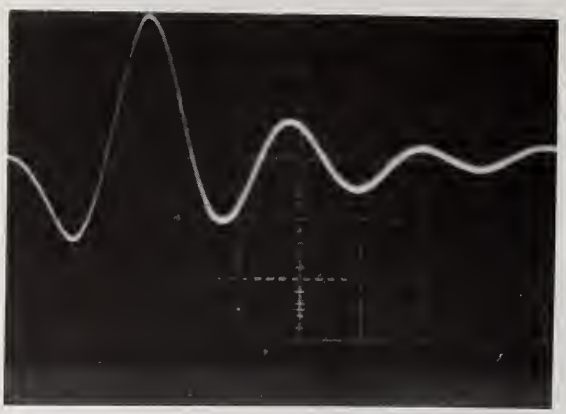

Figure 12b. Electrical output wave from transducer responding to reflection from a plane target normal to direction of sound beam propagation.

Some soft tissue interface acoustic impedance differences are listed in table 1 [7]. It is apparent that the system sensitivity should be such that it should be capable of detecting reflection differences at interfaces down to the order of one part per thousand.

Table 1. Absolute values of acoustic reflection coefficients [7]

	Water	Fat	Muscle	Skin	Brain	Liver	Blood	Skull Bone	Lucite
Water	0.0	0.047	0.02	0.029	0.007	0.035	0.007	0.57	0.35
Fat			0.067	0.076	0.054	0.049	0.047	0.61	0.39
Muscle				0.009	0.013	0.015	0.02	0.56	0.33
Skin					0.022	0.0061	0.029	0.56	0.32
Brain						0.028	0.00*	0.57	0.34
Liver							0.028	0.55	0.32
Blood								0.57	0.35
Skull Bone									0.29

*Clotted and freshly-injected blood can be detected ultrasonically in the live and formalin-fixed brain.

Sensitivity data taken with a typical transceiver used in these experiments are shown in figure 13. A linear scan of the transceiver is made across a specially-constructed target which has step gradations in acoustic impedance ranging from 0.2% to 1.0%. By appropriate settings of the gain and reject controls in the electronic system, it is possible to detect the 0.2% acoustic impedance mismatch in the target. Questions involving the accuracy with which acoustic impedances can be determined at deep body sites remain to be answered. The subsequently-presented experimental data on physical models will show the present status of accuracy and repeatability as the targets are interrogated and the digitized data transmitted to the computer for processing.

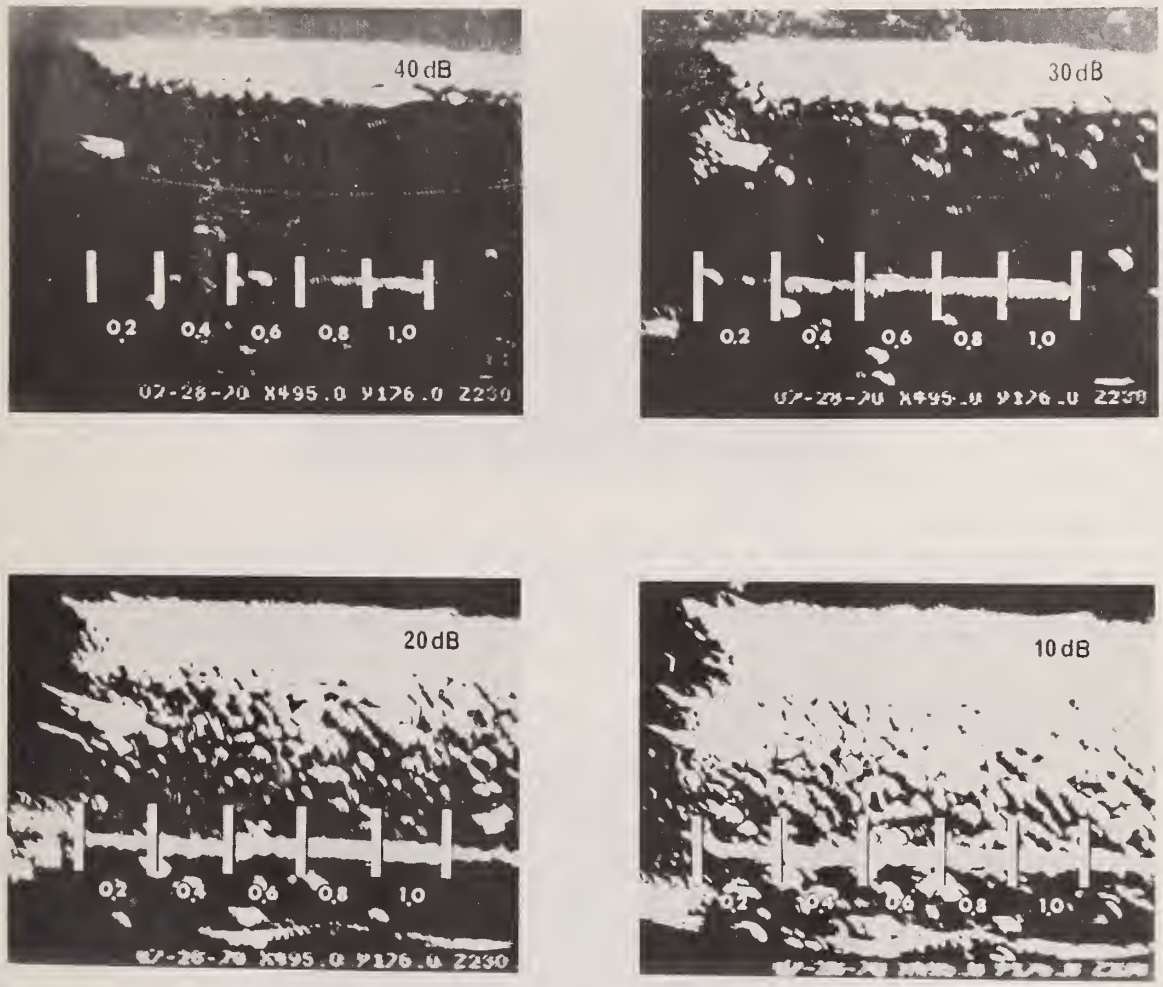

Figure 13. Reflection from a graded set of impedance mismatches. The impedance changes are shown from 0.2% to 1.0% and the horizontal white line above these numbers shows the relative strength of the reflection as a function of system sensitivity indicated as ranging from 40 dB (least sensitive) to 10 dB (most sensitive).

4.2 Experimental Data

All experiments were performed in distilled water maintained at 37 °C in the sound tank. Table 2 shows the results of runs involving damped oscillatory wave interrogation for single-layer lucite targets of different thicknesses. A single run is shown for one thickness of lucite using the non-oscillatory pulse system. Values were inserted for the attenuation coefficient. Because of the differing frequency content of the interrogating pulse, a different $\alpha(0.30\ cm^{-1})$ was used for the non-oscillatory pulse interrogation than was used for the oscillatory wave $\alpha(0.35\ cm^{-1})$. When the same piece of lucite was interrogated by resetting the target in the sound field and the signal reprocessed, the reproducibility of the lucite acoustic impedance was within ±1% of the average of all runs. Table 3 shows the results of separate interrogations of two different multilayer targets (lucite-water-lucite) in the interrogating tank. Since there was no correction for focusing or amplitude drop-off in the interrogating field, the calculated Z_4 value for water deviated from its true value by approximately 20%.

Table 2. 1.7 MHz interrogation of single lucite layer in distilled water

	Lucite Thickness Measured (mm)	Lucite Thickness Computed (mm)	Derived Acoustic Impedance ($g\ cm^{-2}sec^{-1}x10^{-5}$) Lucite Z_1	Water Z_2
Oscillatory Wave	4.89	4.85	3.25	1.46
	6.64	6.59	3.23	1.52
	9.33	9.19	3.25	1.58
	12.28	12.17	3.17	1.59
Non-Oscillatory Wave	6.64	6.51	3.10	1.52

In the calculation, we have used a velocity of 2.68 mm/μs for lucite and have assumed α = 0.35 cm^{-1} and 0.30 cm^{-1} for the oscillatory and non-oscillatory waves, respectively. Literature values [7] for lucite are α = 0.2 cm^{-1} at 1 MHz and Z = 3.2 x 10^5 g $cm^{-2}sec^{-1}$.

Table 3. Oscillatory-wave (1.7 MHz) interrogation of lucite-water-lucite target

Run	Model Thickness (mm) Lucite	Water	Lucite	Computed Thickness (mm) Lucite	Water	Lucite	Derived Acoustic Impedance ($g\ cm^{-2}sec^{-1}x10^{-5}$) Lucite Z_1	Water Z_2	Lucite Z_3	Water Z_4
1	5.98	9.07	6.12	5.98	9.06	6.21	3.14	1.56	2.99	1.93
2	5.98	9.07	6.12	5.98	9.05	6.22	3.05	1.47	3.12	1.81
3	4.86	9.07	4.86	4.88	8.90	4.77	3.22	1.47	3.10	1.77

Lucite in water is, of course, not a very appropriate model for soft tissues of the human body because of its large reflection coefficient (approximately 30%). More appropriate targets which have been interrogated include ρC rubber in water and silastic rubber multilayer sandwiches in water. The silastic sandwiches have been constructed to have impedance differences across the interfaces of approximately 1%. These targets have yielded values which are approximately correct and the results of the ongoing studies will demonstrate the validity of this approach.

This model study has additionally involved interrogation of layered media behind human skull bone sections. Human skull itself presents a multilayered media which considerably modifies the amplitude and temporal character of a transmitted ultrasonic wave. An appreciation of this acoustic wave modification can be obtained by observing the waveforms of figures 14, 15, and 16 [9]. In figure 14, the damped oscillatory wave is that received on a large-aperture focused transceiver when the wave is reflected from a multilayer target in water. Figures 15 and 16 show the result of inserting a human skull bone section at two different skull regions between the transceiver and the target. Figure 17 shows the received signal from an approximately 1% acoustic impedance difference silastic-silastic interface with an intervening human skull section. To date, the results of interrogating a single lucite target in water behind a human skull section, with the reference input waveform recorded on the transceiver from an aluminum block reflector behind the skull, are shown in table 4.

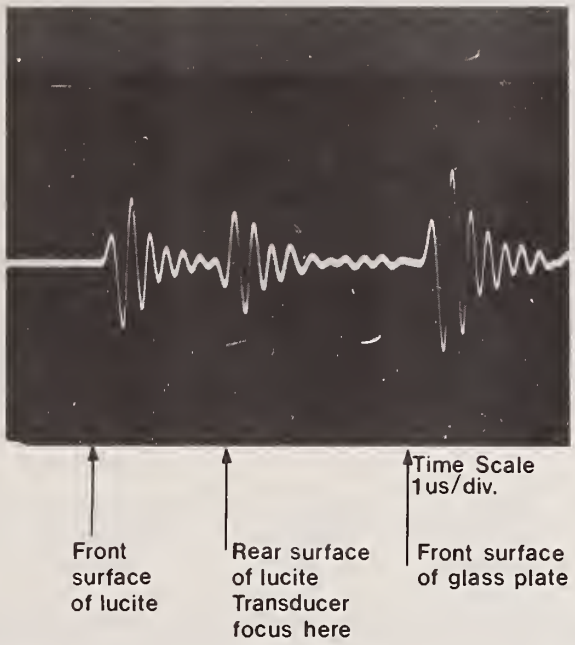

Figure 14. Focused transceiver output from a water-lucite-water-glass series of interfaces without intervening skull bone.

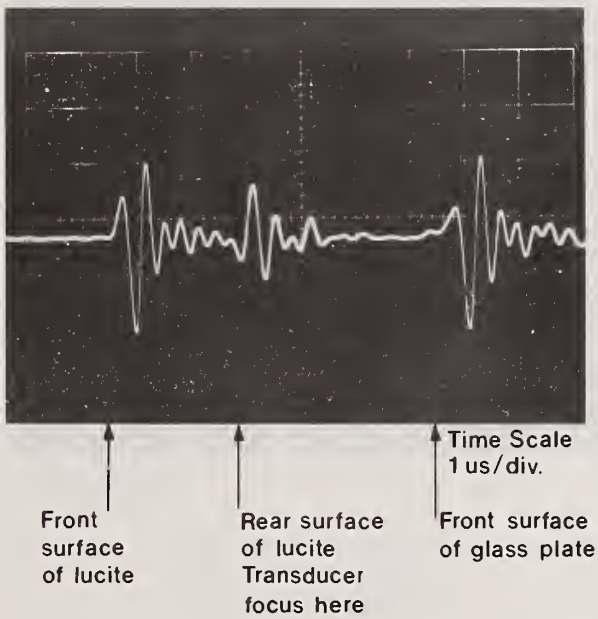

Figure 15. Focused transceiver output from a water-lucite-water-glass series of interfaces with intervening skull bone between the transceiver and the first water-lucite interface.

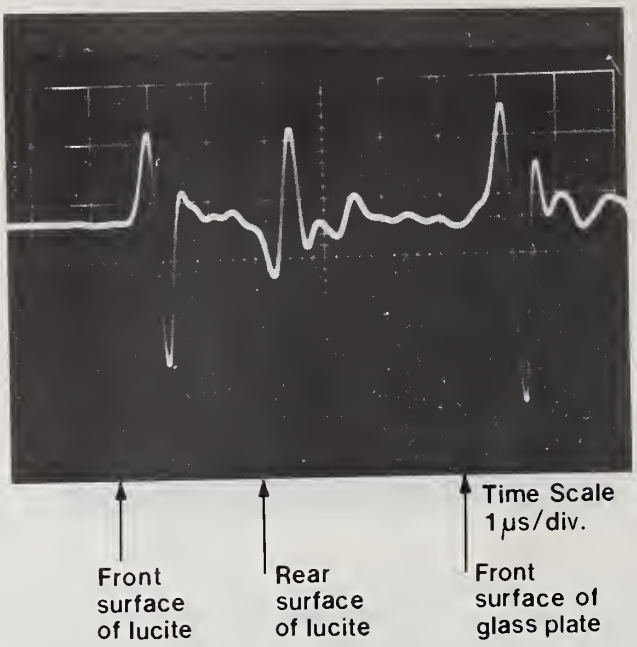

Figure 16. Focused transceiver output from a water-lucite-water-glass series of interfaces with intervening skull bone at a thicker skull bone region than that used for the data of figure 15.

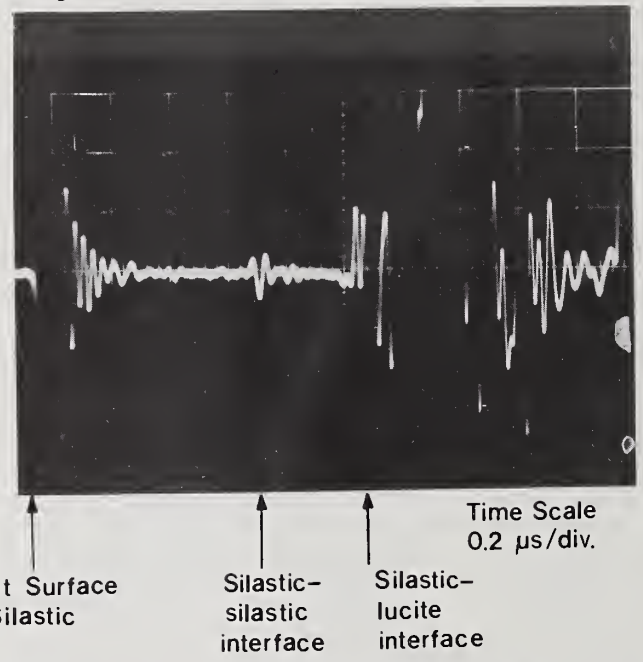

Table 4. Oscillatory-wave interrogation of a single layer of lucite behind human skull section

Skull Position	Test Material	Thickness	Derived Acoustic Impedance ($g\ cm^{-2}sec^{-1}x10^5$) Z_1	Z_2
1	lucite	9.3 mm	2.95	2.08
2	lucite	9.3 mm	3.21	2.12

It is our feeling that this research in the quantitative determination of acoustic impedance as it might be applied to soft tissues is in its early stages of development. Much work needs to be done to relate this particular parameter to the other interacting acoustic parameters mentioned previously. Progress towards the goal of tissue typing through acoustic parameter characterization will be aided by accurate assessment of this parameter.

The authors would like to thank Leland R. Beaumont, John Wolfley, and Kris A. Dines for their contributions to the development of the theoretical ideas presented here, and Narendra T. Sanghvi for help and assistance in implementing the experimental program.

References

[1] Ware, J. A. and Aki, K., Continual and discrete inverse scattering problems in a stratified elastic medium, *J. Acoust. Soc. Am.* 45, 911 (1969).

[2] Boakye, K. A. and Wing, O., On the analysis of realization of cascaded transmission line networks in the time domain, *IEEE Trans. Circuit Theory*, CT-20, 301 (1973).

[3] Jones, J. P., Impediography: a new ultrasonic technique for nondestructive testing and medical diagnosis, in *Ultrasonics International 1973 Conference Proceedings*, p. 214 (IPC Science and Technology Press, U.K., 1974).

[4] Kak, A. C., Beaumont, L. R., and Wolfley, J., Signal processing in the determination of acoustic impedance profiles, School of Electrical Engineering, Purdue University, Research Report TR-EE, 75 (1974).

[5] Rosenfeld, A. and Kak, A. C., *Digital Picture Processing* (Academic Press, New York, 1976).

[6] Van Trees, H. L., *Detection, Estimation, and Modulation Theory* (John Wiley and Sons, Inc., New York, 1968).

[7] Erikson, K. R., Fry, F. J., and Jones, J. P., Ultrasound in medicine: a review, *IEEE Trans. Sonics Ultrason.* SU-21, 144 (1974).

[8] Fry, W. J. and Dunn, F., Ultrasound: analysis and experimental methods in biological research, in *Physical Research in Biological Research, Vol. 4*, p. 261 (Academic Press, New York, 1962).

[9] Fry, F. J. and Sanghir, N., Study and test of ultrasonic technique for diagnosis of cerebral disorders, Final report - Phase 1. NIH Contract NO1-NS-3-2319 (Feb. 1, 1975).

National Bureau of Standards Special Publication 453. Proceedings of Seminar on Ultrasonic Tissue Characterization held at NBS, Gaithersburg, MD, May 28-30, 1975. (Issued Oct. 1976)

Paper 7.2: CURRENT PROBLEMS IN ULTRASONIC IMPEDIOGRAPHY

J. P. Jones[1]

Bolt Beranek and Newman, Inc.
Cambridge, Massachusetts 02138

The term impediography is used to describe a rather general class of signal processing operations which, when applied to pulse-echo ultrasonic signals, yield quantitative information concerning the physical properties of the system under study. The method uses deconvolution of acoustical impulses and their echoes to obtain the impulse response as a function of acoustical travel time. The integral of the impulse response can then be analytically related to various physical parameters such as the specific acoustical impedance. This paper provides a general discussion of the problems associated with the practical implementation of impediography and outlines a number of important research areas which require additional study. Major problem areas discussed include: (1) corrections for non-planar geometry, (2) development of accurate deconvolution algorithms, and (3) corrections and/or development of impediographic processing procedures for attenuation and scattering.

Key Words: Deconvolution, impedance profiling, impediography, impulse response, time-domain deconvolution.

1. Introduction

The term impediography [1-9][2] has been coined to describe a rather general class of signal processing operations which, when applied to input/output signals, yield quantitative information concerning the physical properties of the system under study. Ultrasonic impediography, then, describes signal processing operations upon incident and reflected acoustic waveforms which can be used to determine acoustical properties as a function of spatial location. Ultrasonic impediography offers a means, at least in principle, for quantitatively and non-invasively measuring tissue acoustical properties at appropriate anatomical sites within the body. Such measurements are of diagnostic value since many types of normal and abnormal tissues can be uniquely classified in terms of their acoustical properties [10-15]. Impediography involves (1) a processing operation upon both the incident and reflected acoustical signals to obtain a time domain characterization of system dynamics known as the system impulse response, and (2) a processing operation upon the system impulse response to obtain physical properties as a function of acoustic travel time. In our initial implementations [8-9], the impulse response was obtained by time-domain deconvolution of short duration deterministic incident and reflected waveforms. A profile of specific acoustical impedance vs. acoustic travel time (or position) was generated through analytical relationships involving the integral of the impulse response [8,9]. The term impediography is suggested by the ability of the technique to generate profiles of impedance. The acoustical mapping made with impediography, whether a simple A-scan plot of impedance vs. distance or an impedance profile of an arbitrary cross section, is termed an impedogram.

[1]Present address: School of Medicine, Case Western Reserve University, Cleveland, Ohio 44106

[2]Figures in brackets indicate the literature references at the end of this paper.

The basic principles of impediography can perhaps best be illustrated by a simple example such as that shown in figure 1. Here, an initial medium of constant impedance, Z_0 abuts a test object consisting of two parallel layers each with a constant impedance of Z_1 and Z_2, respectively. For purposes of argument, we assume $Z_2 < Z_0 < Z_1$. An acoustic source, which generates a short pulse, and a receiver, which observes the incident wave as well as the wave that is reflected from the test object, are located in the initial medium. The incident wave produced by the source can be represented mathematically as a function of time by x(t). A typical source-emitted waveform as might be observed at the receiver is shown in the top line of figure 1. The incident wave now propagates into the test object, where impedance changes cause a portion of the incident wave to be reflected. This reflected wave is also observed at the receiver. Given x(t) and the particular physical situation shown schematically in figure 1, the reflected wave, represented by y(t), would appear as shown in the second line of this figure. If reflection is assumed to be a linear process, then the manner in which the test object responds to the incident wave can be characterized by an impulse response function h(t). It is a well-known result that the output of a linear system is the convolution of the input and the impulse response of the system. Thus, the reflected wave (or output) is equal to the convolution of the incident wave (or input) with the impulse response. Given y(t) and x(t), h(t) can be obtained through appropriate deconvolution procedures. A typical result for the physical situation described in figure 1 is shown in the third line of that figure. It can be shown that the integral of the impulse response can be related to various physical parameters, such as specific acoustical impedance. Thus, if we integrate the h(t) shown in figure 1 with respect to the acoustic travel time and perform some simple algebra, we obtain the impedance plot as a function of time (or position) shown in the fourth line of figure 1.

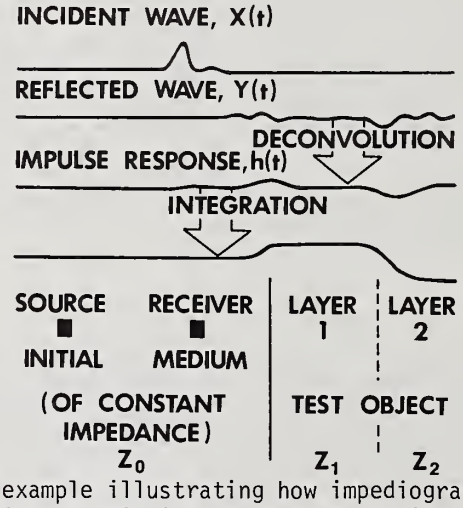

Figure 1. A simple example illustrating how impediography can quantitatively measure the specific acoustic impedance as a continuous function of acoustic travel time.

Although the concept of impediography is quite simple, its practical implementation has proven to be fairly complicated. There are at least four problem areas of current interest: first, appropriate corrections must be formulated for non-planar geometry; second, precise analytical relationships must be obtained relating the impulse response to the specific acoustical impedance and perhaps also to the frequency-dependent attenuation and the frequency-dependent scattering strength; third, accurate, well-conditioned, and stable deconvolution algorithms must be developed for measuring the impulse response; and fourth, the effects of attenuation must either be taken into account or measured concurrently with impediographic processing procedures. Let us now review each of these problem areas in more detail.

Our simple analytical model for impediography has assumed that all reflecting interfaces are plane-parallel structures. Such a model is probably adequate for many situations of interest, particularly if the object is interrogated with a narrow focused beam of ultrasound. For more complicated structures, scanning in conjunction with simple processing may be required to properly account for the effects of non-planar geometry. The limitations of a planar geometry model have yet to be fully assessed.

The second problem area involves obtaining appropriate analytical relationships between the reflected acoustic waveforms and the acoustical properties of the object. A number of iterative methods have been proposed for determining the impedance profile from a knowledge of the incident and reflected signals [16-19]. Such techniques have seen extensive application in geophysics and in the analysis of transmission lines. Although these methods provide a simple means for removing the effects of multiple reflections, they are often inaccurate and feature the rapid accumulation and propagation of errors. To avoid the errors associated with a recursive estimation of impedance, we have developed an integral relationship between the impulse response and the impedance. For example, if the impedance $Z = Z_0$ is constant for all times $t \leq 0$ and Z is a continuous but arbitrary function of time for $t > 0$, then it can be shown [1,7,8] that

$$\int_0^t h_1(\tau)d\tau = \ell n[Z(t)/Z_0]/2$$

where h_1 is the first-order impulse response (*i.e.*, the impulse response which results from only first-order reflections). This result is important since it allows us to obtain the impedance profile of even an impedance continuum and does not require measurements based upon reflections from finite layers of constant impedance.

In certain specialized situations, similar integral relationships can be derived which include the effects of higher-order reflections [7-8]. However, in general such relationships are either indeterminate or non-unique. Fortunately, multiple reflections are usually the result of abrupt, large magnitude impedance excursions. If such is the case, they can be removed through a perturbation analysis on the impulse response in the original formalism [7].

The measurement of attenuation is intimately and irrevocably tied to the measurement of impedance. In fact, in many cases, knowledge of the attenuation may be more important to tissue identification than knowledge of the impedance [8,10]. Although we will return to the question of attenuation later in our presentation, it should be clear that analytical relationships exist between the impulse response and the attenuation. For example, if the transmitted and the reflected impulse responses are measured, then profiles of both the impedance and the attenuation, provided a spectrum analysis of the reflected waveform is obtained. Unfortunately, these procedures suggested for measurement of the attenuation have yet to be implemented.

Impedance profiling is made possible because sound is reflected from the change in acoustical impedance which forms the boundary of the structure in question. In many situations, low amplitude echoes which are highly frequency dependent may be observed from the interior of the structure. These mottling echoes are produced by the scattering of sound from microstructural inhomogeneities, which are inherent to many biological tissues [20]. Since these echoes produced by scattering represent frequency-dependent interfaces, they produce errors in our impediographic profiling. Appropriate corrective measures are required. Scattering, like impedance, velocity, and absorption, is a fundamental tissue property and could well provide a basis for quantitative tissue characterization. Therefore, many situations may require that impediography also provide a measure of the scattering. Such a measure could be obtained either through analytical relationships between the impulse response and the scattering or through analysis of the reflected signal to yield the backscattering strength.

The third problem area to be discussed deals with the development of appropriate deconvolution algorithms for measuring the impulse response. In our initial work on impediography, we tried simple and well-known signal processing procedures that could be carried out without extensive computation [7]. Thus, it was convenient to use a non-anticipatory time-domain deconvolution algorithm in which the convolution integral was approximated by a sum using samples of the continuous functions and in which deconvolution was accomplished through matrix inversion.

If the impulse response is to be obtained from the incident and reflected waveforms using a "standard" time-domain deconvolution algorithm then requirements are placed on the source-emitted waveform and on the manner in which data are sampled. Time-domain deconvolution can be badly degraded if inappropriate input waveforms and/or inappropriate sampling techniques are used. It can be shown [7] that criteria exist for the selection of input waveforms, which, when employed with preferred sampling techniques, will greatly improve the

accuracy and, thereby, enhance the interpretability and utility of records obtained by time-domain deconvolution, especially in the presence of additive noise. A simple analysis indicates that optimal results are obtained with an unconventional source which generates a pressure pulse that is unipolar in shape. Thus, the initial experimental studies of impediography [1-5] made use of a spark source (which easily generates a unipolar pulse). The numerous inconveniences associated with a spark source led to the development of a simple piezoelectric device capable of generating a unipolar pulse [7]. This instrumentation has been used successfully in a number of simple experiments [9]. Accurate impedograms were obtained for a number of highly idealized physical models and for several biological samples. To obtain these results required careful hand analysis of the data as well as preprocessing to remove the effects of multiple reflections and attenuation and to correct for low frequency source drift. Attempts to automate this processing procedure have thus far not been successful. As might be expected, the eye-brain complex is apparently capable of making judgments in the analysis that can be automated only with great difficulty. Obviously more sophisticated processing techniques are required which can circumvent problems of judgment, preprocessing requirement, and the fundamental problem of illconditioning associated with impulse response identification. Although, Prof. Kak has made significant progress in this direction [21], as was indicated in the previous paper, much work remains. There is a considerable literature in applied mathematics, geophysics, control sciences, electroacoustics, and radar/sonar applications which deals with this particular system identification problem and which we in ultrasound have yet to use to full advantage. The practical implementation of impediography would be hastened considerably by translating sophisticated signal processing techniques presently available into impediographic processing procedures, keeping in mind the unique problems associated with ultrasonics and with measurements on biological tissues. Techniques such as homomorphic deconvolution [24] and Kalman filtering [22-23] would seem to be especially promising.

Finally, we consider problems associated with attenuation. As mentioned previously the accurate determination of impedance is dependent upon either the *a priori* knowledge of attenuation or upon a means for its concurrent measurement, and vice versa. There are at least four ways in which both the impedance and the attenuation can be determined. First, if either the impedance or attenuation are known, the unknown parameter can be determined using present impediographic processing procedures. Second, as previously discussed, analytical relationships between attenuation and the impulse response should allow the impedance and attenuation to be concurrently determined. For example, if the reflected impulse response is used with present impediographic processing to obtain an impedance profile, analysis of the transmitted impulse response should allow the attenuation to be determined and the original impedogram to be corrected for attenuation. If the frequency dependence of the attenuation is known, a spectrum analysis of the reflected waveform should be sufficient for determination of the attenuation, provided the measurement is coupled with present impediographic processing. Third, if the properties of an internal reflecting interface or structure are unknown, it might be possible in many situations to calibrate the measuring system on this known object and thereby obtain the necessary corrections to produce an accurate profile of impedance and/or attenuation[3]. Fourth, more sophisticated signal processing techniques may permit corrections for attenuation in the computation of the impulse response. For example, processing techniques based on a time-varying filter and on nonstationary statistics may be useful.

One of the more interesting attenuation problems of current interest involves making quantitative acoustical measurements through human skull. Transskull impediography is difficult because of the rather unique aberrations introduced by the presence of skull bone. An analysis of the propagation of sound through skull shows that the width or spatial characteristics of a focused beam remains virtually unchanged, whereas the waveform is severely altered. Preliminary results of a study now in progress [25] indicate that transskull signal degeneration is a result of frequency-dependent absorption and multipath propagation. Multipath propagation is apparently produced by nonuniform variations in skull thickness and perhaps by mode conversion processes within the skull. Using the results of this study we hope to develop techniques or procedures for removing or taking into account the effects of the skull on acoustical signals.

---

[3]Internal reflecting interfaces of known acoustical properties might include blood (*e.g.*, underlying infarcted heart tissue) and normal structures of the ventricles.

In conclusion, ultrasonic impediography offers a means, at least in principle, for quantiely and non-invasively measuring tissue acoustical properties at appropriate anatosites within the body. However, a number of major problems remain to be solved before iography can be implemented in any practical sense. These problems are extremely enging, are perhaps approachable in the context of recent developments in signal prong and analysis, and deserve the attention of many more interested researchers.

References

Jones, J. P., and Wright, H. A., A new broad-band ultrasonic technique with biomedical implications I: background and theoretical discussions, presented at the 83rd Meeting of the Acoustical Society of America, Buffalo, NY, April 1972.

Jones, J. P., and Wright, H. A., A new broad-band ultrasonic technique with biomedical implications II: preliminary experiments involving human skull bone, presented at the 83rd Meeting of the Acoustical Society of America, Buffalo, NY, April 1972.

Jones, J. P., Impediography: a new approach to non-invasive ultrasonic diagnoses, presented at the 25th Annual Conference on Engineering in Medicine and Biology, Bal Harbor, Florida, 1972.

Jones, J. P., Further experiments with impediography, a new ultrasonic technique with biomedical implications, presented at the 84th Meeting of the Acoustical Society of America, Miami Beach, FL, 1972.

Jones, J. P., Impediography: a new ultrasonic technique for nondestructive testing and medical diagnosis, in *Ultrasonics International 1973 Conference Proceedings*, p. 214 (IPC Science and Technology Press, U.K., 1974).

Jones, J. P., *In Vitro* visualization of liver metastasis using ultrasonic impediography, presented at the 86th Meeting of the Acoustical Society of America, Los Angeles, CA, 1973.

Jones, J. P., *A Study of Ultrasonic Techniques for the Diagnosis of Cerebral Disorders, Phase I: A Preliminary Investigation of Impediography*, (BBN Report No. 2890, NIH Contract No. NO1-NS-3-2319, Oct. 1974).

Jones, J. P., Impediography: a new ultrasonic technique for diagnostic medicine, in *Proceedings of the 19th Annual Conference of the American Institute Of Ultrasound in Medicine* (Seattle, WA, Oct. 1974).

Jones, J. P., A preliminary experimental evaluation of ultrasonic impediography, in *Proceedings of the 19th Annual Conference of the American Institute of Ultrasound in Medicine*, (Seattle, WA, Oct. 1974).

Tanaka, K., Yukishita, K., Ito, K., Ehara, K., and Watanabe, H., Ultrasonic diagnosis of brain tumors, in *Proc. Int. Symp. on Echo-Encephalography*, 38 (1967).

Fry, E. Kelly, Fry, F. J., and Okuyama, D., Ultrasonic differentiation of normal liver structure as a function of age and species, in *Reports of the 6th Int. Cong. on Acoustics*, M1-4 (Tokyo, Japan, August 1968).

Fry, E. Kelly, Eggleton, R. C., and Fry, F. J., Ultrasound echo patterns from normal human and animal liver--relation to detection of pathological states of liver, *Proc. A.I.U.M.* (Denver, CO, Oct. 1971).

Fry, E. Kelly, and Gibbons, L. V., *A Study of Ultrasonic Detection of Breast Disease*, (Report No. PH 86-68-198, U.S. Public Health Service, Cancer Control Program, April 1969).

Fry, E. Kelly, Kossoff, G., and Hindman, H. A. Jr., The potential of ultrasound visualization for detecting the presence of abnormal structures within the female breast, *Proceedings of IEEE Ultrasonics Symposiums*, p. 25 (IEEE, Cat. No. 72 CHO 708-8 SU, New York, 1972).

[15] Fields, S., and Dunn, F., Correlation of echographic visualizability of tissue and biological composition and physiological state, *J. Acoust. Soc. Am.*, 54, 809 (1972).

[16] Ware, J. A., and Aki, K., Continual and Discrete Inverse Scattering Problems in a Stratified Elastic Medium, *J. Acoust. Soc. Am.*, 45, 911 (1969).

[17] Boakye, K. A., and Wing, O., On the analysis and realization of cascaded transmission line networks in the time domain, *IEEE Trans. Circuit Theory*, CT-20, 301 (1973).

[18] Shanks, J. L., Recursion filters for digital frocessing, *Geophysics* 32, 33 (1967).

[19] Tritel, S., and Robinson, E. A., The Stability of Digital Filters, *IEEE Trans. Geosci. Electron.* 2, 6 (1964).

[20] Sigelmann, R. A., and Reid, J. M., Ultrasonic scattering from biological tissues, in *Interaction of Ultrasound and Biological Tissues*, Workshop Proceedings, J. M. Reid and M. R. Sikov, eds. p. 245, (DHEW Pub. 73-8008 BRH/DBE 73-1 1972).

[21] Kak, A. C., Beaumont, L. R., Wolfley, J., *Signal Processing in the Determination of Acoustic Impedance Profiles*, (Purdue University Report TR-EE 75-7, 1974).

[22] Bayless, J. W., and Brigham, E. O., Application of the Kalman Filter to Continuous Signal Restoration, *Geophysics*, 35, 2 (1970).

[23] Crump, N. D., A kalman filter approach to the deconvolution of seismic signals, *Geophysics*, 39, 1 (1974).

[24] Ulrych, T. J., Application of homomorphic deconvolution to seismology, *Geophysics*, 36, 650 (1974).

[25] Study conducted by the Fortune-Fry Research Labs, Indianapolis, IN, and Bolt Beranek and Newman Inc., Cambridge, MA., and supported by the National Institute of Neurological Diseases and Stroke. (NIH Contract No. NO1-NS-3-2319).

CHAPTER 8

ACOUSTIC MICROSCOPY

National Bureau of Standards Special Publication 453. Proceedings of Seminar on Ultrasonic Tissue Characterization held at NBS, Gaithersburg, MD, May 28-30, 1975. (Issued Oct. 1976)

CHAPTER 8. ACOUSTIC MICROSCOPY

Paper 8.1: TISSUE CHARACTERIZATION BY MEANS OF ACOUSTIC MICROSCOPY

L. W. Kessler

Sonoscan, Incorporated
Bensenville, Illinois 60106

The complete characterization of tissue is extremely important for objectively identifying abnormalities and disease states. Optical methods of microscopy have been exploited to a great degree and now the electron microscope is being used in search of diagnostic clues at higher magnification levels. It is well appreciated, however, that these methods provide only limited access to the physical properties of tissue. Furthermore, the physical nature of an abnormality may prohibit its ever being revealed with visual observation techniques. Acoustic microscopy, on the other hand, can reveal new information, the structural elastic characteristics of viable tissue. Acoustic microscopy can also provide quantitative data on these tissue characteristics. As this additional information should have great diagnostic value, a general discussion of the methods and procedures employed is presented.

Key Words: Acoustic imaging; acoustic microscopy; attenuation; frequency dependence; impedance; microstructural analysis; tissue; ultrasound; velocity.

1. Introduction

The application of acoustic microscopy to biological tissues is a new area of study which addresses the problem of delineating the physical characteristics of tissue composition on a microscopic level. Knowledge of the physical characteristics of viable tissue, instead of histologically fixed and stained tissue, can be rendered directly with acoustic microscopy. This will undoubtedly play an important role in increasing our capacity to identify subtle changes in tissue architecture which occur in pathological conditions.

As a technique, acoustic microscopy is analogous to optical microscopy in that high resolution and high magnification images are produced; however, ultrasonic energy, rather than an "optical band" of electromagnetic energy, is transmitted through the sample. Because very high ultrasonic frequencies are employed to produce high resolution, the microscopy regime is new to the medical ultrasonics arena. The high frequencies are associated with large acoustic attenuation values in tissue, thus making small samples necessary. On the other hand, the resolution obtainable is several orders of magnitude better than that achieved in conventional diagnostic ultrasound and the applications are somewhat different. In particular, at frequencies of a few megahertz, *i.e.*, the "macro-range", ultrasonic diagnosis profits from being able to penetrate optically opaque bodies and differentiate soft tissue interfaces without ionizing radiation. The "micro-range" described here, in addition to providing the just-mentioned capabilities on a finer scale, more importantly provides direct access to the elastic properties of fresh tissue at a dimensional level where localized variations in mass density, modulus of elasticity and acoustic attenuation, are much more abundant.

2. Description of the Technique

The following brief description of the technique employed for acoustic microscopy is presented for reference. Interested readers may review the listed references [1-5][1] for more detailed accounts. In the most general sense, in order to produce an acoustic micrograph, a sample is placed between sending and receiving ultrasonic transducers and

[1]Figures in brackets indicate the literature references at the end of this paper.

the point-by-point pattern of sonic transmission is displayed on a CRT. The procedures for mounting specimens in this acoustic microscope (fig. 1) are very similar to those

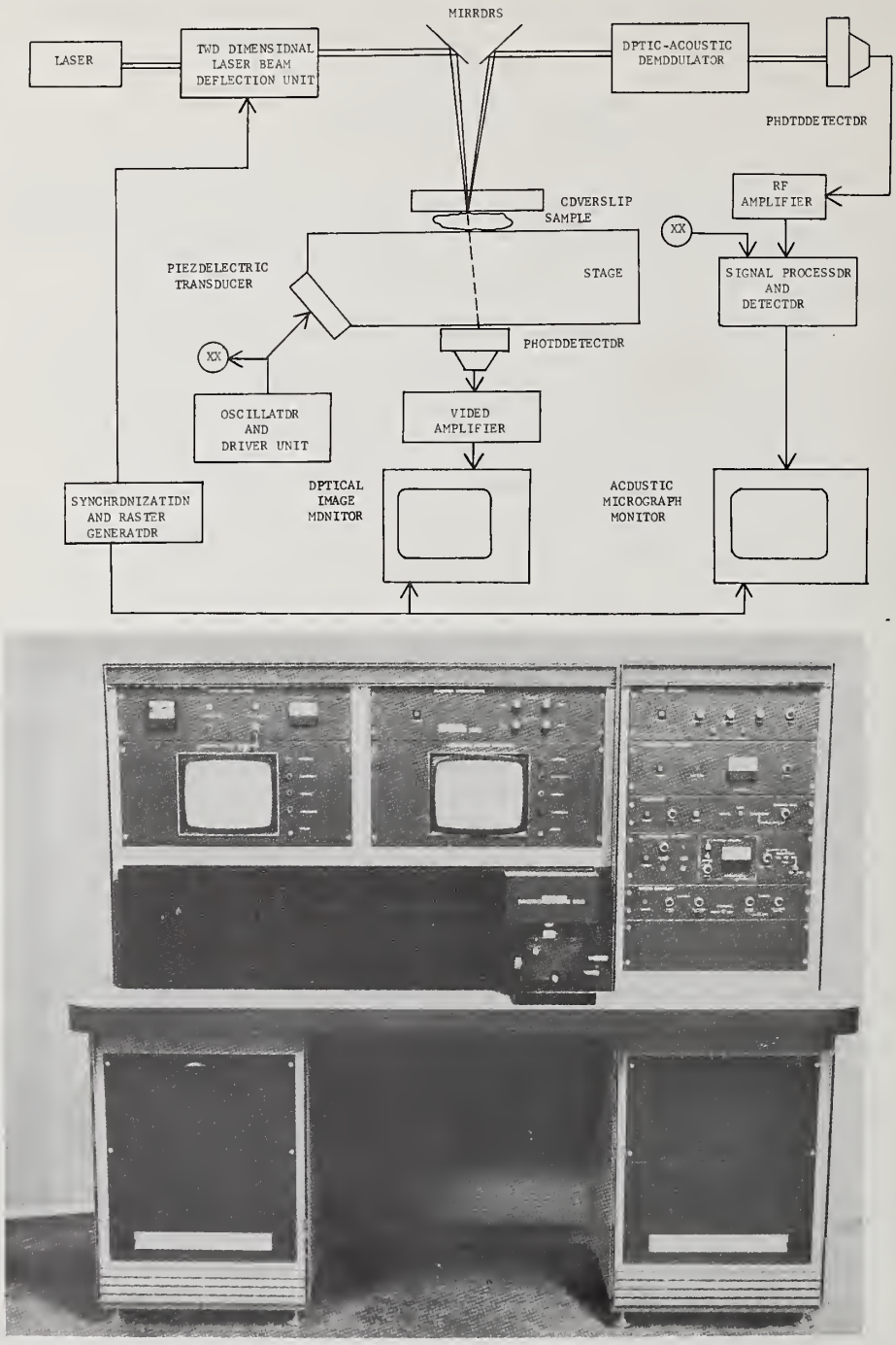

Figure 1. Schematic block diagram and photograph of a completed Sonomicroscope [6] apparatus for producing acoustic micrographs in real time. The instrument employs a scanning laser beam technique for detecting the amplitude and phase of acoustic transmission through a sample. As a by-product of this technique, an optical image of the specimen is simultaneously produced and is presented on a separate TV monitor.

normally encountered in optical imaging. The acoustic energy is coupled directly to the specimen without any need for an acoustically-lossy water bath, although the specimen may be moistened with a thin layer of liquid to insure good acoustic transmission. Biological specimens are placed on a sonically-activated glass stage and are covered with a partially-mirrored coverslip. The transmitted acoustic energy imparts slight oscillatory mechanical perturbations to the coverslip surface. These disturbances, which occur at the acoustic frequency, are proportional to the acoustic amplitudes in each region. These are detected by a focused scanning laser beam probe which drives an opto-acoustic receiver.

An optical image of the specimen is produced simultaneously by detecting the through-transmitted laser light. By virtue of this point-by-point scanning method, the optical and acoustic signals are in perfect register electronically so that corresponding images may be presented on separate side-by-side TV monitors or superimposed on separate color channels of a single color TV monitor [7]. The latter has been especially useful for sorting through and precisely correlating the abundant acoustic and optical image details.

In addition to displaying the acoustic intensity or amplitude throughout the field of view, the Sonomicroscope provides an acoustic interference mode of operation. Here, the acoustic phase may be measured as the wave propagates through various structures within the field of view. Thus, velocity of sound measurements can be made and, under the appropriate conditions, fluctuations of mass density and elasticity can be observed in microscopically-localized regions.

3. Sonomicroscopic Characterization of Tissues

The characterization of tissue microstructure is traditionally accomplished by optical or electron microscopy methods. However, these methods are intrinsically capable of revealing only the physical "electronic properties" of structure defined by the dielectric constant. (The magnetic properties are usually unimportant.) Useful histological methods which alter the natural state of tissues have been developed. These clarify, fix, and selectively stain tissues in order to optically reveal otherwise unobservable aspects of structure. In particular, size, shape, position, and staining characteristics of tissue components encompass the body of information that has been diagnostically available. However, methods have not been capable of translating actual elastic characteristics of tissue to a visible format. The characterization of density and elasticity properties of unaltered tissue structure is now available in acoustic microscopy through the determination of localized attenuation coefficients, acoustic impedance, and velocity of sound. The methods and procedures for producing these quantitative data are described briefly below.

4. Attenuation and Impedance Distribution

In general, the attenuation suffered by an acoustic beam propagating through tissue results from several mechanisms, acting independently or synergistically [8]. As an acoustic beam propagates through an inhomogeneous medium, reflection and refraction at interfaces divert energy away from the primary beam. However, as the spatial extent of acoustic impedance interfaces becomes comparable to or smaller than the dimension of the acoustic wavelength, the process is referred to as scattering. It should be recognized that structures which at clinical diagnostic frequencies may be considered scatterers, may be reflectors at acoustic microscope frequencies. Frictional losses in tissue cause a fraction of the acoustic energy to change into heat. Furthermore, since the physical state of the environment is altered with sound beam propagation, shifts occur in chemical or structural reactions at a molecular level. The frictional and reaction losses are termed absorption.

Attenuation measurements can be made by means of a comparison technique [9]. With the specimen in place and the acoustic image presented on the TV screen, the appropriate region of interest is identified. Positive identification, of course, is made with the assistance of the corresponding optical image as well. The relative image brightness over the region of interest, compared to the situation of having no specimen in place, is a measure of the attenuation. Experimentally, an image brightness level is established with a light meter equipped with an appropriate optical aperture to control its field of view spatially. With the specimen removed, the microscope is refocused on the illuminating sound field alone. Electrical attenuation is then inserted in the signal path of the

irradiation transducer in order to restore the brightness to the previous level. The electrical attenuation inserted is equal to the acoustic attenuation provided by the specimen. Confidence in the method, established by measuring the absorption coefficient in water, indicates that an overall accuracy of ± 10% can be achieved.

A measurement of that part of the attenuation due to reflection losses exclusively will yield the acoustic impedance and scattering. In order to differentiate reflection losses from absorption losses, this measurement procedure may be performed on several samples of the same tissue. The sample can be made sufficiently thin so as to insure that absorption and scattering losses are an insignificant fraction of the observed attenuation. By way of example, if the attenuation of sound within tissue at 100 MHz is still of the order of 1 dB/cm/MHz, then for sample thicknesses of 10, 100, and 1000 micrometers, the expected absorption losses would be 0.1, 1.0, and 10 dB, respectively. Typical sections prepared for optical microscopy are sliced 5-10 micrometers in order to render them reasonably translucent optically.

5. Velocity of Sound Distribution

The velocity of sound has been measured for many soft tissues over the frequency range of 1-10 MHz and the values observed do not vary by more than 100 m/s or less, even though there may be substantial differences in the tissue types [10]. It may be reasoned that at the bulk level of tissue, velocity of sound characteristics of small components are masked by the predominant aqueous constituents. Microscopically, however, the velocity of sound may be measured in individual components of the tissue with the acoustic interferometry mode of operation [3,4].

The principle of measuring changes in velocity of sound can be explained with reference to figure 2. Consider the intersection of two plane, coherent sound beams at

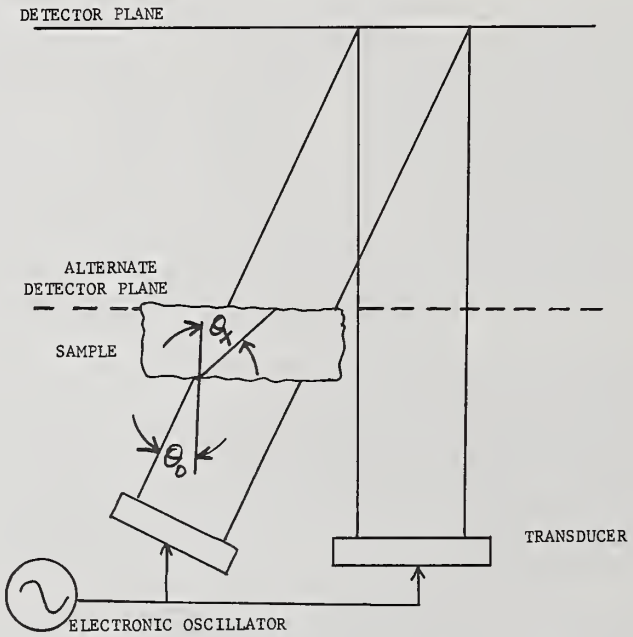

Figure 2. Principle of acoustic interferometry. Two coherent sources of acoustic energy, one passing through the sample and one bypassing the sample, constructively interfere at the detection plane causing a series of fringe lines whose lateral positions are determined by the velocity of sound in the sample. The detection plane, which is shown as being located far away from the sample, is actually located at the alternate position in order to circumvent the large acoustic attenuation losses. However, in order to provide a reference signal for phase detection (there is no room for a sound beam to bypass the sample), it is done electronically.

the detector plane. Depending upon the angle between the beams, a series of regularly-spaced fringe lines, caused by mutual interference, will appear at the detector plane. If an object whose velocity of sound characteristics differ from that of the surrounding medium interrupts one of the beams, localized lateral shifting of the fringe lines will result. The displacement of a fringe, measured graphically, is related to a localized disturbance in transmission time of one sound beam compared with the unperturbed or reference beam.

A simple formula has been derived [11] to calculate the velocity of sound in the "unknown" sample. In the actual set up, high acoustic attenuation requires the object to be placed in close proximity to the detector plane. This is accomplished with the alternate position of the detector plane by electronically simulating a reference beam at normal incidence. The schematic value of figure 2 is still correct, however, for deriving the interferometry equation. An acoustic beam, nominally incident upon the specimen at angle θ_o from the normal will be refracted to angle θ_x within the sample according to Snell's Law,

$$\frac{\sin \theta_o}{C_o} = \frac{\sin \theta_x}{C_x} \tag{1}$$

where C_o and C_x are the velocity of sound values in the unperturbed medium and the unknown sample, respectively. If the thickness of the sample or of the unknown region of a sample is denoted ΔT, then the lateral shift of the fringes, normalized by the unperturbed spacing of the fringes, N, is given by

$$N = \frac{\Delta T \sin \theta_o}{L_o} \left[\frac{1}{\tan \theta_o} - \frac{1}{\tan \theta_x} \right] \tag{2}$$

where L_o is the wavelength of sound in the reference material. Note that N is a dimensionless number, corresponding to the number of fringes of shift in the interferogram. By solving for θ_x and then using the Snell's Law relationship, C_x is readily calculated. Typically θ_o is 10°; however, it depends upon the particular configuration of the stage employed.

The capability for this technique for differentiating velocity of sound regions within the matrix of a tissue is dependent upon the sample thickness. This is consistent with other methods of velocity measurement such as "time of flight" techniques. For example, if fringe line displacements can be measured to the nearest 1/10 fringe, then in a section of tissue 300 micrometers thick, *i.e.*, 20 wavelengths, 7.5 m/s variations in C_x may be discriminated.

6. Results and Discussion

Over the last five years, during the course of development of the acoustic microscopy technique, a variety of biomedical and biological studies were conducted and are still ongoing. The purpose of this section will be to summarize just a few of the highlights, particularly those which may be pertinent to microscopic characterization of the physical properties of tissue.

One of the primary areas of study thus far has been the real-time visualization of dynamic events. A variety of specimens maintained alive in an organ culture state have been examined [2,7,12,13]. For example, isolated beating mouse embryo hearts are being studied for localized sites of action of potentially useful cardioactive agents and drugs [14]. Furthermore, whole embryo specimens have been examined as well [13,15]. Here, the acoustic microscope offers a way of circumventing optical opacity without interfering with the activity and viability of the tissues. The technique permits visualization of soft tissue structures as if they had been fixed and stained histologically.

A detailed study was also conducted on unstained specimens of mouse kidney at frequencies of 100 MHz and 220 MHz [16]. The acoustically-revealed structure has been examined in relation to established microanatomy. High-contrast details corresponding to connective

tissue boundaries of supporting elements such as the cortex and the three medullary regions can be differentiated. In this frequency range, the acoustically-exhibited structures are considered to result from scattering at connective tissue interfaces, resulting from local acoustic impedance discontinuities, rather than from intrinsic acoustic absorption within the microstructure of the tissue.

Acoustic attenuation measurements have also been made with the acoustic microscope. It has been well established that for mammalian tissues such as kidney and brain, the attenuation coefficient exhibits a linear dependence over the frequency range of investigation, *i.e.*, 0.3-10 MHz, and the magnitude is of the order of 1 dB/cm/MHz. The absorption coefficient for water is significantly less than for tissue and exhibits a square-law frequency dependence. Projecting the linear dependence for tissue to higher frequencies and comparing this to the expected absorption in water, leads to speculation that beyond about 500 MHz the attenuation for water might exceed that for tissue. Since tissue is composed mainly of water, this should not be possible.

The attenuation of sound in mammalian kidney tissue was measured at 100 MHz and 220 MHz [9]. The tissue samples were either fresh, fresh-frozen-thawed, or fixed in formalin. The measured attenuation values were found to be *independent* of preparation. The result, presented graphically in figure 3, indicates that the acoustic attenuation in

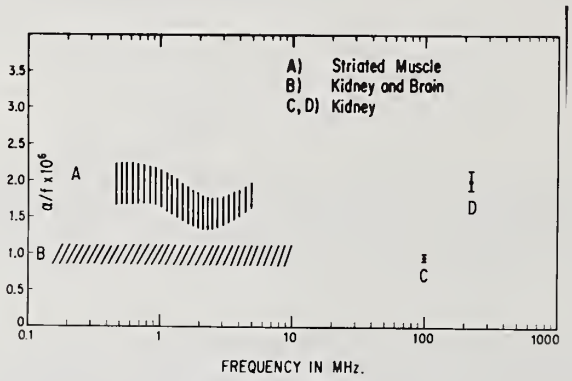

Figure 3. VHF attenuation in mammalian kidney tissue. Data A and B taken from reference 10 and data C and D taken from reference 9.

tissue continues to behave linearly up to a frequency of about 100 MHz. Beyond this frequency, a square-law dependence (or greater) takes over, thereby indicating that the hypothetical crossover point may never actually be reached. This is more in line with intuition.

The use of acoustic microscopy to delineate mechanical variations in hard tissues has been examined and preliminary qualitative results were published [17] for sections of dental tissue. Dentyne and enamel components of this tissue differ greatly in their mechanical properties and this is demonstrated by the acoustic micrographs. Furthermore, in the junction region, where dentyne and enamel components combine in varying proportions, the smooth gradation of density and elasticity is revealed. This type of study is pertinent to other hard tissue investigations, particularly bone pathologies and plaque formation in vessels.

Velocity of sound measurements have recently been initiated with the acoustic microscope. At clinical diagnostic frequencies, only a 100 m/s range in sound velocity has been observed within and among soft tissues. On the microscopic scale, however, we have obtained some evidence which suggests that there are localized regions which are characteri-

zed by velocities of sound 200-800 m/s above that of neighboring tissue structures. Since detailed studies are just getting underway, this conclusion should be regarded only as preliminary.

References

[1] Korpel, A., Kessler, L. W., and Palermo, P. R., An acoustic microscope operating at 100 MHz, *Nature*, 232, 110 (1971).

[2] Kessler, L. W., Korpel, A., and Palermo, P. R., Simultaneous acoustic and optical microscopy of biological specimens, *Nature*, 239, 111 (1972).

[3] Kessler, L. W., Palermo, P. R., and Korpel, A., Practical high resolution acoustic microscopy, in *Acoustical Holography*, Vol. 4, G. Wade, ed., p. 51 (Plenum Press, New York, 1972).

[4] Kessler, L. W., Palermo, P. R., and Korpel, A., Recent developments with the scanning laser acoustic microscope, in *Acoustic Holography*, Vol. 5, P. S. Green, ed., p. 15 (Plenum Press, New York, 1974).

[5] Kessler, L. W., The Sonomicroscope, in *Proceedings of IEEE Ultrasonic Symposium*, J. de Klerk, ed., Cat. No. 74-CHO-896-1 SU, p. 735 (IEEE, New York, 1974).

[6] Manufactured by Sonoscan, Inc., under exclusive license from Zenith Radio Corp.

[7] Kessler, L. W., High resolution visualization of tissue with acoustic microscopy, in *Ultrasonics in Medicine*, M. de Vlieger, ed., p. 250 (Excerpta Medica, 1974).

[8] The synergistic effects of attenuation mechanisms have not received attention as far as this author is aware; however, they may play a significant role in causing the attenuation values observed in tissue to exceed that which can be predicted.

[9] Kessler, L. W., VHF ultrasonic attenuation in mammalian tissue, *J. Acoust. Soc. Am.* 53, 1759 (1973).

[10] See for example: Goldman, D. E. and Heuter, T. F., Tabular data of the velocity and absorption of high-frequency sound in mammalian tissues, *J. Acoust. Soc. Am.* 28, 35 (1956).

[11] Detailed account in preparation.

[12] Eggleton, R. C. and Kessler, L. W., Mouse embryo heart in organ culture visualized by the acoustic microscope, in *Proceedings 1974 meeting of American Institute of Ultrasonics in Medicine*, p. 537 (Plenum Press, New York, 1975).

[13] O'Brien, W. D., Jr. and Kessler, L. W., Examination of mouse embryological development with an acoustic microscope, paper presented at American Society of Zoologists Meeting, Corvallis, Oregon, August 1975. (Manuscript in preparation.)

[14] Study in progress directed by Prof. R. C. Eggleton, Fortune Fry Laboratories, Indiana University Medical School with collaboration of Dr. G. Boder, Eli Lilly and Co.

[15] Ahmed, M. and Kessler, L. W., Microanatomy of a histologically unstained embryo as revealed by acoustic microscopy, in *Acoustic Holography*, Vol. 6, N. Booth, ed., p. 319 (Plenum Press, New York, 1975).

[16] Kessler, L. W., Fields, S. I., and Dunn, F., Acoustic microscopy of mammalian kidney, *J. Clin. Ultrasound*, 2, 317 (1974).

[17] Kessler, L. W., A review of progress and applications in acoustic microscopy, *J. Acoust. Soc. Am.* 53, 246 (1973).

REGISTRATION LIST

SEMINAR ON ULTRASONIC TISSUE CHARACTERIZATION

National Bureau of Standards
Gaithersburg, MD
May 28-30, 1975

Registration List

K. Abel
Becton Dickinson & Co.
P.O. Box 12016
Research Triangle, NC 27709

Robert C. Addison, Jr.
American Optical Corp.
14 Mechanic Street
Southbridge, MA 01550

Jitsuo Akiyama
Dept. of OB-GYN
Okayama University Medical School
Okayama, Japan

Sami J. Al-Banna
Columbia University
620 Mudd Building
New York, NY 10027

W. Watson Alberts
National Institutes of Health
Bethesda, MD 20014

Harold Alsberg
Cal. Tech./JPC
4800 Oak Grove Drive
Pasedena, CA 91103

Frank D. Altieri
National Heart and Lung Institute
Bethesda, MD 20014

Evan D. Anderson
National Science Foundation
1800 G Street, NW
Washington, DC 20550

Thomas L. Anderson
Food and Drug Administration
5600 Fishers Lane
Rockville, MD 20852

Robert Apfel
Yale University
Mason Lab.
New Haven, CT 06520

E. Ronald Atkinson
National Institutes of Health
Bethesda, MD 20014

Richard Banjavic
3321 Sterling Hall
University of Wisconsin
Madison, WI 53706

James E. Barger
Bolt Beranek and Newman Inc.
50 Moulton Street
Cambridge, MA 02138

Ralph W. Barnes
Bowman Gray School of Medicine
Hawthorne Road
Winston-Salem, NC 27103

Ian R. Bartky
Institute for Materials Research
National Bureau of Standards
Washington, DC 20234

G. B. Baum
Albert Einstein Medical School
Yeshiva University
Bronx, NY 10461

Irwin Beretsky
Technicon Instrument Corp.
511 Benedict Avenue
Tarrytown, NY 10956

Harry Berger
Institute for Materials Research
National Bureau of Standards
Washington, DC 20234

Richard B. Bernardi
Picker Corporation
12 Clintonville Road
Northford, CT 06472

Jason C. Birnholz
Stanford University Medical Center
Stanford, CA 94305

Richard Blackmer
General Electric
Schenectady, NY 12345

R. Quentin Blackwell
National Cancer Institute/NIH
9000 Rockville Pike
Bethesda, MD 20014

Marvin A. Blizard
Office of Naval Research
800 N. Quincy Street
Arlington, VA 22217

Francis J. Bonk
Mt. Sinai Hospital
1000 Elbon Road
Cleveland Heights, OH 44106

Joe D. Bourland
Purdue University
Biomedical Engineering Center
West Lafayette, IN 47907

Theodore Bowen
University of Arizona
Tucson, AZ 85721

Herbert S. Bright
7840 Aberdeen Road
Bethesda, MD 20014

Frederick E. Brinckman
Inorganic Materials Division
National Bureau of Standards
Washington, DC 20234

David Brown
University of Cincinnati
2882 Temple Avenue
Cincinnati, OH 45211

Robert L. Brown
Physical Chemistry Division
National Bureau of Standards
Washington, DC 20234

John H. Busser
Alliance for Engineering in Medicine
and Biology
5454 Wisconsin Avenue
Chevy Chase, MD 20015

Norman Caplan
National Science Foundation
1800 G Street, NW
Washington, DC 20854

David Carlson
Iowa State University
Room 266, Biomedical Engineering Bldg.
Ames, IA 50010

D. R. Carroll
USAF
DFEE
USAFA, CO 80840

Steve Charles
1331 Union Avenue
Suite 1123
Memphis, TN 38104

Lawrence Chik
Cleveland Metropolitan General Hospital
Department of Ob-Gyn
Scranton Road
Cleveland, OH 44109

Hyong Jun Choi
Instituto de Pesquises Technologicas
Divisao de Metalurgia
Cidade Universitaria
Sao Paulo, SP, Brazil

C. K. Chow
IBM
P.O. Box 218
Yorktown, NY 10598

Bromley Clarke
B-D Electrodyne
Route 1
Sharon, MA 02067

Frank Coombs
Bureau of Medical Devices/FDA
1901 Chapman Street
Rockville, MD 20852

Melvyn R. Conrad
Johns Hopkins Hospital
Baltimore, MD 21205

Thomas D. Coyle
Institute for Materials Research
National Bureau of Standards
Washington, DC 20234

Frank W. Cuomo
University of Rhode Island
312 East Hall
Physics Department
Kingston, RI 02881

Terry DeGrange
Office of Associate Director
for Programs
National Bureau of Standards
Washington, DC 20234

Gilbert B. Devey
National Science Foundation
1800 G Street, NW
Washington, DC 20550

John L. Doppman
NIH Clinical Center
Bethesda, MD 20014

Gilbert Drouin
Ecole Polytech.
Montreal, Canada

Hal Dufilho
Naval Coastal Systems Lab.
Panama City, FL 32401

Floyd Dunn
University of Illinois
Bioacoustics Research Lab.
Urbana, IL 61801

K. R. Erikson
Rohe Scientific Corp.
2158 S. Hathaway
Santa Ana, CA 92705

Theme T. Everton
St. Mary's Memorial Hospital
Oak Hill Avenue
Knoxville, TN 37865

N. Farhat
University of Pennsylvania
200 South 33rd Street
Philadelphia, PA 19104

David Feinstein
University of Pennsylvania
Biomedical Engr. D2
Philadelphia, PA 19174

Frank P. Finlon
Pennsylvania State University
P.O. Box 30
State College, PA 16801

Dale W. Fitting
University of Tennessee Memorial Hospital
1924 Alcoa Highway
Knoxville, TN 37920

George Flinn
500 Thorn Ridge Cove
Memphis, TN 38111

Michael J. Flynn
Mt. Sinai Hospital
Cleveland, OH 44106

Jeffrey T. Fong
Applied Mathematics Division
National Bureau of Standards
Washington, DC 20234

Leon A. Frizzell
University of Illinois
Bioacoustics Research Lab
Urbana, IL 61801

Lois J. Frolen
Institute for Materials Research
National Bureau of Standards
Washington, DC 20234

F. J. Fry
Indiana University of Medical Center
Indianapolis, IN 46204

Edwin R. Fuller
Inorganic Materials Division
National Bureau of Standards
Washington, DC 20234

Paul M. Gammell
Radionics Limited
195 Graveline Street
Montreal, Quebec, Canada

John B. Garrison
The Johns Hopkins University
Applied Physics Lab.
8621 Georgia Avenue
Silver Spring, MD 20910

David Genova
Eastman Kodak Company
Kodak Park Works, Bldg. #81
Rochester, NY 14650

W. E. Glenn
CBS Labs
High Ridge Road
Stamford, CT 02903

Albert Goldstein
University of Kansas Medical Center
39th & Rainbow
Kansas City, KS 66103

Lester Goodman
National Institutes of Health
9000 Rockville Pike
Bethesda, MD 20014

Stephen A. Goss
University of Illinois
Bioacoustics Research Lab
Urbana, IL 61801

Hans P. Govaars
Searle Radiographics, Inc.
2270 Martin Avenue
Santa Clara, CA 95050

Cary Gravatt
Office of Associate Director
for Programs
National Bureau of Standards
Washington, DC 20234

Robert E. Green, Jr.
Johns Hopkins University
Baltimore, MD 21218

James F. Greenleaf
Mayo Foundation
200 First Street Southwest
Rochester, MN 55901

Martin Greenspan
National Bureau of Standards
Washington, DC 20234

James Griffith
National Institutes of Health
9000 Rockville Pike
Bethesda, MD 20014

F. T. Hambrecht
National Institutes of Health
Bldg. 36, Rm 5A29
Bethesda, MD 20014

L. L. Hamilton
Food and Drug Adminstration
5600 Fishers Lane
Rockville, MD 20852

Mike Haran
Bureau of Radiological Health
Rockville, MD 20852

Jerry Harris
Bureau of Radiological Health
Rockville, MD 20852

Bruce Herman
Bureau of Radiological Health
Rockville, MD 20852

Rob Hertert
U.S. Army Institute of Dental Research
Walter Reed Army Medical Center
Washington, DC 20012

R. C. Heyser
Jet Propulsion Laboratory
California Institute of Technology
Pasadena, CA 91109

Ronald Hileman
Unirad
4765 Oakland
Denver, CO 80239

C. R. Hill
Institute of Cancer Research
Royal Marsden Hospital
Sutton, Surrey
United Kingdom

John D. Hoffman
Institute for Materials Research
National Bureau of Standards
Washington, DC 20234

Charles W. Hohler
University of Rochester School of Med.
601 Elmwood Avenue
Rochester, NY 14642

Edward Holasek
Case Western Reserve University
4617 Archmere Avenue
Cleveland, OH 44109

Alexine D. Holmes
Institute for Materials Research
National Bureau of Standards
Washington, DC 20234

Joseph H. Holmes
Univ. of Colorado Medical Center
4200 East 9th Avenue
Denver, CO 80220

Emanuel Horowitz
Institute for Materials Research
National Bureau of Standards
Washington, DC 20234

C. Howard Hoshall
Johns Hopkins University
8621 Georgia Avenue
Silver Spring, MD 20910

Charles Hottinger
Stanford University
Stanford, CA 94305

Lee L. Huntsman
University of Washington
Seattle, WA 98195

Everette James
Johns Hopkins Hospital
601 N. Broadway
Baltimore, MD 21205

Ronald B. Johnson
Institute for Materials Research
National Bureau of Standards
Washington, DC 20234

Steven A. Johnson
Mayo Foundation
200 First Street Southwest
Rochester, MN 55901

Ronald L. Johnston
University of Illinois
Bioacoustics Research Lab
Urbana, IL 61801

Alan L. Jones
IBM
P.O. Box 6
Endicott, NY 13760

Joie Pierce Jones
Bolt Beranek and Newman, Inc.
50 Moulton Street
Cambridge, MA 02138

Sandra L. Kaefring
University of Iowa
University Hospitals
Iowa City, IA 52242

A. C. Kak
Purdue University
W. Lafayette, IN 47907

Azmi Kaya
University of Akron
Akron, OH 44325

Edward M. Kerwin, Jr.
Bolt Beranek and Newman Inc.
50 Moulton Street
Cambridge, MA 02138

L. W. Kessler
Sonoscan, Inc.
752 Foster Avenue
Bensenville, IL 60106

Donald L. King
Columbia-Presbyterian Medical Center
622 West 168th Street
New York, NY 10032

G. Kossoff
Ultrasonics Institute
Sydney, Austrialia

Frederick Kremkau
Bowman Gray School of Medicine
Winston-Salem, NC 27103

Roman Kuc
Columbia University
St. Luke's Hospital
New York, NY 10025

Ching-Ming Lai
Department of Chemistry
SUNY at Stony Brook
Stony Brook, NY 11794

David R. Larach
Columbia Univ. College of Phys. and Surg.
50 Haven Avenue
New York, NY 10032

John I. Lauritzen
Institute for Materials Research
National Bureau of Standards
Washington, DC 20234

Michael Laviola
Riverside Research Institute
80 West End Avenue
New York, NY 10023

James M. Lawther
Pennsylvania State University
P.O. Box 30
State College, PA 16801

Richard Lawton
General Electric
Schenectady, NY 12345

D. H. Le Croissette
Jet Propulsion Lab
Pasedena, CA 91103

Sidney Lees
Forsyth Dental Center
140 Fenway
Boston, MA 02115

P. P. Lele
Massachusetts Institute of Technology
Cambridge, MA 02139

George K. Lewis
Searle Analytic Inc.
2000 Nuclear Drive
Des Plaines, IL 60018

Bernard Lichtenstein
Technicon Company
511 Benedict Avenue
Tarrytown, NY 10591

William A. Lindgren
Xenotec, Ltd.
401 East Main Street
Middletown, MD 21769

Melvin Linzer
Inorganic Materials Division
National Bureau of Standards
Washington, DC 20234

Carol Lipson
National Bureau of Standards
Washington, DC 20234

Frederic Lizzi
Riverside Research Institute
80 West End Avenue
New York, NY 10023

John A. Long
Providence Hospital
1150 Varnum Street, NE
Washington, DC

Michael L. McCartney
University of Virginia Medical Center
Box 224
Charlottesville, VA 22901

Richard McLeary
Henry Ford Hospital
2799 West Grand Blvd.
Detroit, MI 48202

James S. Main
Lister Hill National Center for
Biomedical Communications
8600 Rockville Pike
Bethesda, MD 20014

John Marangola
Upstate Medical Center
Syracuse, NY 13210

Robert F. Martin
Institute for Materials Research
National Bureau of Standards
Washington, DC 20234

Hewlett E. Melton, Jr.
Medical College of Wisconsin
8700 W. Wisconsin Avenue
Milwaukee, WI 53226

Robert F. Metzker
National Bureau of Standards
Boulder, CO 80302

Reuben S. Mezrich
RCA Labs
Princeton, NJ 08540

Eric B. Miller
National Bureau of Standards
Boulder, CO 80302

James G. Miller
Washington University
St. Louis, MO 63130

Courtney P. Mudd
University of Virginia
37 West Range
Charlottesville, VA 22901

Kiyoshi Nakayama
Johns Hopkins University
Baltimore, MD 21205

Anant K. Nigam
CBS Labs
High Ridge Road
Stamford, CT 06905

Mary B. Noyes
St. Luke's Hospital Center
Ft. Lee, NJ 07024

William O'Brien
University of Illinois
Bioacoustics Research Lab
Urbana, IL 61801

William Oldendorf
UCLA
Los Angeles, CA 90024

Larry Oline
University of South Florida
Flowler Avenue
Tampa, FL 33620

Charles P. Olinger
University of Cincinnati
Cincinnati, OH 45211

Karl C. Ossoinig
University of Iowa
Iowa City, IA

Stephen I. Parks
Inorganic Materials Division
National Bureau of Standards
Washington, DC 20234

M. Parver
NIH Clinical Center
Bethesda, MD 20014

D. M. Perozek
Hewlett Packard Company
Waltham, MA 02154

David J. Phillips
Duke University
Durham, NC 27701

G. J. Posakony
Battelle-Northwest
Box 999
Richland, WA 99352

Roger S. Powell
National Heart and Lung Institute
Bethesda, MD 20014

Judith M. S. Prewitt
National Institutes of Health
Bethesda, MD 20014

Leslie A. Priebe
University of Texas
Austin, TX 78712

T. Allen Pryor
Latter-Day Saints Hospital
Salt Lake City, UT 84143

Bernice T. Radovich
National Cancer Institute
Bethesda, MD 20014

Phillip Rauch
Henry Ford Hospital
2799 W. Grand Blvd.
Detroit, MI 48202

Henry J. L. Rechen
Bureau of Radiological Health/FDA
11113 Dewey Road
Kensington, MD 20795

J. M. Reid
Institute of Applied Physiology
and Medicine
566 18th Avenue
Seattle, WA 98122

Curt W. Reimann
Institute for Materials Research
National Bureau of Standards
Washington, DC 20234

Ron Robinson
Bureau of Radiological Health
Rockville, MD 20852

H. A. F. Rocha
General Electric
Schenectady, NY 12345

Donald S. Rodbell
RPI - Biomedical Engineering
North Hall
SAGE/Tibbetts
Troy, NY

David N. Rosensaft
161 Stouffer
3700 Spruce Street
University of Pennsylvania
Philadelphia, PA 19174

Gaylon S. Ross
Institute for Materials Research
National Bureau of Standards
Washington, DC 20234

Wilfred Roth
University of Vermont
Burlington, VT 05401

Lawrence N. Rothenberg
Memorial Hospital
1275 York Avenue
New York, NY 10021

Robert E. Rousseau
University of Texas
133 Iowa Drive
Santa Cruz, CA 95060

Thomas D. Sachs
University of Vermont
Department of Physics
Burlington, VT 05401

Kiichi Sagawa
Johns Hopkins University
Baltimore, MD 21205

Willima F. Sample
UCLA
Center for the Health Sciences
Los Angeles, CA 90024

Roger C. Sanders
Johns Hopkins Hospital
Baltimore, MD 21205

W. H. Schwarz
Johns Hopkins University
Baltimore, MD 21218

Charles F. Serpan
Nuclear Regulatory Commission
Division of Reactor Safety Research
Washington, DC 20555

Bernard Shacter
National Institutes of Health
Bethesda, MD 20014

Ronald W. Shideler
Analytical Chemistry Division
National Bureau of Standards
Washington, DC 20234

Charles A. Shipley
Johns Hopkins University Applied
Physics Laboratory
Silver Spring, MD 20910

George E. Short, Jr.
Veterans Administration
810 Vermont Avenue, NW
Washington, DC 20420

KoPing K. Shung
Providence Medical Center
556 18th Avenue
Seattle, WA 98122

M. Leon Skolnick
Presbyterian Univ. Hospital
Pittsburgh, PA 15213

James J. Smith
Central Office
Veterans Adminstration
Washington, DC 20420

Stephen W. Smith
Duke University
500 Watts Street
Durham, NC 27701

Adman Sokollu
Case Western Reserve Univ.
School of Medicine
Cleveland, OH 44106

Sidney Soloway
Automation
36 Blue Berry Hill
Wilton, CT 06897

Harold Stewart
Bureau of Radiological Health
Rockville, MD 20852

Milton Stoller
Mediscan, Inc.
544 Tolland Street
East Hartford, CT 06108

Mel E. Stratmeyer
FDA/BRH
12709 Twinbrook Pkwy
Rockville, MD 20852

K. J. W. Taylor
Yale University Medical School
New Haven, CT 06510

Patricia Tornheim
University of Cincinnati
Eden and Bethesda Avenue
Cincinnati, OH 45267

H. Tyrer
Becton Dickinson and Company
P. O. Box 12016
Research Triangle, NC 27709

George A. Uriano
Institute for Materials Research
National Bureau of Standards
Washington, DC 20234

Donald R. Van Deripe
Mallinckrodt Inc.
St. Louis, MO 63147

Bill Varner
Purdue University
W. Lafayette, IN 47906

W. F. Via
University of North Carolina
School of Dentistry
Box 2006
Chapel Hill, NC 27514

Lajos J. Von Micsky
St. Luke's Hospital Center
New York, NY 10025

Olaf T. Von Ramm
Duke University
Durham, NC 27706

Zarko M. Vucicevic
Schieie Eye Institute
University of Pennsylvania
Philadelphia, PA 19104

Robert C. Waag
University of Rochester
Rochester, NY 14627

Ray W. Ware
Veterans Adminstration Hospital
Lexington, KY 40507

Richard L. Webber
NIDR/NIH
Bldg. 10, Room 2B09
Bethesda, MD 20014

P. N. T. Wells
Briston General Hospital
Department of Medical Physics
Bristol, BS1 6SY
United Kingdom

Bryan Westerman
Northwestern Memorial Hospital
Chicago, IL 60611

D. N. White
Queens University
Kingston, Ontario
Canada K7L 3N6

Robert L. Wilson
1480 Poppy Peak Drive
Pasadena, CA 91105

William K. Wilson
Institute for Materials Research
National Bureau of Standards
Washington, DC 20234

Alan A. Winder
MSB Systems, Inc.
3 Evergreen Parkway
Westport, CT 06880

Robert N. Wolfson
1555 Belmar Road
East Cleveland, OH 44118

George J. Yang
Carnegie-Mellon University
Electrical Engineering Dept.
Schenley Park
Pittsburg, PA 15213

Lillian Yin
Food and Drug Adminstration
Rockville, MD 20854

Ellen Yorke
University of Maryland
5401 Wilkens Avenue
Baltimore, MD 21228

Donald E. Yuhas
Washington University
St. Louis, MO 63130

Ivan Zador
Cleveland Metropolitan General Hospital
Department of Ob-Gyn
Scranton Road
Cleveland, OH 44109

James A. Zagzebski
University Hospital
1300 University Avenue
Madison, WI 53706

Janis G. Ziedonis
Roche Medical Electronics
Brickyard Road
Cranbury, NJ 08519

Marvin C. Ziskin
Temple University Medical School
3400 N. Broad Street
Philadelphia, PA 19104

AUTHOR INDEX

AUTHOR INDEX

Adler, L., 25
Ahuja, A. S., 210
Anderson, P. T., 153-163
Atkinson, P., 33,61-70

Beard, C. I., 207,211
Begui, Z. E., 26
Berry, M. V., 33
Birnholz, J. C., 82
Bolt, R. H., 153-154
Busser, J. H., 9

Chivers, R. C., 182,197
Cook, K. W., 25

Devey, G. B., 1,7-10
Donaghy, R. M. P., 153-163
Dunn, F., 2,13,21-28,32,72,127,204
Dussik, K. T., 26

Etzold, K. F., 121-133

Fields, S., 32,72,127,204
Fry, E. K., 32
Fry, F. J., 2,3,143-151,158,231-251
Fry, W. J., 158

Goldman, D. E., 24
Gramiak, R., 182,213-228
Greenleaf, J. T., 2,109-119
Greguss, P., 202
Grimes, R. S., 153-163

Halliwell, M., 61-70
Heuter, T. F., 24,153-154,158
Heyser, R. C., 2,81-95
Hill, C. R., 2,3,34,182,197-212
Hoffman, J. D., 1
Holasek, E., 97-107
Huggins, R. W., 197

Ingard, K. U., 210

Jennings, W., 97-107
Johnson, S. A., 2,109-119
Jones, J. P., 3,232-233,253-258

Kak, A. C., 3,231-251
Kaya, A., 97-107
Kersta, L. N., 56
Kessler, L. W., 3,261-267
Kishimoto, T., 25
Kossoff, G., 2,32,73,135-139

LeCroissette, D. H., 2,81-95
Lele, P. P., 2,3,34,167-196
Lerner, R. L., 182
Lerner, R. M., 213-228
Linzer, M., 9

Mansfield, A. B., 167-196
Mezrich, R. S., 2,121-133
Milan, J., 2,197
Moore, D. H., 170
Morse, P. M., 210
Mountford, R. A., 55,61-70,72,176
Murphy, A. I., 167-196

Namery, J., 167-196
Nicholas, D., 182,197

Ossoinig, K. C., 2,33

Pfander, F., 24
Preston, K., 2,9,51-70
Prewitt, J. H. S., 9
Purnell, E. W., 97-107

Reid, J. M., 1-2,11-17,29-47,61,207-212
Renger, F., 61

Sachs, T. D., 2,153-163
Schentke, K. U., 61
Senapati, N., 167-196
Shung, K. K., 2-3,44,207-212
Sigelmann, R. A., 44,207-212
Sokollu, A., 2,97-107
Stenger, R. J., 170

Taylor, K. J. W., 2,38,71-78
Theisman, H., 24
Twersky, V., 207,209

Vilkomerson, D. H. R., 9,121-133

Waag, R. C., 3,9,34,182,213-228
Wells, P. N. T., 2,38,45,61-70,72,176
Wild, J. J., 11-13,37,61
Wright, S. J., Jr., 153-163

SUBJECT INDEX

AEMB - see "Alliance for Engineering in Medicine and Biology"
AIUM - see "American Institute of Ultrasound in Medicine"
ART - see "algebraic reconstruction"
A-scan pattern recognition - 2,51-60,61-70, 71-78
abdomen - 16
absorption - 1-3,13-14,21-28,34-35,38,42, 44-45,82,88,118,143-151,153-163,168,172, 192,214,219-220,226,232,255,263-264,266
absorption gradient - 2,143-151,153-154
acceptance criteria - 9
acoustic microscopy - 3,261-267
algebraic reconstruction - 109-119
Alliance for Engineering in Medicine and Biology (AEMB) - 6,8
American Institute of Ultrasound in Medicine (AIUM) - 3
anechoic method - 81-95
apodization - 92
arteries - 40
atherosclerotic plaque - 128,132
attenuation - 1-2,13,21-28,29,33,42-44,61-62, 64,81-95,97-107,109-119,121-133,135-139, 143-144,150,153,167-196,231-232,253-254, 256,261,263-264,266
attenuation distribution - 236-237
auditory analysis - 2,51,55-58

bile ducts - 68
blood - 3,13,16,27,29-34,37-39,44,68,207-212, 246,256
bone - 24-26,38,235,266
bowel - 32
Bragg diffraction - 167,175-194,197-206, 213-228
brain - 3,27,86,144-145,147-149,153-163,168, 200,246,256,266
breast - 13,61,109,116-117,121-122,125-127, 135-137,201

CAT - see "computerized axial tomography"
cartilage - 26-27
choroid - 33,107
cirrhosis - 61-70,72,75,193,224-226
collagen - 26-27,32,68,72-73,182,225-226
color display - 2,4,73,97,105-107,138
compressibility - 22,29,31,34,110,207,215
computer analysis - 61,66,71-78,109-119, 231-251
computerized axial tomography - 2,109-119, 154
computerized tomography - see "computerized axial tomography"
computer processing - 2,51-59,97,101-105, 167,169-173
connective tissue - 13,68,266
convolution - 91-95,226
correlation - 237-239,244

deconvolution - 3,45,231-251,253-258
density - 21,24,29,31,67-68,110,144,146,155 158,207,215,261,263,266
dental tissue - 266
dentyne - 266
di-gram - 55
distribution function - 207
Doppler effect - 1,3,11,13-14,158-159,208

echocardiography - 13,33
elasticity - 263,266
elastin - 72
elastogen - 182
emboli - 34,176
enamel - 266
erythrocytes - 207
exit criteria - 9
eye - 2,26,33,38,105

fat - 14,24,27,62-68,132,199-201,246
fibrosis - 68
Fourier transform - 16,55,87-88,90-94,97, 101,169-172,199,213,217-218,220-226
Fraunhofer condition - 216,226
frequency dependence - 1-4,13-15,23-26,30, 33-39,43,81-95,97-107,121,135,138-139,144, 167-196,197-206,207-212,213-228,232,254-255,261,264,266
frequency translation - 51,57-58

geophysics - 69
glioblastoma - 86
Green's function - 215
grey-scale - 71-73,76,138

half-wave resonance - 13,32
heart - 13,34,109,112-113,115-116,167-171, 256,265
Helmholtz equation - 215,219
hematocrit - 34,207-212
hepatitis - 66
hepato-toxic chemicals - 72-76
histogram - 75-77

IEEE Ultrasonic Symposium - 3
image reconstruction - see "computerized axial tomography"
impedance - 1-3,21-22,24,26,31-32,42-43,61, 67,71,110,118,143-151,153,167-168,214, 231-251,253-258,261,263-264,266
impedance distribution - 263-264
impedance gradient - 143-151
impedance profile - 3,231-251,253-258
impediography - 253-258
impulse response - 3,45,46,91,231-251,253-258
Instrumentation Technology Program - 7-10
in vitro conditions - 1,16,40,188
International Symposium on Acoustical Imaging and Holography - 1,3

Kalman filtering - 256
Karhunen-Loeve expansion - 55
kidney - 16,24,27,32,51-52,265-266

lacunar infarct - 162-163
Laue pattern - 202
layer model - 231-251
leukemia - 73-74,76-77,224-226
Linear Frequency Translation (LIFT) - 57-58
liver - 2,24,27,32,51-54,58,61-70,72-73,76 101,131-132,176,180-181,185-190,192,199-204,213,222,224-227,246
Logarithmic Frequency Translation (LOFT) - 57-58
lucite - 148,150,231,249,267
lung - 24,26-27,34
lymph channels - 40
lymphoma - 73

melanoma - 107
mesomorphy - 64
Michelson interferometer - 122-123
Michelson-Morley experiment - 171
microscopy - 3,261-267
mitral valve - 13,15,32
modulus - 21,31-32,67-68,72,261
muscle - 3,24,27,32-33,40,62,68,169-171,174-179,185,187-194,204,246
myocardial infarction - 33,167-171,173,256

NSF - see "National Science Foundation"
NSF Survey Team of Ultrasonic Imaging - 7
National Bureau of Standards (NBS) - 1
National Institutes of Health (NIH) - 1,3
National Science Foundation (NSF) - 1,3,7-10, 51,53
nervous tissue - 24-25
nondestructive evaluation - 1,3,197

optimization - 11,13-14

P-factor - 155,158,160
paraffin oil - 38
pattern recognition - 1,51-59
phase-contrast imaging - 2,121,128-132
phasor - 81,87-89
phoneme - 55
placenta - 33
plaque - 266
polyethylene - 131
polystyrene - 130
portal hypertension - 68,73
portal vein - 203
protein - 2,26

RANN - 1,7-10
R&D incentives - 7
Rayleigh scattering - 14,16,174,199-203,207-212
refractive index - 109-119,215,218-220
relaxation - 23
resonance - 11
retina - 107

saline - 113-116
scattering - 1-3,11-12,14-16,21,29-47,53,68 72,82-83,88,118,153,155,167-196,197-206, 207-212,213-228,232,253-255,263-264,266
scattering, cross-section - 13,16,29,31,35, 36-38,41,42,44,45
scattering, surface - 174
sclera - 33
serum - 27
shear waves - 22-24,26,223
silastic rubber - 248
skin - 62,246
skull - 24,25,147,153-155,158,246,248-250, 256
somatotype - 64
sonar - 2,56
Sonomicroscope - 261-267
Spectra-Color Ultrasonography - 105-107
spectra analysis - 34,55,81-95,97-107,167-196,197,255,256
speech spectrogram - 51,55
spleen - 2,38,71,73-75,77,199-200
splenomegaly - 71-78
sponge - 99-104,136-137
standardization - 29,35-38,42-43,256
statistical analysis - 54-55,61-70,71-78, 185,187-188,190,217-227,256
stomach - 32
streaming phenomena - 158-160
stroke - 162-163
synthetic focus imaging - 109-118

TAST - see "Thermo-Acoustic Sensing Technique"
temperature dependence - 1-2,4,23-25,40,143, 153-163
tendon - 26-27
thalamus - 86
thermal conductivity - 23
thermal effects, 153
thermal gradient, 143-151
Thermo-Acoustic Sensing Technique, 153-163
Time Delay Spectrometry - 81-95
tomography - see "computerized axial tomography"
tuberculosis - 75
tumor - 11,32-33,72-73,75-76,82,86,109,121-122,125-127,132,136,153,158,162-163,201, 235

uterus - 33

veins - 40
velocity - 1-3,14,21-28,29-30,34,72,81-95, 97-107,109-119,121-133,135-139,143-151, 153-163,215-217,219,232,255,261,263,265-267
velocity distribution - 264
velocity gradient - 2
ventricle - 115
viscosity - 23,31-32,210

water - 2,246-247
Weiner spectrum - 55-56

z-transform - 240-241

NBS-114A (REV. 7-73)

U.S. DEPT. OF COMM. BIBLIOGRAPHIC DATA SHEET	1. PUBLICATION OR REPORT NO. NBS SP-453	2. Gov't Accession No.	3. Recipient's Accession No.

4. TITLE AND SUBTITLE

Ultrasonic Tissue Characterization

5. Publication Date: October 1976

6. Performing Organization Code

7. AUTHOR(S)

Melvin Linzer

8. Performing Organ. Report No.

9. PERFORMING ORGANIZATION NAME AND ADDRESS

NATIONAL BUREAU OF STANDARDS
DEPARTMENT OF COMMERCE
WASHINGTON, D.C. 20234

10. Project/Task/Work Unit No. 3130114

11. Contract/Grant No.

12. Sponsoring Organization Name and Complete Address *(Street, City, State, ZIP)*

Same as 9.

13. Type of Report & Period Covered: Final

14. Sponsoring Agency Code

15. SUPPLEMENTARY NOTES

Library of Congress Catalog Card Number: 76-608298

16. ABSTRACT *(A 200-word or less factual summary of most significant information. If document includes a significant bibliography or literature survey, mention it here.)*

An international Seminar on Ultrasonic Tissue Characterization was held at the National Bureau of Standards on May 28-30, 1975. The meeting was co-sponsored by the National Bureau of Standards, the National Science Foundation and the National Institutes of Health. This volume contains extended versions of 20 of the 21 talks presented at the Seminar. Topics covered include techniques for measurement of ultrasonic tissue parameters, the dependence of tissue properties on physical and biological variables (e.g., ultrasonic frequency, temperature) and pattern recognition techniques.

17. KEY WORDS *(six to twelve entries; alphabetical order; capitalize only the first letter of the first key word unless a proper name; separated by semicolons)*

A-scan; absorption; acoustic; attenuation; B-scan; frequency; image; reconstruction; impedance; medical diagnosis; microscopy; pattern recognition; scattering; tissue characterization; tissue parameters, tissue signature; tumor; ultrasonic spectroscopy; ultrasound; velocity.

18. AVAILABILITY

[x] Unlimited

[ ] For Official Distribution. Do Not Release to NTIS

[X] Order From Sup. of Doc., U.S. Government Printing Office Washington, D.C. 20402, SD Cat. No. C13.10:453

[ ] Order From National Technical Information Service (NTIS) Springfield, Virginia 22151

19. SECURITY CLASS (THIS REPORT): UNCLASSIFIED

21. NO. OF PAGES: 274

20. SECURITY CLASS (THIS PAGE): UNCLASSIFIED

22. Price: $3.55

USCOMM-DC 29042-P74

NBS TECHNICAL PUBLICATIONS

PERIODICALS

JOURNAL OF RESEARCH reports National Bureau of Standards research and development in physics, mathematics, and chemistry. It is published in two sections, available separately:

• **Physics and Chemistry (Section A)**
Papers of interest primarily to scientists working in these fields. This section covers a broad range of physical and chemical research, with major emphasis on standards of physical measurement, fundamental constants, and properties of matter. Issued six times a year. Annual subscription: Domestic, $17.00; Foreign, $21.25.

• **Mathematical Sciences (Section B)**
Studies and compilations designed mainly for the mathematician and theoretical physicist. Topics in mathematical statistics, theory of experiment design, numerical analysis, theoretical physics and chemistry, logical design and programming of computers and computer systems. Short numerical tables. Issued quarterly. Annual subscription: Domestic, $9.00; Foreign, $11.25.

DIMENSIONS/NBS (formerly Technical News Bulletin)—This monthly magazine is published to inform scientists, engineers, businessmen, industry, teachers, students, and consumers of the latest advances in science and technology, with primary emphasis on the work at NBS. The magazine highlights and reviews such issues as energy research, fire protection, building technology, metric conversion, pollution abatement, health and safety, and consumer product performance. In addition, it reports the results of Bureau programs in measurement standards and techniques, properties of matter and materials, engineering standards and services, instrumentation, and automatic data processing.

Annual subscription: Domestic, $9.45; Foreign, $11.85.

NONPERIODICALS

Monographs—Major contributions to the technical literature on various subjects related to the Bureau's scientific and technical activities.

Handbooks—Recommended codes of engineering and industrial practice (including safety codes) developed in cooperation with interested industries, professional organizations, and regulatory bodies.

Special Publications—Include proceedings of conferences sponsored by NBS, NBS annual reports, and other special publications appropriate to this grouping such as wall charts, pocket cards, and bibliographies.

Applied Mathematics Series—Mathematical tables, manuals, and studies of special interest to physicists, engineers, chemists, biologists, mathematicians, computer programmers, and others engaged in scientific and technical work.

National Standard Reference Data Series—Provides quantitative data on the physical and chemical properties of materials, compiled from the world's literature and critically evaluated. Developed under a world-wide program coordinated by NBS. Program under authority of National Standard Data Act (Public Law 90-396).

NOTE: At present the principal publication outlet for these data is the Journal of Physical and Chemical Reference Data (JPCRD) published quarterly for NBS by the American Chemical Society (ACS) and the American Institute of Physics (AIP). Subscriptions, reprints, and supplements available from ACS, 1155 Sixteenth St. N.W., Wash. D. C. 20056.

Building Science Series—Disseminates technical information developed at the Bureau on building materials, components, systems, and whole structures. The series presents research results, test methods, and performance criteria related to the structural and environmental functions and the durability and safety characteristics of building elements and systems.

Technical Notes—Studies or reports which are complete in themselves but restrictive in their treatment of a subject. Analogous to monographs but not so comprehensive in scope or definitive in treatment of the subject area. Often serve as a vehicle for final reports of work performed at NBS under the sponsorship of other government agencies.

Voluntary Product Standards—Developed under procedures published by the Department of Commerce in Part 10, Title 15, of the Code of Federal Regulations. The purpose of the standards is to establish nationally recognized requirements for products, and to provide all concerned interests with a basis for common understanding of the characteristics of the products. NBS administers this program as a supplement to the activities of the private sector standardizing organizations.

Consumer Information Series—Practical information, based on NBS research and experience, covering areas of interest to the consumer. Easily understandable language and illustrations provide useful background knowledge for shopping in today's technological marketplace.

Order **above** *NBS publications from: Superintendent of Documents, Government Printing Office, Washington, D.C. 20402.*

Order **following** *NBS publications—NBSIR's and FIPS from the National Technical Information Services, Springfield, Va. 22161.*

Federal Information Processing Standards Publications (FIPS PUBS)—Publications in this series collectively constitute the Federal Information Processing Standards Register. Register serves as the official source of information in the Federal Government regarding standards issued by NBS pursuant to the Federal Property and Administrative Services Act of 1949 as amended, Public Law 89-306 (79 Stat. 1127), and as implemented by Executive Order 11717 (38 FR 12315, dated May 11, 1973) and Part 6 of Title 15 CFR (Code of Federal Regulations).

NBS Interagency Reports (NBSIR)—A special series of interim or final reports on work performed by NBS for outside sponsors (both government and non-government). In general, initial distribution is handled by the sponsor; public distribution is by the National Technical Information Services (Springfield, Va. 22161) in paper copy or microfiche form.

BIBLIOGRAPHIC SUBSCRIPTION SERVICES

The following current-awareness and literature-survey bibliographies are issued periodically by the Bureau:

Cryogenic Data Center Current Awareness Service. A literature survey issued biweekly. Annual subscription: Domestic, $20.00; Foreign, $25.00.

Liquified Natural Gas. A literature survey issued quarterly. Annual subscription: $20.00.

Superconducting Devices and Materials. A literature survey issued quarterly. Annual subscription: $20.00. Send subscription orders and remittances for the preceding bibliographic services to National Bureau of Standards, Cryogenic Data Center (275.02) Boulder, Colorado 80302.

U.S. DEPARTMENT OF COMMERCE
National Bureau of Standards
Washington, D.C. 20234

OFFICIAL BUSINESS

Penalty for Private Use, $300

POSTAGE AND FEES PAID
U.S. DEPARTMENT OF COMMERCE
COM-215

SPECIAL FOURTH-CLASS RATE
BOOK